Regulation of peptidoglycan synthesis during cell division in *Escherichia coli*

Alexander J F Egan

Centre for Bacterial Cell Biology

Institute for Cell and Molecular Biosciences

Thesis submitted for the degree of Doctor of Philosophy

Newcastle University

March 2014

Declaration

I hereby declare that this thesis is my own work and effort and that it has not been submitted elsewhere for any award. Any contribution made to the project by others is explicitly acknowledged in this thesis.

Alexander J F Egan

Abstract

Bacteria surround their cytoplasmic membrane with an essential, stress-bearing macromolecule, the peptidoglycan (PG) layer. During growth and division cells extend this layer through the action of membrane-anchored peptidoglycan synthases. Presumably, sacculus growth is facilitated by dynamic multiprotein complexes which are guided by cytoskeletal elements. These complexes contain all the necessary peptidoglycan synthases and hydrolases for the enlargement of the sacculus, along with their regulators. Biochemical and genetic data gathered in recent years provides evidence for the existence of these complexes, but the molecular mechanisms they employ, and how cell wall synthesis is coordinated with the synthesis of other cell envelope layers, remain largely unknown.

In this work we have elucidated key biochemical features of a regulator of PG synthesis, LpoB. Its high resolution structure was solved by NMR spectroscopy and the interaction interface of LpoB with the major peptidoglycan synthase active during cell division in *Escherichia coli*, PBP1B, was determined. We show that LpoB interacts with the non-catalytic UB2H domain of PBP1B, situated between the glycosyltransferase and transpeptidase domains.

Several other proteins have previously been implicated in the regulation of PBP1B. Here we optimised an *in vitro* glycosyltransferase assay and investigated the effect of interacting proteins on peptidoglycan synthesis. We have shown the first evidence that multiple interaction partners, LpoB and FtsN, exert a simultaneous synergistic regulatory effect on PBP1B GTase. We also identified novel, functional interactions of PBP1B. YbgF and TolA are both members of the Tol-Pal complex which is required for outer membrane stability and its proper invagination during cell division. TolA was shown to interact with PBP1B via its transmembrane region (domain I) and moderately stimulates the GTase activity of the synthase. YbgF also interacts with PBP1B and is the first example of a negative modulator of PG synthetic activity, inhibiting the regulation of PBP1B TPase by Lpo, which is relieved by TolA. We propose that YbgF and TolA function to fine tune the regulation of PBP1B during division which allows for a proper coordination between cell wall synthesis and constriction of the OM during division in *E. coli*.

In summary, this work significantly enhances our understanding of the regulation of the bifunctional PG synthase active during cell division, PBP1B.

Acknowledgements

I would like to acknowledge Newcastle University, the Centre for Bacterial Cell Biology within the Institute for Cell and Molecular Biosciences and the BBSRC for funding and support throughout. I must particularly thank Waldemar Vollmer, not only for his excellent supervision and guidance, but for giving me the opportunity to learn all I could from him, a process which is still ongoing and will be for as long as I'm permitted. It has been an honour and privilege to hone my skills in his lab along with my colleagues and friends, to all of whom I owe gratitude; Masters Khai Bui and Jacob Biboy for sharing their support and wisdom, Daniela Vollmer for being a great lab-mother, and fellow students, particularly Adam Lodge for his unparalleled ability to make the lab a fun place to be. Finally Manuel Banzhaf, for teaching me how to become a good and effective scientist in the beginning.

I would also like to thank Andrew Gray, Nicolas Jean, Alexandra Koumoutsi, Catherine Bougault, André Zapun, Jules Phillipe, Tanneke den Blaauwen, Carol Gross, Jean-Pierre Simorre, Athanasios Typas and Eefjan Breukink. All of whom provided vital assistance in collaborative projects, and enhanced the significance of my contributions to the field.

I have been lucky to be surrounded by such supportive friends and colleagues throughout my time at the CBCB. The people of this centre; particularly Flo, Flint and Adam, have made it an excellent place to work.

Finally I must thank my Motherness, Simon and my dad, the Fuzzyman, for nurturing my interest in science and supporting my early studies of the subject.

And Emily, whose love and support kept me going throughout.

Abbreviations

ABC	ATP binding cassette
Amp	ampicillin
APS	ammonium peroxodisulphate
ATP	adenosine-5'- triphosphate
AUC	analytical ultracentrifugation
BSA	bovine serum albumin
CPM	counts per minute
C-terminal	carboxy-terminal
Da / kDa	Daltons / kilodaltons
ddH_20	MilliQ water
D-iGlu	D-isoglutamic acid
DNA	deoxyribonucleic acid
DNase	deoxyribonuclease
DTSSP	3,3'-dithiobis(sulfosuccinimidylpropionate)
ECL	enhanced chemiluminesence
EDC	1-Ethyl-3-(3-dimethylaminopropyl)carbodimide hydrochloride
EDTA	ethylenediaminetetraacetic acid
FRET	förster resonance energy transfer
× *g*	acceleration due to gravity
Glc*N*Ac	*N*-acetylglucosamine
GTase	glycosyltransferase
HEPES	(4-(2-hydroxyethyl)-1-piperazineethanesulfonic acid)
His- / -His	hexahistidine tag (N- / -C terminal)
HPLC	high pressure liquid chromatography
IEX	ion exchange chromatography
IM / CM	inner membrane / cytoplasmic membrane
IMAC	immobilised metal affinity chromatography
Kan	kanamycin
LB	Luria Bertani
meso-Dap	*meso*-diaminopimelic acid
min	minute
Moe.	moenomycin
MOPS	3-(*N*-morpholino)propanesulfonic acid
Mur*N*Ac	*N*-acetylmuramic acid

MW	molecular weight
NaAcetate	sodium acetate
Ni-NTA	nickel^{2+} - nitrilotriacetic acid
NO	nucleoid occlusion
N-terminal	amino-terminus
OM	outer membrane
P	phosphate
PBP	penicillin binding protein
PG	peptidoglycan
PMSF	phenylmethanesulphonyl fluoride
rpm	revolutions per minute
RT	room / ambient temperature
SDS	sodium dodecyl sulphate
PAGE	polyacrylamide gel electrophoresis
SEC	size exclusion chromatography
s-NHS	sulfo-*N*-hydroxysuccinimide
SPR	surface plasmon resonance
TEMED	tetramethylethylenediamine
TM	transmembrane
TP	transpeptidation
TPase	transpeptidase
Tris	tris(hydroxymethyl)aminomethane
U.V.	ultraviolet
UDP	uridine diphosphate

Index of figures and tables

1. Introduction

1.1 Growth and morphogenesis of *Escherichia coli*

All propagating bacteria cycle between growth and division, during which all cellular components are replicated in a controlled manner for inheritance by each daughter cell. An important example of this is the bacterial cell wall peptidoglycan (murein) sacculus (1). The sacculus is a continuous net-like macromolecule which encloses the cytoplasmic (or inner) membrane (IM). It determines the shape of the cell and is required to protect the cell against osmotic challenges. How this large and essential component of the cell is synthesised for inheritance by the daughter cells while maintaining a uniform morphology is a fundamental, but largely unanswered question in microbiology (2–4).

The peptidoglycan cell wall forms part of the basis for the separation of bacteria into either Gram-positive or Gram-negative categories. In Gram-negative bacteria, like the proteobacteria, the PG is 3 – 6 nm thick, and likely a single layer which is associated with an outer membrane (OM). In some species the PG and OM are connected through covalent binding of the cell wall to Braun's lipoprotein which is embedded in the outer membrane (5). In Gram-positive bacteria, such as the firmicutes, the cell wall is thicker (10 – 20 nm) and contains covalently attached secondary cell wall polymers including teichoic acids and capsular polysaccharides (6).

Peptidoglycan is composed of glycan chains made of alternating *N*-acetylmuramic acid (Mur*N*Ac) and *N*-acetylglucosamine (Glc*N*Ac) residues linked by β-1,4 glycosidic bonds. These chains are cross-linked by short peptides, which are composed of the following sequence in *E. coli*: L-Ala-D-iGlu-*m*-Dap-D-Ala-D-Ala (*m*-Dap, *meso*-diaminopimelic acid). New peptides can be connected to neighbouring peptides in existing cross-links to form multimeric cross-links between two or more glycan chains (7). In Gram-positive species, the sequence of the peptide varies, and many of these species also modify the glycan chain through *O*-acetylation or *N*-deacetylation (8). The architecture of the cell wall has been debated over the last few decades with particular focus on the mainly single layered sacculus from Gram-negative bacteria (9). A current model of a single layered sacculus is based on several observations. The enhanced elasticity of purified sacculi in the direction of the long axis suggests that the glycan chains are oriented perpendicular to this direction with the more flexible peptide cross-links oriented parallel to the long axis. A single layer is also supported by the determined thickness of 3 – 6 nm (10–12). Further evidence is that the length of glycan chains isolated from *E. coli* varied dramatically with an average of 25

to 35 disaccharide units, which would give them a length of 25 – 35 nm (13, 14). Given the observed thickness the model that glycans run away from the cytoplasmic membrane in an alternative scaffold-like manner proposed by Dmitriev *et al.* (2005) is unlikely. A recent study on the cell wall of *B. subtilis* suggested it has the same architecture, but with multiple layers (16), but it remains unclear.

The mechanisms by which the sacculus grows during the elongation and division of the cell are largely unknown. According to a current model, membrane-associated multienzyme complexes consisting of enzymes for peptidoglycan synthesis and hydrolysis are controlled spatially and/or functionally from inside the cell by cytoskeletal elements, along with other associated proteins (17, 18). The actin-like MreB is required for the maintenance of rod shape in many bacterial species and has been shown to localise in dynamic patches/filaments on a helical path along the length of the cell depending on ongoing PG synthesis (19–22). This association between MreB and the cell wall synthesis machinery, the so called elongosome, acts to maintain a constant diameter of the cell during growth by an unknown mechanism (1). Cell division is orchestrated by the tubulin-like FtsZ along with more than 12 other essential division proteins (23). These, with other accessory proteins associate to form the divisome complex for cell pole synthesis during division. Given the parallels with the elongosome, these complexes are believed to share a common evolutionary past (24). Recent studies have shown that in *E. coli*, *C. crescentus* and presumably other species, a pre-septal phase of PG synthesis occurs in the transition between elongation and division, elongating the cell from a specific zone (mid-cell) dependant on FtsZ (25, 26).

In *E. coli* and likely other Gram-negative γ-proteobacteria growth is also regulated from the outer membrane by recently identified lipoproteins LpoA and LpoB (27, 28), which will be discussed later (1.3.3.1). Gram-negative bacteria, with their additional layer to the cell envelope, employ a constrictive mode of cell division such that the synthesis of the septum, splitting of this septum, and the invagination of the outer membrane occur simultaneously. In contrast, many Gram-positive species synthesise the septal cell wall completely prior to its splitting for cell separation as shown in figure 1.1.

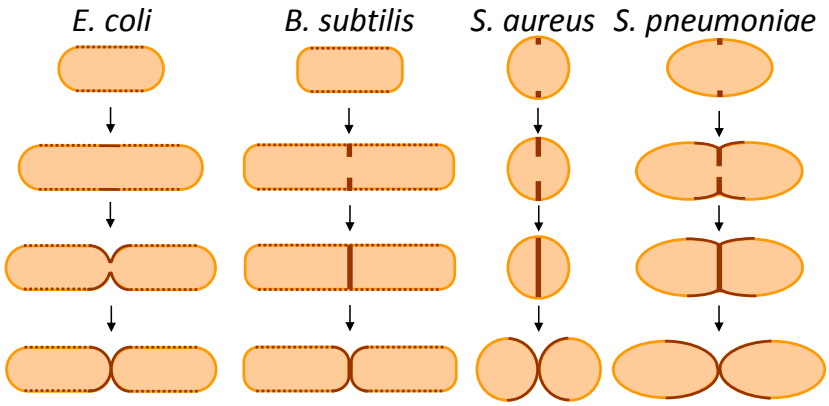

Figure 1.1 Modes of growth and division in different bacterial species (1)

Sites of peptidoglycan synthesis during growth and cell division in different bacterial species. The rod-shaped *E. coli* and *B. subtilis* elongate by insertion of new peptidoglycan (brown dots) into the lateral wall. The ovococcus *S. pneumoniae* elongates from a specific growth zone at mid-cell and coccal species such as *S. aureus* lack an elongation phase altogether, simply synthesising a division septa via zonal synthesis (dark brown lines). This zonal synthesis is also adopted by the other species but while Gram-positives all fully synthesise a complete division septum prior to splitting, Gram-negatives synthesise and split the septum simultaneously with constriction of the cell.

1.2 Peptidoglycan synthesis and hydrolysis

1.2.1 The peptidoglycan precursor lipid II

Synthesis of the peptidoglycan cell wall begins in the cytoplasm with the synthesis of the nucleotide activated precursors UDP-Glc*N*Ac and UDP-Mur*N*Ac. The Glm enzymes (GlmM, GlmS and GlmU) catalyse the conversion of fructose-6-P into UDP-Glc*N*Ac, which is converted to UDP-Mur*N*Ac by MurA and MurB. The amino acid ligases MurC, MurD, MurE and MurF catalyse the sequential addition of L-Ala, D-iGlu, *m*-Dap and D-Ala-D-Ala, respectively (29). The D-Ala-D-Ala dipeptide is synthesised by the Ddl ligases and added in a single step by MurF. Racemases are required for the creation of D- amino acids from their L-enantiomers (29, 30).

The next steps occur at the cytoplasmic face of the inner membrane when the transferase MraY catalyses the formation of undecaprenyl-pyrophosphoryl-Mur*N*Ac(pentapeptide), which is referred to as lipid I (31). The glycosyltransferase MurG then transfers a Glc*N*Ac residue from UDP-Glc*N*Ac to lipid I forming the peptidoglycan precursor lipid II (undecaprenyl-pyrophosphoryl-Mur*N*Ac(pentapeptide) -Glc*N*Ac) (31).

1.2.2 Growth of the sacculus

For the synthesis of peptidoglycan, lipid II is flipped across the cytoplasmic membrane by FtsW/RodA flippases (32) where it is the substrate of glycosyltransferase (GTase) reactions, the first peptidoglycan synthesis reaction at the periplasmic face of the cytoplasmic membrane, which polymerises lipid II into the glycan chains (33). Structural and biochemical data shows that the GTase enzymes act processively (34, 35) with the growing glycan chain as the donor and lipid II as acceptor in the reaction. A catalytic base residue (glutamate) is required for the deproptonation of Glc*N*Ac 4-OH of lipid II forming an activated nucleophile which then directly attacks the C1 of the lipid-linked Mur*N*Ac of the growing glycan chain, causing the release of the undecaprenol pyrophosphate moiety as shown in figure 1.2A (35–37). Peptides protruding from different glycan chains are cross-linked by transpeptidase (TPase) reactions, typically DD-TPases in *E. coli*. LD-TPases also exist, but are more common in other species (38). DD-TPases (here referred to as TPases) use a pentapeptide as donor and a tri-, tetra, or pentapeptide as acceptor. The terminal D-Ala of the donor is released during the reaction (39) which links the 4th residue of the donor to the 3rd residue of the acceptor (*m*-Dap).

The catalytic serine forms an acyl-enzyme complex with the tetrapeptide which is then attacked by the amino group of *m*-Dap of another peptide leading to the cross-linkage of two glycan chains (dimeric cross-link) (40) to produce the net-like peptidoglycan structure (Fig. 1.2 B).

There are several models for the growth of the sacculus. Most agree that growth is achieved via insertion of new peptidoglycan into the existing layer. One model suggests that the insertion occurs by a bulk addition of a large section of newly synthesised material (15), another that two glycan chains are synthesised simultaneously, adjacent to existing chains in the cell wall (41). Both of these theories require the hydrolysis of the existing sacculus prior to the insertion of the new material, which could potentially lead to lysis when the internal pressure of the cell is considered and is thus an unsafe mechanism for the cell. As such, Koch proposed a "make before break" strategy in which new covalent bonds must be formed prior to the hydrolysis of the old/existing bonds in the sacculus (42). Following this, Höltje proposed a "three for one" model in which three new glycan chains are synthesised, cross-linked and attached underneath a single docking strand in the existing sacculus which is simultaneously hydrolysed and removed allowing the insertion of the three new strands immediately in its place (17) (Fig. 1.3). This growth mechanism would allow for the safe enlargement of the peptidoglycan sacculus, and also provides a basic explanation for the maintenance of shape, given that the existing sacculus is used directly as a template. The model also explains the high amount of peptidoglycan turnover observed in growing cells (see 1.2.4).

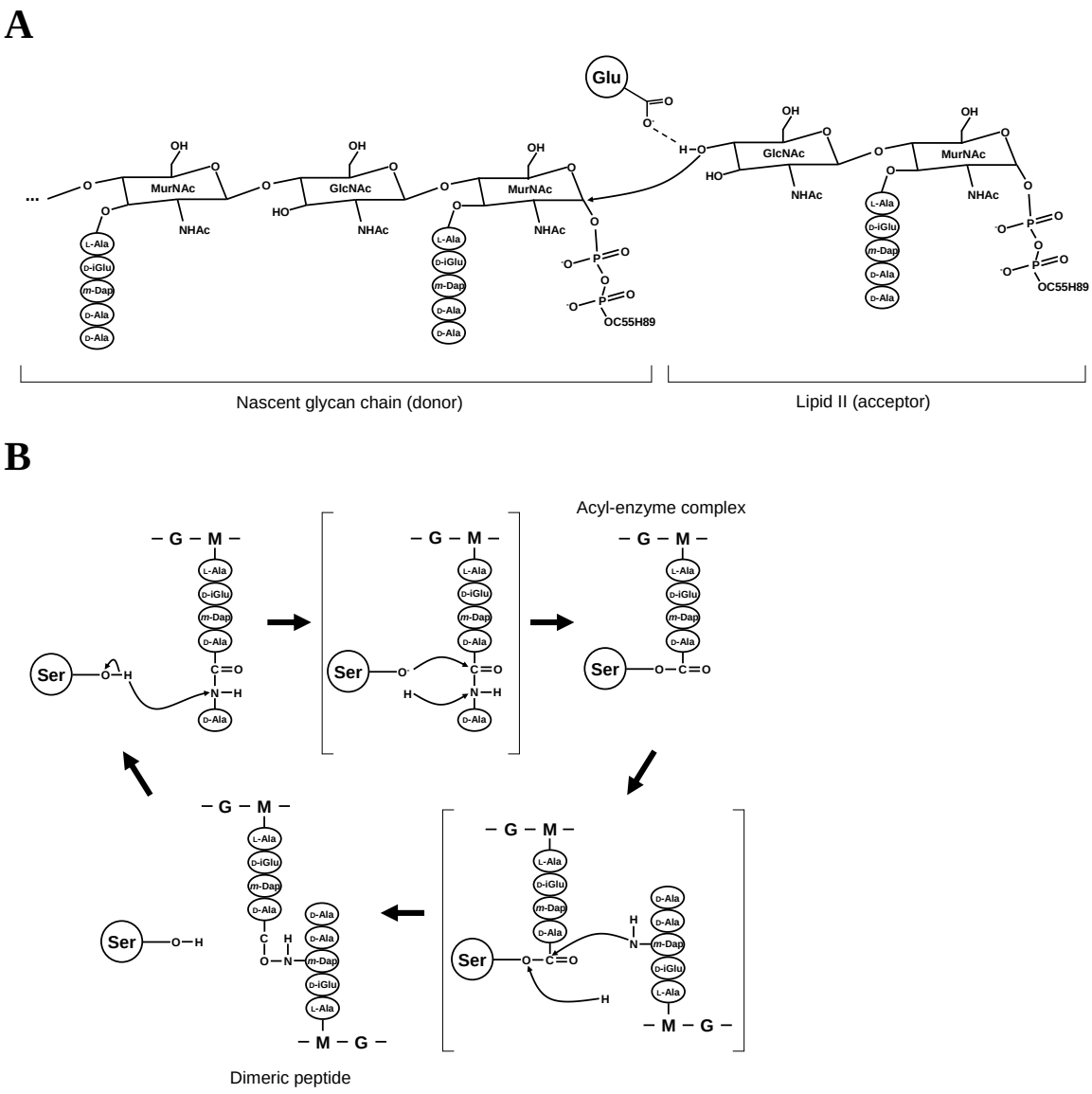

Figure 1.2 The PG synthetic reactions in *E. coli*

(A) The glycosyltransferase reaction, catalysing the addition of lipid II (acceptor) to the growing glycan chain (donor). The basic Glu residue is key for catalysis, it deprotonates the Glc*N*Ac 4-OH of lipid II forming a nucleophilic intermediate which attacks the C1 of the lipid linked Mur*N*Ac of the growing glycan chain forming a β-1,4-glycosidic linkage and causing the loss of the undecaprenol pyrophosphate.
(B) The transpeptidation or acyl transferase reaction. The catalytic Ser residue attacks the carboxy-terminal D-Ala-D-Ala bond of a pentapeptide via its γOH forming an acyl-enzyme complex, which is then attacked by the amino group of *m*-Dap of another peptide leading to a cross-linked peptide dimer. The catalytic residue is returned to its original state and free to catalyse the reaction again. G, Glc*N*Ac; M, Mur*N*Ac.

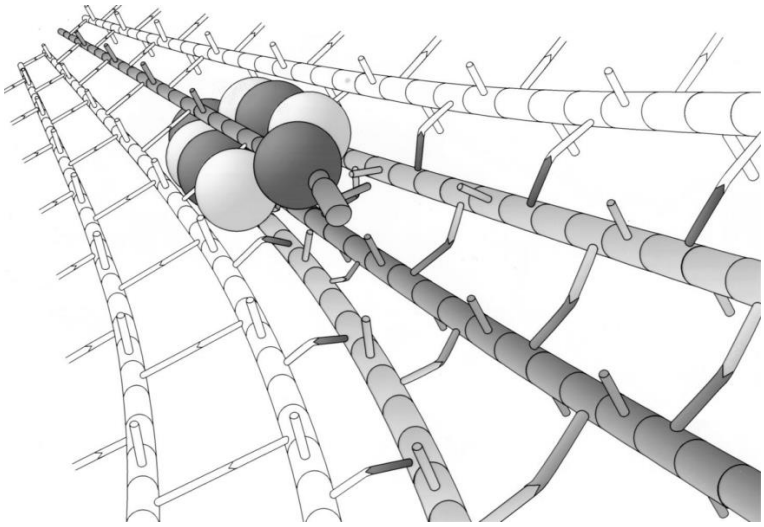

Figure 1.3 The three for one model as proposed by Höltje (17)

The proposed multi-enzyme peptidoglycan synthesis complex (represented as various grey and white spheres) polymerises and cross-links three new glycan chains (the three grey strands) to the existing sacculus while simultaneously removing the guiding or docking strand (single dark grey strand).

1.2.3 Synthesis of the cell poles

Until cell division, growth of the sacculus occurs along the lateral cell wall in order to produce a cell with the proper morphology, in the case of *E. coli* this is a rod of uniform cylindrical diameter. At the point of division the cell must switch to the production of peptidoglycan that no longer conforms to the maintenance of the constant diameter but instead to a constrictive pattern (Fig. 1.1). The underlying mechanism behind this switch is unknown. Recent data suggests that the cytoskeletal elements MreB and FtsZ play a role by coordinating a pre-septal phase of cell wall synthesis. A direct interaction between MreB and FtsZ as well as a co-localisation prior to division was observed (43). Additionally, integral proteins of the elongosome and divisome were also shown to interact and co-localise during this phase of growth (44).

1.2.4 Peptidoglycan turnover

As implied above, peptidoglycan hydrolases are an essential component of the proposed multienzyme complexes for the growth of the sacculi and for the splitting of septal PG during division (45). There are several classes of PG hydrolases, defined by their catalytic activity including the lytic transglycosylases, endopeptidases (EPases), carboxypeptidases (CPases) and Mur*N*Ac-L-alanine amidases which are further defined

by their specific substrates (Fig. 1.4). These hydrolases cleave the various covalent bonds within the sacculus and cause the release of 40 – 50% of the total PG during the cell cycle (46). The fragments released are then recycled efficiently in a process referred to as peptidoglycan turnover (47).

The three-for-one model of PG synthesis explains this relatively high turnover as the removal of the docking strand. However, the mechanisms of peptidoglycan synthesis during both the elongation of the sacculus and cell division remain largely unknown. This model requires the existence of multienzyme complexes of both PG synthases and hydrolases and though this has not yet been isolated from cells, work in this field has identified several interactions between different synthases, hydrolases and various regulatory proteins, which will be discussed in detail in the following sections.

E. coli possesses 17 periplasmic PG hydrolases, single mutations in these confer no phenotype. Interestingly, three EPases together are essential for elongation; YebA, Spr and YdhO (48). Also, several of the amidases are required for daughter cell separation during cell division (1.4.2.3).

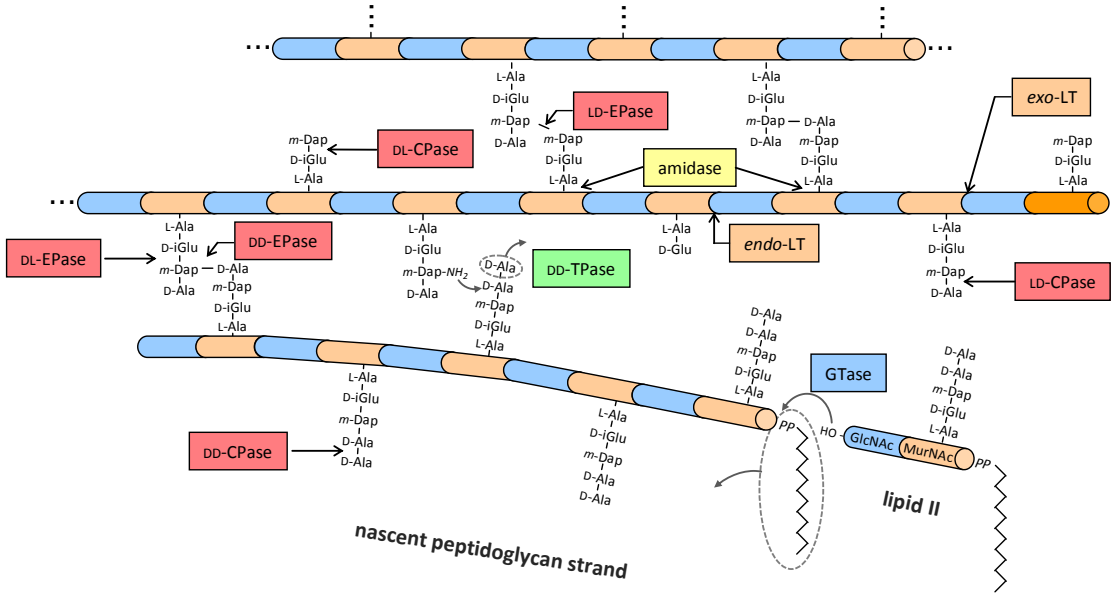

Figure 1.4 Peptidoglycan synthesis and hydrolysis (1)

A new glycan chain is synthesised from lipid II by glycosyltransferase (GTase) reactions and is attached to peptidoglycan through transpeptidase (TPase) reactions. Peptidoglycan is modified and hydrolysed by various hydrolases: DD-, LD- or DL-carboxypeptidases (CPases) remove a terminal amino acid from the peptide (DD-CPase cleave between D-Ala-D-Ala, LD- between *m*-Dap-D-Ala and DL- between D-iGlu-*m*-Dap), DD-, LD- or DL- endopeptidases (EPases) hydrolyse cross-links as shown, lytic transglycosylases (LTs) cleave within (endo-LTs) or at the terminal (exo-LTs) of glycan strands producing 1,6-anhydro-Mur*N*Ac, and amidases hydrolyse the amide bond between Mur*N*Ac and L-Ala.

1.3 Peptidoglycan synthases of *E. coli*

Peptidoglycan synthases fall into three categories; bifunctional GTase/TPase (class A penicillin binding proteins (PBPs)), monofunctional TPase (class B PBPs), and monofunctional GTase (39).

1.3.1 Bifunctional synthases - Class A PBPs

PBP1A, PBP1B and PBP1C are the 3 class A PBPs in *E. coli*. PBP1A and PBP1B have a major and semi-redundant role in peptidoglycan synthesis, either one can be deleted but a loss of both is lethal. (49). The role of PBP1C is unknown. Both enzymatic activities of PBP1A and PBP1B have been demonstrated *in vitro* with lipid II substrate. An excellent characterisation of PBP1A was carried out by Born *et al.* 2006 (50) in which it was found to polymerise lipid II to form a cross-linked peptidoglycan product with 18 – 26% of the peptides participating in cross-links and glycan chains of ~ 20 disaccharide units in length. Remarkably, PBP1A could also attach newly synthesised PG material to existing sacculi *in vitro*, supporting the previously discussed models for growth of the sacculus. The catalytic residues Glu94 and Ser473 are essential for GTase and TPase activities respectively (50).

PBP1B exists as two isoforms in the cell, PBP1Bα and PBP1Bγ which differ in the length of their short cytoplasmic region. PBP1Bγ is a truncated version of α with translation starting at Met46 (51). A third version was originally characterised, PBP1Bβ, but found to be an artificial cleavage of PBP1Bα by OM protease OmpT which occurred during disruption of the cell envelope for purification (52). PBP1B forms homodimers *in vitro* with a K_D of 0.13 μM, and evidence suggests that these dimers also exist *in vivo* (53, 54). The enzyme is most efficient in its dimeric form and like PBP1A is able to polymerise lipid II into a cross-linked peptidoglycan product *in vitro*, producing glycans with an average length of > 25 disaccharide units with ~ 50% of peptides participating in cross-links (53). The catalytic residues Glu233 and Ser510 are essential for GTase and TPase activity respectively (36, 40). A more detailed characterisation of PBP1B's GTase activity revealed that several other conserved residues are essential for catalysis and for *in vivo* function, these include Asp234, Phe237, His240, Thr267, Gln271 and Glu290 (36). Of these residues, Glu290 is proposed to be important in the proper removal of the undecaprenol pyrophosphate, the others are proposed to maintain the structure of the active site for the correct positioning of the catalytic Glu233, and may also interact with the substrate, which is consistent

with that of *S. aureus* class A PBP PBP2 (55). A high resolution crystal structure of PBP1B in complex with a GTase inhibitor moenomycin has been solved (56). It showed the GTase domain proximal to the transmembrane helix, with a hydrophobic region which is presumed to imbed into the periplasmic leaflet of the cytoplasmic membrane, a small non-catalytic domain exists between the GTase and TPase domains called UB2H for its homology to domain 2 of UvrB (figure 1.5). The structure also revealed the possible residues involved in the interaction with moenomycin, which inhibits GTase activity by mimicking the growing glycan within the domain, which is also referred to as lipid IV (two lipid II disaccharides)(57). Other than Glu233 and Glu290, Asn275, Arg286, Ser358 and Lys355 were identified as possibly forming hydrogen bonds with moenomycin. Using the structural data, a model for the progression of a growing glycan through the PBP1B molecule was proposed and is shown in figure 1.5B (56). This model has the glycan growing perpendicular to the membrane delivering a pentapeptide to the TP domain for use in cross-linking reactions which is consistent with the evidence that class A PBPs act processively, requiring ongoing GTase for TPase activity (50, 53).

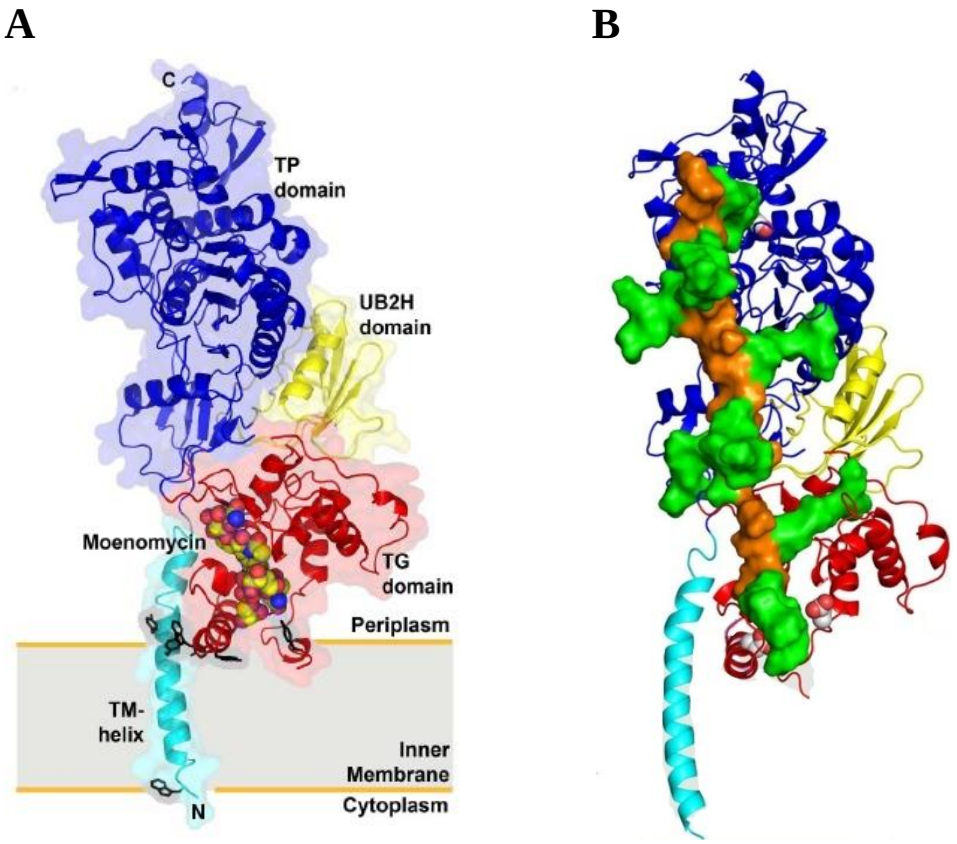

Figure 1.5 Crystal structure of *E. coli* PBP1B (56)

(A) Structure of PBP1B represented as a ribbon diagram with the TM, UB2H, GT and TP domains colour coded in cyan, yellow, red and blue respectively. Bound moenomycin is represented as van der Waals spheres and tryptophan located near the cytoplasm/periplasm-membrane interface shown as black sticks.
(B) Domain colour coding as A. Active sites (Glu233 and Ser510) shown as van der Waals spheres. A growing glycan is modelled in with lipid IV in place of moenomycin. The glycan is produced such that it progresses perpendicular to the membrane, bringing a peptide within range of the TPase domain to allow for cross-linking reactions to take place.

1.3.2 Monofunctional synthases

E. coli has three monofunctional synthases, a GTase MtgA and the Class B PBPs, PBP2 and PBP3, which are TPases. Class B PBPs have an N-terminal membrane anchor, followed by a non-catalytic domain and a TPase domain. The non-catalytic domain is thought to act as a 'pedestal' for the TP domain, to optimally position it for its PG cross-linking activity in the cell (58), it is also required for the correct folding of the protein as isolated TP domains are intrinsically unstable (59). There are three monofunctional synthases in *E. coli*, including two class B PBPs (PBP2 and PBP3) and the monofunctional GTase (MtgA).

The TPase activity of a class B PBP had not been demonstrated *in vitro* until recently. Banzhaf *et al.* 2012 showed that PBP2 was able to form cross-links in the presence of PBP1A and purified PG sacculi, contributing to the attachment of newly synthesised material to the sacculi. The gene encoding PBP2 (*mrdA*) is essential. Cells with a temperature sensitive version, or those treated with the PBP2 specific β-lactam antibiotic mecillinam no longer grow as rods, but into spheres before lysing, indicating that PBP2 is required for elongation (61). This is supported by its cellular localisation, which was shown to be to the lateral wall during elongation and to mid-cell early in division, though it leaves mid-cell before completion of septation (61).

PBP3 is encoded by the *ftsI* gene (filamentous temperature sensitive), so named as it is an essential gene for cell division. PBP3 localises to mid-cell during cell division and it's activity is essential for the process as treatment of cells with the PBP3 specific β-lactam aztreonam blocks septation (62). However, though PBP3 binds to a range of β-lactam antibiotics and is capable of transferring the donor moiety of an artificial thioester substrate to a D-amino acid acceptor *in vitro* the TPase activity has not yet been established with natural substrate (63).

MtgA is a membrane bound monofunctional GTase capable of catalysing the formation of non cross-linked glycan chains *in vitro* but is dispensable for cell viability (64, 65). It localises to mid-cell during division and interacts with PBP3 along with other proteins essential for cell division (66), though its cellular function remains unclear.

1.3.3 Interactions of peptidoglycan synthases

Several interactions between different peptidoglycan synthases and other proteins have been identified (1). As implied above, PBP1A is required for the *in vitro* activity of

PBP2 through direct protein-protein interaction, which was demonstrated both *in vitro* and *in vivo*. PBP2 also has an effect on the synthetic activity of PBP1A, significantly enhancing the rate of its GTase activity (60). PBP1B interacts with PBP3 both *in vitro* and *in vivo* with a K_D of 0.4 μM determined by SPR. The interaction was also seen by bacterial two-hybrid system which showed that the first 56 amino acids of PBP3 are sufficient, suggesting the interaction takes place between the membrane proximal portions of the proteins (67). This interaction has an important context in the cell. A significant proportion of the cellular PBP1B localises at mid-cell during division dependant on the presence but not activity of PBP3, as treatment with aztreonam has no effect. The over-expression of PBP1B also suppresses the thermosensitivity of a mutant strain possessing a temperature sensitive PBP3 (*pbpB2158*), presumably by stabilising the protein through direct interaction (68). PBP1B and PBP3 are thought to provide the major peptidoglycan synthesis during cell division, with PBP1A and PBP2 active predominantly in cell elongation. However PBP1A and PBP1B are able to perform the role of the other, given their redundancy in the cell. In the absence of PBP1B, PBP1A shows an enhanced localisation to mid-cell (60). The mechanisms behind this redundancy are unknown.

1.3.3.1 Lipoprotein activators of PBPs

In *E. coli* and presumably other Gram-negative bacteria peptidoglycan synthesis is also controlled from the outside the sacculus by outer membrane lipoproteins LpoA and LpoB which are essential for the activities of PBP1A and PBP1B, respectively (27, 28). The cell requires either PBP1A-LpoA or PBP1B-LpoB for growth, with the depletion of one of the *lpo* genes in the absence of the other or in the absence of its non-cognate class A PBP resulting in cell lysis.

The Lpo proteins show the same preference for sub-cellular localisation as their cognate PBP, with LpoA localising to the lateral wall and LpoB predominantly to mid-cell. The septal localisation of LpoB is dependent on the activity of PBP3, as it is diminished in cells treated with aztreonam presumably because it requires ongoing septal PG synthesis (27).

The Lpo proteins are thought to interact with small non-catalytic domains within their cognate class A PBPs, for LpoB this is the UB2H domain mentioned in 1.3.1 and for LpoA a similar region predicted in PBP1A called ODD (Outer membrane docking domain). It was shown that LpoB could no longer be cross-linked to PBP1B lacking its

UB2H domain in the cell (27). Both Lpos stimulate the PG synthetic activities of their cognate PBP *in vitro*, in both cases increasing the peptides in cross-links by 20% and increasing GTase rate by 1.5-fold (27, 28, 69). Though the activities of PBP1A and PBP1B have been shown independently of their cognate Lpo *in vitro*, it is believed that this effect is essential *in vivo* (27, 28).

The crystal structure of PBP1B shows that the UB2H domain, which is required for interaction with LpoB, is no further than ~60 Å away from the inner membrane. The fact that the distance from the IM to the PG sacculus is ~ 90 Å and thus the UB2H domain is inside the PG sacculus from the point of view of LpoB means that it must reach through the pores in the sacculus in order to activate its cognate synthase, which is presumably also true of LpoA (4, 27). Thus, the activation would be most efficient if the peptidoglycan were stretched making the pores wider and the converse true when the sacculus was relaxed. This simple homeostatic mechanism would allow the cell to passively adjust the rate of peptidoglycan synthesis to the overall growth rate of the cell, if intracellular growth exceeded PG synthesis the pores would become stretched allowing for the activation of the major synthases. This hypothesis is supported by the results of a recent study using high resolution imaging (AFM) and fluorescence microscopy, showing the existence of pores in isolated sacculi (70).

1.4 Multiprotein complexes for peptidoglycan synthesis in growth and division of *E. coli*

As mentioned above, the current theories for peptidoglycan synthesis suggest the existence of multienzyme complexes specialised for cell elongation and division. The evidence for these two distinct complexes will be discussed in this section.

1.4.1 The elongosome

The actin-like MreB is required for peptidoglycan synthesis at the lateral wall during cell growth which presumably is by controlling peptidoglycan synthesis and hydrolysis through various protein-protein interactions to form the elongosome which is proposed to include MreB, MreC, MreD, RodZ, RodA and PBP2. All of which are required for cell elongation as a loss of any one results in spherical cells (4). The complex was shown to associate with the final two enzymes in the lipid II synthesis pathway MraY and MurG, supporting its function as a PG synthesis complex (71). MreB is a soluble

cytoplasmic protein which forms actin like filaments dependant on ATP and associates with the inner face of the cytoplasmic membrane via an amphiphatic helix (72, 73). The formation of properly functioning filaments requires the presence of RodZ presumably through the stabilisation of the MreB 1A domain by direct protein-protein interaction (74–77). MreB is known to interact with the integral membrane protein MreC, which forms homodimers and also interacts with another integral membrane protein MreD in the cell forming the MreBCD complex (78, 79). RodA is a member of the SEDS family of integral membrane proteins (shape, elongation, division and sporulation) and is essential for elongation in *E. coli* (80). It is thought to be the lipid II flippase of the elongosome, responsible for the delivery of the PG substrate to the synthases. Consistent with this, RodA is associated with PBP2, and therefore PBP1A which are proposed to form the peptidoglycan synthesis core of the elongosome (60, 81). Unpublished work from Manuel Banzhaf (Newcastle University) shows that PBP2 interacts with MreC. Presumably PBP2 interacts with MreC in complex with MreB and MreD. The interaction between PBP2 and MreC was also observed in *H. pylori* (82) and a co-localisation of PBP2 and MreBCD was seen in *C. crescentus* (83). These data support the proposal that PBP2 is an integral member of the elongosome.

1.4.2 The divisome

The cell division complex assembles at mid-cell for the synthesis and cleavage of septal peptidoglycan to produce the new cell poles of the daughter cells. There are more than 12 proteins essential for cell division, a loss of any leading to the formation of long filamentous cells with no division septa, the proteins involved are summarised in Table 1.1. The assembly of the divisome is initiated by the tubulin-like FtsZ which polymerises into filaments via head to tail association dependant on GTP (84–86). These filaments, along with essential accessory proteins (discussed below) associate proximal to the inner face of the cytoplasmic membrane into a ring-like structure at the site of prospective cell division, referred to as the Z-ring which is thought to contribute to the constrictive force during cytokinesis (87, 88). FtsZ rings have also been seen *in vitro* by atomic force microscopy (89). In the cell, the ring is dynamic, with a constant exchange of FtsZ subunits with free cytoplasmic FtsZ molecules with a time-scale of 9 seconds (90). It is stabilised at mid cell by several positive regulators which will be discussed in detail below, in addition to this there are two mechanisms which negatively

Table 1.1 Divisome proteins of *E. coli*

Function / Category	Protein (gene)[1]	Role / Remarks[2]
Cytoskeletal element	• FtsZ (***ftsZ***)	• Tubulin-like, polymerises with GTP to form the Z-ring at mid-cell
Membrane attachment of FtsZ and regulation of z-ring dynamics	• FtsA (***ftsA***), ZipA (***zipA***), ZapA (*zapA*), ZapB (*zapB*), ZapC (*zapC*), ZapD (*yacF / zapD*)	• Membrane attachment of FtsZ polymers (FtsA, ZipA) • Stabilisation of z-ring and regulation of dynamics (ZapA, ZapB, ZapC, ZapD)
Divisome maturation, stability and PG binding	• FtsK (***ftsK***), FtsQ (***ftsQ***), FtsL (***ftsL***), FtsB (***ftsB***)	• Recruitment of downstream divisome proteins (FtsK, FtsQLB) and DNA transport (FtsK)
	• FtsW (***ftsW***)	• Lipid II flippase (FtsW)
	• FtsN (***ftsN***), DamX (*damX*), DedD (*dedD*), RlpA (*rlpA*)	• PG binding (FtsN, DamX, DedD, RlpA), divisome stability (FtsN) and regulation of PG synthesis (FtsN)
PG synthesis (and its regulation)	• PBP1B (*mrcB*), PBP3 (***ftsI***), MtgA (*mtgA*)	• Synthesis of PG from precursor (PBP1B, PBP3, MtgA)
	• LpoB (*lpoB*)	• Activation of PBP1B (LpoB)
PG hydrolysis (and its regulation)	• MltA (*mltA*), Slt70 (*sltY*)	• Hydrolysis of existing sacculus (MltA, Slt70)
	• AmiA (*amiA*), AmiB (*amiB*), AmiC (*amiC*)	• Septal PG cleavage for daughter cell separation (AmiA, AmiB, AmiC)
	• FtsE (***ftsE***)[3], FtsX (***ftsX***)[3], EnvC (*envC*), NlpD (*nlpD*)	• Control of septal PG cleavage (FtsEX, EnvC, NlpD)
OM Invagination	• Pal (*pal*), TolA (*tolA*), TolB (*tolB*), TolQ (*tolQ*), TolR (*tolR*)	• OM invagination and stability during division (TolA, TolB, TolQ, TolR, Pal) • PG binding (Pal)

[1] Genes essential for division are shown in bold.
[2] For detailed discussion and references, see text.
[3] Only essential in low osmolarity growth medium.

regulate Z-ring formation and therefore cell division at any other site but mid-cell. The Min proteins (MinC, MinD and MinE) prevent Z-ring assembly near the cell poles and a loss of these causes mis-placed divisions leading to the formation of DNA-free mini-cells. MinC and MinD form the inhibitor complex which oscillates from pole to pole driven by the membrane bound MinE in an ATP dependant manner, which results in the average concentration of MinC-MinD being lowest at mid cell once the cell is long enough to divide (91–93). The second mechanism is the so called occlusion of Z-ring formation from the nucleoid by SlmA, the functional analogue of which is Noc in *B. subtilis*. These proteins prevent cell division near the chromosomal DNA to avoid bisecting the nucleoid, which would be lethal (94, 95). SlmA dimers bind to specific sites on the chromosome and form high-order nucleoprotein complexes which interact with FtsZ, causing a disruption of its polymerisation (96–98). *B. subtilis* Noc, though achieving the same occlusion effect, acts via a different mechanism and unlike SlmA has not been shown to interact directly with FtsZ, its inhibitory effect may be on downstream members of the divisome/positive regulators of FtsZ (99, 100). Together the nucleoid occlusion mechanism and the Min system ensure a precise placement of division sites in *E. coli* with daughter cells deviating in length by only a few percent (101, 102). The precision of selection is robust, able to successfully place a division site in *E. coli* cells forcibly grown into irregular shapes in nanofabricated channels (103).

Once the Z-ring has coalesced, the remaining divisome proteins of *E. coli* assemble at mid-cell in a hierarchical manner in two steps (Fig. 1.6) with FtsA, ZipA, ZapA, ZapB, ZapC, ZapD, FtsE and FtsX assembling early at the future division site long before constriction is apparent, at ~ 40% of the cell cycle, with constriction visible after ~ 60% (1, 104). Their localisation is simultaneous with FtsZ and also coincides with the phase of pre-septal elongation discussed previously, in fact it has been suggested that these early cell division proteins control the PG synthetic components of the elongosome for this phase of growth (4, 105). Prior to constriction the divisome matures, also in a hierarchical manner (Fig. 1.6), with the localisation of the late division proteins FtsK, FtsQ, FtsL, FtsB, FtsW, PBP3(-PBP1B) and FtsN simultaneous with the departure of PBP2, and presumably other elongosome components, from mid-cell (61, 104). The precise mechanism of how the recruitment of division proteins is controlled is unknown but is dependent on multiple protein-protein interactions between the constituents.

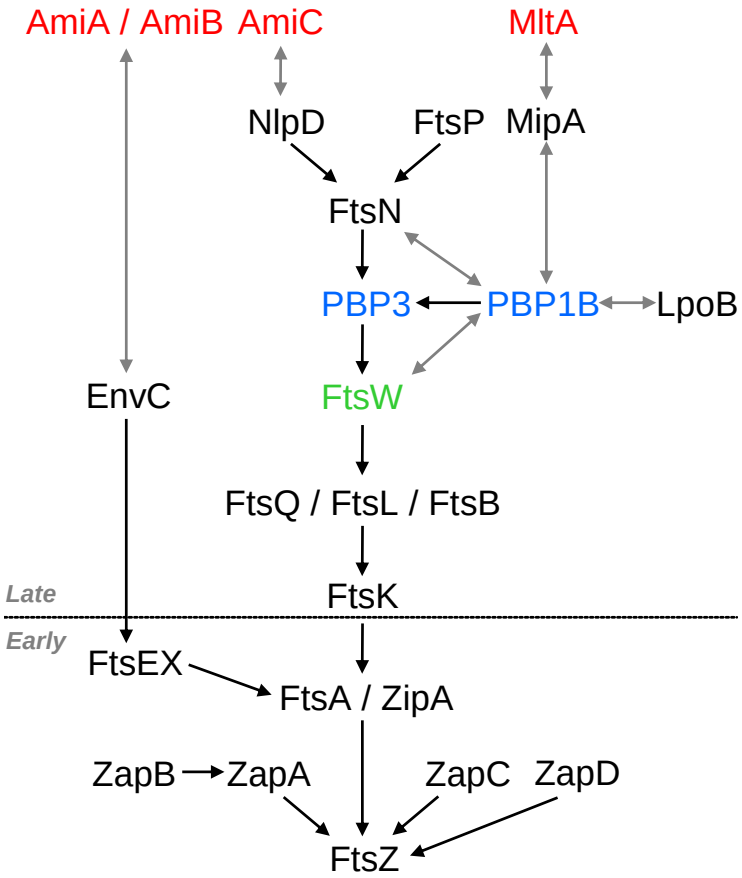

Figure 1.6 Hierarchical recruitment of proteins for the maturation of the divisome (1)

Starting in the cytoplasm, the divisome in built up in a hierarchical manner with the early proteins localising before septation begins (FtsZ and associated proteins). Black arrows denote dependency on mid cell localisation which is through direct protein-protein interaction in most cases. Grey arrows show further important interactions within the divisome, particularly peptidoglycan enzymes (synthases shown in blue, hydrolases in red) within the late proteins of the divisome, which also includes the lipid II flippase FtsW (green). PBP1B-LpoB are not essential for cell division, as they are redundant with PBP1A-LpoA. The hydrolases shown are also not essential for division, however the amidases are essential for daughter cell separation.

1.4.2.1 The early divisome proteins

As mentioned in 1.4.2 the Z-ring is stabilised at mid-cell by positive regulators. ZipA and FtsA are essential for cell division, both interacting with the C-terminal domain region of FtsZ (106). Their interaction stabilises the Z-ring and anchors it to the inner membrane (107, 108). FtsA is an actin-like protein that has a non-canonical sub-domain architecture in the form of the 1c domain, it polymerises bidirectionally into protofilaments associated with the membrane by an amphipathic helix (24, 109, 110). ZipA consists of three domains; a membrane spanning domain within the inner membrane, a C-terminal domain which binds to FtsZ and causes bundling of FtsZ

filaments *in vitro*, and a long central linker region (111). Several other cytoplasmic Z-ring associated proteins, ZapA, ZapB, ZapC and ZapD, promote Z-ring formation but are dispensable for cell division. ZapA, ZapC and ZapD interact with FtsZ promoting association of Z-ring filaments thus stabilising the ring further to the effects of FtsA and ZipA (112–116). There are certain conditions at which some Zap proteins are required, such as the necessity of ZapA for division in cells with reduced numbers of FtsZ. ZapB interacts with ZapA and also forms filaments *in vitro*. These were observed to localise inside the Z-ring, which presumably stabilises the structure via ZapA (117–119). ZapA and ZapB are also involved in proper chromosome segregation during division, through interaction with a protein which structures the chromosomal terminus region into a macrodomain, MatP, which is then relocated and orientated with the division site (120).

FtsE and FtsX form a complex within the inner membrane referred to as FtsEX. FtsEX is an ATP binding cassette (ABC) transporter homologue that binds to FtsZ via the ATP binding protein FtsE, with a mid-cell localisation dependant on FtsA and ZipA (121–123). FtsE is essential for division in low-osmolarity growth medium (124) and the role of FtsEX was recently shown to be in the recruitment and regulation of peptidoglycan hydrolases (discussed in section 1.4.2.3).

1.4.2.2 Maturation of the divisome

To begin septation the divisome must be matured through the addition of the essential 'late' division proteins FtsK, FtsQ, FtsL, FtsB, FtsW, PBP3 and FtsN along with non-essential constituents. These assemble to the putative, early, divisome simultaneously in an interdependent and hierarchical manner (Fig. 1.6) (125).

FtsK is a multidomain protein involved in chromosome segregation during cell division as well as a role as a core divisome protein interacting with FtsZ, FtsQ, FtsL and PBP3 in bacterial two-hybrid assays (126, 127). The C-terminal domain forms a hexameric ring which directionally transports DNA during decatenation of sister chromosomes in the fraction of cells in which chromosome catenation occurs (128–131). The inner membrane spanning and periplasmic part of FtsK is essential for cell division, forming a core part of the divisome believed to stabilise the recruitment and presence of downstream proteins (130, 132). Mutations in *ftsA* and *ftsQ* are able to bypass the necessity for FtsK, presumably by stabilising the divisome in its absence (133).

FtsK is required for the recruitment of a pre-formed complex of FtsQ, FtsL and FtsB (125, 134). Each is an integral membrane protein with a short cytoplasmic loop

and a periplasmic domain, with the C-terminal part of FtsQ essential for FtsL, FtsB and FtsW recruitment (135, 136) and the C-terminal of FtsL required for its own recruitment through interaction with FtsQ but not FtsB, though the C-terminal of FtsB is also required for its interaction with FtsQ (137). FtsQLB complexes with stoichiometries of 1:1:1 and 2:2:2 have been modelled, the latter being consistent with the crystal structure of FtsQ showing it as a homodimer, but which is adopted in the cell remains unknown though small angle X-ray scattering analysis of a homologous complex from *S. pneumoniae* is consistent with a 1:1:1 complex (138, 139). In addition to FtsB, FtsL and FtsK FtsQ has been shown to interact with FtsW and PBP3 by bacterial two-hybrid (126, 127) and FtsQLB is required for the recruitment of FtsW, though this necessity can be by-passed by expressing either ZapA-FtsL or ZapA-FtsB fusion proteins (140).

FtsW, like RodA, is a member of the SEDS (shape, elongation, division and sporulation) family proteins (141). FtsW is an integral membrane protein with 10 transmembrane regions and is responsible for flipping lipid II from the inner face of the cytoplasmic membrane to the periplasmic face where it is the substrate of the PG synthases (32). Consistent with this function FtsW interacts with PBP3, PBP1B and MtgA and is required for the recruitment of PBP3, and therefore PBP1B, to the divisome (66, 142–144). As well as FtsW, PBP3 interacts with FtsL, FtsQ, PBP1B and FtsN (67, 127, 145). PBP3, like FtsW, can be recruited to the divisome independently of the FtsQLB complex using a FtsW-ZapA fusion. This targeting of FtsW-PBP3 also stabilises recruitment of FtsQLB in cells depleted of FtsA suggesting that sub-complexes within the divisome form prior to their recruitment such as discrete FtsQLB and FtsW-PBP3-(presumably)-PBP1B complexes (140).

FtsN is the final essential division protein in the hierarchy and interacts with both early and late divisome components including FtsA, ZapA, FtsQ, PBP3, FtsW and PBP1B as shown by various techniques (126, 127, 142, 143, 145, 146). It is a bitopic membrane protein with a short cytoplasmic region, a single transmembrane domain and a flexible periplasmic region which features three α-helices followed by a proline/glutamate rich unstructured region and a globular C-terminal SPOR domain which binds to peptidoglycan (147). The SPOR domain binds to peptidoglycan *in vitro* but is not essential for cell division (148). This is presumably due to a redundancy with other SPOR domain containing proteins which also localise to division sites, DamX, DedD and RlpA, as mutants lacking multiple SPOR domain proteins show division defects (149, 150). The precise role of FtsN in cell division is not known. The transmembrane domain along with the three α-helices of the periplasmic region is the

only portion of the protein essential for cell division for yet unknown reasons (148, 151, 152). The interaction of FtsN with PBP1B was shown to have a functional context, with FtsN increasing the activity of PBP1B at conditions where its dimerisation is not favoured, presumably by stabilising PBP1B dimers. Given this functional context, FtsN may play a role in activation of PBP1B in the cell, further supported by its interaction with FtsW and PBP3 (145). Another role of may be to provide the signal for completed divisome assembly to the cytoplasmic elements, supported by the interaction of FtsN with ZapA and the 1c domain of FtsA (146) and the existence of FtsA mutants which are able to divide without FtsN (153). In addition to this, FtsN appears to stabilise the completed core divisome. Depletion of FtsN leads to the disassembly of already assembled divisome components from PBP3 down the hierarchy to the cytoplasmic proteins (154). Also, overexpression of FtsN rescues the phenotypes of FtsK, FtsQ and FtsA mutants, which are implicated in core divisome stability themselves (152). FtsP (SufI) is a recently characterised protein involved in cell division, though its precise role is unknown. It localises late to the division site depending on the presence of core divisome proteins FtsZ, FtsQ, FtsL and FtsN (155), though a direct interaction between FtsP and any division proteins have not yet been shown. FtsP is dispensable under normal growth conditions, but it is required for division under various stress conditions, such as oxidative stress and DNA damage (156) and also in the absence of *ftsEX* at high osmolarity (124). The crystal structure of FtsP showed it to be structurally similar to the multicopper oxidase protein family, but it does not bind copper (155). Fig. 1.7 shows a summary of the known interactions between the essential division proteins, along with the major PG synthase PBP1B.

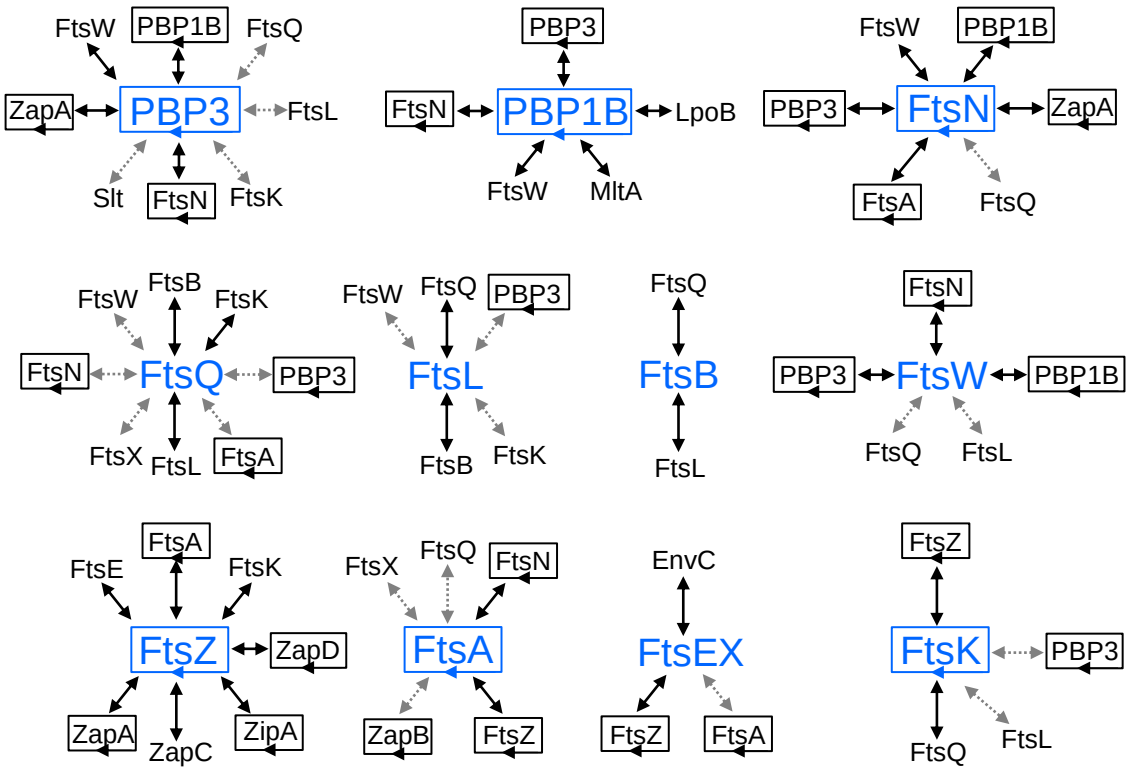

Figure 1.7 Interactions of the essential(*) divisome proteins and PBP1B (1)

The known protein-protein interactions of the essential cell division proteins are shown above, along with those of the major synthase active during division PBP1B thought this is not essential(*). Solid black lines represent direct interactions clearly demonstrated *in vitro* and *in vivo*. Dashed grey lines represent interactions shown with only bacterial two-hybrid assays. Rectangular arrows enclosing proteins represents homodimerisation or multimerisation.

1.4.2.3 Daughter cell separation

As mentioned above, the process of daughter cell separation in *E. coli* and presumably other Gram-negative species requires the co-ordinated constriction of multiple layers of all cell envelope simultaneously with the synthesis and splitting of the new cell poles. Mainly, the amidases are required for the splitting of the septum through hydrolysis of the amide bond between Mur*N*Ac and L-Ala, thus releasing the peptide from the glycan chain and in the cases where these form a cross-link, reversing the linkage (157). *E. coli* has four amidases; the soluble periplasmic AmiA, AmiB and AmiC along with the OM bound lipoprotein AmiD (157–159). AmiB and AmiC both localise to the division site, and AmiA is more diffuse throughout the periplasm (160, 161). AmiA is a zinc metalloenzyme with specificity for polymeric peptidoglycan, requiring at least a tetrasaccharide sized fragment (162). AmiA, AmiB and AmiC play a major role in separation of daughter cells, mutants lacking two or more form chains of non-separated

cells with an increased OM permeability, these phenotypes are exacerbated by the loss of DD-endopeptidases and/or lytic transglycosylases (163, 164). During the process of daughter cell separation approximately 1/3 of the newly synthesised peptidoglycan is removed by the septum splitting hydrolases (165, 166). Consistent with the finding that AmiC removes fluorescent peptides incorporated into the sacculus during its growth in cell division (167).

Recent work provided significant insight into the regulation of the amidases during cell division. Specific activator proteins, EnvC and NlpD, were discovered to be recruited to the division site depending on FtsEX and FtsN, respectively (161, 168). The periplasmic EnvC activates AmiA and AmiB and the outer membrane lipoprotein NlpD activates AmiC. Expression of a miss-localisation mutant of EnvC causes cell lysis, presumably due to inappropriate activation of AmiA and AmiB at sites away from mid-cell (161). In addition to NlpD, FtsN is required for mid-cell localisation of AmiB and AmiC in addition to NlpD. Active PBP3 is required for the recruitment of AmiA, AmiB and AmiC as this is impaired in cells treated with cephalexin (169). Importantly, the activators EnvC and NlpD still localise under these conditions, suggesting the recruitment of the amidases requires ongoing septal PG synthesis and that mechanisms exist to ensure their activators are present prior to their arrival (169). The mechanism of activation employed by EnvC was recently shown to be dependent on conformational changes in the ABC transporter homologue FtsEX, likely in turn dependant on ATP hydrolysis (170). The current model is that EnvC interacts with the periplasmic region of FtsX, hydrolysis of ATP by FtsE drives conformational changes which are transduced through FtsX and EnvC to AmiB causing the removal of an α-helix sequestered in the active site of the enzyme, a mechanism which appears to be conserved between the septum cleaving amidases (171).

1.4.2.4 Outermembrane constriction

The outer membrane of Gram-negative bacteria protects the cell from many cell-wall targeting antibiotics and antibacterial enzymes by preventing access to the periplasm (172). In *E. coli* the outer membrane is firmly attached to the peptidoglycan cell wall by the highly abundant outer membrane lipoprotein Lpp, a proportion of which is covalently linked to the peptidoglycan (5, 173). Other abundant outer membrane proteins such as OmpA and Pal interact non-covalently with peptidoglycan. The deletion of *pal* or *lpp* causes reduced OM integrity, with leakage of periplasmic contents,

increased sensitivity to chemicals (and other environmental insults such as osmotic shock and mechanical stress) and blebbing off of vesicles (174, 175). Overexpression of Pal rescues *lpp* null mutants, however the converse is not true, indicating that Pal has a more specific role than a tethering of the OM to the peptidoglycan (175). Pal is part of the Tol-Pal operon along with *ybgC, tolQ, tolR, tolA, tolB* and *ybgF* the products of which (excluding *ybgC* and *ybgF* whose functions are currently unknown) form the Tol-Pal complex, which is well conserved in Gram-negative species (176). The Tol-Pal complex has been implicated in aiding outer membrane constriction during cell division. Cells deficient in a functional complex form short chains at low osmotic growth conditions along with a reduced outer membrane integrity, thus the Tol-Pal complex plays a role in daughter cell separation (177).

The Tol-Pal complex consists of the integral inner membrane proteins TolQ, TolR and TolA, the periplasmic protein TolB and the outer membrane lipoprotein Pal (176). Each of these proteins localises to mid-cell during division dependant on FtsN, with TolQ and TolA localising independently of the other Tol-Pal components (177). TolA was later shown to localise to mid-cell independently of FtsN in *ftsA* mutant cells which no longer require FtsN for division, suggesting that its localisation requires other components of the divisome rather than FtsN directly (153). Protein-protein interactions within the Tol-Pal complex can potentially form a transenvelope complex physically connecting the inner and outer membranes (177).

TolQ consists of two cytoplasmic regions and three transmembrane regions, TolR and TolA are both anchored within the cytoplasmic membrane by a single transmembrane region at their N-terminals with the majority of the protein located in the periplasm (178). The periplasmic part of TolR features a C-terminal amphipathic helix which is thought to associate with the periplasmic leaflet of the cytoplasmic membrane (179). The structure of TolR from *H. influenzae* suggests this helix may self associate forming homodimers with a large hydrophobic groove thought to play an important role in its function (180, 181). TolA is divided into three domains; the N-terminus including the transmembrane domain is domain I, domain II is a mainly α-helical, elongated region and domain III forms a globular head (182, 183). TolB features two distinct domains, a C-terminal six-bladed β-propeller domain along with a globular N-terminal domain. The extreme N-terminus of TolB features a flexible 12 amino-acid peptide which is sequestered into a cleft between the N and C-terminal domains upon binding of TolB to Pal (184, 185).

TolQ, TolR and TolA interact to form a cytoplasmic membrane complex (186, 187). Domain II of TolA interacts with YbgF, a non-essential protein of unknown function encoded by the last gene in the *tol-pal* operon (188). YbgF consists of a C-terminal TPR domain, which interacts with TolA, and a N-terminal α-helical coiled-coil domain which associates into a trimer, though the interaction of TolA and YbgF has a stoichiometry of 1:1 (188). TolA also interacts with the N-terminal 12 amino-acid region of TolB which is referred to as the TolA box for this reason. Thus, when TolB is bound to Pal it cannot interact with TolA (185) and evidence suggests there may be several different interaction states of the Tol-Pal proteins within the cell envelope though there are conflicting models which are summarised (Fig. 1.8) (177, 189). TolA was cross-linked *in vivo* to Pal via domain III, and subsequent studies using the same technique mapped separate interaction sites of Pal with TolA and TolB (190, 191). However, studies with purified proteins could not confirm the interaction between TolA and Pal or the existence of a ternary TolA-TolB-Pal complex (185).

TolA may undergo conformational changes driven by TolQ and TolR dependent on the proton motive force (pmf), which presumably provides energy for the invagination of the outermembrane during division, however the details of this are not understood (181). Gerding *et al.* proposed that pmf dependant conformational changes in TolA produce cycling between Pal bound and unbound states facilitating transient connections between the outer membrane and PG and the inner and outer membranes respectively (177). In addition, TolB may cycle between Pal-bound and Pal-unbound states, the later allowing interaction with TolA domain III (Fig 1.8).

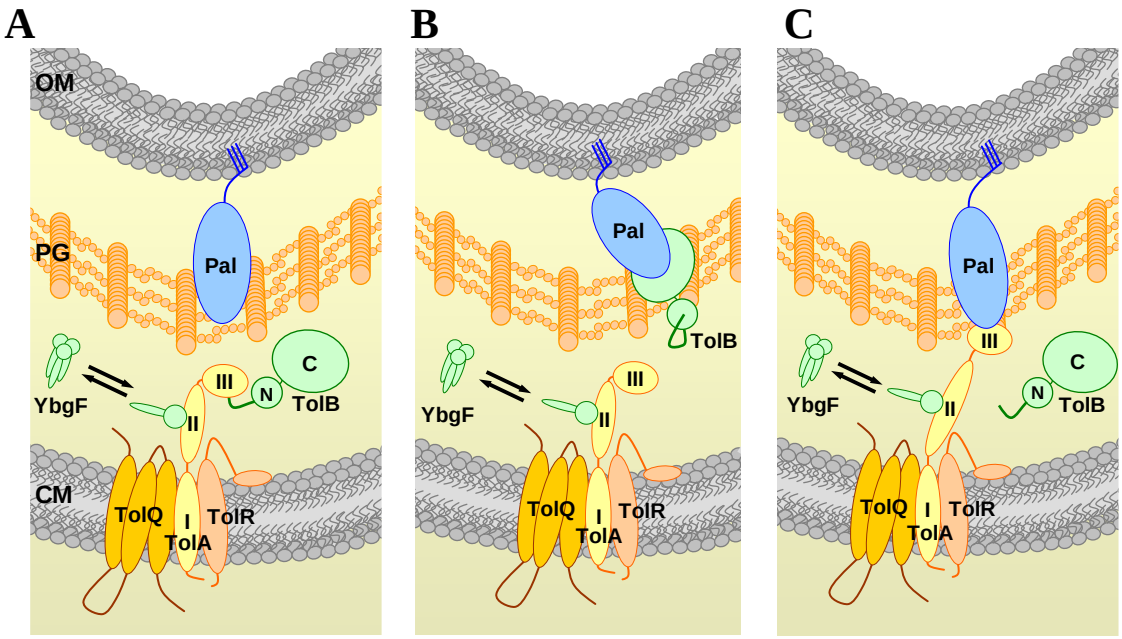

Figure 1.8 Proposed interaction states of the Tol-Pal complex (1)

Different proposed interaction states of the Tol-Pal complex between the cytoplasmic membrane (CM), peptidoglycan cell wall (PG) and outer membrane (OM) are shown in panels A, B and C. Proteins are represented with their structural features as linked ovals or spheres. Panel A shows Pal bound to peptidoglycan, which occludes its TolB binding site, and TolB bound to domain III of TolA via its N-terminal TolA box (depicted as a green line). TolA forms an integral membrane complex with TolQ and TolR and also interacts with YbgF via domain II. Panel B shows Pal binding to the C-terminal domain of TolB, causing the sequestration of the TolA Box, after their respective dissociation from PG and TolA. Panel C shows Pal bound to domain III of TolA, whether or not TolB interacts with Pal or TolA in this state is unclear, and the interaction between TolA and Pal is disputed. Whether Pal is able to bind to peptidoglycan when bound to TolA is also unknown. *In vitro* data support the states depicted in Panels A and B, while *in vivo* cross-linking data suggests all three are possible. Thus, either a transient transenvelope complex exists linking the CM, PG and OM (all three panels), or a cycling between panels A and B maintains sufficient contact between the layers for proper invagination. The role of YbgF in this is not yet known. Alone, it forms a homotrimer but interacts with TolA domain II with a stoichiometry of 1:1.

The PBP1B-LpoB complex spans from the cytoplasmic membrane to the outer membrane and thus could contribute to the constriction of the outer membrane during division, presumably through a passive connection of the envelope layers. This hypothesis is supported by the observation that cells lacking both a functional Tol-Pal system (*pal*$^-$) and LpoB show a severe lysis phenotype, while the single mutants do not (27). Further to this, in a *pal*$^-$ background, miss-localisation of LpoB to the inner membrane through changing its protein sorting signal is as detrimental as an LpoB deletion, suggesting that its localisation to the OM is required to support constriction in the absence of a functional Tol-Pal system. For unknown reasons PBP1A-LpoA, though they too have the capacity for physically linking the cytoplasmic and outer membranes, do not share this function (27) In *C. crescentus*, which lacks PBP1B-LpoB, the Tol-Pal proteins are essential, (192).

1.5 Aims

The discovery that peptidoglycan synthesis is regulated from both inside the cell and outside the sacculus has intriguing implications for the mechanism of envelope constriction during cell division. Therefore, in this work the following questions will be investigated.

1. What are the biochemical properties of LpoB, and what is its high resolution structure?
2. How does LpoB interact with PBP1B, and how does this lead to activation of the synthase? Do other PBP1B interaction partners play a role in the regulation of peptidoglycan synthesis during cell division?
3. How is peptidoglycan synthesis coordinated with constriction of the outer membrane during cell division?

2. Materials and Methods

2.1 Microbial methods

2.1.1 Bacterial storage and growth

E. coli strains were cultivated in Luria Bertani (LB) liquid media (10 g/L NaCl, 5 g/L Yeast extract, 10 g/L tryptone, pH 7.2 – 7.5) or on LB agar plates (10 g/L NaCl, 5 g/L Yeast extract, 10 g/L tryptone, 1.5% agar, pH 7.2 – 7.5) at 30 or 37°C depending on strain/experiment. Alternatively M9 liquid media was used (5.29 g/L Na_2HPO_4, 3 g/L KH_2PO_4, 0.5 g/L NaCl, 1 g/L NH_4Cl, 2 mM thiamine, 1 mM $MgSO_4$, 0.1 mM $CaCl_2$, 0.3% Glucose, pH 6.8 – 7.2). Growth of liquid culture was aided by orbital shaking and was monitored by measuring the optical density at a wavelength of 578 nm (OD_{578}). For short-term storage strains were plated on LB agar containing the appropriate antibiotic, grown at 37°C overnight and stored at 4°C. For long term storage, liquid cultures in LB media in the exponential growth phase (OD_{578} of 0.4-0.6) were mixed with sterile glycerol to a final concentration of 10% and stored at -80°C.

2.1.2 Preparation of competent *E. coli*

Cells were grown in 100 ml LB to an OD_{578} 0.4-0.6. Cell were harvested via centrifugation (4000 × *g*, 10 min, 4°C) and resuspended in 30 ml ice-cold TFB1 buffer (100 mM RbCl, 50 mM $MnCl_2$, 10 mM $CaCl_2$, 30 mM KCH_3COO, 15% glycerol, pH 5.8 adjusted with acetic acid) and incubated at 4°C for 90 min. Cells were centrifuged (4000 × *g*, 10 min, 4°C) and resuspended in 4 ml ice-cold TFB2 buffer (10 mM MOPS, 10 mM RbCl, 75 mM $CaCl_2$, 15% glycerol, pH 6.8 adjusted with KOH). Aliquots of 100 µl were either immediately used for transformation (2.1.3) or stored at -80°C.

2.1.3 Transformation of competent cells

An aliquot of competent cells (100 µl) was thawed on ice, to which 1 – 10 µl plasmid DNA or ligation mix was added. The cells were incubated for 10 min on ice and subsequently heat shocked by incubating at 42°C for 1 min before being placed back on ice for 10 min. LB medium (900 µl) was added to the cells prior to incubating for 1 h at 37°C with gentle shaking, after which the cells were plated on LB agar plates containing the selection appropriate antibiotic.

2.1.4 Isolation of plasmid DNA from *E. coli*

Plasmid DNA was purified from *E. coli* cells using either PeqlabGOLD Plasmid mini-prep kit or Sigma-Aldrich GenElute HP plasmid midi-prep kit as per the manufacturer's instructions.

2.2 Protein Methods

2.2.1 Sodium Dodecyl Sulphate-polyacrylamide gel electrophoresis (SDS-PAGE)

Proteins were separated according to their molecular weights using discontinuous SDS-PAGE. Samples are mixed in a 2:1 ratio with loading buffer (4 ml 1 M Tris/HCl, 5.1 ml 75% glycerol, 0.6 g SDS, 0.4 ml 0.1% bromphenol blue and 10% β-mercaptoethanol), boiled for 10 min and centrifuged at 10000 rpm for 20 seconds prior to being loaded onto a polymerised acrylamide gel at 10%, 12% or 15% acrylamide (w/v). The gels were mounted in a BioRad gel tank system and a voltage of 90 – 150 V was applied for 1-2 h. Gels were routinely stained with coomassie staining solution (1 g/L coomassie brilliant blue R250, 50% methanol, 40% water and 10% acetic acid) for 15 min and destained in destaining solution (30% methanol, 60% ddH_2O and 10% acetic acid) until background was cleared. Alternatively gels were stained with a zinc staining kit (BioRad) or a silver staining kit (Sigma) as per the manufacturer's instructions. The recipe for stacking and resolving gels are shown in table 2.1.

Table 2.1 SDS-PAGE gel recipe for 2 gels

Component	Stacking Gel	Resolving gel (10%)	Resolving gel (12%)	Resolving gel (15%)
ddH_2O	2.45 ml	3.1 ml	2.4 ml	1.4 ml
Buffer (I & II)[1]	1.25 ml(II)	2.5 ml(I)	2.5 ml(I)	2.5 ml(I)
Acrylamide solution[2]	0.75 ml	3.3 ml	4 ml	5 ml
10% SDS	50 µl	100 µl	100 µl	100 µl
2% TEMED	250 µl	500 µl	500 µl	500 µl
1.4% APS	250 µl	500 µl	500 µl	500 µl

[1]Buffer I, 1.5 M Tris/HCl, pH 8.8; Buffer II, 0.5 M Tris/HCl, pH 6.8.
[2]Acrylamide solution is Rotiphorese (Roth, Germany).

2.2.2 Determination of protein concentration in solution

Performed using a BCA protein assay kit (Thermo scientific) as per the manufacturer's instructions. If necessary, samples were diluted to keep the absorbance in the range of the standard curve (Fig. 2.1). Alternatively, protein concentration was determined using a Nano-Drop spectrophotometer with ND1000 V3.7.1 software.

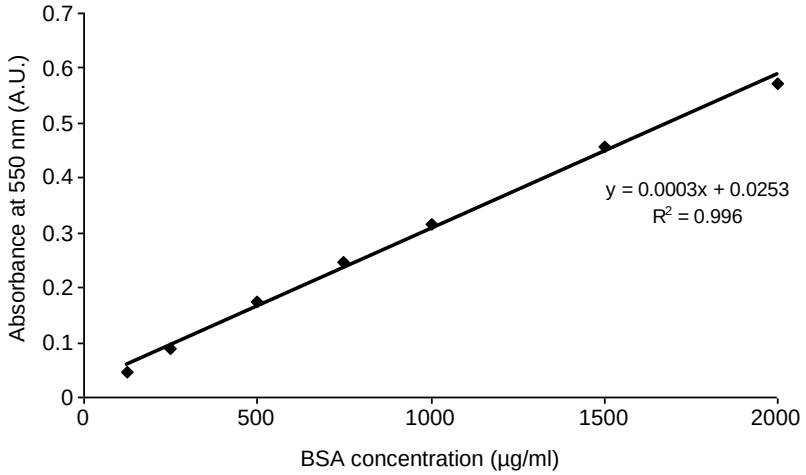

Figure 2.1 Example BSA standard curve

Absorbance measured at 550 nm plotted against concentration of standard (BSA).

2.2.3 Scanning of SDS-PAGE gels

Gels or blots were placed between 2 clear plastic sheets and scanned using an Epson Perfection V350 scanner and professional software package, images were subsequently cropped and aligned using Paint.net version 2.61.

2.2.4 Western blot, immunodetection and ECL visualisation

Proteins were separated by SDS-PAGE (2.2.1) and transferred onto a nitrocellulose membrane using a Bio-Rad wet-blot system. Transfer occurred as per the manufacturer's instructions in a 20 mM Tris, 192 mM glycine, 0.1% SDS, 10% methanol buffer at 300 mA for 1 h. Nitrocellulose membrane was incubated overnight at 4°C with shaking in Tris-buffered saline (TBS) blocking buffer (10 mM Tris/HCl, 0.09% NaCl pH 7.5 + 0.5% casein). The membrane was incubated with specific antibody dissolved in TBS for 90 min at RT. The membrane was washed 3 times in TBST (TBS + 0.1% Tween-20) for 5 min before incubation with the secondary antibody (typically α-rabbit-HRP) dissolved in TBS for 90 min at RT. The membrane was again washed 3 times before the proteins are visualised using enhanced chemiluminescence (ECL) kit from GE Healthcare as per the manufacturer's instructions. Films were exposed as appropriate (10 s – 10 min) and developed using an automatic developer machine (Konica SRX-101A). Alternatively, blots were visualised with an ImageQuant LAS4000mini biomolecular imager (GE Healthcare). Images were processed with the accompanying software and/or Paint.net version 2.61.

2.3 Protein purification methods

2.3.1 Protein overproduction

Unless otherwise stated in the specific protein preparation methods (2.3.5), the typical procedure for protein overproduction was as follows. *E. coli* BL21 (DE3) strain containing the appropriate over-expression plasmid (see appendix, 5.1.9) was grown overnight in LB with the appropriate antibiotic to select for plasmid retention along with 0.2% glucose to repress translation. The overnight pre-culture was diluted 1 in 50 into 1 – 3 L of pre-warmed LB (with the appropriate antibiotic) and grown at 30°C to an OD_{578} of 0.4 – 0.6 at which point protein over-production was induced with 1 mM IPTG for 3 h. Cells were then cooled on ice for 10 min prior to harvesting (see 2.3.2 below).

2.3.2 Immobilised metal affinity chromatography (IMAC)

Detailed here is the general procedure for the first step of purification of proteins possessing a poly-histidine tag (His-tag) from cell lysate or solubilised membrane extract. Performed using an ÄKTA Prime^{+} system (GE Healthcare) with a 5 ml HisTrap HP column (GE Healthcare). UV absorbance chromatograms were collected with PrimeView software v5.0 (GE Healthcare), a typical chromatogram is shown (Fig. 2.2). After the induction of over-expression detailed above, cells were harvested by centrifugation at 10000 × *g* for 15 min at 4°C using a Beckman-Coulter Avanti centrifuge. Cells were then resuspended in purification specific buffer (Buffer I) generally consisting of either Tris or HEPES buffers, NaCl and imidazole at varied pH depending on the pI of the protein. DNase (Sigma), protease inhibitor cocktail (Sigma) at 1 in 1000 concentration and PMSF to a final concentration of 100 µM was added prior to disruption of cells with a digital sonifier (Branson). The cell lysate yielded was then separated into soluble and membrane fractions via ultracentrifugation at 130,000 × *g* for 1 h at 4°C using a Beckman-Coulter Optima L-100 XP ultracentrifuge. At this point during soluble protein preps the lysate is ready for application to the IMAC column, for membrane protein preps the membrane pellet yielded by the ultracentrifugation is resuspended in buffer containing a high concentration of detergent (2% Triton X-100) and NaCl specific for the prep (Extraction buffer) which acts to solubilise membrane associated proteins. Cell lysates or membrane extracts are applied to the column, which was previously equilibrated with specific buffer, at a flow rate of 1

ml/min. After the sample had flowed through the column flow rate is increased to 2 ml/min and the column is washed with 6 × volume (30 ml) of specific buffer until a baseline in the UV absorbance trace is reached, at which point buffer flow is changed to the elution buffer, which typically consisted of the same components as the original buffer but with a high (400 mM) imidazole concentration to elute bound His-tagged proteins. Samples collected during the purification such as the applied sample, flow-through, washes and elution fractions were analysed by SDS-PAGE to assess protein content and purity. If purity were sufficient, protein is dialysed into specific storage buffer, typically containing 10% glycerol for cryoprotection, overnight at 4°C using Spectra/Pore dialysis tubing with a MW cut-off of 6 to 8 kDa (Spectrum Laboratories Inc.) If the desired purity levels were not achieved a second step of purification would be carried out, as detailed in 2.3.3 and/or 2.3.4 below.

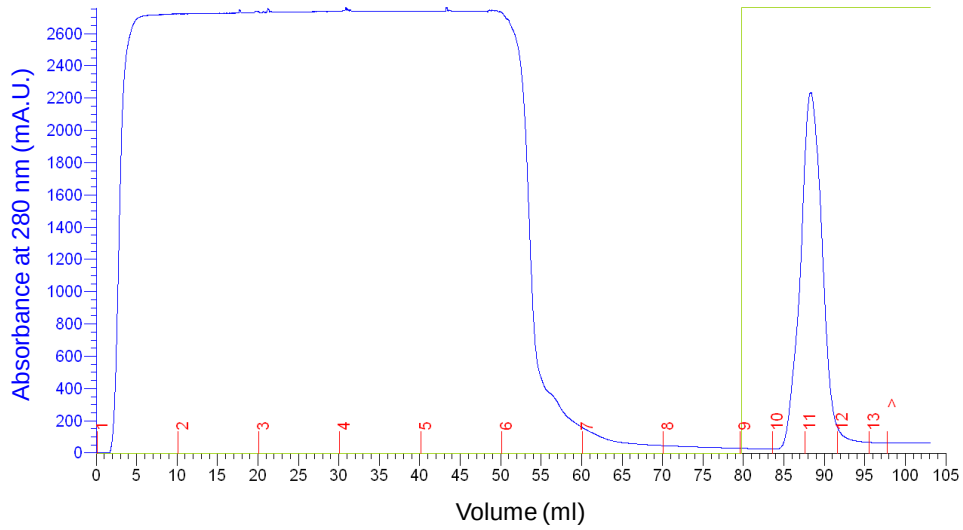

Figure 2.2 Typical HisTrap UV chromatogram

A typical chromatogram from a HisTrap column purification with the UV absorbance at 280 nm plotted against the volume (ml) of buffer flowed through the system, the blue line is the UV absorption signal, the green represents the concentration of elution buffer (%). The red numbers indicate the fractions collected. The first ~50 ml represents the unbound proteins/molecules of the crude lysate flowing through, the return to low absorbance results from the washing away of these unbound molecules. The second peak results from the elution of bound protein/molecules from the column.
Note: the Triton X-100 present during membrane protein purification gives a significant absorption on this UV chromatogram and should be considered.

2.3.3 Ion-exchange chromatography (IEX)

Performed using an ÄKTA Prime$^+$ system (GE Healthcare) with a 5 ml HiTrap HP -Q (anion) or –SP (cation) exchange column (GE healthcare) depending on the charge of the protein in the buffer used. UV absorbance chromatograms were collected with PrimeView software v5.0 (GE Healthcare). Proteins are applied at a flow-rate of 0.5 ml/min in a low ionic strength buffer (Buffer A) with a pH at which the protein is sufficiently positively or negatively charged, this is calculated using ProteinCalculator v3.3 (C. Putnam). Protein samples yielded from IMAC are dialysed into this buffer as detailed above. After protein application, the column is washed with 4 × volume buffer A, or an alternative wash buffer where necessary (to reduce detergent concentration for example). Bound proteins are typically eluted with a gradient from low (buffer A) to high ionic strength (buffer B). Retention time of proteins depends on the charge at the particular pH and thus different proteins are separated. For specific gradients and buffer compositions see details in 2.3.5.

2.3.4 Size exclusion chromatography (SEC)

Performed using an ÄKTA Prime$^+$ system (GE Healthcare) with either a Superdex75 HiLoad 16/60 or a Superdex200 HiLoad 16/600 column (GE healthcare). UV absorbance chromatograms were collected with PrimeView software v5.0 (GE Healthcare). Note, all solutions used must be filtered (0.45 μm) and degassed. The column is first washed with 1.5 × volume H_2O prior to equilibration with 1.5 × volume running buffer (See specific purifications below). Chromatography was typically performed at a flow rate of 1 ml/min with fractions of 2 ml collected. Fractions were analysed by SDS-PAGE for protein content and purity.

2.3.5 Conditions for specific protein purifications

Below are the specific details for individual protein preparations regarding buffer composition and details of purification steps undertaken. For specific over-production constructs and strains, and for the precise composition of proteins produced see the appendix (section 5).

PBP1B

The previously published protocol (53) was adapted. Protein overproduction and purification procedure was as detailed in 2.3.1, 2.3.2 for a membrane protein after which His-tags were removed by digestion with 50 U/ml restriction grade thrombin (Novagen). Thrombin cleavage was performed during dialysis of protein against digestion buffer for 20 h at 4°C. The protein was then sequentially dialysed against dialysis buffers I, II and III in order to gently reduce NaCl concentration prior to ion exchange chromatography as detailed in 2.3.3 using a HiTrap SP HP 5 ml column. After binding of dialysed PBP1B to the column a wash with IEX wash buffer was performed in order to reduce the Triton concentration in the column. The elution gradient in this case is from 0 to 100% buffer B over 70 ml at a flow rate of 5 ml/min. Fractions of 2 ml were collected and analysed by SDS-PAGE, those containing sufficiently pure PBP1B were dialysed against storage buffer overnight and subsequently aliquotted in volumes of 100 to 500 µl and stored at -80°C. SDS-PAGE analysis of final protein samples shown in figure 2.3 A. Typically ~1 mg of PBP1B (see 5.1.8) per litre of culture was obtained (0.001 g/L). Prep specific buffers are detailed below.

- Buffer I: 25 mM Tris/HCl, 10 mM $MgCl_2$, 1 M NaCl, pH 7.5.
- Extraction buffer: 25 mM Tris/HCl, 10 mM $MgCl_2$, 1 M NaCl, 20 mM imidazole, 20% glycerol, 2% Triton X-100, pH 7.5.
- IMAC elution buffer: 25 mM Tris/HCl, 10 mM $MgCl_2$, 1 M NaCl, 400 mM imidazole, 20% glycerol, 0.2% Triton X-100, pH 7.5.
- Digestion buffer: 25 mM Tris/HCl, 10 mM $MgCl_2$, 1 M NaCl, 0.5 mM EGTA, 20% glycerol, pH 7.5.
- Dialysis buffer I: 10 mM NaAcetate, 1 M NaCl, 10% glycerol, pH 5.0.
- Dialysis buffer II: 10 mM NaAcetate, 300 mM NaCl, 10% glycerol, pH 5.0.
- Dialysis buffer III: 10 mM NaAcetate, 100 mM NaCl, 10% glycerol, pH 5.0.
- IEX buffer A: 10 mM NaAcetate, 100 mM NaCl, 10% glycerol, 0.2% Triton X-100, pH 5.0.
- IEX wash buffer: 10 mM NaAcetate, 100 mM NaCl, 10% glycerol, 0.2% Triton X-100, pH 5.0.
- IEX buffer B: 10 mM NaAcetate, 2 M NaCl, 10% glycerol, 0.2% Triton X-100, pH 5.0.
- Storage buffer*: 10 mM NaAcetate, 10 mM $MgCl_2$, 500 mM NaCl, 10% glycerol, pH 5.0.

*Note: Final PBP1B buffer composition consists of storage buffer and 0.2% Triton X-100 as it is not removed by dialysis.

His-UB2H

Protein overproduction and purification procedure was as detailed in 2.3.1 and 2.3.2 for a soluble protein. His-UB2H requires a second step of purification, namely SEC as detailed in 2.3.4 using the Superdex75 HiLoad 16/60 column. After SEC, His-UB2H containing fractions were identified and their purity assessed via SDS-PAGE, these were then concentrated using a VivaSpin 6 column (Sartorius stedim biotech) and stored at -80°C in aliquots of 100 to 500 µl. SDS-PAGE analysis of final protein samples shown in figure 2.3 B. Typically approximately 0.008 g/L of His-UB2H (see 5.1.8) was obtained. Prep-specific buffers are detailed below.

- Buffer I: 25 mM Tris/HCl, 10 mM $MgCl_2$ 500 mM NaCl, 40 mM imidazole, pH 7.5.
- IMAC Elution buffer: (25 mM Tris/HCl, 10 mM $MgCl_2$ 500 mM NaCl, 400 mM imidazole pH 7.5.
- SEC buffer: 25 mM Tris/HCl, 1 M NaCl, 10% glycerol, pH 7.5.

PBP3

This protocol was developed by Khai Bui in the lab. Protein overproduction and purification procedure differed to that above. XL1-Blue strain containing the PBP3 plasmid (see appendix, section 5.1.9) was grown in LB supplemented with 5% glycerol to an OD_{578} of 0.6 at 30°C, overexpression of protein was induced overnight with 0.05 mM IPTG. Cells were harvested as detailed in 2.3.2 with an additional step, such that cells were first resuspended in buffer I and harvested again (cell pellet wash) and resuspended in buffer II. After lysis and extraction (2.3.2) solubilised membrane proteins were applied to 1 ml of Ni-NTA beads (QIAGEN) equilibrated with extraction buffer. The mix was incubated for 4 h at 4°C, beads were then washed with 3 x 10 ml IMAC wash buffer I followed by 4 x 10 ml IMAC wash buffer II. Remaining bound protein was eluted with 10 x 1 ml IMAC elution buffer into tubes containing 10 µl of 100 mM EGTA (final concentration of 1 mM). Samples were analysed by SDS-PAGE, those containing sufficiently pure PBP3 were dialysed against storage buffer overnight and subsequently aliquotted in volumes of 100 to 500 µl and stored at -80°C. SDS-PAGE analysis of final protein samples shown in figure 2.3 C. Typically, 0.9 mg of His-

PBP3 (see 5.1.8) per litre of culture was obtained. Prep specific buffers are detailed below.

- Buffer I: 25 mM HEPES/NaOH, pH 8.0.
- Buffer II: 25 mM HEPES/NaOH, 1 M NaCl, pH 8.0.
- Extraction buffer: 25 mM HEPES/NaOH, 10 mM $MgCl_2$, 1 M NaCl, 20 mM imidazole, 2% Triton X-100 pH 8.0.
- IMAC wash buffer I: 25 mM HEPES/NaOH, 10 mM $MgCl_2$, 1 M NaCl, 20 mM imidazole, 10% glycerol, 0.2% Triton X-100 pH 8.0.
- IMAC wash buffer II: as IMAC wash buffer I with 40 mM imidazole.
- IMAC elution buffer : 25 mM HEPES/NaOH, 10 mM $MgCl_2$, 1 M NaCl, 400 mM imidazole, 10% glycerol, 0.2% Triton X-100 pH 8.0.
- Storage buffer* : 25 mM HEPES/NaOH, 10 mM $MgCl_2$, 1 M NaCl, 1 mM EGTA, 10% glycerol, pH 8.0.

*Note: Final buffer composition is storage buffer plus 0.2% Triton X-100 as this is not removed by dialysis.

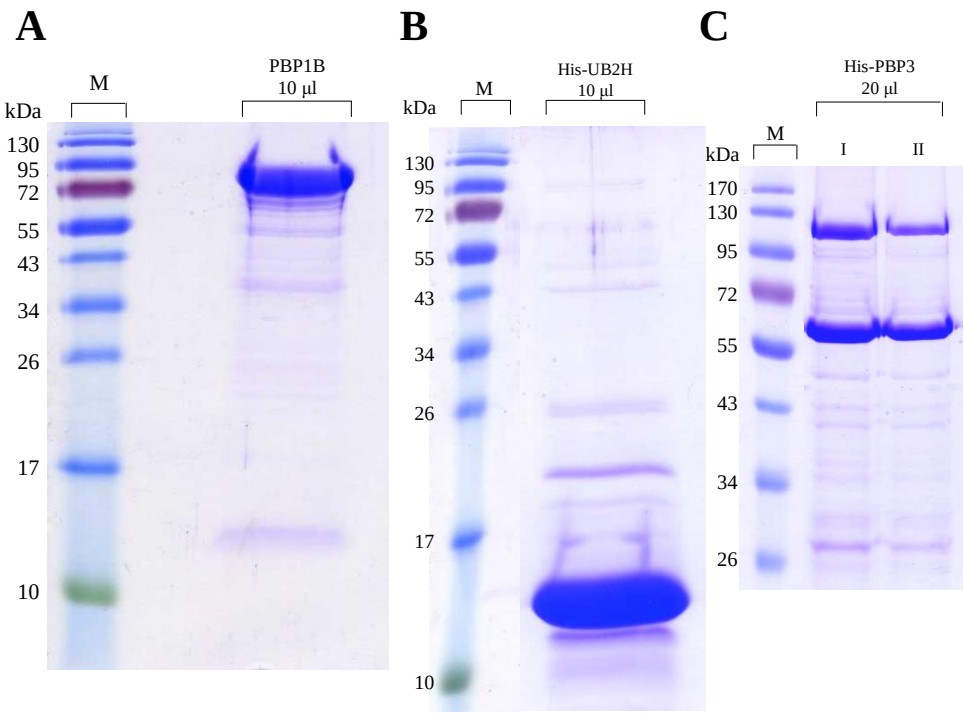

Figure 2.3. SDS-PAGE of purified PBP1B and UB2H domain

Final protein pool purity of PBP1B (A) His-UB2H (B) and His-PBP3 (C) assessed by Coomassie-stained 15% SDS-PAGE. Volume of protein sample loaded in each instance is indicated above. In the case of His-PBP3, of which two pools are shown indicated by I and II, a strong apparent dimer band exists at ~120 kDa even after boiling in SDS for resolution by SDS-PAGE. Whether PBP3 forms homodimers or not is unknown. This band may also result from formation of artificial di-sulphide bridges in the denatured proteins during transition of the sample from the stacking to resolving gel. At this point the reducing agent (β-mercaptoethanol) is removed potentially allowing the oxidisation of cysteines in the protein (PBP3 has 2 Cys residues).

LpoB(sol)

Protein overproduction and purification procedure was as detailed in 2.3.1 and 2.3.2 for a soluble protein. After which His-tags were removed by digestion with 50 U/ml restriction grade thrombin (Novagen) during dialysis of protein against IEX buffer A for 20 h at 4°C. After dialysis, thrombin was removed from the sample by ion exchange chromatography (5 ml HiTrap Q HP column), at the conditions of IEX buffer A LpoB carries little charge and does not bind to the column matrix. The majority of contaminants, including thrombin, do bind at these conditions and are therefore removed from the sample. SEC was performed as detailed in 2.3.4. Finally, the protein was dialysed against storage buffer overnight and concentrated using a VivaSpin 6 MW c.o column (Sartorius Stedim Biotech) prior to storage in aliquots of 100 to 500 µl at -80°C. SDS-PAGE analysis of final protein samples shown in figure 2.4 A. Prep-specific

buffers are detailed below. Typically 20 mg of pure protein per litre of culture was obtained. His-LpoB(sol) was purified by the same procedure, without the IEX step, see appendix table 5.1.8 for protein sequence details.

- Buffer I: 25 mM Tris/HCl, 10 mM $MgCl_2$ 500 mM NaCl, 40 mM imidazole, pH 7.5.
- IMAC Elution buffer: 25 mM Tris/HCl, 10 mM $MgCl_2$ 500 mM NaCl, 400 mM imidazole, pH 7.5
- Digestion buffer / IEX buffer A : 25 mM Tris/HCl, 100 mM NaCl, 10% glycerol, pH 8.2.
- IEX buffer B: 25 mM Tris/HCl, 1 M NaCl, pH 8.2.
- SEC Buffer: 25 mM Tris/HCl, 1 M NaCl, 10% glycerol, pH 7.5.
- Storage buffer: 25 mM Tris/HCl, 10 mM $MgCl_2$ 500 mM NaCl, 10% glycerol, pH 7.5.

His-LpoA(sol)

The protocol was optimised by Giles Callens in the lab. Protein overproduction and purification procedure was as detailed in 2.3.1 and 2.3.2 for a soluble protein. After which a second purification step via ion exchange chromatography (5 ml HiTrap Q HP column) as detailed in 2.3.3 followed by a third step of SEC as detailed in 2.3.4. Finally, the protein was dialysed against storage buffer overnight and concentrated using a VivaSpin 6 column (Sartorius stedim biotech) prior to storage in aliquots of 100 to 500 µl at -80°C. SDS-PAGE analysis of final protein samples shown in figure 2.4 B. Prep-specific buffers are detailed below. Typically 20 mg of pure protein per litre of culture was obtained. See appendix table 5.1.8 for protein sequence details.

- Buffer I: 25 mM Tris/HCl, 10 mM $MgCl_2$ 500 mM NaCl, 40 mM imidazole, pH 8.0.
- IMAC Elution buffer: 25 mM Tris/HCl, 10 mM $MgCl_2$ 500 mM NaCl, 400 mM imidazole, pH 8.0.
- IEX buffer A: 20 mM Tris/HCl, pH 8.0.
- IEX buffer B: 20 mM Tris/HCl, 300 mM NaCl, pH 8.0.
- SEC Buffer: 20 mM Tris/HCl, 500 mM NaCl, pH 8.0.
- Storage buffer: 25 mM Tris/HCl, 10 mM $MgCl_2$ 500 mM NaCl, 10% glycerol, pH 7.5.

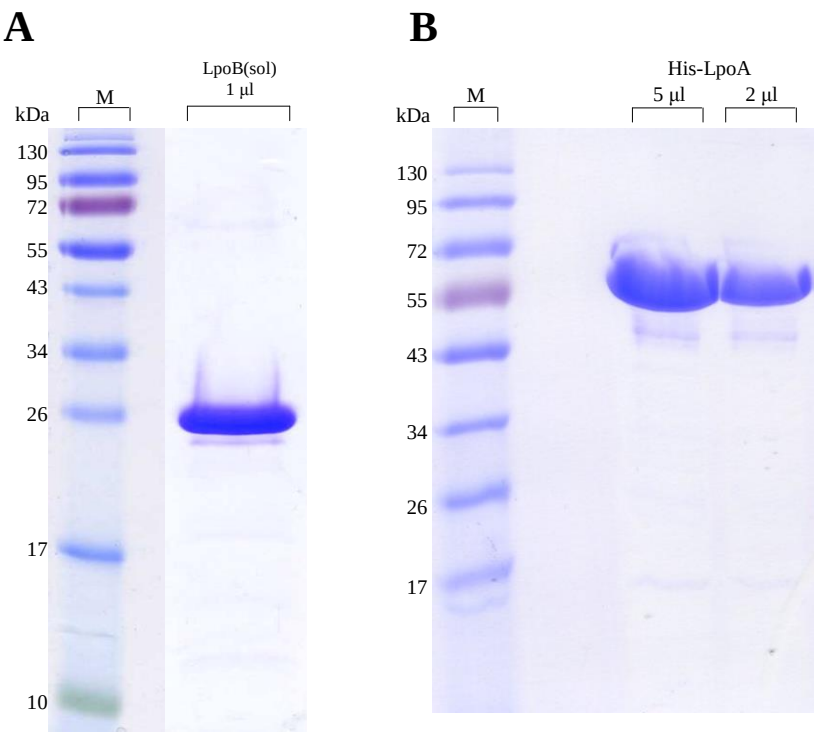

Figure 2.4. SDS-PAGE of purified LpoB(sol) and His-LpoA(sol)

Final protein pool purity of LpoB(sol) (A) and His-LpoA(sol) (B) assessed by coomassie-stained 15% and 12 % SDS-PAGE.

FtsNΔ1-57-His

The previously described procedure (145) was optimised in this work. Protein overproduction and purification procedure was as detailed in 2.3.1 and 2.3.2 for a soluble protein. Final purity assessed by SDS-PAGE shown in figure 2.5A. Prep-specific buffers are detailed below. Typically 145 mg of pure protein per litre of culture was obtained and stored at -80°C in aliquots of 100 to 500 µl. See appendix table 5.1.8 for protein sequence details.

- Buffer I: 25 mM Tris/HCl, 1 M NaCl, 40 mM imidazole, pH 6.0.
- IMAC Elution buffer: 25 mM Tris/HCl, 1 M NaCl, 400 mM imidazole, pH 6.0.
- Storage buffer: 25 mM Tris/HCl, 500 mM NaCl, 10% glycerol, pH 6.0.

FtsN-His

The previously described procedure (145) was optimised in this work. Protein overproduction and purification procedure was as detailed in 2.3.1 and 2.3.2 for a

membrane protein, with a slight variation in both procedures. Cells were grown to an OD_{578} of 0.4 and induced for only 2 h at 37°C before harvesting. IMAC procedure had additional washes, with 6 × column volumes (30 ml) of IMAC wash buffer, designed to ensure a reduction in Triton concentration before elution of bound FtsN-His. Final purity assessed by SDS-PAGE shown in figure 2.5 B Prep-specific buffers are detailed below. Typically 15 mg of pure protein per litre of culture was obtained and stored at -80°C in aliquots of 100 to 500 µl. See appendix table 5.1.8 for protein sequence details.

- Buffer I: 25 mM Tris/HCl, 1 M NaCl, pH 6.0.
- Extraction buffer: 25 mM Tris/HCl, 1 M NaCl, 40 mM imidazole, 1% Triton X-100, pH 6.0.
- IMAC wash buffer: 25 mM Tris/HCl, 1 M NaCl, 40 mM imidazole, 0.25% Triton X-100, pH 6.0.
- IMAC Elution buffer: 25 mM Tris/HCl, 1 M NaCl, 400 mM imidazole, 0.25% Triton X-100 pH, 6.0.
- Storage buffer*: 25 mM Tris/HCl, 500 mM NaCl, 10% glycerol, pH 6.0

*Note: Final FtsN-His buffer composition consists of storage buffer and 0.25% Triton X-100 as it is not removed by dialysis.

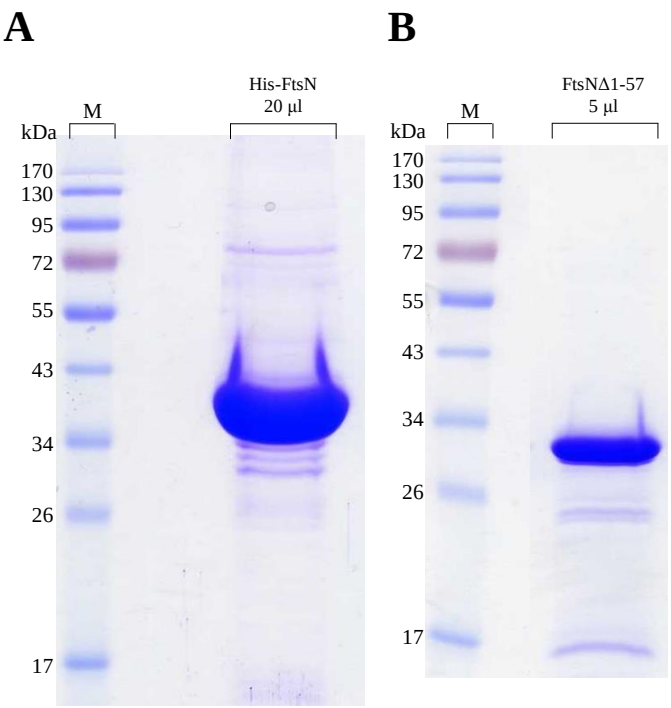

Figure 2.5. SDS-PAGE of purified FtsN-His and FtsNΔ1-57-His

Final protein pool purity assessed by coomassie-stained 12% SDS-PAGE for FtsNΔ1-57-His (A) and FtsN-His (B).

YbgF and TolA(sol)

Purification procedure for both of these protein constructs was the same. Protein overproduction and purification procedure was as detailed in 2.3.1 and 2.3.2 for soluble proteins. After which the His-tags were removed by digestion with 50 U/ml restriction grade thrombin (Novagen) during dialysis of protein against digestion buffer for 20 h at 4°C. Thrombin was removed by SEC as detailed in 2.3.4. Finally, the protein was dialysed against storage buffer overnight and concentrated using a VivaSpin 6 column (Sartorius stedim biotech) prior to storage in aliquots of 100 to 500 µl at -80°C. Final purity assessed by SDS-PAGE shown in figure 2.6 A and B. For both proteins, approximately 8 mg of pure protein per litre of culture was obtained and stored at -80°C in aliquots of 100 to 500 µl. See appendix table 5.1.8 for protein sequence details. Prep-specific buffers are detailed below.

- Buffer I: 25 mM Tris/HCl, 10 mM $MgCl_2$ 500 mM NaCl, 40 mM imidazole, pH 7.5.
- IMAC Elution buffer: 25 mM Tris/HCl, 10 mM $MgCl_2$ 500 mM NaCl, 400 mM imidazole, pH 7.5.
- Digestion buffer: 25 mM Tris/HCl, 10 mM $MgCl_2$ 500 mM NaCl, pH 7.5.
- SEC buffer: 25 mM Tris/HCl, 500 mM NaCl, 10% glycerol, pH 7.5.
- Storage buffer: 25 mM Tris/HCl, 10 mM $MgCl_2$ 500 mM NaCl, 10% glycerol, pH 7.5.

TolB-His

Protein overproduction and purification procedure was as detailed in 2.3.1 and 2.3.2 for soluble proteins. The protein required a second step of purification to remove co-eluted contaminants after IMAC. SEC was performed using a superdex75 HiLoad 16/60 column as detailed in 2.3.3. TolB-His containing fractions were identified and their purity assessed via SDS-PAGE, these were then concentrated using a VivaSpin 6 column (Sartorius stedim biotech) and stored at -80°C in aliquots of 100 to 500 µl. SDS-PAGE analysis of final protein samples shown in figure 2.6 C. Typically approximately 1.3 mg per litre of culture was obtained. See appendix table 5.1.8 for protein sequence details. Prep-specific buffers are detailed below.

- Buffer I : 25 mM Tris/HCl, 500 mM NaCl, 20 mM imidazole, pH 8.0.
- IMAC Elution buffer: 25 mM Tris/HCl, 500 mM NaCl, 400 mM imidazole, pH 8.0.
- SEC buffer: 25 mM Tris/HCl, 1 M NaCl, 10% glycerol, pH 8.0.

- Storage buffer: 25 mM Tris/HCl, 500 mM NaCl, 10% glycerol, pH 8.0.

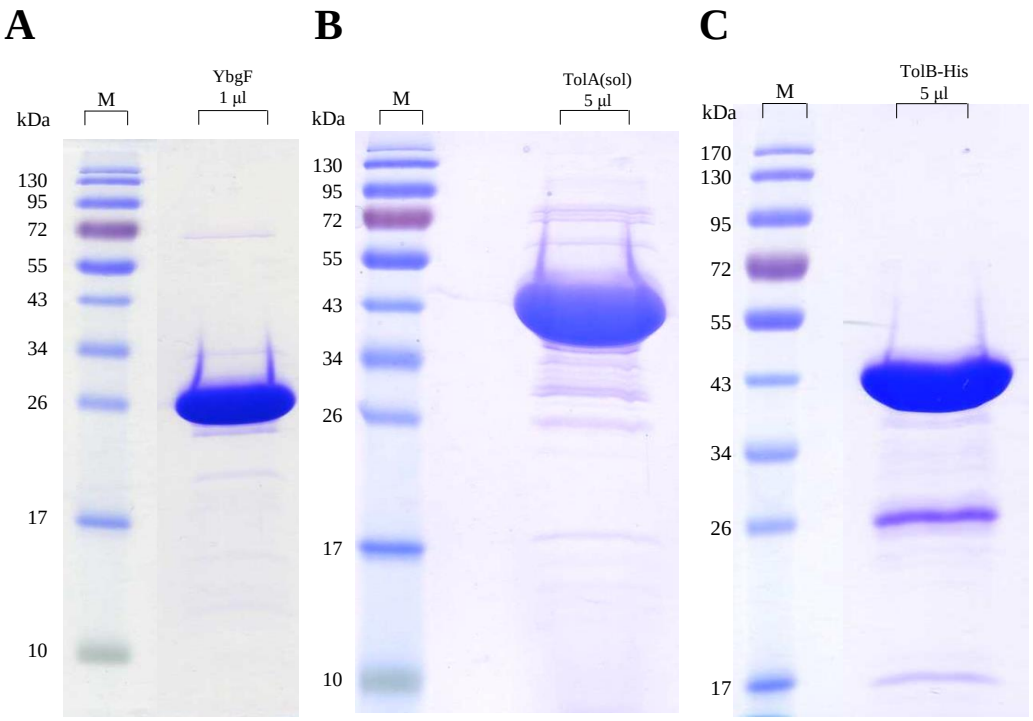

Figure 2.6. SDS-PAGE of purified YbgF, TolA(sol) and TolB-His

Analysis of purified protein pools of YbgF (A) TolA(sol) (A) and TolB-His (A) by coomassie-stained SDS-PAGE (12 or 15%). 5 µl of protein sample loaded in each instance.

TolA-His and tag-less TolA

Full length TolA was purified in both a C-terminally tagged form, or in a tag-less form. Protein overproduction and purification procedure was as detailed in 2.3.1 and 2.3.2 for a membrane protein. In the case of TolA-His IMAC featured several additional wash steps. The column was washed with 20 ml extraction buffer, prior to 30 ml wash I, 30 ml wash II and finally 20 ml wash III before elution. This yielded TolA-His at a sufficient purity without the need for any subsequent purification steps. Appropriate elutions were pooled and dialysed against TolA-His storage buffer overnight and subsequently aliquotted in volumes of 100 to 500 µl and stored at -80°C. SDS-PAGE analysis of final protein samples shown in figure 2.7 A. Typically 2.5 mg of TolA-His per litre of culture was obtained. Prep specific buffers are detailed below. For tagless TolA, N-terminally tagged TolA was produced and purified by the same method as TolA-His. Appropriate elution fractions were pooled and dialysed for 20 h against digestion buffer, with 50 U/ml restriction grade thrombin added (Novagen). The sample

was then dialysed against IEX buffer A for application to HiTrap HP SP (5 ml) as 2.3.3. In this case step-wise elutions were performed as opposed to a gradient. After application the column was washed with 10 ml IEX buffer A followed by elution of TolA with IEX elution I. Remaining protein (e.g. thrombin, among others) were then eluted with IEX elution II. Fractions containing pure TolA were pooled and dialysed against TolA storage buffer overnight and subsequently aliquotted in 200 µl volumes and stored at -80°C. SDS-PAGE analysis of final protein samples shown in figure 2.7 B. Typically 0.38 mg of pure protein was obtained per litre of culture. See appendix table 5.1.8 for protein sequence details.

- Buffer I: 25 mM Tris/HCl, 10 mM $MgCl_2$, 1 M NaCl, 10% glycerol, pH 7.5.
- Extraction buffer: 25 mM Tris/HCl, 10 mM $MgCl_2$, 1 M NaCl, 5 mM imidazole, 10% glycerol, 2% Triton X-100. pH 7.5.
- IMAC Wash I : As extraction buffer with 0.2% Triton X-100.
- IMAC Wash II: As Wash II with 20 mM imidazole.
- IMAC Wash III: 25 mM Tris/HCl, 10 mM $MgCl_2$, 500 mM NaCl, 40 mM imidazole, 10% glycerol, 0.2% Triton X-100, pH 7.5.
- IMAC elution buffer : 25 mM Tris/HCl, 10 mM $MgCl_2$, 1 M NaCl, 400 mM imidazole, 20% glycerol, 1% Triton X-100, pH 7.5
- Digestion buffer : 25 mM HEPES/NaOH, 10 mM $MgCl_2$, 100 mM NaCl, 10% glycerol, pH 7.5.
- IEX buffer A: 25 mM HEPES/NaOH, 10 mM $MgCl_2$, 100 mM NaCl, 10% glycerol, pH 6.0.
- IEX elution I : 25 mM HEPES/NaOH, 10 mM $MgCl_2$, 500 mM NaCl, 10% glycerol, pH 7.5.
- IEX elution II: 25 mM HEPES/NaOH, 10 mM $MgCl_2$, 1 M NaCl, 10% glycerol, pH 7.5.
- TolA-His storage buffer*: 25 mM Tris/HCl, 10 mM $MgCl_2$, 500 mM NaCl, 10% glycerol, pH 7.5
- TolA storage buffer*: 25 mM HEPES/NaOH, 10 mM $MgCl_2$, 100 mM NaCl, 10% glycerol, pH 7.5.

*Note: Final buffer composition consists of storage buffer and 0.2% Triton X-100 as it is not removed by dialysis.

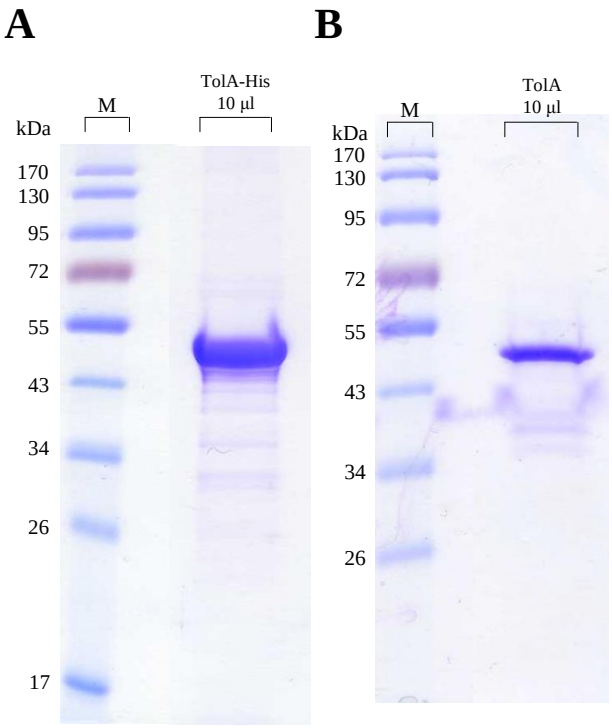

Figure 2.7 SDS-PAGE of purified TolA-His and TolA

Analysis of purified protein pools of TolA-His (A) and TolA (B) by coomassie-stained SDS-PAGE (12%). 10 µl of protein sample loaded in each instance.

His-Pal(sol)

Protein overproduction and purification procedure was as detailed in 2.3.1 and 2.3.2 for a soluble protein. A second step of purification was required, SEC was performed as detailed in 2.3.3 using the Superdex200 HiLoad 16/60 column. After SEC, His-Pal(sol) containing fractions were pooled and concentrated using a VivaSpin 6 column (Sartorius stedim biotech) and stored at -80°C in aliquots of 100 to 500 µl. SDS-PAGE analysis of final protein samples shown in figure 2.8. Typically 48.7 mg of His-Pal(sol) per litre of culture was obtained. See appendix table 5.1.8 for protein sequence details. Prep-specific buffers are detailed below.

- Buffer I: 25 mM Tris/HCl, 10 mM $MgCl_2$, 500 mM NaCl, 20 mM imidazole, 10% glycerol, pH 7.5
- IMAC elution buffer: 25 mM Tris/HCl, 10 mM $MgCl_2$, 500 mM NaCl, 400 mM imidazole, pH 7.5
- SEC buffer: 25 mM HEPES/NaOH, 10 $MgCl_2$, 1 M NaCl, 10% glycerol, pH 7.5.
- Storage buffer: 25 mM HEPES/NaOH, 10 $MgCl_2$, 500 mM NaCl, 10% glycerol, pH 7.5.

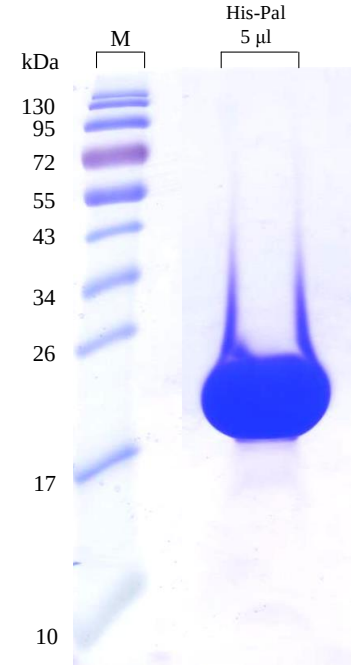

Figure 2.8. SDS-PAGE of purified His-Pal(sol)

Analysis of purified His-Pal(sol) protein by coomassie-stained SDS-PAGE (15%).

2.3.6 Protein overproduction for NMR spectroscopy

For structural determination by NMR spectroscopy proteins must be labelled with ^{15}N and ^{13}C. For this work LpoB(sol) was overproduced and purified from cells grown in [^{15}N, ^{13}C]-M9 media, in which the only sources of these two elements were [^{15}N]-ammonium chloride and [^{13}C]-glucose (Cambridge Isotope Laboratories Inc, USA). BL21 (DE3) pET28-His-LpoB(sol) was inoculated from glycerol stock 1 in 70 in 7 ml LB with 50 µg/ml kanamycin and grown for 8 h at 37°C, 100 ml of M9 with 50 µg/ml kanamycin was inoculated with 1 ml of pre-culture and grown overnight at 37°C. Cells were harvested by centrifugation at 4500 rpm for 20 min at room temperature. Cells were then resuspended in 1 ml of fresh M9 media and used to inoculate the remaining 900 ml. Cells were then grown and protein over-production induced as in 2.3.1 followed by purification of LpoB(sol) as detailed in 2.3.5.

2.3.7 Purification of antibodies from immunised rabbit serum

Antibodies were purified from antisera derived from rabbits immunised with the particular antigen (Eurogentec, Belgium), in this work antibodies were produced against *E. coli* YbgF, TolA, TolB and Pal proteins purified as detailed above (2.3.5). Antibody purification was achieved via affinity chromatography using the purified protein antigen coupled to a sepharose bead matrix (as detailed in section 2.4.3). The beads were washed with 10 ml buffer I (10 mM Tris/HCl, 1 M NaCl, 10 mM $MgCl_2$, 0.1% Triton X-100, pH 7.2) followed by 5 ml elution buffer I (100 mM glycine/HCl, 0.1% Triton X-100, pH 2.0) and equilibrated with 30 ml buffer I. 10 ml of serum was diluted with 35 ml diluent buffer (10 mM Tris/HCl, 0.1% Triton X-100, pH 7.4) and centrifuged at 4500 rpm for 10 min at 4°C to remove insoluble debris. The supernatant was then incubated with the bead matrix for 20 h with gentle mixing at 4°C. The mix was then transferred to a 10 ml gravity column, the collected bead matrix was washed with 30 ml buffer I followed by 20 ml buffer II (10 mM Tris/HCl, 150 mM NaCl, 10 mM $MgCl_2$, 0.1% Triton X-100, pH 7.2). Bound antibodies were eluted with 10 × 1 ml elution buffer I into 1.5 ml microfuge tubes containing 200 µl of elution buffer II (2 M Tris/HCl, pH 8.0) and 300 µl of glycerol. Fractions were then thoroughly mixed by inversion, 20 µl samples were taken for SDS-PAGE analysis (Fig. 2.9 A) before freezing at -80°C. Fractions were pooled depending on their antibody content (e.g. fractions 2 to 7 as pool I and fractions 1, 8, 9 and 10 as pool II from Fig. 2.7 A) The pooled antibodies were tested for specificity against western blots with lysates from a standard *E. coli*

laboratory strain (BW25113) and an antigen deletion strain (figure 2.9 B). BW25113 and BW25113Δ*tolA* / BW25113Δ*tolB* / BW25113Δ*pal* strains were grown to an OD of 0.5. 1 ml was harvested by centrifugation, resuspended in 100 µl PBS and lysed by addition of 100 µl SDS-PAGE loading buffer and boiling for 10 min. Lysate (20 µl) was resolved by SDS-PAGE and blotted as detailed in 2.2.4.

A

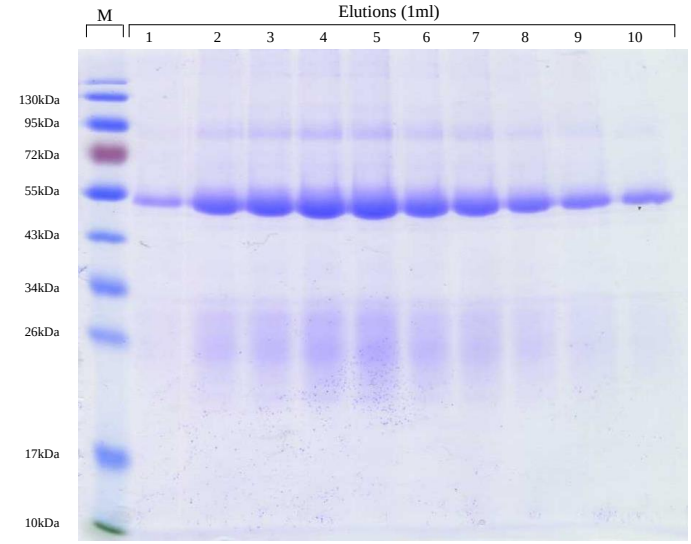

B

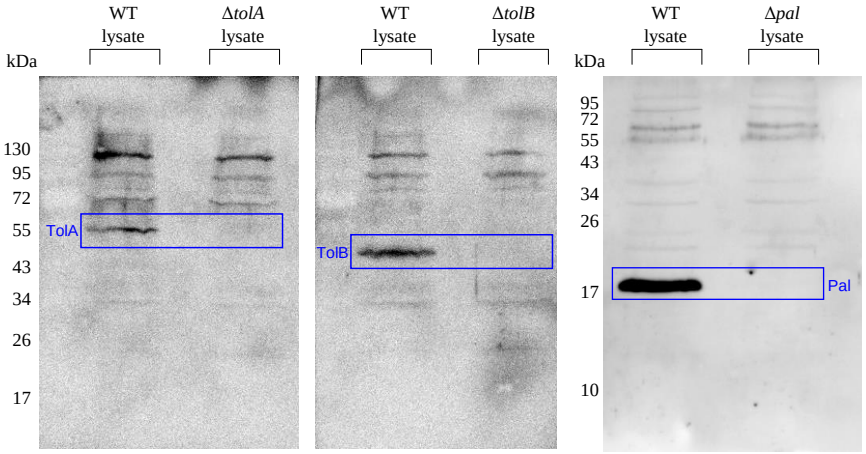

Figure 2.9 SDS-PAGE of antibody prep elutions and test western blot

(A) Coomassie-stained 15% SDS-PAGE gel of the α-TolB antibody purification elutions. The heavy (~50 kDa) and light (~30 kDa) immunoglobulin chains are apparent. These were also apparent in the α-YbgF, α-TolA and α-Pal purifications (not shown).
(B) Test western blot for the α-TolA, α-TolB (at 1 in 2000 dilution) and α-Pal (at 1 in 5000 dilution) antibodies. Immunodetection performed as detailed in 2.2.4.

2.4 Advanced protein methods

2.4.1 Analytical size exclusion chromatography (SEC)

Samples were prepared in high salt buffer (25 mM Tris/HCl, 10 mM $MgCl_2$, 1 M NaCl, pH7.5) to appropriate final concentrations (see specific results). Samples were then incubated at 4°C for 30 min before dialysis overnight against running buffer (25 mM Tris/HCl, 100 mM NaCl, pH 7.5). SEC assays were performed using an ÄKTA Prime$^+$ with a Superdex75 or 200 24 ml column (GE Healthcare). UV absorbance trace was collected with PrimeView software v5.0 (GE Healthcare). The column was washed with 1.5 × volume of filtered and degassed ddH_2O followed by equilibration with 1.5 × volume running buffer. Proteins of known MW; Albumin, Carbonic anhydrase and cytochrome C (Sigma) were run on the column in running buffer to provide a standard curve to calculate the approximate MW of protein complexes depending on their elution volumes, this was derived by plotting the elution volumes of the standards against their LogMW (Fig. 2.10). The samples were loaded onto the column in a volume of 400 µl. SEC was performed at a flow-rate of 0.5 ml/min, with 1 ml fractions collected. The elution volumes of protein(s) were determined from the peaks in the UV chromatograms using the attached software, SDS-PAGE of the collected fractions were run to identify the proteins within these peaks.

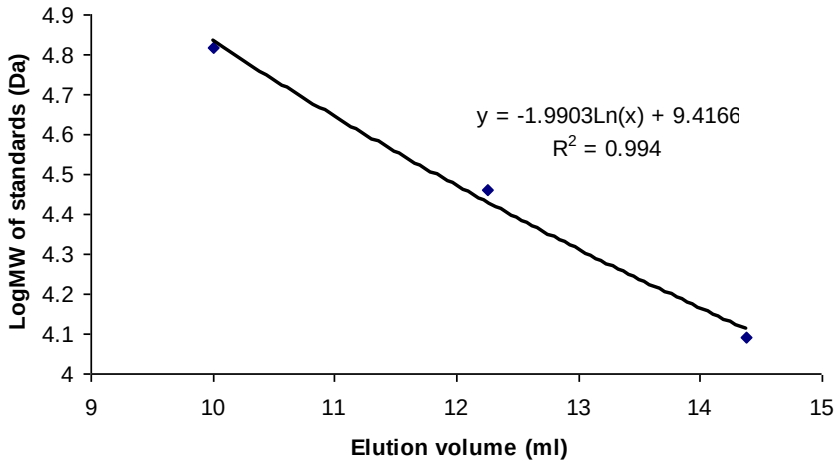

Figure 2.10 SEC assay standard curve

The elution volumes of three separate standard runs were averaged and used to produce this standard curve for the Superdex 75 (24 ml) gel filtration column.

2.4.2 Preparation of membrane fraction for affinity chromatography

This protocol was adapted form previously published method (193). Membrane proteins were isolated from 2 L of *E. coli* MC1061 grown at 37°C to an $OD_{(578)}$ of 0.5 – 0.6. Cells were harvested via centrifugation at 10000 x g for 15 min at 4°C and resuspended in 10 ml buffer I (10 mM Tris/Maleate, 10 mM $MgCl_2$, pH 6.8). DNase, protease inhibitor cocktail (Sigma) at 1 in 1000 concentration was added to the suspension before disruption with a Branson digital sonifier. The cell lysate yielded was then separated into soluble and membrane fractions via ultracentrifugation at 130,000 x g for 1 h at 4°C using a Beckman-Coulter optima L-100 XP ultracentrifuge, the supernatant (soluble fraction) was discarded. Membrane pellet was resuspended in 10 ml buffer II (10 mM Tris/Maleate, 10 mM $MgCl_2$, 1 M NaCl, 2% Triton X-100, pH 6.8) and stirred at 4°C overnight to extract membrane proteins. The extraction was then ultracentrifuged as previous, the supernatant was then diluted with 10 ml of membrane fraction (MF) dialysis buffer (10 mM Tris/Maleate, 10 mM $MgCl_2$, 50 mM NaCl, pH 6.8) and then dialysed against 3 L of this buffer overnight. For high salt affinity chromatography, this buffer contained 400 mM NaCl.

2.4.3 Affinity chromatography

This protocol was adapted form previously published method (193). Proteins were coupled to CNBr-activated Sepharose beads (GE Healthcare) as per the manufacturer's protocol. Coupling of 10 mg of protein to 0.8 g of re-hydrated sepharose beads was performed overnight at 4°C with gentle agitation in AC coupling buffer (100 mM $NaHCO_3$, 10 mM $MgCl_2$, 500 mM NaCl, 0.1% Triton X-100, pH 8.3), beads were then washed with 2 column volumes coupling buffer. Remaining coupling sites were blocked with AC block buffer (200 mM Tris/HCl, 10 mM $MgCl_2$, 500 mM NaCl, 0.1% Triton X-100, pH 8.0) overnight with gentle agitation. Beads were then washed with alternating AC block buffer and AC acetate buffer (100 mM sodium acetate, 10 mM $MgCl_2$, 500 mM NaCl, 0.1% Triton X-100, pH 4.8) for 3 cycles before finally being washed with and resuspended in AC binding buffer (10 mM Tris/Maleate, 10 mM $MgCl_2$, 50 mM NaCl, 0.05% Triton X-100, pH 6.8). As a control one batch of sepharose beads were treated the same with no protein added (producing Tris-Sepharose).

Affinity chromatography was performed by the addition of 10 ml of membrane extract containing 50 mM NaCl (400 mM NaCl for high salt AC), this was then incubated at

4°C overnight with gentle agitation. The flow through was collected, followed by washing with 50 ml of AC wash buffer (10 mM Tris/Maleate, 10 mM $MgCl_2$, 50 mM NaCl, 0.05% Triton X-100, pH 6.8). Retained proteins were eluted with 20 ml AC elution buffer I (10 mM Tris/Maleate, 10 mM $MgCl_2$, 150 mM NaCl, 0.05% Triton X-100, pH 6.8) followed by 20 ml AC elution buffer II (10 mM Tris/Maleate, 10 mM $MgCl_2$, 1 M NaCl, 0.05% Triton X-100, pH 6.8), each elution was incubated for 10 min prior collection. High salt affinity chromatography was performed using AC high salt wash (10 mM Tris/Maleate, 10 mM $MgCl_2$, 400 mM NaCl, 0.05% Triton X-100 pH 6.8) and AC high salt elution buffer (10 mM Tris/Maleate, 10 mM $MgCl_2$, 2 M NaCl, 0.05% Triton X-100 pH 6.8). Fractions were stored at -80°C for later analysis by western blot immunodetection.

2.4.4 Proteomic approach for the identification of putative interactions

The approach described in (27) was adopted with changes. Affigel-10 beads (300 µl) (Sigma) were washed by centrifugation (4000 rpm, 4 min, 4°C) with 3 × 2 ml MilliQ H_2O, followed by 2 × 2 ml coupling buffer (50 mM NaH_2PO_4, 500 mM NaCl, pH 8.0). 2 mg of protein was immobilised to the beads in 500 µl coupling buffer overnight at 4°C with gentle mixing, control beads were treated the same but lacked protein. Beads were then washed with 2 × 2 ml blocking buffer (200 mM Tris/HCl, 500 mM NaCl, pH 8.0) followed by incubation for 2 h at 4°C in 1 ml blocking buffer with gentle mixing. Beads were then washed with 2 × 2 ml elution buffer (10 mM Tris/HCl, 500 mM NaCl, 0.2% N-Lauroylsarcosine, pH 8.0) to remove any weakly immobilised protein before equilibration with 2 × 2 ml binding buffer (10 mM Tris/Maleate, 10 mM $MgCl_2$, 100 mM NaCl, 0.05% Triton X-100, pH 7.5). Membrane extract was prepared as in 2.4.2 and dialysed into binding buffer, 1.5 ml was applied to the bead samples and incubated for 20 h at 4°C with gentle mixing. Beads were then washed as above with 3 × 2 ml binding buffer, the final wash was transferred to a new 2 ml microfuge tube before elution of bound protein with 250 µl elution buffer. The samples were transferred to a new microfuge tube to which 750 µl of ethanol was added, samples were then incubated overnight at -20°C prior to centrifugation at 14,000 rpm, 20 min at 4°C. The supernatant was discarded, leaving any bound protein as a precipitated pellet ready for analysis by MALDI-PMF mass spectrometry once dried. This was performed by Dr. Joe Gray at the Pinnacle facility, Newcastle University.

2.4.5 *In vitro* glycosyltransferase activity assay

The continuous fluorescence GTase assay described previously (194, 195) was optimised in this work. Reactions were performed in a medium-binding black 96-well microplate (Greiner Bio One ref. 655076, Freickenhausen, Germany) in a FLUOstar OPTIMA microplate reader (BMG Labtech, Offenburg, Germany). The reaction mix (60 µl) comprised of lysine-dansylated lipid II (10 µM) in 50 mM HEPES (pH 7.5), 150 mM NaCl, 25 mM $MgCl_2$, 0.5 µg/ml *Streptococcus globisporus* muramidase, and between 0.02 and 0.065% Triton X-100 (Roche Diagnostics, Mannheim, Germany). Negative controls had GTase activity blocked by 50 µM moenomycin (Flavomycin, Hoechst, Frankfurt, Germany). Enzyme concentrations were between 0.25 or 1 µM, which were mixed with interaction partners or control proteins at equimolar ratios or in excess depending on the assay, and incubated for 5 min at 25 or 30°C, depending on the necessary conditions, before the initiation of reactions. Appropriate protein storage buffer was added to the enzyme alone to ensure no unspecific effect was occurring. GT activity was measured over a time course of 20 min at 25 or 30°C, measurements were taken every 30 or 20 seconds with an excitation at 340 nm and emission recorded at 520 nm. Reactions were initiated via the addition of the lipid II dissolved in H_2O to the pre-incubated reaction components. Data is presented as the mean fluorescence at a given time-point as a percentage of the initial fluorescence. Errors bars show the standard deviation of the particular data point. Changes in reaction rate are determined by calculation of the gradient of the curve at its steepest point (greatest rate).

2.4.6 *In vitro* peptidoglycan synthesis assay

Method was adapted from (50). Standard reaction conditions were 10 mM HEPES/NaOH pH 7.5, 10 mM $MgCl_2$, 150 mM NaCl and a varied Triton X-100 concentration from 0.025 to 0.08%. Sufficient amount of [^{14}C]-Glc*N*Ac lipid II to make a final concentration of 15 µM in 100 µl was dried and resuspended in 5 µl of 0.2% Triton X-100. Proteins along with HEPES/NaOH pH 7.5, $MgCl_2$ and NaCl were diluted to the desired molar concentrations in 95 µl and incubated on ice for 10 min. The reaction mix was then added to the lipid II, briefly vortex mixed and incubated with shaking at 37°C in an Eppendorf thermomixer for 1 h. Samples were then incubated for 5 min at 100°C to stop the reaction before digestion with muramidase to produce muropeptides for HPLC analysis (see 2.5.4).

2.4.7 Peptidoglycan binding assay

An assay to determine protein binding to isolated peptidoglycan sacculi was performed as described (148). All steps were carried out on ice with cold buffers unless otherwise stated. Approximately 100 μg of peptidoglycan sacculi from *E. coli* MC1061 was pelleted via centrifugation, washed with 100 μl of binding buffer (10 mM Tris/Maleate, 10 mM $MgCl_2$, 50 mM NaCl, pH 6.8) and resuspended to a final volume of 100 μl with binding buffer and 10 μg of the analyte protein. A control sample without peptidoglycan was treated the same way. Samples were incubated for 30 min on ice before pelleting by centrifugation at 13,000 rpm for 15 min at 4°C. The supernatant was collected as the unbound fraction. Samples were washed with 200 μl of binding buffer followed by centrifugation as before. The supernatant was collected as the wash fraction prior to the resuspension of the pellet in 2% SDS. The samples were gently stirred for 1 h at RT before a final centrifugation step. Samples were analysed by SDS-PAGE.

2.4.8 Surface Plasmon Resonance (SPR) assay

This method was adapted from (193). Performed using a ProteOn XPR36 system and associated software (BioRad) with a GLC general amine coupling sensorchip in a running buffer of 10 mM Tris/Maleate, 150 mM NaCl, 0.05% Triton X-100, pH 7.5. For the creation of a PBP1B surface, 10 mg/ml ampicillin in 0.1 M sodium acetate pH 4.6 was coupled to appropriate lanes on the chip surface by general amine coupling as per the manufacturer's instructions (N-ethyl-N'-(dimethylaminopropyl)-carbodimide hydrochloride, N-hydroxysuccinimide method). PBP1B was then immobilised to the ampicillin matrix via the application of 3 μg/ml PBP1B at a flow rate of 30 μl/min for 5 min at 35°C. As a control, an identical ampicillin surface was exposed to PBP1B buffer with no protein present. After binding, the surface was washed with regeneration buffer (10 mM Tris/Maleate, 1M NaCl, 0.05% Triton X-100, pH 7.5) before digestion of free ampicillin with 1 μM β-lactamase (VIM-4, Adeline Derouaux). Surface was then washed with regeneration buffer followed by running buffer prior to injection of analyte protein. For the creation of surfaces of protein which do not bind to ampicillin (e.g. FtsN) these were immobilised by amine coupling directly to activated GLC surface as per the manufacturer's instructions.

Binding assays were performed at 25°C in running buffer. flow rates varied from 75 – 100 μl/min, with an injection time of 3 or 5 min. The 6 flow cells of the ProteOn system allowed for the simultaneous measurement of the change in response in RUs of

a blank (buffer only) and 5 analyte concentrations, typically in the range of 0.1 to 4 µM. For kinetic calculations several repeat runs (at least 3) across a range of analyte concentrations were performed from which R_{eq} was calculated using the associated software. R_{eq} is the response (RU) at which association and dissociation is at equilibrium. These values were then applied to a Scratchard plot, in which they are plotted against R_{eq}/C where C is the concentration of the analyte in µM. The gradient of the resulting slope yielded is $-K_D^{-1}$ in µM.

2.4.9 *In vitro* cross-linking / pulldown assay

An assay using Ni-NTA bead resin to pull-down multi-protein complexes *in vitro* via the Histidine tag of one of the participating proteins was developed in this work. Proteins were mixed at appropriate concentrations in 200 µl of binding buffer (10 mM HEPES/NaOH, 10 mM $MgCl_2$, 150 mM NaCl, 0.05% Triton X-100, pH 7.5) and incubated at RT for 10 m. Interacting proteins were then cross-linked via the addition of formaldehyde to a final concentration of 0.2% (by volume) and incubated for a further 10 – 15 min at 37°C. Excessive cross-linking was blocked via the addition of Tris/HCl, pH 7.5 to a final concentration of 100 mM, at this point an aliquot is taken as the 'applied' sample. A negative control features the tag-less proteins incubated in the same manner without the His-tagged protein present. Samples were then added to 100 µl washed and equilibrated Ni-NTA beads (QIAGEN) suspended in 1.3 ml binding buffer and incubated with gentle mixing overnight at 4°C. Beads were washed with 5 × 1.5 ml wash buffer (10 mM HEPES/NaOH, 10 mM $MgCl_2$, 150 mM NaCl, 0.05% Triton X-100, 50 mM imidazole, pH 7.5) before the elution of bound proteins by directly boiling in 75 µl of SDS-PAGE loading buffer, this also acts to reverse the cross-linking. The elution sample was then diluted 1:1 with H_2O prior to analysis via SDS-PAGE along with the applied sample.

2.4.10 *In vitro* cross-linking (non-reversed approach)

An assay with a similar approach to 2.5.9, using non-denaturing SDS-PAGE to detect multi-protein complexes *in vitro*, developed with the assistance of undergraduate project student Ann-Kristin Hov. Protein sample preparation was as in 2.5.10, but in 100 µl of binding buffer with the goal being the resolution of proteins/complexes on a 4 – 20% gradient gel via SDS-PAGE instead of a pull-down using Ni-NTA beads. Proteins were then detected by western blotting as in 2.2.4 using specific antibodies. The key aspect of this technique is the comparison of the species produced by the cross-linking of each

protein alone and in the presence of the others. As such an assay testing for a ternary complex will feature 4 samples; protein A, protein B, protein C and a mixture of A, B and C. Samples were incubated with SDS loading buffer without β–mercaptoethanol added at a 2:1 ratio for 10 min at RT. Samples were then resolved on a 4 – 20% SDS-PAGE gradient gel (Generon, Maidenhead, UK). Using the example above, 3 20 µl samples of the mixture are prepared, each being loaded and resolved next to one of the individual protein samples as shown in table 2.8. MW marker used was the Spectra multicolour high range protein ladder (Thermo Scientific, Rockford, USA) as this has a range of 40 to 300 kDa.

Table 2.2 Example gel loading and immunodetection scheme

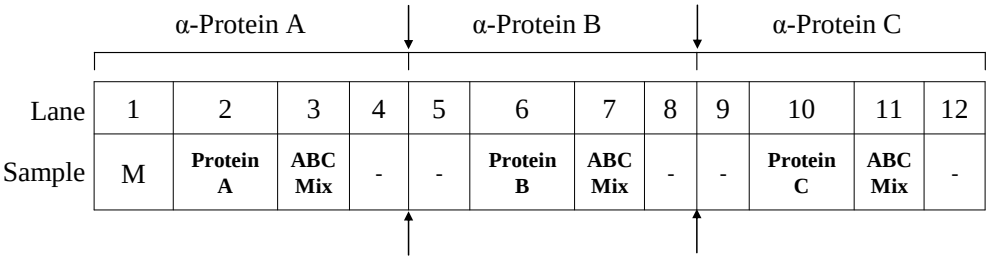

Lane	1	2	3	4	5	6	7	8	9	10	11	12
Sample	M	**Protein A**	**ABC Mix**	-	-	**Protein B**	**ABC Mix**	-	-	**Protein C**	**ABC Mix**	-

M = MW marker, – denotes an empty well. The arrows indicate where the blot would be cut for separate immunodetection in this example.

2.4.11 *In vivo* cross-linking / co-immunoprecipitation assay

This method was described in (67) and modified. *E. coli* BW25113 cells were grown in 150 ml LB medium at 37°C to an OD_{578} of 0.6. Cells were harvested by centrifugation (4000×g, 15 min, 4°C) and resuspended in 6ml of cold CL buffer (50 mM NaH_2PO_4, 20% sucrose, pH 7.4) to which freshly prepared DTSSP solution (20 mg/ml in H_2O) was added, the cells were incubated with mixing at 4°C for 1 h. DTSSP is used as it is water soluble, and its cross-links readily reversible by reduction during SDS-PAGE sample preparation. Cross-linked cells were harvested by centrifugation (4000 × *g*, 15 min, 4°C) and resuspended in 6 ml CL buffer II (100 mM Tris/HCl, 10 mM $MgCl_2$, 1 M NaCl, pH 7.5), 1/1000 of PIC and PMSF protease inhibitors were added along with a small amount of DNase. The cells were then disrupted by sonication with a Branson Digital Sonifier operating at 10 W for 15 min in total (Pulse 30 s, pause 60 s). The lysate was ultracentrifuged (130,000 × *g*, 60 min, 4°C), the supernatant discarded and the membrane fraction was resuspended in 2.5 ml CL buffer III (25 mM Tris/HCl, 10 mM $MgCl_2$, 1 M NaCl, 20% glycerol, 1% Triton X-100) and incubated with mixing

overnight at 4°C to solubilise membrane proteins. After a second ultracentrifugation (130,000 × *g*, 60 min, 4°C) to remove remaining debris 2 × 1.2 ml of the supernatant was diluted via the addition of 0.6 ml CL buffer IV (75 mM Tris/HCl, 10 mM $MgCl_2$, 1 M NaCl, pH 7.5). 15 µg of specific antibody was then added to one of the samples and incubated for 5 h at 4°C with mixing. The other was incubated in parallel with no antibody added, as a control. 2 × 100 µl Protein G-coupled agarose (Pierce / Thermo-Fisher Scientific, Rockford, USA) were washed with 3 × 200 µl CL buffer IV and 1 × 200 µl CL wash buffer (2 parts CL buffer III + 1 part CL buffer IV) before incubation with the immunoprecipitated samples overnight at 4°C with mixing. The beads were then washed with 10 ml CL wash buffer before being boiled for 10 min in 50 µl SDS-PAGE loading buffer (4.2.1). The supernatant was collected and analysed via SDS-PAGE followed by western blot and immunodetection. TrueBlot Anti-Rabbit-HRP (eBiosciences, San Diego, USA) was used as the secondary antibody.

2.4.12 Bocillin binding assay

This method was described in (196) with modifications. PBP1B or PBP3 (10 µg in 50 µl) were incubated at 37°C with 1 ng/µl of the fluorescently labelled β-lactam Bocillin (Molecular Probes, Life Technologies, UK) for 10 min. A control featured the same amount of protein blocked by incubation with 1 ng/µl Penicillin G prior to incubation with Bocillin. Samples were resolved by SDS-PAGE and the gel was scanned with a Typhoon scanner using the blue FAM channel at 488 nm. The result of an assay using His-PBP3 is shown below (Fig. 2.11).

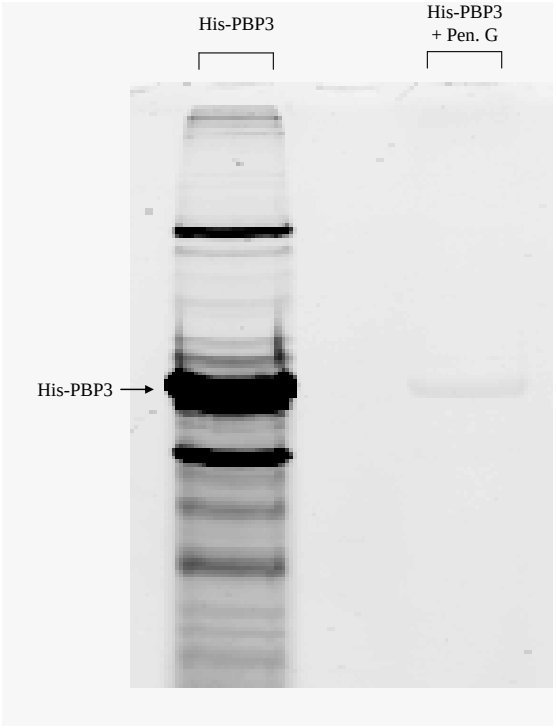

Figure 2.11 Bocillin binding assay for His-PBP3

His-PBP3 was purified as described above (2.3.5) and tested for β-lactam binding to demonstrate correct folding of the protein. As shown above, His-PBP3 does indeed bind bocillin, as does the apparent dimer band and some of the degradation products. Bocillin binding is blocked by pre-incubation with Penicillin G.

2.4.13 *In vivo* protein copy number estimation by quantitative western blot

BW25113 (WT) and BW25113Δ*ybgF* cultures were grown in 50 ml of LB to an OD of 0.3. The culture was then back-diluted 1 in 50 into 50 ml fresh LB and grown to an OD of 0.3. Cells were then cooled on ice for 10 min prior to harvesting of 5 ml by centrifugation (10000 × *g*, 10 min, 4°C). At this point a viable count was also performed to determine the number of cells per ml of culture. The pellets were resuspended in 100 µl TBS and lysed by addition of 100 µl SDS-PAGE loading buffer with boiling for 10 min. 3 × 20 µl samples of BW25113 lysate were resolved by SDS-PAGE along with purified YbgF standards (0, 1, 2, 4, 8 and 16 ng) loaded in 20 µl of BW25113*ΔybgF* lysate. YbgF was detected with specific antibody after western blot. Images were analysed using ImageQuant LAS4000 software, giving the chemiluminescence signal derived from YbgF bands over the background (signal at the same height as YbgF in the 0 ng sample). A standard curve was plotted using the known YbgF standards and the amount of YbgF in the BW25113 lysate samples was calculated. This was then converted to molecules per cell using the viable count data.

2.5 Cell wall analysis methods

2.5.1 Isolation of peptidoglycan from *E. coli*

The previously described protocol for isolation of peptidoglycan from *E. coli* (14) was adapted. A 600 ml culture was grown to an OD between 0.4 to 0.8 in LB media. Cells were then rapidly cooled in an ice-water bath for 10 min before harvesting by centrifugation at 8000 × *g* for 20 min at 4°C. Cells were then resuspended in 6 ml of ice-cold H_2O. The resulting suspension was slowly added (drop-wise) to 6 ml of boiling 8% SDS and boiled for a further 30 min. The lysate was then cooled to RT and ultracentrifuged at 130,000 × *g* for 1 h at RT, the pellet was washed free of SDS by repeated resuspension in 60°C H_2O and ultracentrifugation. The presence of SDS was tested for by the Hyashi test as detailed in 2.6.2. Once the pellet was free of SDS it was resuspended in 900 µl of 10 mM Tris/HCl, 10 mM NaCl, pH 7.0 and transferred to a 2 ml microfuge tube, 100 µl of 3.2 M imidazole at pH 7.0 was added followed by 15 µl of a 10 mg/ml α-amylase solution, samples were then incubated at 37°C for 2 h to digest remaining glycogen. 20 µl Pronase E (10 mg/ml) solution pre-incubated for 2 h at 60°C was then added, samples were incubated for a further 1 h at 60°C to remove covalently attached lipoproteins. 1 ml of 4% SDS was then added to samples prior to boiling for 15 min. The samples were then cooled to RT and washed free of SDS as before. The SDS-free sample was then resuspended in 400 µl of 0.02% NaN_3 solution and stored at 4°C.

2.5.2 Sodium dodecyl sulphate test by Hyashi

The absence of SDS was tested/confirmed using a previously described assay (197). The test determines the presence of SDS by testing for the formation its water insoluble complex with methylene blue resulting in a blue coloured outcome. In a 1.5 ml microfuge tube, a sample of 335 µl is vortex mixed with 170 µl of 0.7 M sodium phosphate, 7 µl of 0.5% methylene blue and 1 ml of chloroform. The sample was free of SDS when the organic phase at the bottom of the tube shows no blue colouration.

2.5.3 Preparation, detection and analysis of muropeptides

Muropeptides were obtained by incubation of peptidoglycan, either produced in the *in vitro* synthesis assay described above (2.5.7) or from isolated PG samples from cells (2.5.1) with muramidase (cellosyl) by the established protocol (14). A sufficient amount

of 4 × cellosyl digest buffer (80 mM sodium phosphate, pH 4.8) was added to samples for a final concentration of 20 mM sodium phosphate, followed by 10 µg of cellosyl (Hoechst, Germany), samples were then incubated at 37°C for 1 to 2 h (for *in vitro* synthesised PG) or overnight (for isolated sacculi). Samples were incubated at 100°C for 15 min before centrifugation at 14,000 rpm for 10 min. An equal volume of 0.5 M sodium borate, pH 9.0 was added to each sample, after which a small spatula-full of sodium borohydride powder was added and the samples were centrifuged at 3000 rpm for 30 min. The pH was adjusted to between 3 and 4 with 20% phosphoric acid, samples are then ready for HPLC analysis. Alternatively samples were stored at -20°C for later analysis. HPLC analysis was performed using an Agilent Technologies series 1200 HPLC system with a reversed phase column - Prontosil 120-3-C18-AQ 3 µm (Bischoff) at 55°C using a linear gradient from 100% solvent A (50 mM sodium phosphate, pH 4.31 + 0.0002% NaN_3) to 100% solvent B (75 mM sodium phosphate, pH 4.95 + 15 % Methanol) over 140 min. Muropeptides were detected by a UV-detector at 205 nm, [^{14}C]-labelled muropeptides were detected by a scintillation counter (LabLogic). The values (mAU or counts per min) were recorded in an HPLC chromatogram by Laura software v4.1.7.70 (LabLogic Systems Ltd), which was subsequently used for data analysis (integration). The chemical structures of detected muropeptides are shown in figure 2.12. The percentage of peptides involved in cross-links was calculated using the formula 100% - % of monomeric muropeptides.

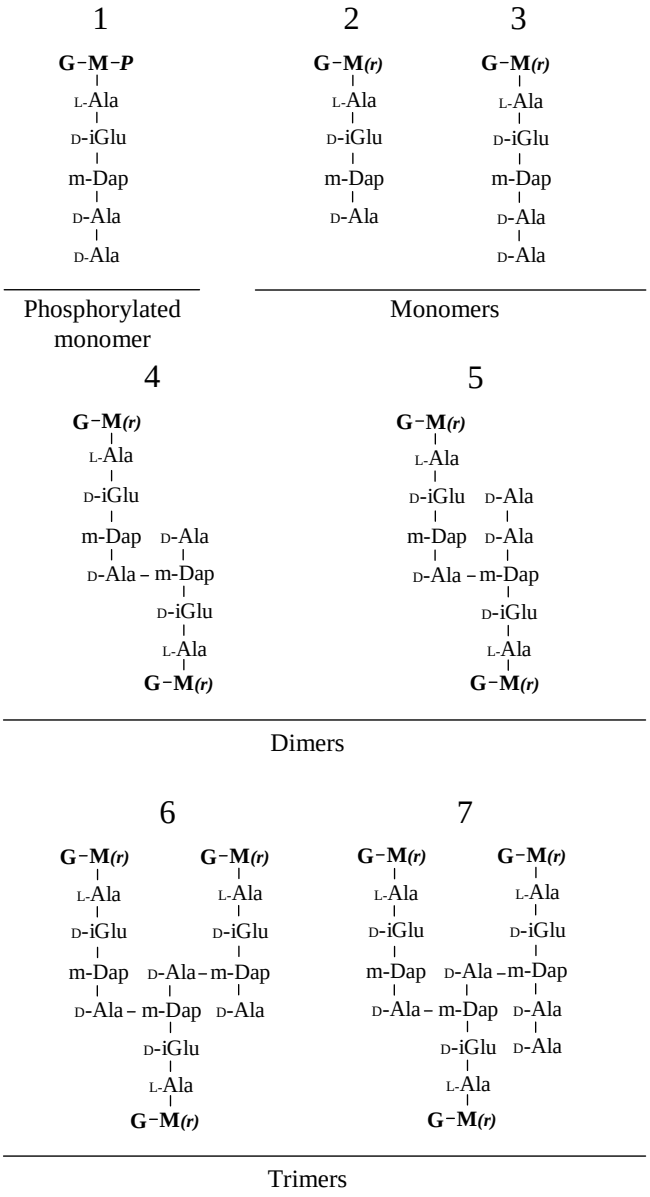

Figure 2.12 Chemical structure of detected muropeptides

The chemical structures of muropeptides detected by HPLC from *in vitro* PG synthesis assays. 1, Penta-P, the product of un-reacted substrate and/or glycan chain ends; 2, Tetra-peptide, the product of both GTase and CPase activities; 3, Penta-peptide, the product of GTase alone; 4, TetraTetra-, the product of GTase, TPase and CPase activities; 5, TetraPenta-, product of GTase and TPase activities; 6, TetraTetraTetra-, product of GTase, TPase and CPase activities; 7, TetraTetraPenta-, the product of GTase and TPase activities. G, Glc*N*Ac; M, Mur*N*Ac; M(*r*), reduced Mur*N*Ac (*N*-acetylmurmitol).

3. Results

3.1 Biochemical and structural properties of a regulator of PG synthesis, LpoB

3.1.1 Introduction

LpoB is required for the activity of the major peptidoglycan synthase active during cell division, PBP1B, in the cell. LpoB interacts with and stimulates the GTase and TPase activities of PBP1B *in vitro* and, like its cognate synthase, localises at mid-cell during division (27, 28). However, many aspects of the regulation of peptidoglycan synthesis in *E. coli* remained unclear. In this section we address questions about the nature of the structure of LpoB, whether it exists in a homo-multimeric state, the specific interaction residues/domains of its interaction with PBP1B and whether it participates in additional protein-protein interactions.

3.1.2 LpoB is a monomer

In this work we pursued a characterisation of LpoB. We therefore optimised the protocol for overproduction and purification of hexahistidine tagged LpoB lacking its lipoprotein signal sequence, LpoB(sol) (2.3.5). Two versions of LpoB are used in this work, one which retains the his-tag and one where this was removed by thrombin cleavage. One aspect of characterisation used analytical SEC assays (2.4.1), whereby proteins are separated according to their MW and shape. The apparent MW of LpoB(sol) in SEC was 45.5 kDa (Fig. 3.1 A), which is more than double its calculated MW of 20.34 kDa. Thus, whether LpoB self-interacts to form a homodimer was investigated. First, a series of SEC assays were set up in which 50 μM LpoB(sol) was resolved in buffers of increasing ionic strength, which is known to dissociate many ionic protein interactions. The running buffer consisted of 10 mM Tris/HCl, 10 mM $MgCl_2$ and either 100 mM, 1 M or 2 M NaCl, pH 7.5. There was no shift in the elution volume of LpoB with increasing ionic strength (Fig. 3.1 A) indicating that LpoB does not dimerise through ionic interaction. However, this does not discount that a homodimer could form via hydrophobic interaction. Thus another approach was used to confirm this result.

Analytical ultracentrifugation was carried out by Dr. Alexandra Solovyova at Newcastle University's Pinnacle facility in which His-LpoB(sol) at 15 μM (0.35 mg/ml) in 10 mM Tris/HCl, 10 mM $MgCl_2$, 100 mM NaCl, pH 7.5 was subjected to sedimentation velocity analysis. A single species with a molecular weight of 22.58 kDa and a sedimentation coefficient of 1.754 was observed (Fig. 3.1 B). The calculated MW

of His-LpoB(sol) is 22.64 kDa, thus AUC confirmed that LpoB exists as a monomer at the conditions used. The AUC data explained the observed apparent MW in SEC. Globular proteins of ~20 kDa typically have a sedimentation co-efficient of 1.2 – 1.4. A sedimentation co-efficient of >1.7 indicates that LpoB has regions of significant flexibility or disorder in its structure. Such flexibility could cause an abnormal migration in SEC as these regions can exclude the protein from pores it would otherwise penetrate if it were more globular/compact, increasing the rate of its transit through the column.

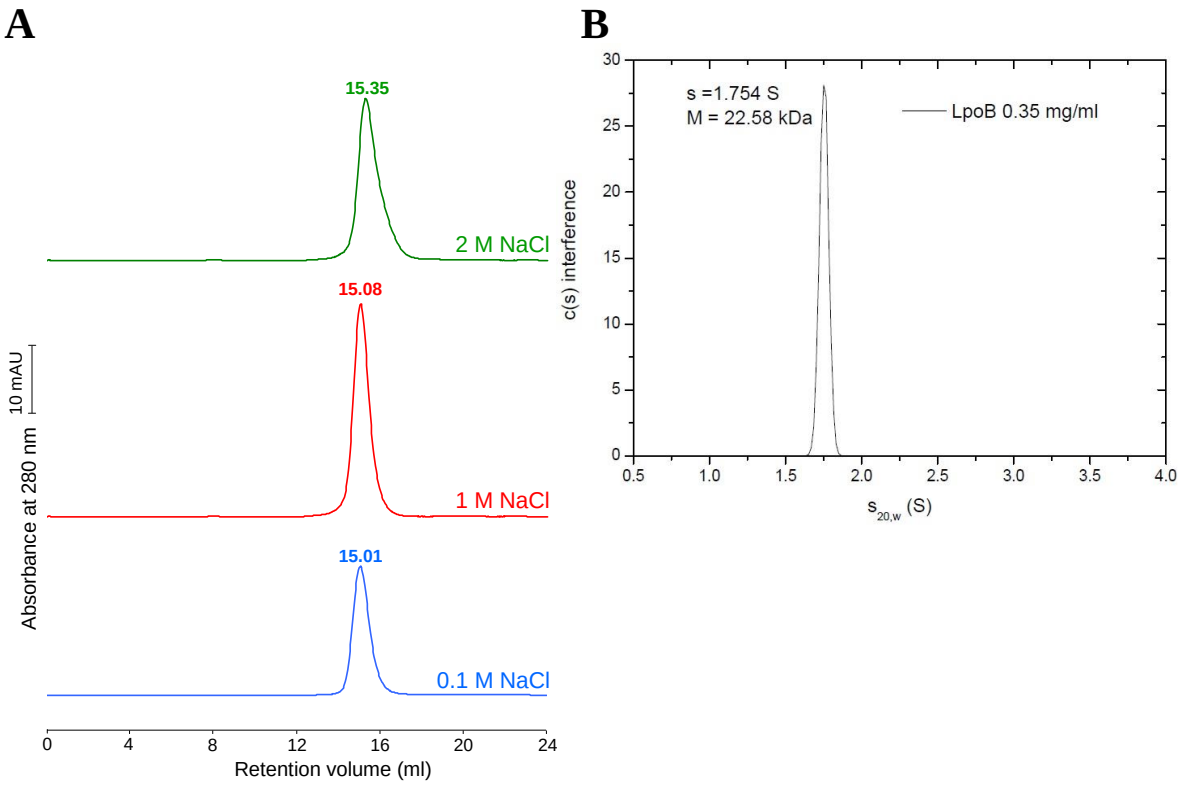

Figure 3.1 LpoB exists as a monomer *in vitro*

(A) Chromatograms of LpoB(sol) resolved at 100 mM, 1 M and 2 M NaCl in a 24 ml Superdex200 column. The retention volume in ml is shown at the top of each peak. No significant shift in the retention of LpoB(sol) was observed from 0.1 to 2 M NaCl. The apparent MW was calculated from the elution volumes derived from two runs, and was 45.5 ± 3.3 kDa.
(B) AUC results of a sedimentation velocity experiment. The Rayleigh interference is plotted against the sedimentation coefficient of His-LpoB(sol) in sedimentation velocity AUC. A single species was detected with a MW of 22.58 kDa and a sedimentation co-efficient (S) of 1.754. Figure courtesy of Dr. Alexandra Solovyova.

3.1.3 The high resolution structure of LpoB was solved by NMR spectroscopy

Work to try and determine the structure of LpoB began with attempts to obtain protein crystals of LpoB(sol) for X-ray crystallography. Despite many attempts at optimisation we never obtained LpoB crystals. After observing that the properties of LpoB suggested disorder/flexibility in its structure (3.1.2) we opted for NMR spectroscopy. Fortunately, LpoB is small enough for high resolution structural determination by this technique. LpoB(sol) was produced (2.3.6) in both singly labelled [^{15}N] and doubly [^{15}N,^{13}C] labelled forms. Labelled LpoB samples were sent to our collaborators Catherine Bougault, Jean-Pierre Simorre and Nicholas Jean at the Institute de Biologie Structurale (IBS) in Grenoble, France who solved its high resolution structure by NMR spectroscopy (Fig. 3.2 B). The structure confirmed that LpoB possesses areas of flexibility suggested by AUC (3.1.2), with a long flexible, unstructured N-terminal region spanning 52 amino acid residues (between Val21 and Pro73). Theoretically this region could maximally stretch to 145 Å. The globular domain (His74 to Gln213) features both α-helical and β-sheet structures, with a three stranded anti-parallel β-sheet flanked by a short two stranded parallel sheet and four α-helices. The three stranded β-sheet of the globular domain has a large positively charged patch on the surface of the protein (Fig. 3.2 C), which contains residues conserved across 68 distinct LpoB sequences (Fig. 3.2 D) which may be the region of its interaction with PBP1B (see 3.1.7).

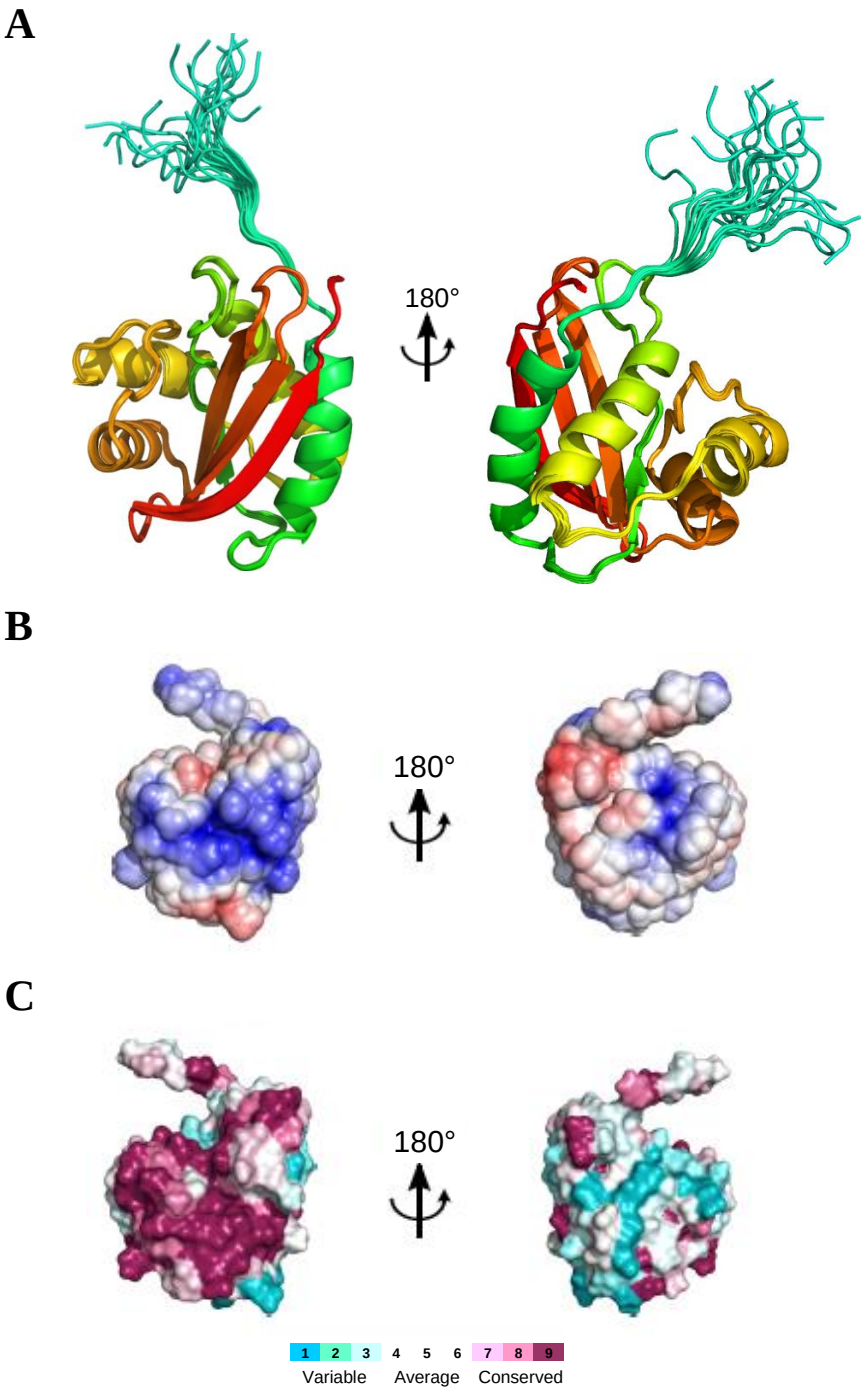

Figure 3.2 Structure of LpoB(sol) solved by NMR spectroscopy

(A) Ribbon representation of the structure of LpoB(sol) shown from residue T52 for clarity.
(B) Electrostatic surface representation of LpoB globular domain, with positively charged residues shown in blue, and negatively charged residues in red.
(C) Surface representation of LpoB globular domain showing conservation of residues indicated by the colour code below.
Images provided by Jean-Pierre Simorre.

3.1.4 A screen for novel interaction partners of LpoB found none

This work was done with the assistance of a Masters student, Jad Sassine. The proteomic approach described in 2.4.4 was used to screen for interaction partners of LpoB, using immobilised LpoB(sol) to pull-down binding protein(s) from *E. coli* membrane extract. Table 3.1 shows the top 5 hits from MALDI-PMF mass spectrometry analysis of eluted proteins performed by Dr. Joe Grey at Newcastle University's Pinnacle facility. The top hit was LpoB, which is to be expected due to bleeding of the immobilised protein from the bead matrix. The second and third hits were the cytoplasmic transcriptional activator Cap/Crp complex. Given the OM localisation of LpoB it is unlikely it interacts with a cytoplasmic protein complex, therefore these were disregarded. The fourth hit was a hypothetical protein (HMPREF9536_05050) from *E. coli* MS84-1. This was also likely non-specific as it is from a different strain than that used to prepare the membrane extract. To confirm this a BLAST analysis of the peptide was performed (blastp of pepide INGIAR), which gave putative fimbrial proteins from various *E. coli* strains. The fifth hit was PBP1B, which is expected as it is known to interact with LpoB. No other significant hits were found, simply abundant cytoplasmic proteins such as ribosomal subunits, transcriptional activators and stress/repair proteins. These data indicate that LpoB only has one main binding partner, its cognate PG synthase PBP1B, in the cell detectable by this method. However, this result does not rule-out the existence of other weak interactions in the cell.

Table 3.1 Top 5 hits from MALDI-PMF analysis

Hit Number	Name
1	Penicillin-binding protein activator **[LpoB]**
2	Catabolite Gene Activator Protein **[Cap]**
3	cAMP receptor protein **[Crp]**
4	Hypothetical protein HMPREF9536_05050 [*Escherichia coli* MS 84-1] (Putative fimbrial protein)
5	Penicillin-binding protein 1B **[PBP1B]**

Data collection performed by Dr. Joe Gray, analysis performed by Jad Sassine and myself.

3.1.5 Kinetic characterisation of the PBP1B-LpoB interaction

A kinetic characterisation of the interaction between PBP1B and LpoB was carried out using surface plasmon resonance (SPR) as detailed in section 2.4.8. PBP1B was immobilised to the sensorchip surface by binding to immobilised ampicillin, ensuring PBP1B molecules are orientated in the same way. Any remaining, free ampicillin was digested with β-lactamase and the surface was washed with 1 M NaCl to dissociate any PBP1B dimers. A control surface was prepared in the same way, without immobilisation of PBP1B. LpoB(sol) at concentrations of 0.5, 1, 2, 3 and 4 μM was injected over the PBP1B and control surfaces to produce SPR curves (response units against time). The interaction was observed, with on/off rates too rapid for determination of k_a/k_d as indicated by the immediate increase and decrease in response upon injection of LpoB(sol) and switch back to running buffer, respectively (Fig. 3.3 A). The dissociation constant (K_D) of the interaction was determined using a Scratchard plot. The response at equilibrium (R_{eq}) was calculated using the associated software for each of the concentrations of LpoB(sol) injected minus the response signal from the control surface. R_{eq} was then plotted against R_{eq} divided by the concentration of analyte injected in μM (R_{eq}/C). The slope of the line produced from this plot is $-K_D^{-1}$ (Fig. 3.3 B). For the interaction of PBP1B-LpoB a K_D of 0.81 ± 0.08 μM was determined (n = 3).

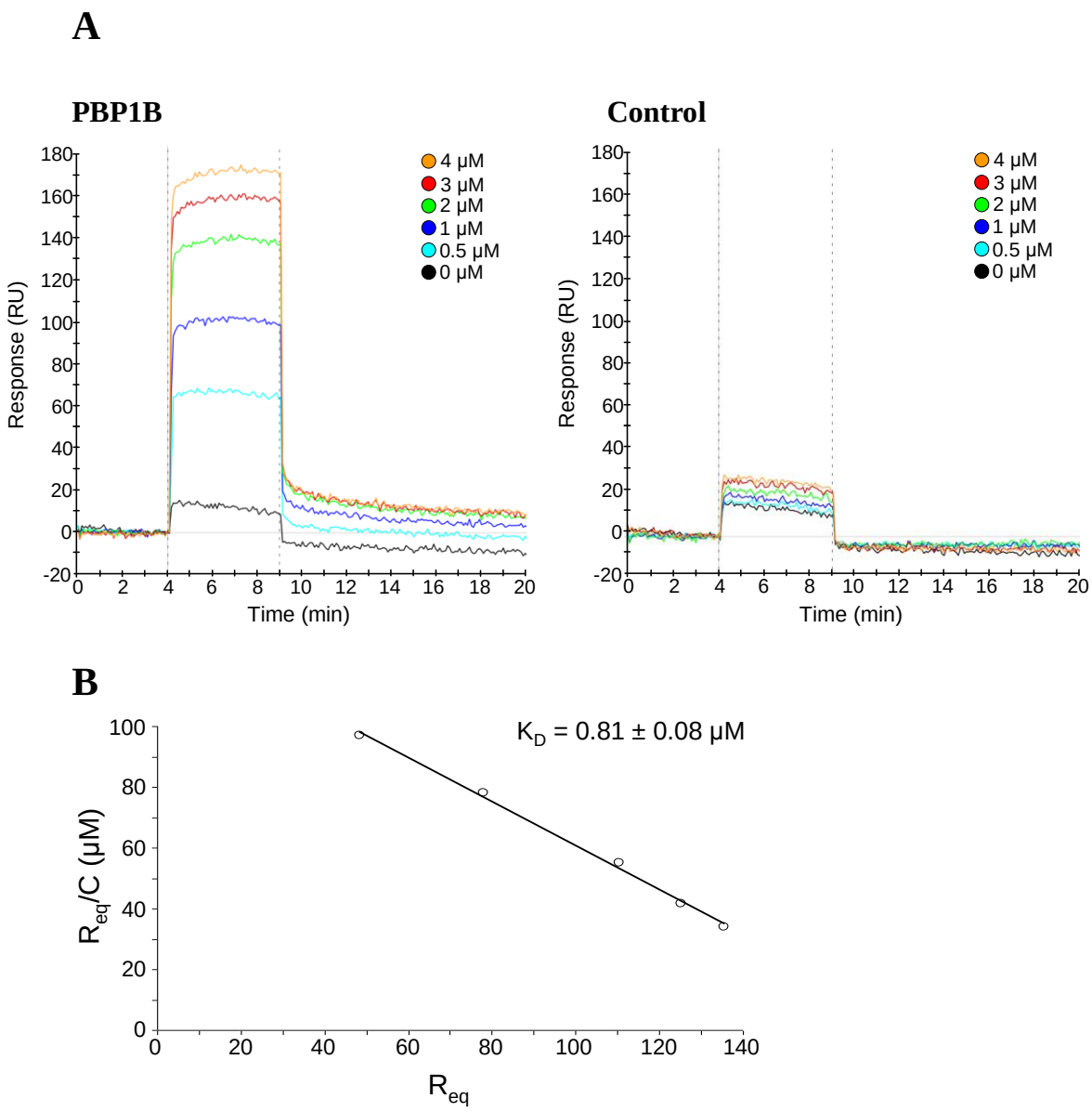

Figure 3.3 Interaction of LpoB(sol) with PBP1B by SPR

(A) SPR curves (response against time) of LpoB(sol) injected over PBP1B and control surfaces. At 4 min LpoB was injected in running buffer at the concentrations shown for 5 min, followed by a return to running buffer. The flow rate was 75 µl/min.
(B) Scratchard plot of PBP1B-LpoB interaction. Response at binding equilibrium (R_{eq}) of 3 replicates was used to determine the K_D of interaction by plotting the R_{eq}/C (where C is the analyte concentration) against R_{eq}. The slope of the linear regression is $-K_D^{-1}$.

3.1.6 LpoB shows no interaction with FtsN or PBP3 in SPR

Affinity chromatography showed that FtsN and PBP3 were weakly retained by LpoB immobilised to Sepharose beads and incubated with membrane extract derived from *E. coli* MC1061 (2.4.3) (Manuel Banzhaf, Newcastle University). Whether these are direct interactions or the result of their participation in a multiprotein complex consisting of LpoB and PBP1B was investigated using SPR. PBP1B or PBP3 were immobilised via ampicillin, and FtsN immobilised by general amine coupling. The control surface consisted of ampicillin digested by β-lactamase. LpoB(sol) bound to the PBP1B surface but not to the PBP3, FtsN or control surfaces (Fig. 3.4), Therefore the retention of FtsN and PBP3 by LpoB-sepharose is likely indirect via PBP1B.

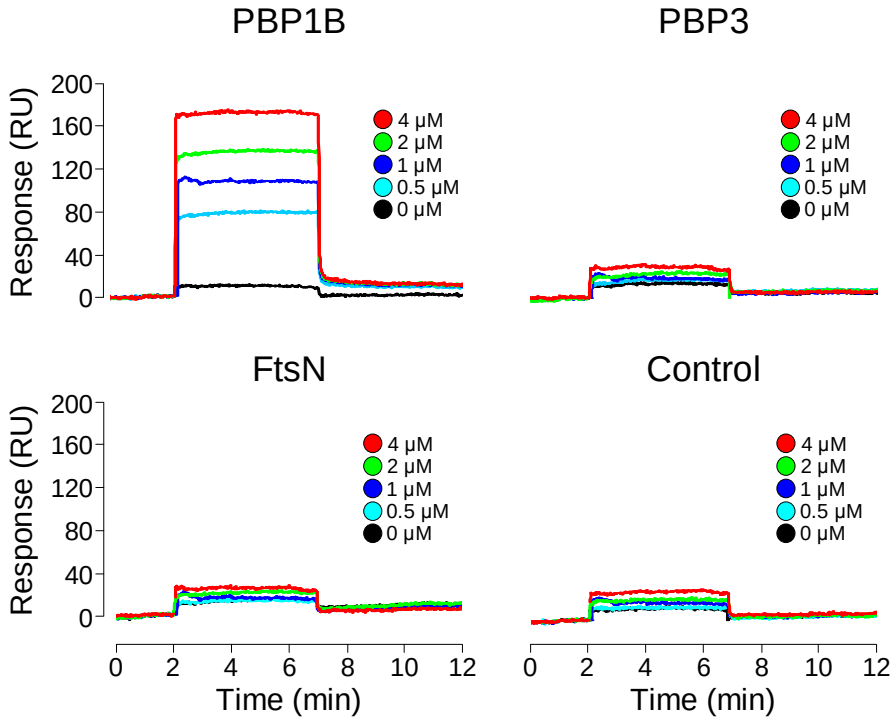

Figure 3.4 LpoB does not interact with PBP3 or FtsN

SPR curves (response against time) of LpoB(sol) injected over PBP1B and control surfaces. At 2 min LpoB was injected in running buffer at the concentrations shown for 5 min, followed by a return to running buffer. The flow rate was 75 µl/min. No change in response seen for control, PBP3 or FtsN surfaces.

3.1.7 LpoB interacts with the UB2H domain of PBP1B

The activators of PG synthesis LpoA and LpoB co-occur in the γ-proteobacteria and enterobacteria, respectively, with small non-catalytic domains in their cognate PBP. ODD in PBP1A and UB2H in PBP1B (27). LpoB does not interact with a version of PBP1B lacking its UB2H domain in the cell (27). This however required confirmation as there are other possible explanations why this result *in vivo* was negative, for example a lack of proper protein folding and/or stability of PBP1BΔUB2H. We therefore tested for a direct interaction between LpoB and the isolated UB2H domain. We optimised a procedure for the overproduction and purification of His-UB2H (2.3.5). Using an analytical SEC assay (2.4.1) with a Superdex75 column His-LpoB(sol) (250 μM) and His-UB2H (330 μM) were resolved alone and in combination. A shift in the elution volume of UB2H was seen in the presence of His-LpoB(sol) which was not seen in the presence of His-LpoA(sol) (250 μM) (Fig. 3.5). The LpoB-UB2H co-elution peak had an apparent MW of ~49.1 kDa; LpoB alone,~39.8 kDa; and UB2H alone ~21.3 kDa. However, due to the abnormal migration behaviour of LpoB in SEC (3.1.2) the stoichiometry of this interaction could not be determined by this method. Section 3.1.2 presents evidence against the homodimerisation of LpoB indicating that the peak at 39.8 kDa is produced by monomeric LpoB (due to the difference in the pore matrix, Superdex200 and Superdex75 columns give slightly different apparent MWs of the same proteins). His-UB2H alone elutes at the approximate MW of a dimer, its calculated MW is 13.5 kDa. We therefore tested the effect of high ionic strength on His-UB2H in SEC. Fig. 3.6 shows the result of this experiment, a minor peak with an apparent MW of ~12.4 kDa appeared at 1 M NaCl, suggesting that UB2H does indeed form homodimers *in vitro* that were partially disrupted by high NaCl concentration.

Of note is the requirement of a high salt pre-incubation step in the procedure (2.4.1) without which the interaction between LpoB and UB2H is not seen in SEC. We hypothesise that this step is necessary to disrupt non LpoB-interacting UB2H homodimers present in the stored sample, which contained only 500 mM NaCl which is not sufficient to disrupt dimerisation of His-UB2H (Fig. 3.6). The necessity for the high salt incubation to see the complex, and the fact that the apparent MW of the complex is roughly the sum of the proteins alone in SEC, are consistent with a stoichiometry of 1:1.

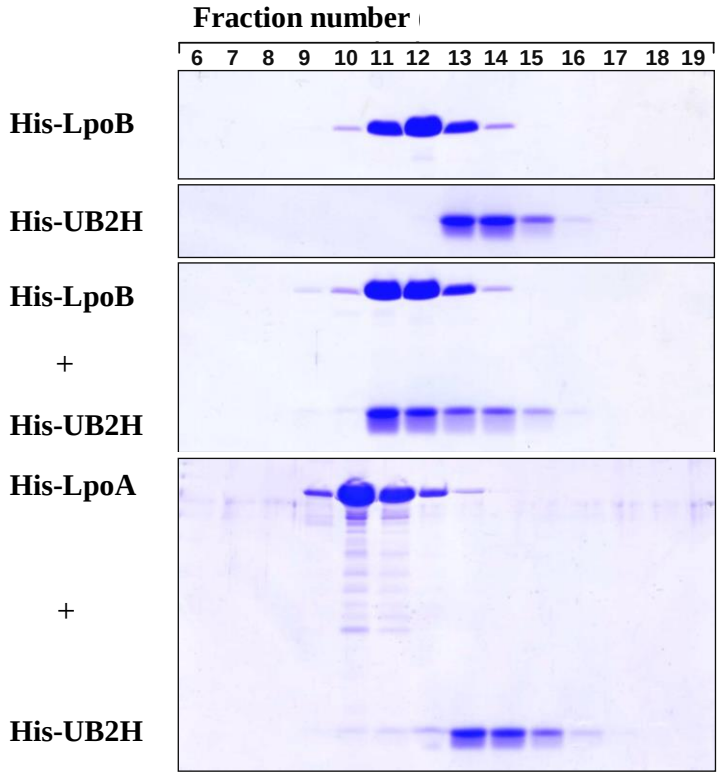

Figure 3.5 His-LpoB and His-UB2H form a complex resolvable by SEC

Coomassie-stained SDS-PAGE gel of samples from 1 ml fractions collected during SEC of His-LpoB(sol), His-UB2H, His-LpoB(sol) and His-UB2H or His-LpoA(sol) and UB2H. His-UB2H alone eluted in fractions 13, 14 and 15. In the presence of LpoB the majority of UB2H eluted earlier, in fractions 11 and 12, together with LpoB. This shift is not seen when His-LpoA(sol) was present.

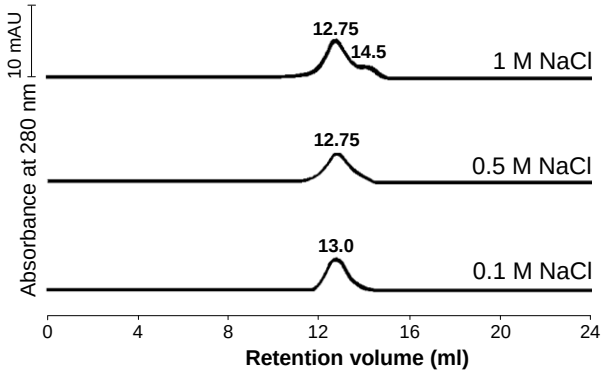

Figure 3.6 His-UB2H forms dimers *in vitro* which are partially disrupted by high NaCl concentration

Chromatograms of His-UB2H (130 µM) resolved in buffers of increasing ionic strength in a 24 ml Superdex75 column. Retention volumes are shown above each peak in ml. Buffers used were 10 mM Tris/HCl, 10 mM $MgCl_2$, pH 7.5 and either 0.1, 0.5 or 1 M NaCl. The major peak was calculated to be 21.8 ± 0.6 kDa, which persists at all conditions. However, at 1 M NaCl a new minor peak appears with a MW of ~12.4 kDa, consistent with a monomer of His-UB2H (the calculated MW of His-UB2H is 13.5 kDa).

Next, the interaction between LpoB and UB2H was investigated by NMR spectroscopy following on from the determination of the structure of LpoB (3.1.3). Using the same sample preparation method and buffer conditions as for SEC, His-UB2H was added to [^{13}C,^{15}N]-LpoB(sol). The sample was then sent to our collaborators at the IBS, Grenoble. [^{1}H,^{15}N]-BEST-TROSY-HSQC spectra of [^{13}C,^{15}N]-LpoB(sol) alone and in the presence of His-UB2H were recorded by Nicholas Jean and Catherine Bougault. They identified chemical shift perturbations in 42 residues, which were mapped on to the surface of LpoB and found to concentrate on the conserved region shown in figure 3.2. These data were further refined, reducing the number of potential residues using the "HADDOCK web server for data-driven biomolecular docking" which also generated potential participating residues of UB2H. With this information, Alexandra Koumoutsi of the EMBL, Heidelberg constructed a number of plasmids encoding LpoB and PBP1B versions with single or multiple alanine substitutions of these residues for phenotypic testing and also overproduction and purification. Several residues that had been implicated in the chemical shift perturbation measurement were discounted as they had no effect on the survival of cells carrying the version in the absence of the native copy and PBP1A. Additionally, a more subtle test of cellular fitness was used, in which cells were grown in the presence of the PBP1A and PBP1B specific inhibitor cefsulodin (to which PBP1A is more sensitive). Some PBP1B and LpoB versions carrying single, double or multiple substitutions showed various degrees of impact on cellular fitness in this assay. These include; D163, E166, E187, N188, R190 and Q191 in PBP1B and D106, N110, R111, Y178, and M195 in LpoB. Four versions of PBP1B carrying combinations of these substitutions were purified for interaction studies. PBP1B; E166A, D163A/E166A, E187A/N188A/R190A/Q191A and D163A/E166A/E187A/N188A/R190A/Q191A. Additionally three versions of LpoB were also purified for testing, LpoB(sol); D106A/M195A, N110A/R111A and Y178A.

The K_D of interaction of PBP1B and LpoB versions was determined using SPR as previously described (3.1.5), with PBP1B versions immobilised to a GLC sensorchip surface via ampicillin and LpoB(sol) versions injected at various concentration ranges (0, 0.5, 1, 2, 3 and 4 µM; 0, 2, 4, 8, 12, 16 µM; and 0, 5, 10, 20, 30 and 40 µM) (Fig. 3.7) (Fig. 3.7). The PBP1B version with substitutions in all six residues showed the strongest phenotype and had a severe impairment of the physical interaction with LpoB with a 50-fold increase in K_D. Though residues D163 and E166 gave phenotypes, substitution of these alone has the smallest impact on interaction with LpoB. However, the PBP1B version possessing these residues but with substitution of the other four,

while severely impaired, is fitter (in terms of cellular fitness) and has a stronger interaction with LpoB than the mutant lacking all 6 residues. Thus, the role of all 6 residues in the interaction of PBP1B and LpoB was validated. In LpoB, a double substitution of D106 and M195 caused the greatest loss in cellular fitness, and causes a 9.9-fold increase in K_D. The substitution of residues N110 and R111 also impaired cellular fitness and interaction affinity, but to a slightly lesser degree with a 4.8-fold increase in K_D. An Ala substitution of Y178 LpoB causes the largest decrease in affinity, a 23.6-fold increase in K_D. Interestingly, this impact is not mirrored by cellular fitness compared to the other residues tested. The *in vitro* biochemical data presented here were collated along with that from the phenotypic and NMR experiments and used to generate a final interaction interface in HADDOCK by Jean-Pierre Simorre (Fig. 3.8).

Versions of LpoB with a truncated or missing N-terminal linker region, LpoBΔ1-56 and LpoBΔ1-73, were also purified for interaction studies. *In vivo*, OM localised version of LpoB with these truncations (LpoBΔ23-56 and LpoBΔ23-73) were unable to support the growth of cells in the absence of the wild-type copies of LpoB and PBP1A. However, the partial or complete loss of the flexible N-terminal region had no impact on the interaction with PBP1B. Both LpoBΔ1-56 and LpoBΔ1-73 interacted with PBP1B with a similar K_D value to the wild type version of 0.71 ± 0.08 µM and 0.73 ± 0.16 µM, respectively.

The effect of the substitutions / truncations described in this section on the ability of LpoB to stimulate the activities of PBP1B is described later in this work (section 3.2.3).

A

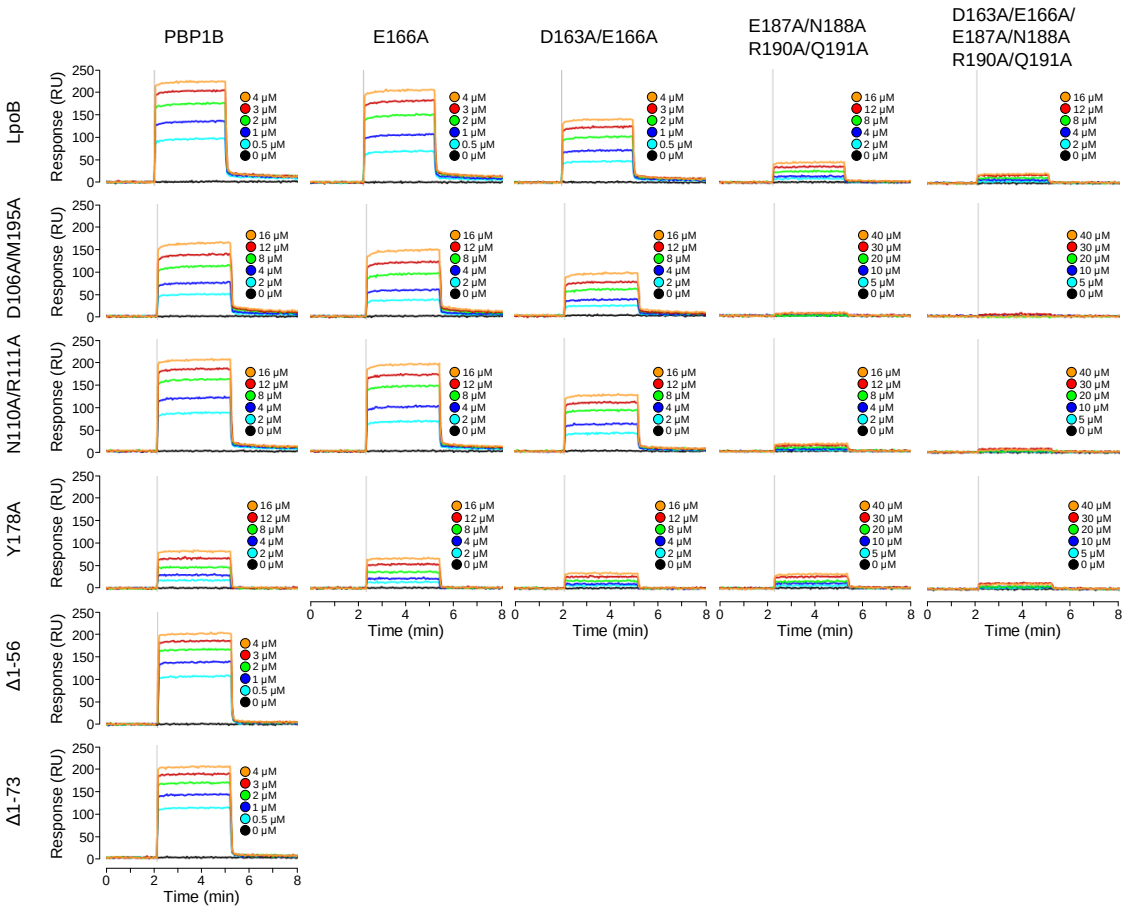

B

	PBP1B	E166A	D163A E166A	E187A N188A R190A Q191A	D163A E166A E187A N188A R190A Q191A
LpoB	0.81 ± 0.08	1.41 ± 0.05	1.43 ± 0.04	27.7 ± 5.81	40.5 ± 1.63
D106A M195A	8.01 ± 0.30	12.6 ± 0.39	6.05 ± 0.12	n.b.	n.b.
N110A R111A	3.90 ± 0.12	14.1 ± 0.15	7.01 ± 0.03	34.2 ± 0.33	n.b.
Y178A	19.1 ± 0.32	28.0 ± 0.54	43.0 ± 5.14	70.7 ± 0.35	n.b.
LpoBΔ1-56	0.71 ± 0.08				
LpoBΔ1-73	0.73 ± 0.16				

Figure 3.7 Interactions between PBP1B and LpoB versions assayed by SPR

(A) Representative SPR sensorgrams of LpoB versions (indicated to the left) injected over immobilised PBP1B versions (indicated above). The concentrations of LpoB versions are shown next to each sensorgram.
(B) Dissociation constants (K_D values) in µM determined by SPR. Values are the mean ± SD of 3 independent experiments, n.b., insufficient binding for calculation of K_D.

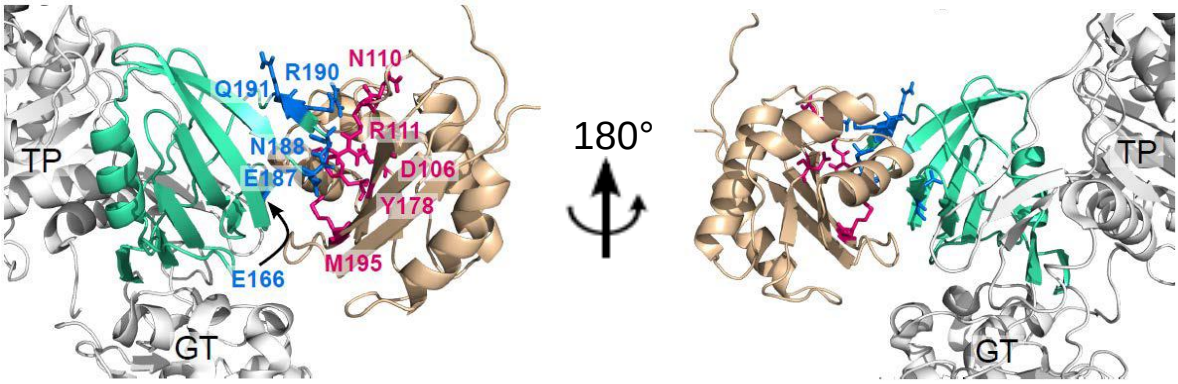

Figure 3.8 The interaction interface of PBP1B and LpoB

Final HADDOCK model of the LpoB-PBP1B interaction interface after collation of NMR, phenotypic, and biochemical (interaction) data (Fig. 3.7). The structures are shown as ribbons with UB2H in green and LpoB in wheat. The TP and GT domains of PBP1B are also partially shown (in grey). Residues in UB2H and LpoB participating in the interaction are shown in stick format in blue and magenta, respectively. This figure was provided by Jean-Pierre Simorre.

3.1.8 Conclusions and discussion

The biochemical and structural characterisation of LpoB in this section reveals a protein which likely acts as a monomer in the cell, reaching from the OM via a long flexible unstructured linker region. Loss of this region did not compromise its ability to interact with PBP1B *in vitro* but impaired *in vivo* functionality, as cells expressing OM anchored versions of LpoB either completely lacking this linker (LpoBΔ23-73), or with a significant truncation (LpoBΔ23-56) cannot fully complement a deletion of *lpoB* (results communicated by Alexandra Koumoutsi), suggesting that this linker is required for the globular domain of LpoB to span the distance from the OM to PBP1B. The structure also showed that the size of the globular domain of LpoB is no wider than 30 Å, and can fit through pores in the PG sacculus, which were calculated to range from 40 to 60 Å depending on the turgor (198, 199).

Interestingly, LpoB has structural similarity to the N-terminal domain of TolB (TolB_N, see (184)). This was observed by Jean-Pierre Simorre using the Dali server (200), which also identified similarity with a lipoprotein of unknown function from *Neisseria meningitidis*, GNA1162 (201). LpoB has the inverse orientation to TolB_N, with α-helix 1 of LpoB corresponding to the last α-helix of TolB_N. LpoB also lacks the motif with which TolB interacts with TolA, the so-called 'TolA box' (see section 1.4.2.3). This similarity may point to a link between PBP1B-LpoB and the Tol-Pal complex, with overlapping and/or interlinked functions during cell division. This was therefore investigated in section 3.3 of this work.

An attempt to find novel protein-protein interaction partners of LpoB through a proteomic approach yielded only one significant hit, its cognate PG synthase PBP1B, suggesting it may be the only binding partner of LpoB in the cell. However, this result does not rule out the existence of other, weaker interactions of LpoB.

The dissociation constant (K_D) of the interaction between PBP1B and LpoB was determined to be 0.8 µM by SPR. This value is within a similar range of other known interaction partners of PBP1B, of which the K_D was also determined by SPR (PBP1B-PBP1B, 0.13 µM (53); PBP1B-PBP3, 0.4 µM (67)). Also using SPR, LpoB was found to show no direct interaction with FtsN or PBP3 immobilised to the chip surface. These data suggest that the retention of FtsN and PBP3 from *E. coli* membrane extract by LpoB-sepharose is indirect, via PBP1B. This observation suggests that LpoB, FtsN and PBP3 are able to interact with PBP1B simultaneously to form a multiprotein complex.

This is in agreement with the multiprotein complexes hypothesis for PG synthesis and is explored further in section 3.2 of this work.

The observation that LpoB no longer interacts with a version of PBP1B lacking the UB2H domain in the cell by Typas *et al.* (27) was built upon in this work. Here we purified isolated UB2H to show a direct interaction with LpoB by SEC and chemical shift perturbation assays (NMR spectroscopy). The specific residues involved were determined to be D163, E166, E187, N188, R190 and Q191 in PBP1B, and D106, N110, R111, Y178 and M195 in LpoB. These residues in LpoB map to the conserved positively charged patch on the three-stranded β-sheet. Thus, these data indicate that PBP1B and LpoB interact through a large interface that involves several amino acids in both proteins.

3.2 Regulation of class A PBPs involved in cell division

3.2.1 Introduction

In recent years genetic and biochemical data has built up the evidence for multi-protein complexes for the synthesis of the bacterial cell wall peptidoglycan, the elongosome and the divisome (see 1.4). Yet, the molecular mechanisms of how these proposed complexes achieve their functions and, importantly, how PG synthases are regulated within them remain unclear.

Section 3.1 explored the biochemical and structural properties of LpoB, an activator of the major synthase active during cell division PBP1B. In the course of this work the interaction interface between the two proteins was elucidated. In this section, the effect of this interaction on the PG synthesis activities of PBP1B and possible mechanisms of activation were explored. Typas *et al.* and Paradis-Blau *et al.* showed that LpoA and LpoB both stimulated the TPase activity of their cognate synthase (27, 28) and that LpoB has a minor effect on the GTase activity of PBP1B (28). Here, we optimised an established continuous GTase assay to measure the effect of binding partners on the class A PBPs, which was previously not possible by this assay. The effect of PBP3 and FtsN, both essential for cell division in *E. coli*, as well as LpoB on PBP1B activity was tested. Further to section 3.1.7 the effect of Ala substitutions in the PBP1B-LpoB interaction interface on the activation of the synthase was investigated. Also, the effect of PBP2 and LpoA on the GTase activity of PBP1A was tested, as PBP1A is redundant with PBP1B in the cell and thus can be active during cell division. The scheme of the continuous fluorescence GTase activity assay and the *in vitro* PG synthesis (TPase) assay used in this section are outlined below (Fig. 3.9).

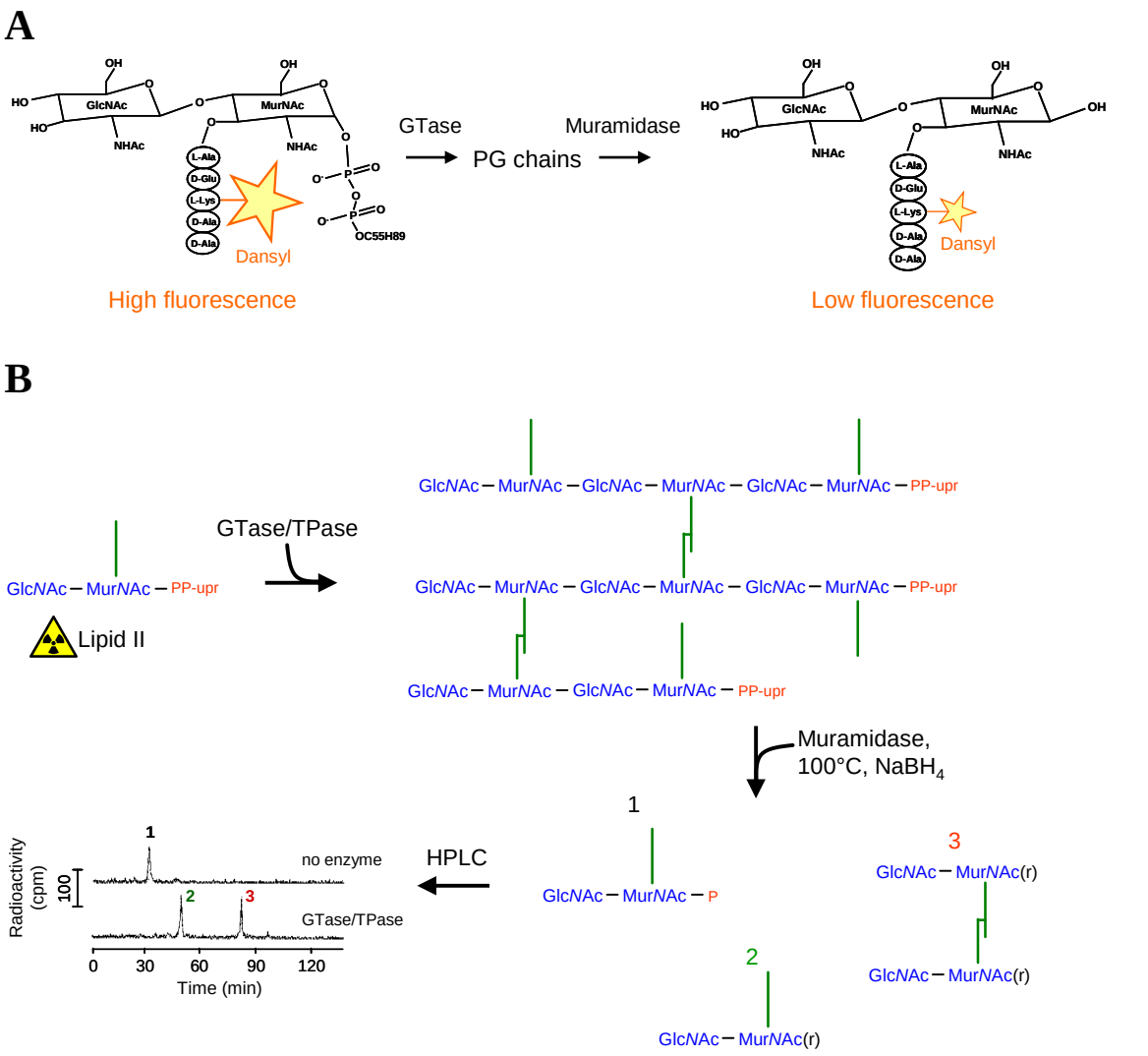

Figure 3.9 General scheme of PG synthesis activity assays used in this work

(A) Continuous fluorescence GTase activity assay. The PG substrate lipid II is modified with a fluorescent Dansyl moiety at the 3rd residue (Lys) of the pentapeptide stem. The polymerisation of this substrate into glycan chains results in the loss of the lipid moiety (see Fig. 1.2) altering the environment of the dansyl group, and leading to a decrease in fluorescence which is measured over the course of 20 min in a plate reader with fluorescence detection. The modified lipid II substrate was provided by Eefjan Breukink. (B) *In vitro* PG synthesis assay. PG synthases are incubated with radioactive lipid II substrate (m-Dap version) in the presence or absence of binding partner(s). The resulting PG is boiled to remove the lipid moiety, digested with muramidase (cellosyl) and the resulting muropeptides are reduced with sodium borohydrate and the products (here; 1, 2 and 3) are separated by HPLC. All muropeptides detected in this work are shown in Fig. 2.12. The percentage of peptides in cross-links, resulting from TPase activity, is calculated as 100% - the % of monomeric (uncross-linked) muropeptides. Glc*N*Ac, *N*-acetylglucosamine; Mur*N*Ac, *N*-acetylmuramic acid; Green lines, peptide stems; *P*, Phosphate; upr, undecaprenol pyrophosphate. The [^{14}C]-lipid II substrate was provided by Eefjan Breukink.

3.2.2 Optimisation of the continuous fluorescence GTase assay

The *in vitro* PG synthesis assay established by Born *et al.* (50) provides good insights into the activity of PG synthases. However, one limitation as that it is an end-point measurement, and thus yields no information about the rate of the two reactions. Particularly, monitoring the GTase activity is laborious by this method, and not practical for many samples. For this work the continuous fluorescence assay first described by Schwartz *et al.* (194) and modified by Offant *et al.* (195) was optimised further to allow for the assessment of the effect of binding partners on the GTase activity of PBP1A and PBP1B. The optimisation was carried out during a two week visit to the laboratory of Dr. André Zapun at the IBS, Grenoble. The assay was then set up at the CBCB in Newcastle for continued experimentation. The reaction conditions previously contained a high concentration of DMSO (25%). We reasoned that this high DMSO concentration may negatively impact protein-protein interactions. Indeed, the presence of DMSO prevented the interaction between PBP1B and LpoB (Fig. 3.10 A) and furthermore caused aggregation of PBP1B (Fig 3.10 B). Consequently DMSO was removed from the reaction conditions.

However, the removal of DMSO caused new issues with the optimisation. Without DMSO in the reaction little to no GTase activity was observable at the concentration of detergent used (0.2% Triton X-100). Therefore, the next step of optimisation was to find the optimum concentration of Triton X-100 detergent. Fig. 3.10 C shows reactions using PBP1B (1 µM) with 0.2% and 0.08% Triton X-100 in the presence or absence of 25% DMSO. In the presence of 0.2% Triton, PBP1B is poorly active but its activity was rescued by the presence of DMSO, which is interesting considering 25% DMSO causes aggregation of PBP1B. Fortunately, the GTase activity of PBP1B was observable in the presence of 0.08% Triton. Reactions were also performed from 0.04 to 0.125% Triton (0.04% being the minimum possible at the time, as it was present in the enzyme storage buffer). In this series a clear negative impact of increased Triton concentration was seen, but in each case PBP1B activity was still observable (appendix Fig. 5.5). Therefore, the Triton X-100 concentration in series of samples was carefully adjusted, particularly when binding partners with Triton X-100 in their storage buffer (e.g. PBP3 and FtsN) were tested. Different binding partners confer different amounts of Triton X-100, some conferring none. Therefore, in the following sections the concentration differs between experiments but is always the same within a series of samples and is given in the legends of each figure.

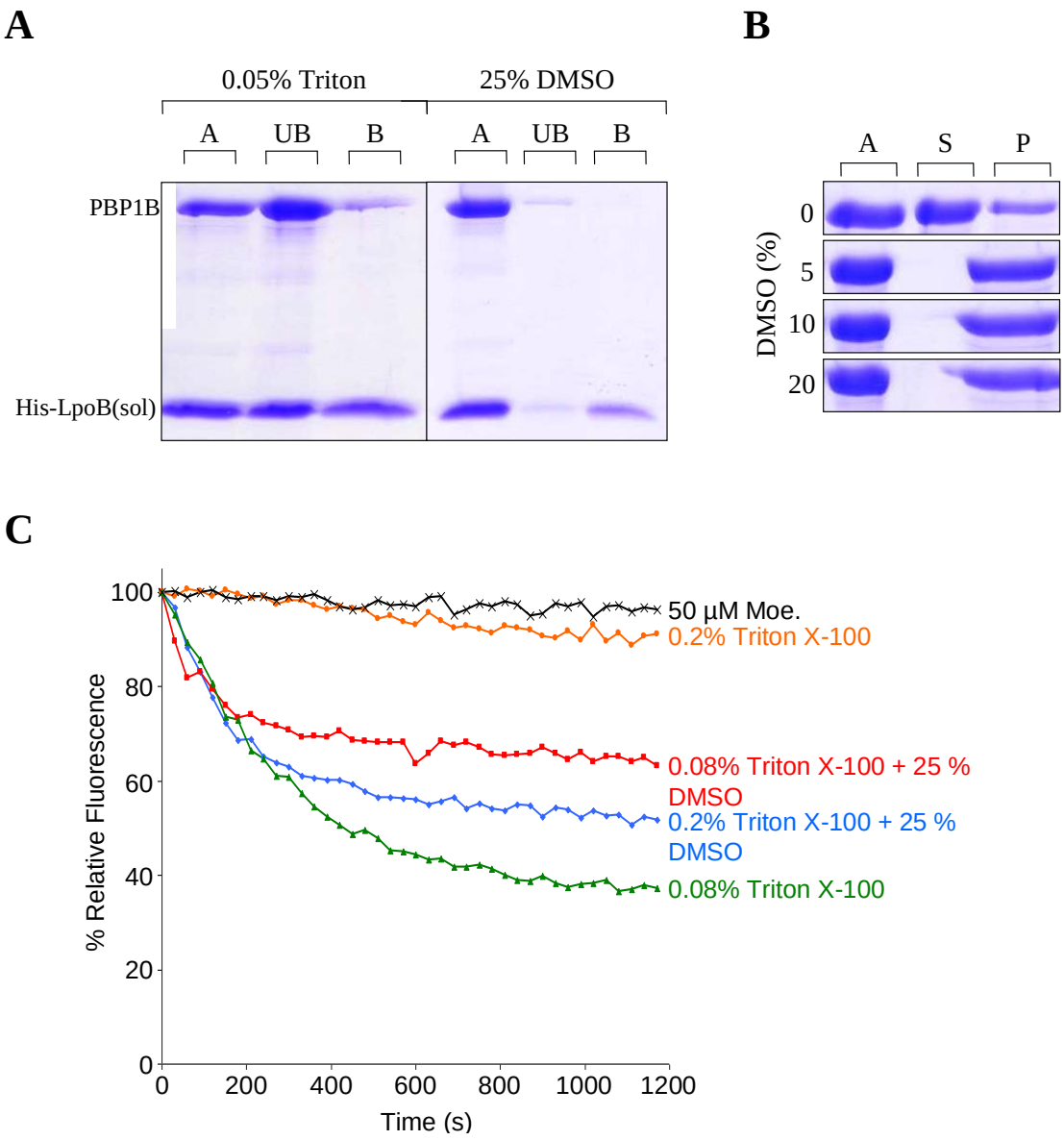

Figure 3.10 Optimisation of the continuous fluorescence GTase assay

(A) Coomassie-stained SDS-PAGE gel of an *in vitro* pulldown experiment using His-LpoB(sol) (2 µM) and PBP1B (1 µM). The procedure was as described (2.5.10) without the use of cross-linker. The presence of 25% DMSO prevented binding of PBP1B to His-LpoB(sol). A, applied sample; UB, unbound protein; B, bound protein.
(B) Coomassie-stained SDS-PAGE gel of PBP1B samples (20 µg in 300 µl, ~0.7 µM) subjected to ultracentrifugation (30 min at 470,000 × *g*) in buffers with 0, 5, 10 or 20% DMSO. The GTase assay standard buffer conditions were used with a Triton X-100 concentration of 0.05%. The samples were kept at 30°C. A, applied; S, supernatant; P, pellet resuspended in 300 µl 5% SDS. PBP1B is aggregated by DMSO at 5, 10 and 20% concentrations as shown by its absence from the supernatant and appearance in the pellet.
(C) The GTase rate of PBP1B (1 µM) was tested at 0.08% and 0.2% Triton X-100 in the presence and absence of 25% DMSO. Each curve is the relative fluorescence, taking the fluorescence at time 0 as 100%, plotted against time (s). The rate of reaction was decreased at high Triton X-100 concentration (0.2%). Addition of DMSO rescues activity at high Triton X-100 concentration. In this assay, optimum activity was seen at low Triton X-100 concentration (0.08%). Addition of moenomycin (Moe.) blocks GTase activity as expected.

3.2.3 LpoB stimulates the GTase activity of PBP1B

With the GTase assay optimised the effect of LpoB on PBP1B activity was investigated. It was previously shown that LpoB has a mild stimulatory effect on PBP1B GTase activity, increasing it 1.5-fold (28). In fact, this work shows that LpoB has a significantly greater effect than previously reported. The presence of LpoB increased the maximal GTase reaction rate 8.0 ± 0.9-fold (Fig. 3.11). As expected, the non-cognate LpoA has no effect on PBP1B GTase.

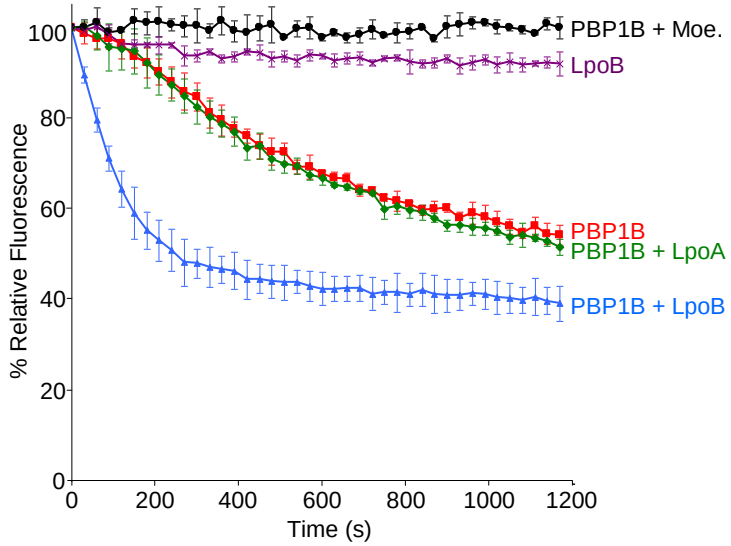

Figure 3.11 LpoB stimulates the GTase activity of PBP1B

GTase reactions of PBP1B (0.5 µM) alone and in the presence of LpoA(sol) (1.5 µM), LpoB (sol) (1.5 µM) or moenomycin (50 µM), and of LpoB(sol) alone. The Triton X-100 concentration was 0.04%. LpoB stimulated the rate of reaction 8.0 ± 0.9-fold (n = 4). LpoA had no effect on PBP1B, and LpoB alone had no effect on the substrate.

The effect of several Ala substitutions in PBP1B and LpoB and also of truncating the long, flexible N-terminal region of LpoB on the K_D of interaction was investigated in this work (3.1.7). The effect of these same substitution / truncation versions on the stimulation of PBP1B was also tested by GTase and TPase assays. The PBP1B versions (PBP1B; E166A, D163A/E166A, N187A/E188A/R190A/Q191A, and D163A/E166A/N187A/E188A/R190A/Q191A) are as active as the native version in both GTase and TPase assays (Fig. 3.12). The effect of native LpoB(sol) on the PBP1B Ala substitution versions mirrored the effect on the K_D of interaction. Substitution of D163 and E166 in PBP1B had a minor effect on its stimulation, and the multiple substitutions were severely impaired with the 6 residue substitution near-insensitive to stimulation (Fig 3.12). The effects on both GTase and TPase activities are similar,

consistent with the fact that PBP1B acts processively and that the GTase and TPase domains are coupled (53). The effect of the Ala substitutions in LpoB (LpoB(sol); D106A/M195A, N110A/R111A and Y178A) on its ability to stimulate PBP1B also mirrored the effect seen on K_D with the exception of LpoB Y178A. Of the LpoB versions, Y178A had the highest K_D of interaction with PBP1B, but has the least impact on its stimulation *in vitro* and has the least impact on cellular fitness. We would expect that such an impairment of interaction would impair the stimulation of PBP1B also. The reason for this unexplained result is unknown. The effect of D106A/M195A was more severe than N110A/R11A, which was more severe than Y178A. Again, the GTase and TPase activities were affected in similar ways. The truncation (LpoBΔ1-56) or loss (LpoBΔ1-73) of the N-terminal region had no effect on the ability of LpoB to stimulate PBP1B, which is consistent with the fact that its loss had no effect on the interaction.

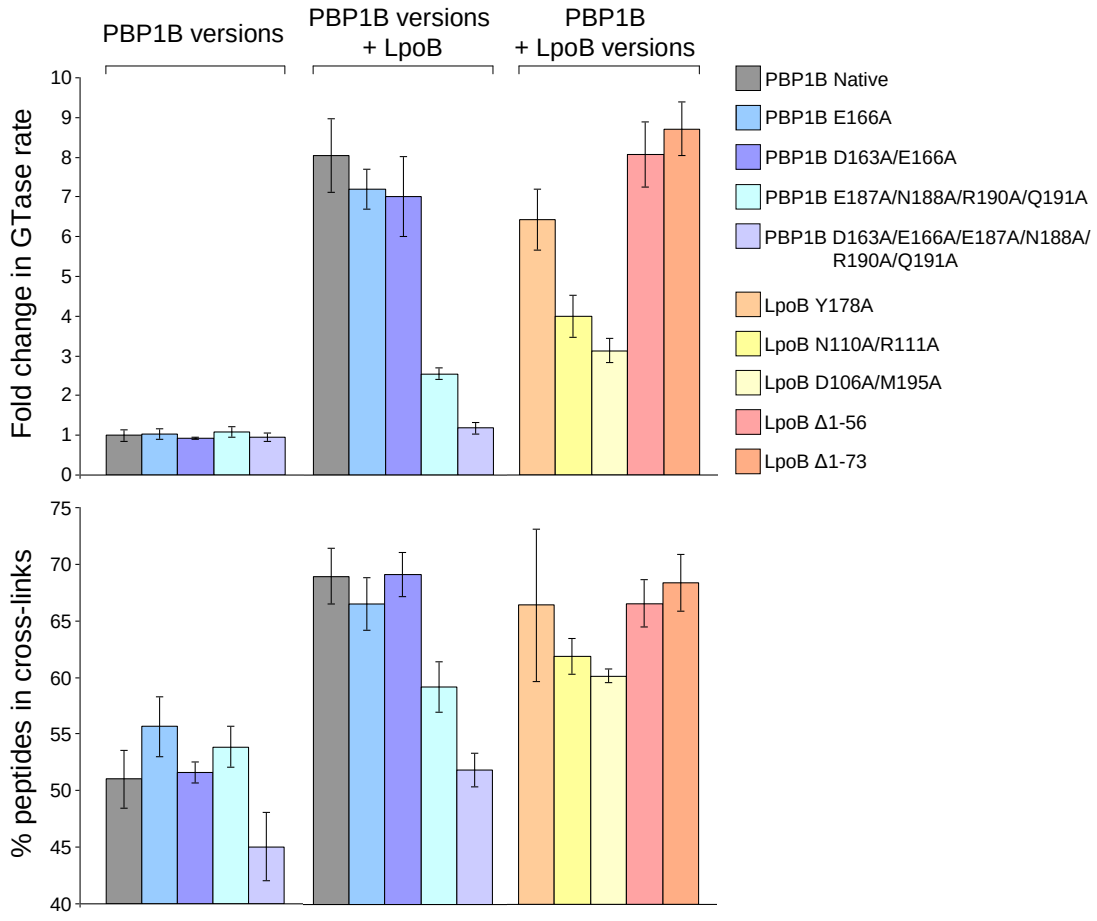

Figure 3.12 Effect of Ala substitutions and N-terminal truncations on the stimulation of PBP1B activity

The GTase and TPase activities of PBP1B versions in the presence or absence of LpoB versions are represented as the fold change in rate (GTase) compared to the mean rate of PBP1B alone and percentage of peptides in cross-links (TPase). Data for both activities are the mean ± SD (n = 3 – 6).

3.2.4 LpoB is able to restore GTase activity of PBP1B at low pH

The GTase activity of PBP1B requires the glutamate residue at position 233 to deprotonate the Glc*N*Ac 4-OH of lipid II (36). In order to carry out this catalysis Glu233 itself needs to be deprotonated, and the reaction is therefore slowed down at low pH. In order to gain insights into the stimulatory mechanism of LpoB its effect on PBP1B at low pH conditions was tested. GTase reactions of PBP1B (0.5 µM) at pH 7.5, 5.0 and 4.5 were conducted in parallel with and without LpoB(sol) (1 µM) or LpoB(sol) storage buffer (Fig. 3.13). PBP1B GTase activity at pH 5.0 and 4.5 is indeed slower than at pH 7.5, with a more severe effect at pH 4.5. At both conditions LpoB was able to significantly increase the rate of reaction (pH 5.0, ~9-fold; pH 4.5, ~12-fold).

Data shown in section 3.1.7 show that LpoB interacts with the non-catalytic UB2H domain of PBP1B situated between the TP and GT domains. Therefore, we suggest that binding of LpoB causes conformational changes in PBP1B which exerts an allosteric effect on the GTase domain, affecting the environment of the catalytic Glu 233.

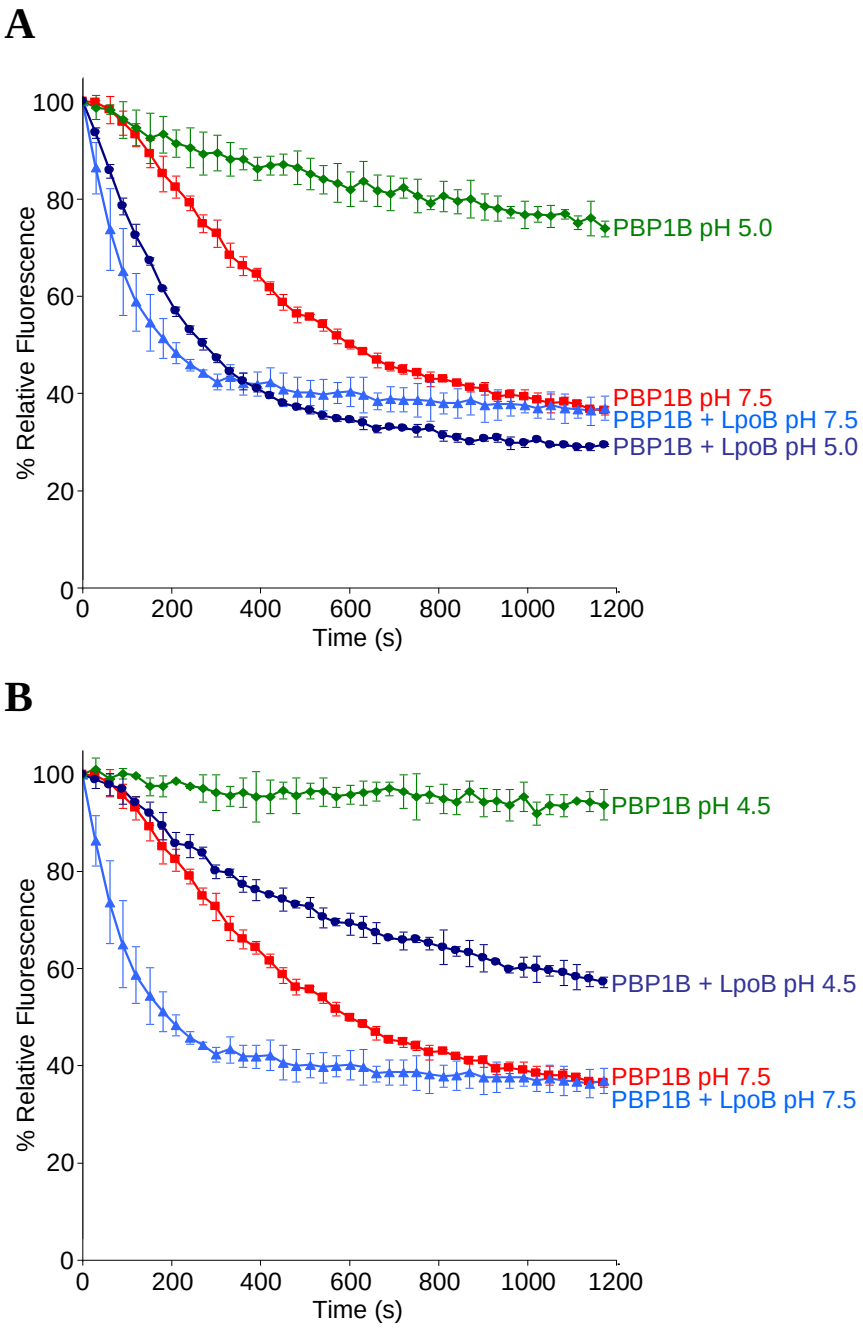

Figure 3.13 The effect of LpoB of PBP1B GTase activity at pH 5.0 and 4.5

GTase reactions of PBP1B (0.5 µM) alone and in the presence of LpoB(sol) (1 µM) at pH 5.0 (A) and pH 4.5 (B) with reactions at the standard pH of 7.5 included as a positive control. The Triton X-100 concentration was 0.04%. LpoB(sol) stimulates PBP1B GTase activity at these low pH conditions, at which PBP1B alone is poorly active (n = 3).

3.2.5 FtsN stimulates the GTase activity of PBP1B

A potential regulatory effect of FtsN on PBP1B was previously described by Müller *et al.* (145) who showed that FtsN possessing its transmembrane and short cytoplasmic domains was able to stimulate PBP1B at low enzyme concentration (38 nM). Using the newly optimised GTase activity assay FtsN was shown to stimulate the activity of PBP1B at 0.5 µM (Fig. 3.14) and 1 µM (not shown), not previously seen due to the limitation of the end-point *in vitro* PG synthesis assay. The presence of FtsN increased the rate of reaction by 3.2 ± 0.2-fold. Of note is the fact that FtsNΔ1-57 still interacts with PBP1B but had no effect on GTase activity, suggesting that this effect required the TM and short cytoplasmic domains of FtsN (residues 1 to 57). This is in agreement with Müller *et al.* (145) (Fig. 3.14). FtsN alone had no effect on the substrate.

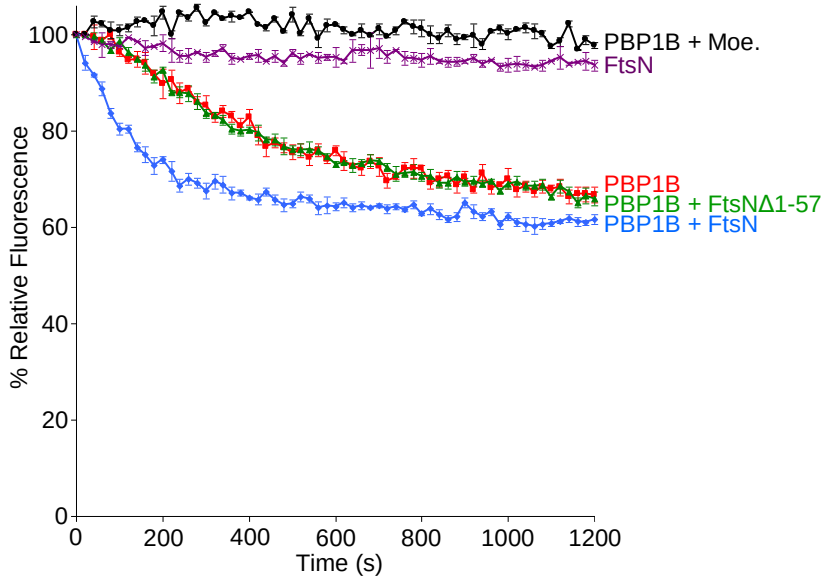

Figure 3.14 Effect of FtsN on PBP1B GTase activity

GTase reactions of PBP1B (0.5 µM) with and without FtsN-His (1 µM), FtsNΔ1-57-His (1 µM) or moenomycin (50 µM), and FtsN-His alone. The Triton X-100 concentration was 0.04%. FtsN, but not the soluble version lacking its TM and cytoplasmic domains, increases the rate of reaction by 3.2 ± 0.2-fold (n = 4).

3.2.6 PBP3 has no effect on the GTase activity of PBP1B or its stimulation by LpoB and FtsN

PBP3 is the class B PBP essential for cell division in *E. coli*. It interacts with PBP1B and FtsN, forming a ternary complex (67). Data in this work suggest that PBP3, PBP1B and LpoB also form a ternary complex *in vitro* (3.1.6). Therefore, the effect of PBP3 on the GTase activity of PBP1B was investigated. PBP3 (1 µM) had no effect on the GTase activity of PBP1B (1 µM) (Fig. 3.15). In the presence of PBP3 (1 µM) the stimulatory effect of LpoB and FtsN on PBP1B was unaffected (Fig. 3.16).

The class B PBP essential for cell elongation, PBP2, was also included in this experiment. Interestingly, PBP2 had a moderate stimulatory effect on PBP1B. In the presence of PBP2 (1 µM) the rate of reaction increased 2.0 ± 0.4-fold (Fig. 3.15).

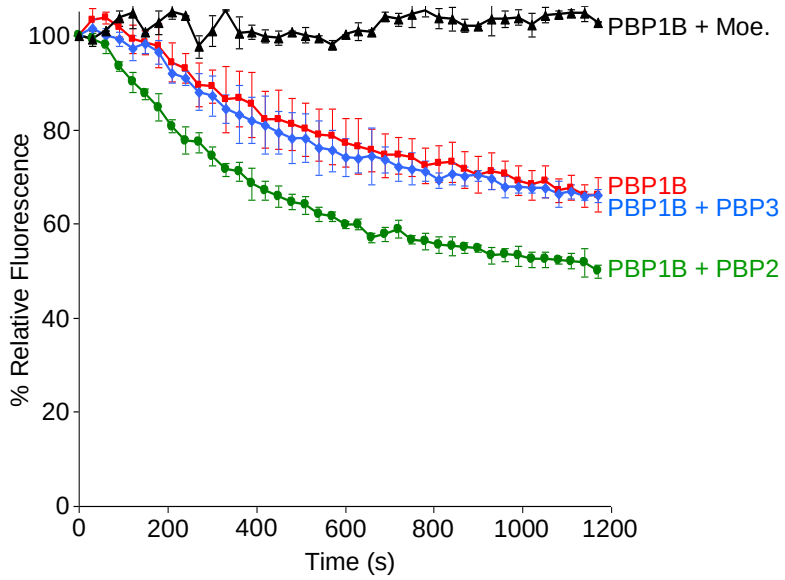

Figure 3.15 Effect of PBP3 and PBP2 on PBP1B GTase activity

GTase reactions of PBP1B (1 µM) alone and in the presence of either PBP3 (1 µM), PBP2 (1 µM) or moenomycin (50 µM). The Triton X-100 concentration was 0.065%. PBP3 had no effect on the rate of PBP1B GTase activity. PBP2 increases the rate of reaction by 2.0 ± 0.4-fold (n = 6).

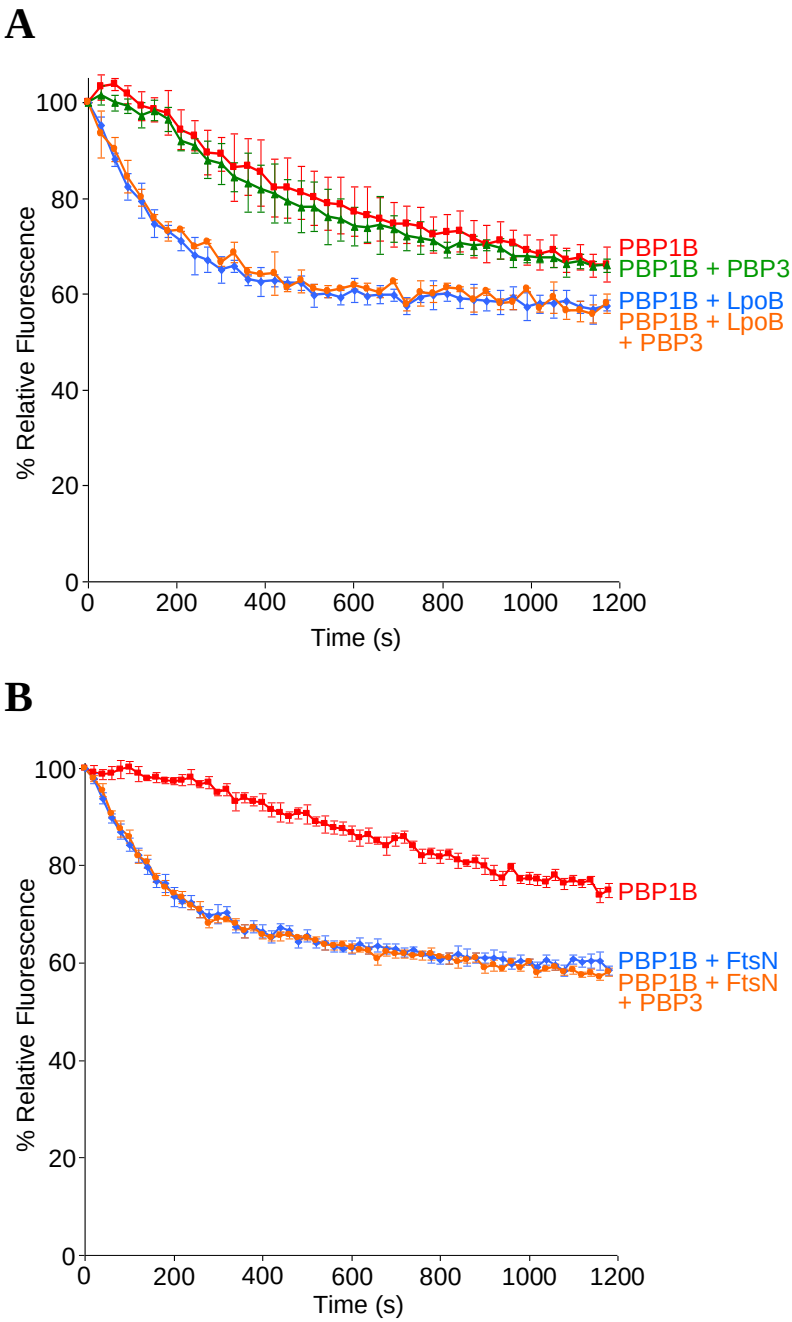

Figure 3.16 PBP3 has no effect on LpoB or FtsN mediated stimulation of PBP1B GTase activity

(A) GTase reactions of PBP1B (1 µM) alone and in the presence of LpoB(sol) (1 µM), PBP3 (1 µM) or a combination of the two interaction partners. The Triton X-100 concentration was 0.065%. The presence of PBP3 had no effect on the stimulation of PBP1B by LpoB (n = 4).
(B) GTase reactions of PBP1B (0.5 µM) alone and in the presence of FtsN (1 µM) with and without PBP3 (1 µM). The Triton X-100 concentration was 0.065%. PBP3 had no effect on the stimulation of PBP1B by FtsN (n = 4).

3.2.7 PBP5 has no effect on PBP1B GTase activity

PBP5 is a major DD-carboxypeptidase in *E. coli*. The PBP5 gene (*dacA)* is in the same operon as PBP2 and RodA (202). Mutants lacking PBP5 exhibit various morphological defects at certain growth conditions such as branching and kinks, which become exacerbated with the loss of other PG hyrdolases such as PBP4 and PBP7 (203). It was suggested that PBP5 along with other hydrolases play a role in regulating the balance between PG synthesis during cell growth and division (204) as deletion of *dacA* in a temperature sensitive *ftsK* mutants (*ftsK44* and *ftsK3531*) suppresses the division defect and overproduction of PBP5 alone causes cells to become spherical (205–207).

A sub-population of the cell's PBP5 pool localises at the septum dependant on its enzymatic activity (208) and an interaction between PBP1B and the PBP5 has been seen by the laboratory of Dr. Eefjan Breukink (unpublished). Thus, whether PBP5 has any effect on PBP1B GTase activity was investigated. PBP5 (1 µM) had no effect on PBP1B (1 µM) GTase activity in this assay. PBP5 was incubated with the substrate alone in order to ensure its carboxypeptidase activity did not affect the fluorescence.

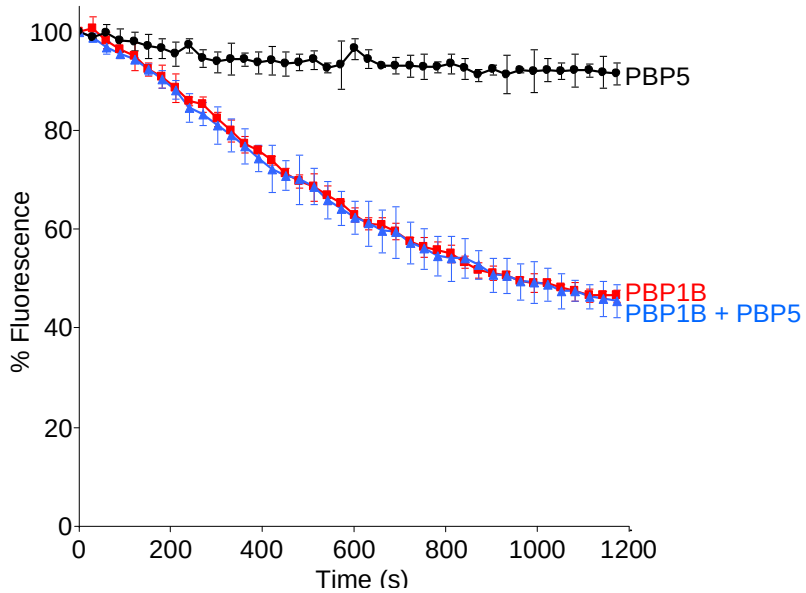

Figure 3.17 PBP5 has no effect on PBP1B GTase activity

GTase reactions of PBP1B (1 µM) with and without PBP5 (1 µM), and PBP5 alone. Triton X-100 concentration was 0.04%. The presence of PBP5 has no effect on the rate of PBP1B GTase activity, nor does PBP5 alone affect the fluorescence of the substrate (n = 3).

3.2.8 PBP1B forms a ternary complex with FtsN and LpoB

The data shown in section 3.1.6 suggest that PBP3, FtsN and LpoB are able to interact with PBP1B simultaneously. PBP3 and FtsN do not interact with LpoB but were retained from *E. coli* membrane extract by LpoB-sepharose, likely indirectly via PBP1B. The interaction site for LpoB and PBP3 within PBP1B are distinct. LpoB interacts with the UB2H domain (3.1.7), and PBP3 likely interacts with the TM domain or membrane proximal parts of PBP1B as it was shown to require the first 56 residues of PBP3 (67). The specific interactions sites/domains of PBP1B-FtsN are unknown. Therefore we tested whether soluble FtsN (Δ1-57) interacts with the UB2H domain of PBP1B using analytical SEC. Two protein concentration conditions were used; 33 μM of FtsNΔ1-57-His with 66 μM His-UB2H, and 130 μM of FtsNΔ1-57-His with 260 μM His-UB2H. FtsNΔ1-57 shows no binding to His-UB2H by SEC (Fig. 3.18). This suggests that the interaction sites/domains of FtsN and LpoB within PBP1B are distinct.

Next, we aimed to test the hypothesis that a ternary complex of LpoB, FtsN and PBP1B forms. Exploiting the fact that LpoB and FtsN show no direct interaction (3.1.6) a pulldown approach was devised using Ni^{2+}-NTA beads. Using FtsN-His, we tested whether both PBP1B and LpoB were retained together, the key aspect being that the retention of LpoB would require the presence of PBP1B. Initial attempts were unsuccessful, possibly due to loss of protein during the wash steps. This problem was overcome by cross-linking interacting proteins with formaldehyde (0.2%). LpoB(sol) was retained by FtsN-His only in the presence of PBP1B (Fig. 3.19). The relatively weak retention of LpoB by FtsN-His and PBP1B is no reflection of an attenuated binding between PBP1B and LpoB, as retention of LpoB by His-PBP1B at the same conditions is similar (Fig. 3.19).

It is important to note that this technique does not distinguish between two possibilities; 1) binding of single LpoB and FtsN molecules to the same PBP1B molecule, or 2) binding of an LpoB molecule to one of the two PBP1B molecules in a dimer and of FtsN to the other.

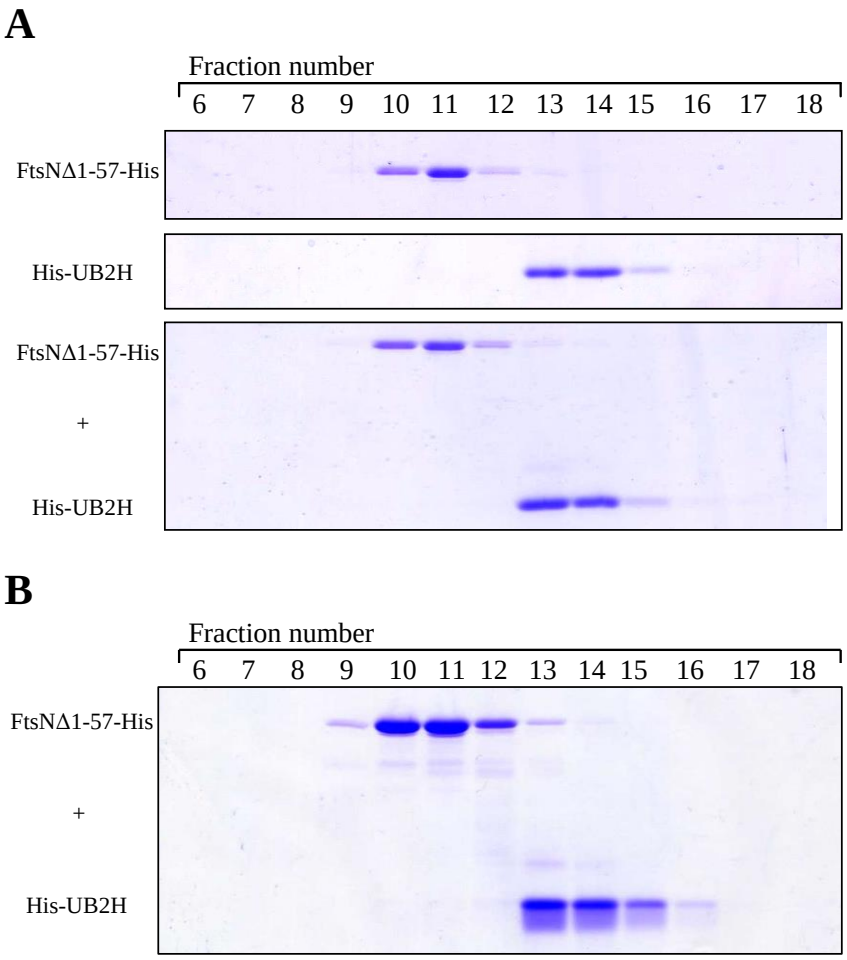

Figure 3.18 FtsNΔ1-57 shows no interaction with UB2H in SEC

The resulting Coomassie-stained SDS-PAGE gels of samples from 1 ml fractions collected during SEC of FtsNΔ1-57-His, His-UB2H or FtsNΔ1-57-His and His-UB2H. His-UB2H alone was eluted in fractions 13, 14 and 15 and there is no shift in the presence of FtsNΔ1-57-His. (A) Gels of the 33 µM FtsNΔ1-57-His and 66 µM His-UB2H experiments. (B) Gel of the 130 µM FtsNΔ1-57-His and 260 µM His-UB2H experiment.

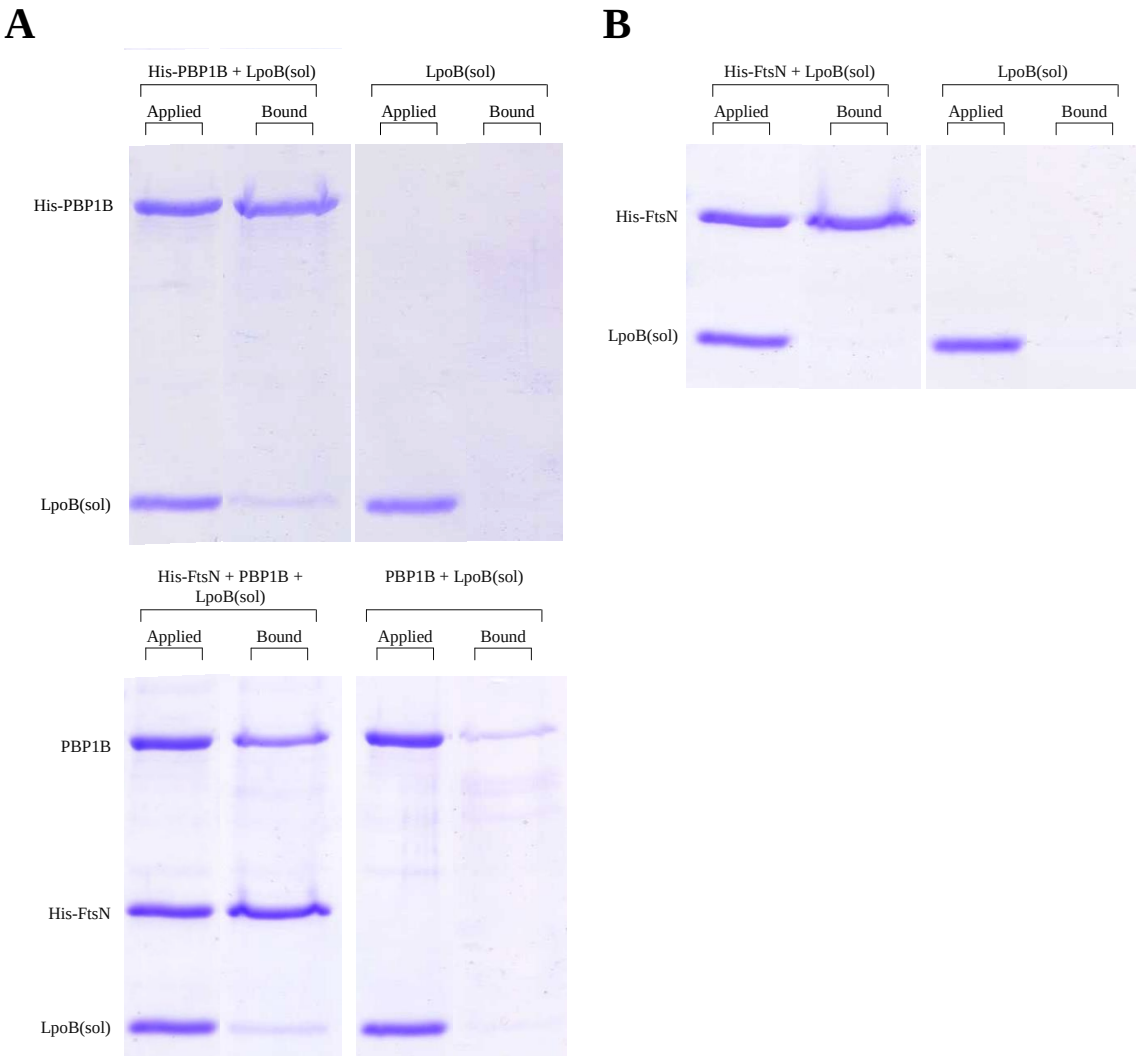

Figure 3.19 Ternary complex of PBP1B, LpoB and FtsN

Coomassie-stained SDS-PAGE gels of three pull-down experiments performed in parallel. Applied, proteins incubated with the Ni^{2+}-NTA beads; Bound, proteins retained after the wash steps. (A) His-PBP1B (1 µM) incubated with LpoB(sol) (2 µM) prior to cross-linking and incubation with Ni-NTA beads. LpoB(sol) was retained by His-PBP1B. (B) FtsN-His (1 µM) alone did not retain LpoB. (C) FtsN-His (1 µM) incubated with PBP1B (1 µM) and LpoB(sol) (2 µM) prior to cross-linking and incubation with Ni-NTA beads. Both LpoB and PBP1B were retained by FtsN-His.

3.2.9 LpoB and FtsN synergistically stimulate the GTase activity of PBP1B

PBP1B is able to interact with LpoB and FtsN simultaneously (3.2.8), and both LpoB and FtsN stimulate its GTase activity (3.2.3 and 3.2.5). Therefore, we investigated whether LpoB and FtsN are able to stimulate PBP1B in a synergistic manner.

In order to observe a synergistic stimulatory effect the reaction conditions needed to be adjusted such that the overall rate was decreased. This was achieved by decreasing the amount of PBP1B used and decreasing the reaction temperature from 30°C to 25°C. The GTase rate of PBP1B (0.25 μM) in the presence of both LpoB (0.5 μM) and FtsN (0.5 μM) is greater than in the presence of LpoB or FtsN alone. At these conditions LpoB stimulated 9.3 ± 0.9-fold, FtsN 4.6 ± 0.4-fold. LpoB and FtsN together stimulated 16.9 ± 0.9-fold (Fig. 3.20 A). Though it is possible that two sub-populations of enzymatically active complexes exist within the reaction (PBP1B-LpoB and PBP1B-FtsN) the evidence presented in 3.1.6 and 3.2.8 suggests that this synergistic effect is the result of both binding partners exerting their stimulatory mechanisms on PBP1B simultaneously. This result is in agreement with the multiprotein complexes for PG synthesis model.

Whether the synergistic stimulation of the GTase activity of PBP1B has an effect on its TPase activity was also investigated, using the *in vitro* PG synthesis assay Fig. 3.9). There was no change in the percentage of peptides in cross-links of PG produced by PBP1B (1 μM) in the presence of both LpoB (1 μM) and FtsN (1 μM) (64.7 ± 1%) compared to the presence of LpoB only (64.6 ± 1.3%) (Fig. 3.20 B). FtsN has a minor stimulatory effect on the TPase activity of PBP1B at these conditions, increasing the percentage of peptides in cross-links from 48.6 ± 4.0% to 54.2 ± 1.9% which is statistically significant with a p value of 0.025 by homoscedastic T-test.

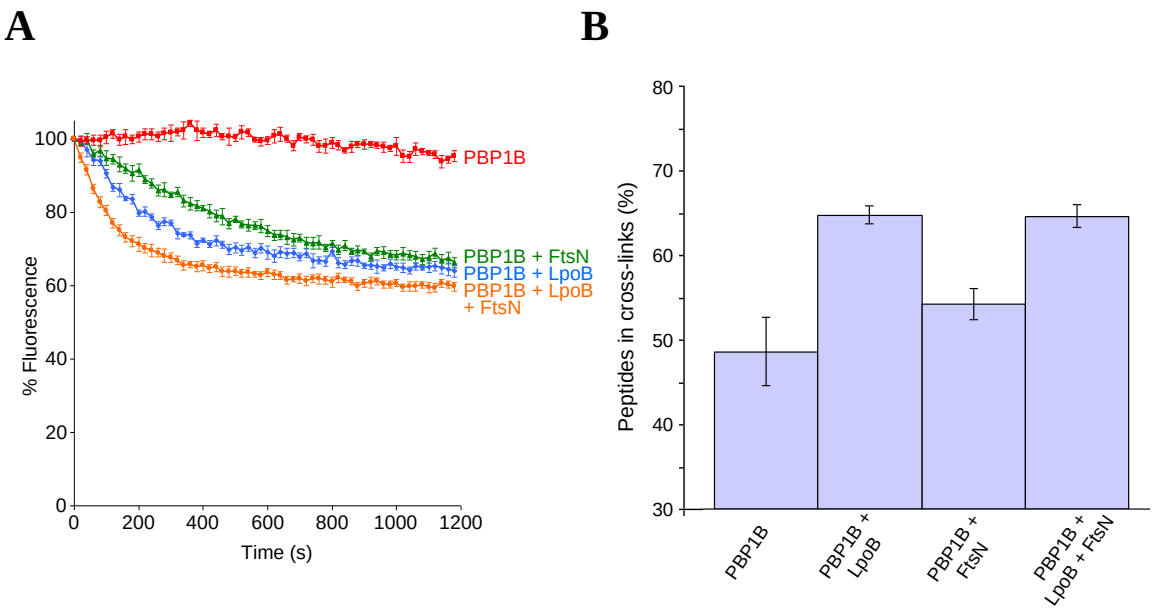

Figure 3.20 LpoB and FtsN exert a cumulative stimulatory effect on PBP1B GTase, but not TPase, activity

(A) GTase reactions of PBP1B (0.25 µM) in the presence of either LpoB(sol) (0.5 µM), FtsN-His (0.5 µM) or LpoB(sol) and FtsN-His. The Triton concentration was 0.04% and the temperature was decreased to 25°C in order to slow the reaction for sufficient resolution. PBP1B has the greatest rate of GTase activity in the presence of both LpoB and FtsN (n = 8).
(B) The percentage of peptides in cross-links in PG produced by PBP1B (1 µM) alone and in the presence of either LpoB(sol) (1 µM), FtsN-His (1 µM) or LpoB(sol) and FtsN-His. The presence of FtsN has no effect on the percentage of peptides in cross-links produced by PBP1B-LpoB, but has a mild effect on PBP1B alone (n = 4).

3.2.10 PBP2 stimulates the GTase activity of PBP1A

PBP1A and PBP1B are redundant for PG synthesis during cell division in *E. coli* (49). Therefore, the regulation of PBP1A is also of interest in the context of this work.

At the time of experimentation, Manuel Banzhaf (Newcastle University) had demonstrated an interaction between PBP1A and the class B PBP essential for cell elongation, PBP2. Furthermore, he had shown that the presence of PBP2 enhanced the rate of consumption of [^{14}C]-lipid II by PBP1A using an SDS-PAGE based method (60). Using the newly optimised GTase assay this result was confirmed. PBP2 (0.5 µM) increased the GTase rate of PBP1A (0.5 µM) 4.4 ± 0.75-fold (Fig. 3.21 A). PBP2 alone had no effect on the substrate. Interestingly PBP1A's non-cognate class B PBP PBP3 had a moderate stimulatory effect, increasing the rate of reaction 1.8 ± 0.3-fold. This result mirrored the effect of PBP2 on PBP1B (3.2.6). The effect of PBP2 on PBP1A was later published (60).

Whether or not the cognate OM lipoprotein of PBP1A, LpoA, had any effect on its GTase activity was also investigated by the continuous GTase assay. LpoA (1.5 µM) had no effect on the GTase rate of PBP1A (0.5 µM), nor did LpoB (1.5 µM) (Fig. 3.21 B).

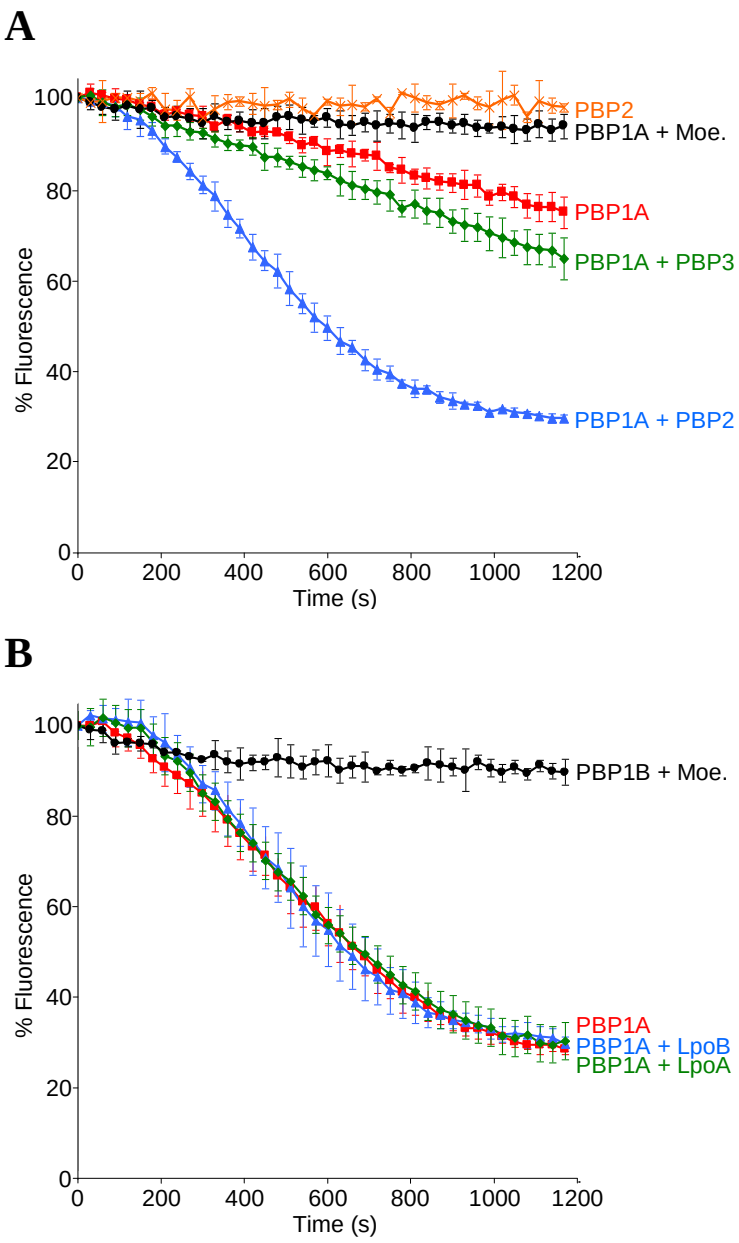

Figure 3.21 The effect of LpoA and PBP2 on the GTase activity of PBP1A

(A) GTase reactions of PBP1A (0.5 µM) in the presence of PBP2 (0.5 µM), PBP3 (0.5 µM), or moenomycin (50 µM). PBP2 was also incubated with the substrate alone. The Triton X-100 concentration was 0.065%. PBP2 stimulated the GTase activity of PBP1A 4.4 ± 0.75-fold. PBP3 also moderately increased the rate of reaction by 1.8 ± 0.3-fold (n = 6).
(B) GTase reactions of PBP1A (0.5 µM) in the presence of LpoA(sol) (1.5 µM), LpoB(sol) (1.5 µM), or moenomycin (50 µM. The Triton X-100 concentration was 0.02%. Neither LpoA nor LpoB had any effect on PBP1A GTase (n = 4).

3.2.11 Conclusion and discussion

The work in this section adds to the growing evidence supporting the model of multiprotein complexes for the synthesis of the peptidoglycan cell wall. Here we investigated the functional implications of the interactions of PBP1B with PBP3, FtsN and LpoB, testing whether the proteins may form a PG synthetic sub-complex.

The recently identified OM lipoprotein regulator of PBP1B, LpoB, was shown to affect the activity of its cognate synthase significantly more than previously reported using a newly optimised continuous GTase activity assay in this work. LpoB increased the rate of reaction 8.0 ± 0.9-fold. LpoB also stimulated PBP1B at low pH conditions at which the enzyme was poorly active alone. Given that LpoB interacts via the UB2H domain of PBP1B (3.1.7), we postulate that its stimulatory effect on both activities of PBP1B are through prompting conformational changes in the synthase upon binding. These changes may positively affect both active sites simultaneously. Explaining how a relatively small protein is able to directly affect two active sites with distinct catalytic activities (formation of a nucleophilic intermediate in the case of the GTase activity, and the acyl-enzyme intermediate of Ser510 with the carboxyl-terminal D-Ala D-Ala bond in the case of the TPase activity (40) spaced 65.8 Å apart (56). The domain of LpoB required to stimulate both activities is only maximally 30 Å in diameter, and does not undergo significant conformational changes upon binding to UB2H as determined by NMR spectroscopy. A long-range allosteric effect was recently shown to occur with PBP2a from *Staphylococcus aureus*. The TPase domain of PBP2a is opened upon binding of PG fragments to a site ~60 Å̊ away (209). However, whether the effect on both activities represents a true change in both catalytic sites is unclear. In all PBP1B and LpoB versions with a perturbed interaction interface the GTase and TPase activities were affected in similar ways, suggesting that the two activities are interdependent, which is consistent with previous work (53). These data may also suggest that LpoB primarily activates one of the two PBP1B activities, which in turn affects the second. A recent study by Lupoli *et al.* (69) supports this hypothesis. The Lupoli study suggested that LpoA and LpoB may affect the activity of their cognate PBP differently. They suggest that LpoA primarily affects the TPase domain of PBP1A, which is also supported by this work and Typas *et al.* (3.2.10)(27). They also suggest that an increase in PBP1B GTase activity caused by LpoB is independent of its TPase because blocking the activity with penicillin had no effect, which again is confirmed by this work as the substrate used in the continuous fluorescence assay cannot be used as a substrate for

TPase activity due to the addition of the Dansyl moiety. Thus there is no TPase activity in the GTase assay.

Even with these recent advances, the stimulatory mechanism of LpoB remains unclear. A hypothesis, along with further work to test this, is discussed in section 4 of this work.

Khai Bui (Newcastle University) found that PBP3 has no effect on the TPase activity of PBP1B by *in vitro* PG synthesis assay. In this work PBP3 was also found to have no effect on the GTase activity of its cognate class A PBP. In contrast to this finding, the class B PBP essential for cell elongation PBP2 was found to stimulate the activity of its cognate class A PBP PBP1A, increasing the rate of reaction 4.4 ± 0.75-fold at the conditions tested. Thus, the GTase activity of the major class A PBPs of *E. coli* is stimulated conversely. The primary synthase involved in cell elongation PBP1A is stimulated by the class B PBP essential for elongation (PBP2) but not by its cognate OM lipoprotein regulator (LpoA) and the primary synthase involved in cell division PBP1B is not stimulated by the class B essential for division (PBP3) but by its cognate OM lipoprotein regulator (LpoB). It is perhaps important to note that LpoB shares PBP1B's localisation at mid-cell but does not require its presence to localise. This converse regulation may reflect the observed role of each class A PBP in the differing modes of PG synthesis.

An unexpected finding from this work is that each class B PBP had a mild stimulatory effect on the GTase activity of its non-cognate class A PBP. PBP2 affected PBP1B and PBP3 affected PBP1A to a similar degree with increases of 2 ± 0.4 and 1.8 ± 0.3-fold, respectively. Although the class A PBPs have their 'preferred' roles in elongation and division each is able to take over the function of the other in its absence, as the deletion of one has no significant phenotype. Thus, these data suggest that the redundancy could result from the fact that PBP1A and PBP1B are stimulated, albeit mildly, by their non-cognate class B PBP. Whether PBP1A or PBP1B interact with their non-cognate class B is currently unknown. No interaction was detected by affinity chromatography (Manuel Banzhaf, Newcastle University), but this does not exclude that there are weak interactions. The stimulatory effects suggest they do interact, which should be investigated. Recent evidence shows that PBP2 and PBP3 interact with each other, co-localising at mid-cell early during division (44). Speculatively, even in the presence of PBP1B it is feasible that PBP1A participates in PG synthesis early during division. Perhaps in the absence of PBP1B PBP1A is able to persist through

simultaneous interaction with PBP3 and PBP2. Whether PBP2 localisation at mid-cell persists for longer during division in the absence of PBP1B should be tested.

The role of the essential cell division protein FtsN in the regulation of PBP1B PG synthesis activities was suggested by Müller *et al.* (145). Data presented in this work confirmed the results of this study and that FtsN requires its TM and cytoplasmic domain in order to stimulate PBP1B GTase activity. This work elaborates on the functional interaction between PBP1B and FtsN, showing that stimulation also occurs at ~13-fold higher enzyme concentration than previously reported. FtsN also had a mild stimulatory effect on the TPase activity of PBP1B, not previously seen at higher enzyme concentration. These data strengthen the evidence for a role of FtsN in regulating PBP1B in the cell.

One of the main aims of this work was to test whether multiple interaction partners are able to exert a synergistic stimulatory effect on PG synthesis. Indeed, FtsN is able to work in consort with LpoB to increase the GTase activity of PBP1B even further than either protein alone, likely via an LpoB-PBP1B-FtsN ternary complex. This is the first piece of direct evidence for a multi-protein complex enhancing PG synthesis. Given that the stimulatory effect of FtsN requires its TM and cytoplasmic domains while LpoB interacts with the UB2H domain of PBP1B, it is possible that the mechanisms of stimulation are different. FtsN likely acts via the membrane proximal part of PBP1B, which opens up several possibilities for its mechanism. These include; a direct effect on key residues of the GTase active site, which is located near the cytoplasmic membrane in the cell, improvement of substrate binding and/or processivity of the newly forming glycan chain, or the hypothesis of Müller *et al.* (145) such that FtsN binding acts to stabilise dimerisation of PBP1B. However, further experiments are needed to elucidate key aspects for the mechanism and are discussed in section 4.

3.3 A physical and functional link between the Tol-Pal complex and the peptidoglycan synthesis machinery

3.3.1 Introduction

The study by Gerding *et al.* (177) provided the first direct evidence of the involvement of the Tol-Pal complex in cell division, particularly in ensuring the correct timing of OM invagination and stability (see 1.4.2.3). The localisation of the Tol-Pal proteins at mid-cell is dependent on the divisome (153). Alongside several other possibilities, this suggests a physical link may exist. A lack of further investigation in this area left the question of the role of Tol-Pal in division poorly understood.

Using data from the same chemical genomics screen which lead to the discovery of LpoB (27, 210) a correlation between strains lacking *mrcB* (PBP1B) or *lpoB* (LpoB) with the strain lacking *ybgF* was noted by Athanasios Typas, with correlation coefficients of 0.469 and 0.424, respectively. Simultaneously to this, the laboratory of Eefjan Breukink discovered a putative interaction between YbgF and PBP1B through identification of proteins cross-linked to specific residues in PBP1B *in vivo* by mass spectrometry. The *ybgF* gene is a largely uncharacterised member of the *tol-pal* operon. YbgF is a soluble periplasmic protein known to exist as stable trimers, but which interacts with domain II of TolA with a stoichiometry of 1:1 via its C-terminal tetratricopeptide repeat (TPR) domain. TPR motifs are known to be protein-protein interaction modules and often participate in complex formation (188). Nothing is known about the function of the protein. Hence one of the aims of this collaborative project was to investigate a possible involvement in peptidoglycan synthesis during cell division, which could explain the phenotypic correlation with *mrcB* and *lpoB* mutants.

The work presented in this section is part of a large collaborative project in cooperation with the groups of Carol Gross at the University of California San Francisco, Tanneke den Blaauwen at the University of Amsterdam, Athanasios Typas at the European Molecular Biology Laboratory Heidelberg and Eefjan Breukink at the University of Utrecht.

In this section *in vitro* data, including interaction and enzymatic activity studies, will be presented that demonstrates a more direct role of Tol-Pal in cell division. Collective data from the collaborative group provided insights into the cellular biology context of these *in vitro* data and will also be discussed.

3.3.2 YbgF interacts with PBP1B

We aimed to establish whether the observed phenotypic correlation between YbgF and PBP1B/LpoB, and whether the interaction of YbgF and PBP1B *in vivo* represents a direct physical link. We established a protocol for purification of mature hexahistidine tagged YbgF (His-YbgF) and a version with the tag removed (YbgF) (2.3.5). Interaction studies were undertaken including affinity chromatography with immobilised YbgF, SPR assays and *in vivo* cross-linking / co-immunoprecipitation assays using anti-YbgF antibodies.

Purified YbgF was coupled to CNBr-activated sepharose beads, remaining active groups were blocked with Tris. *E. coli* MC1061 membrane extract was applied to these beads and to control beads lacking protein (2.4.3). PBP1B, LpoB and FtsN were specifically retained by YbgF-sepharose in the presence of low NaCl concentration (50 mM) (Fig. 3.22 A). PBP3, PBP1A, LpoA or MltA did not bind to immobilised YbgF (Fig. 3.22 A). Affinity chromatography was also performed in the presence of high NaCl concentration (400 mM) but PBP1B, LpoB and FtsN were not retained at these conditions (Fig. 3.22 B).

The observed interactions were further investigated *in vivo* using chemical cross-linking / co-immunoprecipitation (2.4.11). Interacting proteins within the periplasm of *E. coli* BW25113 and a *ybgF*$^-$ mutant (BW25113Δ*ybgF*) were cross-linked using DTSSP. Membrane extracts were then produced to which 10 µg of YbgF antibody was added (controls had no antibody added). The samples were incubated with Protein-G agarose beads, to which the antibody bound along with its antigen and any proteins the antigen was cross-linked to. Beads were washed before elution of bound antibody / proteins and reversal of the cross-links by reduction with β-mercaptoethanol. Proteins were resolved by SDS-PAGE and transferred to nitrocellulose membrane by western blot. Potential binding partners were detected with specific antibody. Antibodies against PBP1B, LpoB, FtsN, PBP1A or LpoA were used. Only PBP1B was co-immunoprecipitated with YbgF (Fig. 3.23 A and B), suggesting that the observed binding of LpoB and FtsN in affinity chromatography was indirect via PBP1B. Immunoprecipitation of PBP1B with YbgF was specific, as shown by the absence of PBP1B in the sample derived from the *ybgF*$^-$ mutant strain. Next, we tested whether a loss of LpoB, LpoA, FtsN, the UB2H domain of PBP1B or a block in cell division by incubation with the PBP3 specific inhibitor aztreonam had an impact on the interaction between PBP1B and YbgF. Membrane extracts of strains *lpoA*$^-$, *lpoB*$^-$, JOE309 pJC83 (*ftsN*$^-$ with inducible copy of FtsN on a plasmid for depletion), CAG606366 (*mrcB*ΔUB2H) and BW25113 treated with 1 µg/ml

aztreonam for 1 h at 37°C were used for anti-YbgF IP. The FtsN depletion was carried out as previously described (125). Cells were observed to be filamentous under a microscope for both the FtsN depletion and the cell division block (+ aztreonam) cultures. None of these altered conditions caused a loss of the interaction between PBP1B and YbgF (Fig. 3.23 A).

To show that the interaction between PBP1B and YbgF is direct *in vitro*, SPR assays with PBP1B immobilised to the chip surface via ampicillin were carried out (as in 3.1.5). A PBP1A surface was included, further to the ampicillin alone surface. YbgF was injected at 0, 0.1, 0.2, 0.3, 0.4 and 0.5 µM in running buffer at a flow-rate of 75 µl/min for 5 min. YbgF bound to the PBP1B surface, at significantly greater amounts than to the PBP1A or control surfaces (Fig. 3.24 A). Next, the range of YbgF concentrations injected was increased in order to calculate the K_D by Scratchard plot, which was determined to be 0.28 ± 0.05 µM (Fig. 3.24 B and C).

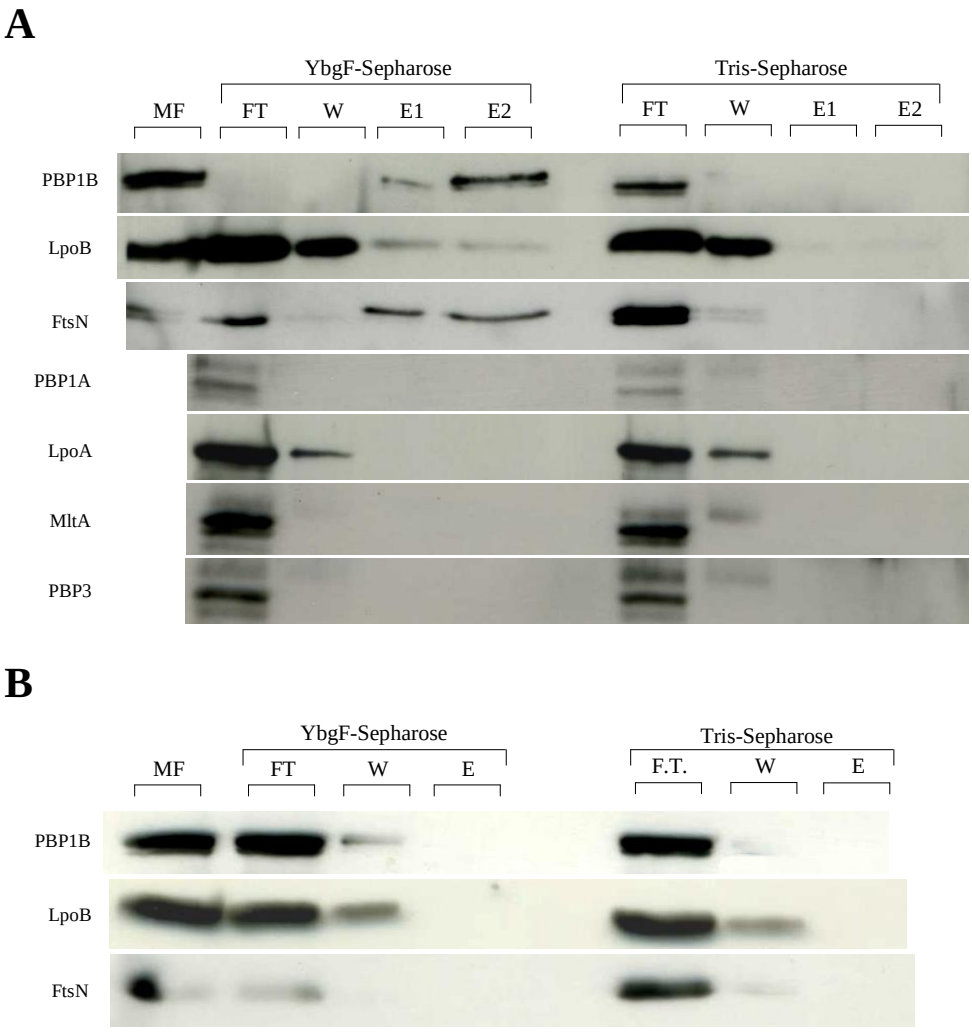

Figure 3.22 Affinity chromatography with YbgF-sepharose

(A) Low salt affinity chromatography samples from YbgF- and Tris-sepharose resolved by SDS-PAGE, the presence of specific potential binding partners were detected by western blot (antibodies used are indicated to the left). M.F, applied membrane fraction; FT, flow through; W, wash; E1, elution 1 (150 mM NaCl); E2, elution 2 (1 M NaCl). PBP1B, LpoB, FtsN, PBP1A, LpoA, MltA and PBP3 were detected. PBP1B, LpoB and FtsN showed binding to YbgF-sepharose but not to the control material (Tris-Sepharose).
(B) High salt affinity chromatography samples from YbgF- and Tris-sepharose resolved by SDS-PAGE. Proteins which bound at low salt were detected (antibodies indicated to the left). MF, applied membrane fraction; FT, flow through; W, wash; E, elution (2 M NaCl). At high salt PBP1B, LpoB and FtsN show no binding to YbgF-sepharose.

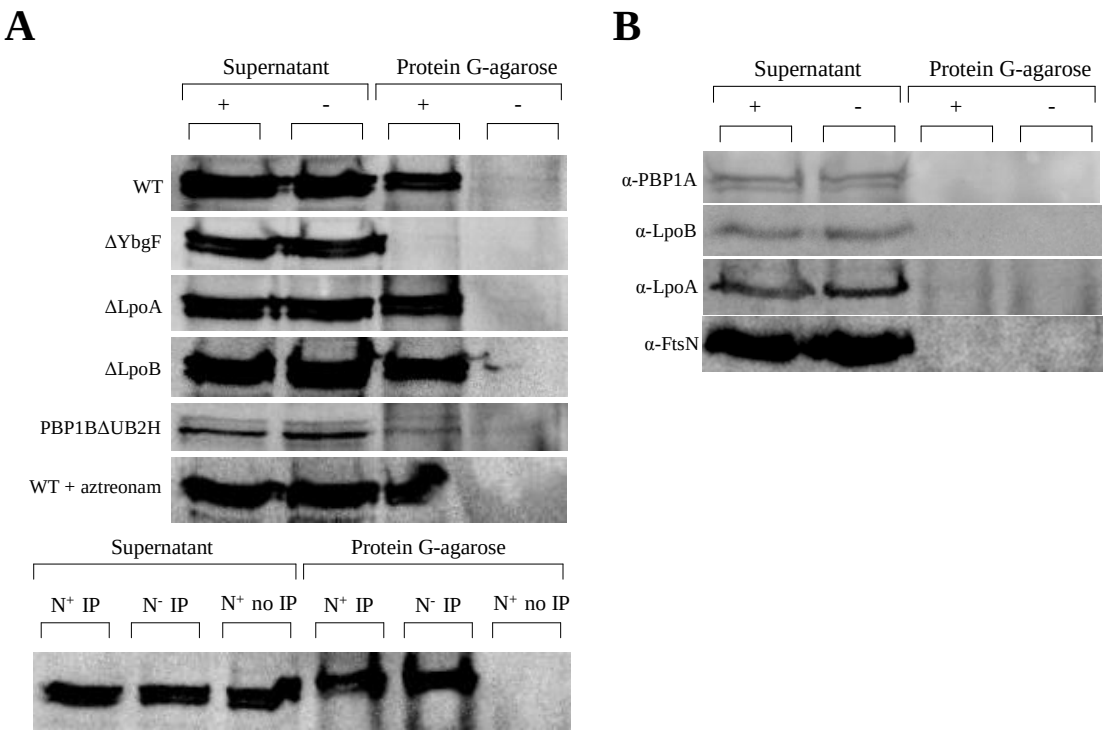

Figure 3.23 PBP1B interacts with YbgF *in vivo*

(A) Western blot detection (with anti-PBP1B antibodies) of supernatant and retained proteins from YbgF immunoprecipitation from wild type and *ybgF*$^-$ membrane extract. (+, with antibody; -, without antibody). PBP1B was specifically co-immunoprecipitated with YbgF. The interaction of PBP1B and YbgF is not affected by the loss of LpoB, FtsN, LpoA, the UB2H domain of PBP1B or by a block of PBP3 activity. N^+ IP, immunoprecipitation without FtsN depletion; N^- IP, immunoprecipitation with FtsN depletion.
(B) Western blot detection (anti-PBP1A, LpoB, LpoA and FtsN) of supernatant and retained proteins from YbgF immunoprecipitation (+, with antibody; -, without antibody) from wild type membrane extract. None of the detected proteins were co-immunoprecipitated with YbgF.

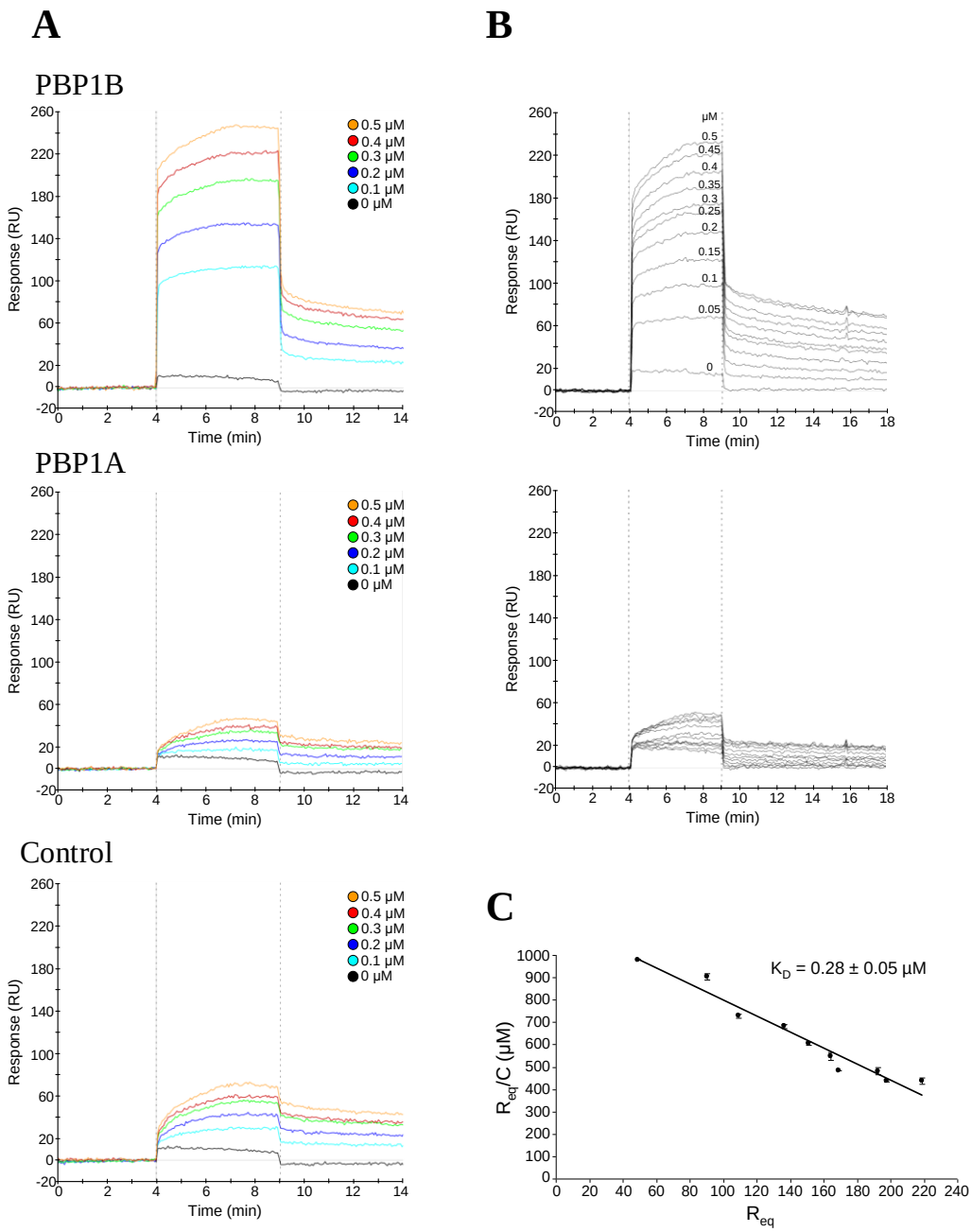

Figure 3.24 Interaction of YbgF with PBP1B by SPR

(A) SPR sensorgrams (response units against time) of YbgF at concentrations of 0.1, 0.2, 0.3, 0.4 and 0.5 µM injected at 75 µl/min over PBP1B, PBP1A, and control surfaces in running buffer for 5 min.
(B) SPR sensorgrams of YbgF at an increased concentration range from 0.05 to 0.5 µM (indicated above the corresponding curve) over PBP1B and control surfaces.
(C) Scratchard plot, using data derived from B.

3.3.3 TolA interacts with PBP1B via its TM domain (domain I)

An interaction between TolA and PBP1B *in vivo* was observed by collaborator Andrew Gray at the UCSF by cross-linking / co-immunoprecipitation using TolA and PBP1B antibodies produced during this work. Whether the interaction was direct was investigated *in vitro* by SPR and cross-linking / pulldowns. We developed a protocol for the purification of hexahistidine tagged TolA lacking its transmembrane region (His-TolA(sol)) and a version from which the tag was removed (TolA(sol)) (2.3.5).

For SPR, PBP1B was immobilised via ampicillin to the chip surface, and TolA(sol) was injected at concentrations of 0, 0.5, 1, 2, 3 and 4 µM in running buffer at a flow rate of 100 µl/min for 3 min. However, TolA(sol) did not bind to the PBP1B surface greater than its binding to the control (Fig. 3.25 A). Suggesting that the *in vivo* interaction is either indirect or the interaction is via domain I of TolA, which is missing in TolA(sol). Thus full length TolA was purified (2.3.5), however the protein was not suitable for SPR as the concentration was too low to attain meaningful data. Therefore the interaction was investigated using *in vitro* cross-linking / pulldown experiments. His-PBP1B in combination with TolA and TolA(sol) or TolA-His and TolA(sol)-His in combination with PBP1B were tested. Interaction was observed between His-PBP1B and TolA and between TolA-His and PBP1B. Consistent with SPR results, there was no significant binding detected between TolA(sol) and PBP1B in either combination (Fig. 3.25 B and C). These data show that TolA interacts with PBP1B and suggest that the binding requires the TM domain, domain I, of TolA.

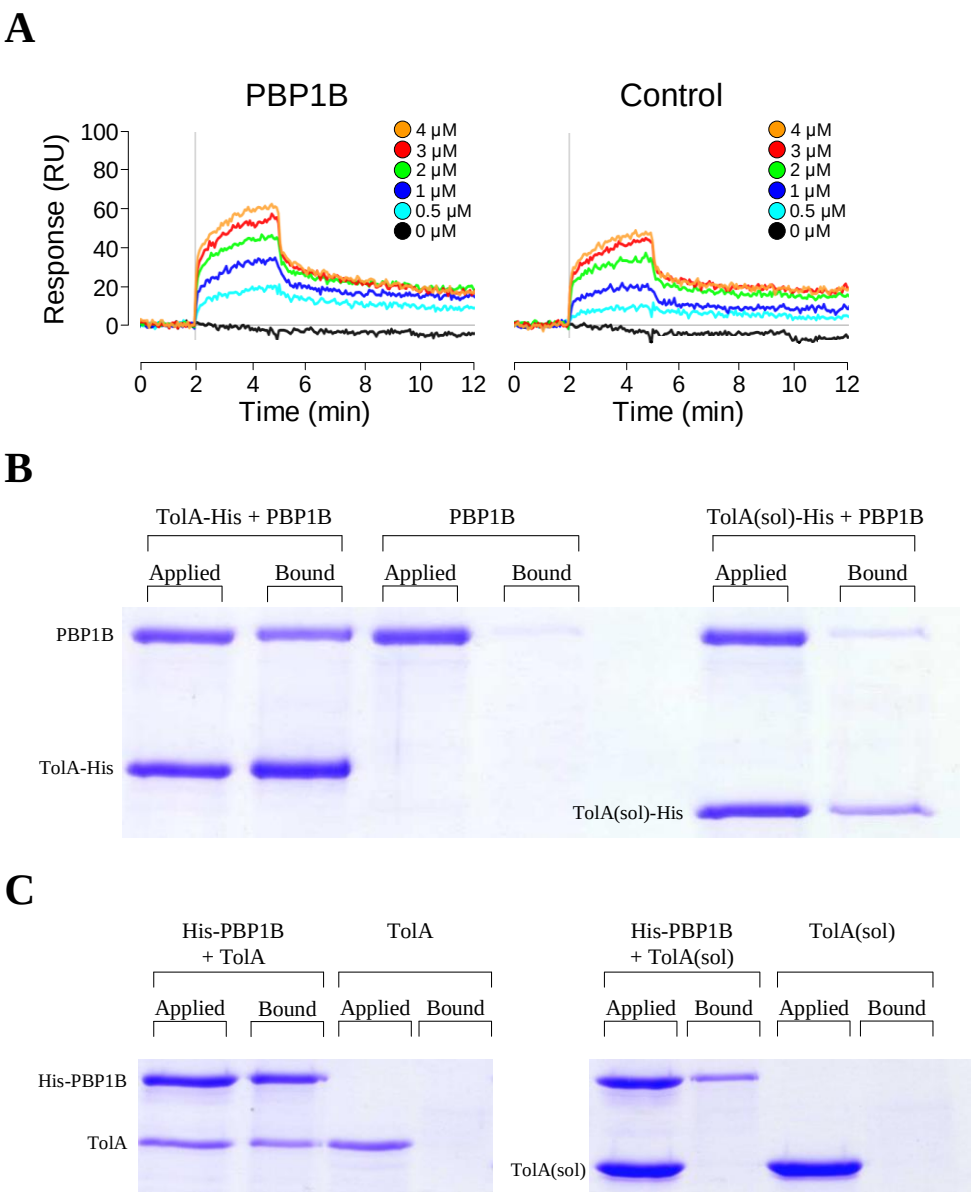

Figure 3.25 Interaction of PBP1B and TolA

(A) SPR sensorgrams (response units against time) of TolA(sol) injected over PBP1B immobilised via ampicillin at concentrations of 0, 0.5, 1, 2, 3 and 4 µM. No significant difference in the response units is seen between the PBP1B and the control surfaces indicating no binding of TolA(sol) to PBP1B had occurred.
(B) Coomassie-stained SDS-PAGE gels of an *in vitro* cross-linking / pulldown experiment using full length TolA-His and TolA(sol)-His with PBP1B. Full length TolA, but not its soluble version retained PBP1B greater than the Ni-NTA beads alone.
(C) Coomassie-stained SDS-PAGE gels of an *in vitro* cross-linking / pulldown experiment using His-PBP1B with TolA and TolA(sol). His-PBP1B retained full length TolA but not TolA(sol).

3.3.4 TolB shows no interaction with PBP1B *in vitro*

LpoB was found to have remarkable similarity to the N-terminal domain of TolB (3.1.8). Whether or not TolB was able to interact with PBP1B was investigated by SPR and affinity chromatography. An SPR experiment was performed with PBP1B immobilised to the chip surface as previously. Initially, TolB-His was injected at concentrations of 0, 0.5, 1, 2, 3 and 4 µM in running buffer at a flow rate of 100 µl/min for 3 min. TolB-His showed significant non-specific binding to the chip surface at these conditions, giving responses of >150 RUs with no difference between the PBP1B and control surfaces. Next TolB-His was injected at 0, 0.1, 0.2, 0.3, 0.4 and 0.5 µM in an attempt to reduce the non-specific binding. Again, no difference in the response was seen between PBP1B and control surfaces suggesting the TolB does not interact with PBP1B at these conditions (Fig. 3.26 A).

To confirm this result, affinity chromatography samples prepared by Manuel Banzhaf (Newcastle University) using MC1061 membrane extract applied to PBP1B-sepharose were analysed. These had been stored at -80ºC since their creation. Anti-LpoB and Anti-TolB antibodies were used for detection, LpoB gave the expected positive result as published but no binding of TolB was seen at these conditions (Fig. 3.26 B).

Thus, there is no binding of PBP1B and TolB-His at the conditions tested, suggesting that the proteins do not interact. Further tests such as *in vivo* cross-linking co-immunoprecipitation could be used to confirm the result. Even with the structural similarity TolB shares no sequence homology with LpoB, and lacks the conserved interaction patch of LpoB-PBP1B (3.1.7), which could explain the lack of interaction.

A

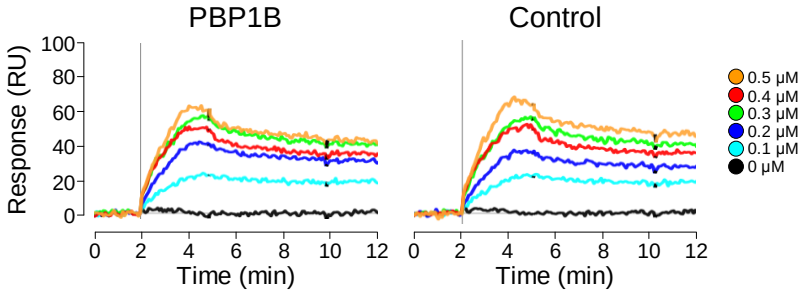

B

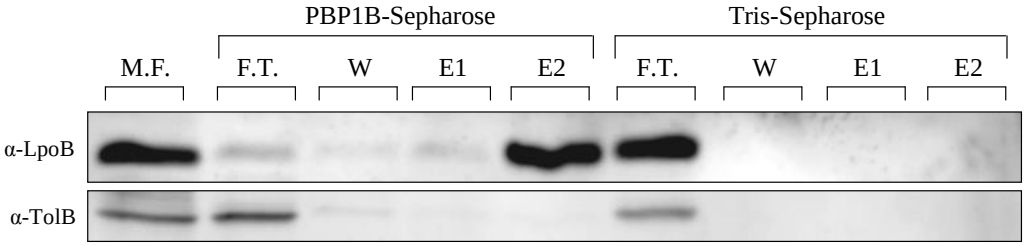

Figure 3.26 No interaction detected between TolB and PBP1B *in vitro*

(A) SPR sensorgrams (response units against time) of TolB-His at concentrations of 0, 0.1, 0.2, 0.3, 0.4 and 0.5 µM injected over PBP1B immobilised via ampicillin. TolB-His showed significant non-specific binding to the chip surface, which was exacerbated at higher protein concentration. No significant difference in the response units was seen between the PBP1B and the control surfaces.
(B) Low salt affinity chromatography samples from PBP1B- and Tris-sepharose resolved by SDS-PAGE, the presence of LpoB and TolB was detected with specific antibody after western blot (indicated to the left). MF, applied membrane fraction; FT, flow through; W, wash; E1, elution 1; E2, elution 2.

3.3.5 PBP1B, LpoB, YbgF and TolA form a quaternary complex *in vitro*

With interactions between TolA and YbgF and PBP1B established, we next aimed to test whether TolA and YbgF are able to interact with PBP1B simultaneously to form a ternary complex. We also tested whether TolA and YbgF can interact to form ternary complexes with PBP1B-LpoB.

First, His-LpoB(sol) was used in an *in vitro* cross-linking / pulldown experiment to test whether it could retain YbgF via PBP1B, as in 3.2.8 with the demonstration of LpoB-PBP1B-FtsN ternary complex. Indeed, His-LpoB(sol) was able to retain YbgF via PBP1B (Fig. 3.28 A). Next, the same approach was used with TolA in place of YbgF. Again, a ternary complex was observed (Fig. 3.27 B).

As both YbgF and TolA independently interact with PBP1B, the pulldown approach is not appropriate to show a ternary complex as it could not distinguish between separate PBP1B-YbgF and PBP1B-TolA complexes at the conditions used. Therefore an alternate approach was developed in this work with the assistance of undergraduate student Ms Ann-Kristin Hov. Cross-linked complexes were resolved by SDS-PAGE without boiling or the use of reducing agent before western blotting and detection of proteins with specific antibodies (2.4.11). The aim was to test whether all three proteins featured in the same band. PBP1B, YbgF and TolA were observed to be part of multiple complexes together, these were of differing MW labelled i, ii and iii (Fig. 3.28 A). However, though it is clear the higher MW bands in the TolA and YbgF sections of the blot are a result of cross-linking to PBP1B, two of the bands (ii and iii) are present in both the PBP1B alone and the mix samples. Therefore, to ensure the accuracy of the result a control experiment with PBP1A in the place of PBP1B was performed (Fig. 3.28 B). The high MW bands containing both TolA and YbgF were present only in the sample with PBP1B and thus the three proteins are able to interact simultaneously to form a ternary complex *in vitro*.

LpoB is able to form a ternary complex with PBP1B and both YbgF and TolA independently, and PBP1B interacts with both TolA and YbgF simultaneously in the absence of LpoB. Therefore the four proteins could interact to form a quaternary complex. This hypothesis was tested using the *in vitro* cross-linking / pulldown approach using His-LpoB(sol) incubated with PBP1B, YbgF and TolA. His-LpoB was able to retain PBP1B, YbgF and TolA simultaneously (Fig. 3.29). Although it is possible that this is the result of two independent ternary complexes data presented later in this work (3.3.9) supports the existence of a quaternary complex.

A

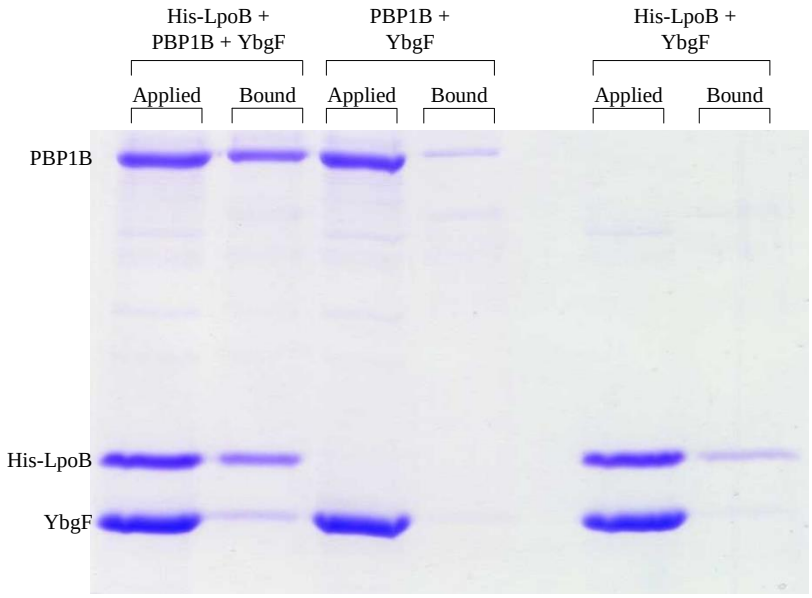

B

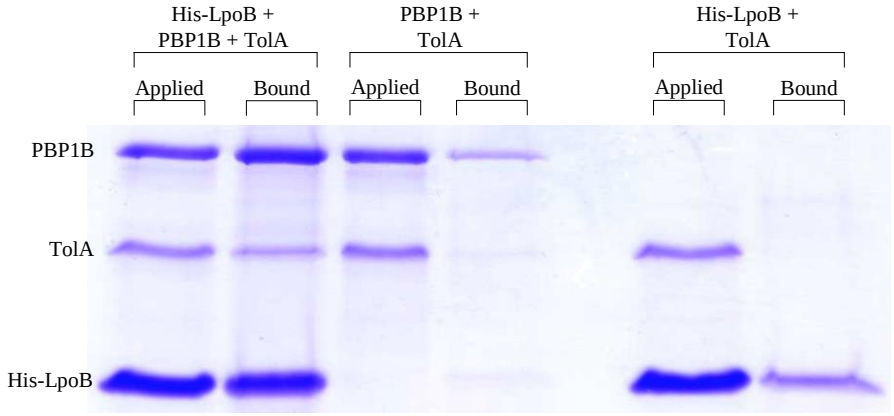

Figure 3.27 *in vitro* cross-linking / pulldown assays of His-LpoB with PBP1B and YbgF or TolA

Coomassie-stained SDS-PAGE gels of *in vitro* cross-linking / pulldown experiments. Applied, proteins incubated with Ni-NTA beads; Bound, proteins retained after the wash steps.
(A) His-LpoB(sol) (2 µM), PBP1B (1 µM) and YbgF (4 µM) were incubated in the combinations shown and cross-linked prior to incubation with Ni-NTA. Both YbgF and PBP1B were retained by His-LpoB(sol) in greater amounts than the Ni-NTA beads alone, retention of YbgF by His-LpoB(sol) required the presence of PBP1B.
(B) His-LpoB(sol) (4 µM), PBP1B (1 µM) and TolA (1 µM) were incubated in the combinations shown and cross-linked prior to incubation with Ni-NTA. Both TolA and PBP1B were retained by His-LpoB(sol) in greater amounts than the N-NTA beads alone, retention of TolA by His-LpoB(sol) requires the presence of PBP1B.

A

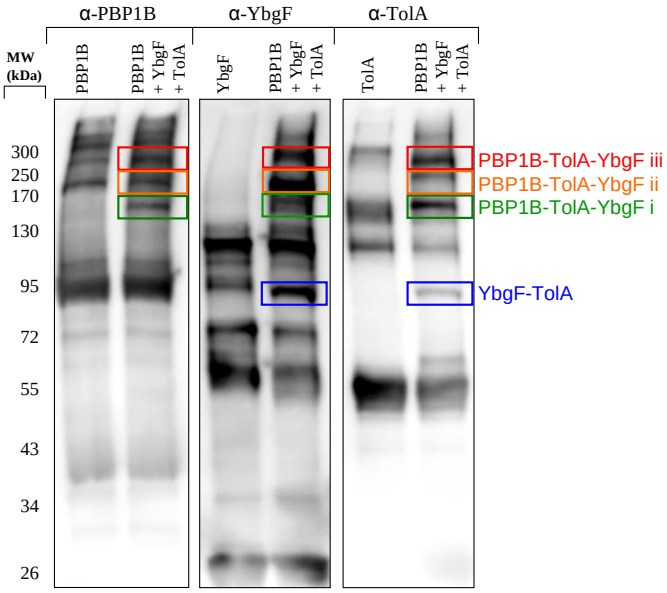

B

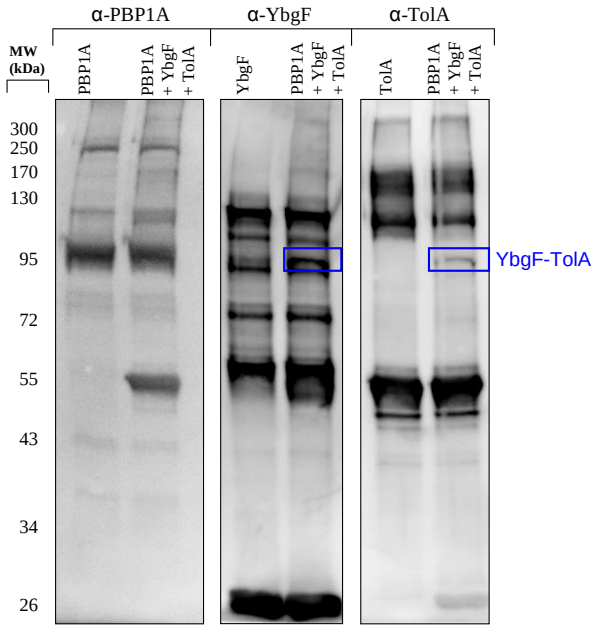

Figure 3.28 ***in vitro*** **cross-linking of PBP1B/PBP1A with TolA and YbgF**

Lanes from the immunodetection of blot sections framed according to which primary antibody was used for detection (indicated above) with their protein content indicated.
(A) Samples of PBP1B (1 µM), TolA (1 µM), YbgF (4 µM) or a combination of the three were cross-linked and resolved by SDS-PAGE. The presence of specific proteins were detected with antibody (indicated above) after western blot. The apparent protein complexes are highlighted with coloured boxes and labelled with the constituent proteins in text of the same colour.
(B) Using PBP1A (1 µM) instead of PBP1B shows the bands containing YbgF and TolA present at high MW are specific to PBP1B.

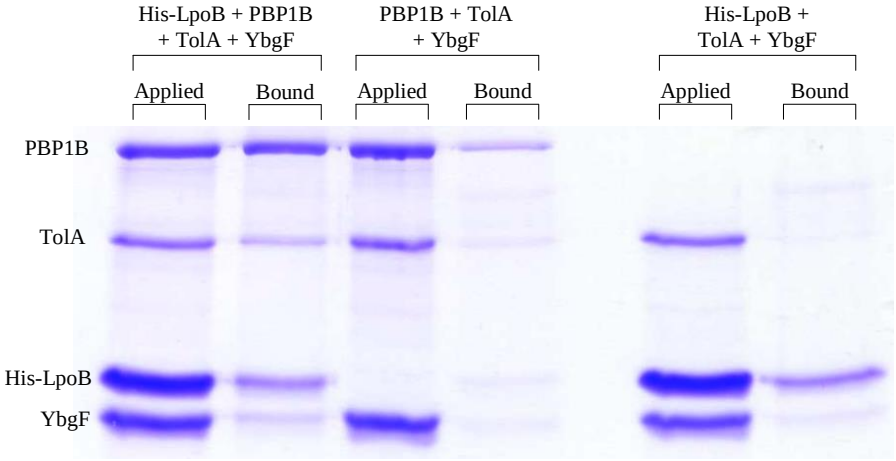

Figure 3.29 *in vitro* cross-linking pulldown assay: His-LpoB with PBP1B, TolA and YbgF

Coomassie-stained SDS-PAGE gel of *in vitro* cross-linking / pulldown experiment. Applied, proteins incubated with the Ni-NTA beads; Bound, proteins retained after the wash steps. His-LpoB(sol) (4 µM), PBP1B (1 µM), TolA (1 µM) and YbgF (4 µM) were incubated in the combinations indicated above, cross-linked and incubated with Ni-NTA beads. YbgF, TolA and PBP1B were retained by His-LpoB(sol). Retention of YbgF and TolA at these amounts by His-LpoB only occurred in the presence of PBP1B.

3.3.6 TolA moderately stimulates the GTase activity of PBP1B, synergistically with LpoB and FtsN

Having established direct protein-protein interactions of YbgF and TolA with PBP1B with and without LpoB, whether these interactions had an effect on the PG synthesis activities of PBP1B was investigated.

Firstly, the effects of the proteins on the GTase activity of PBP1B, alone and in the presence of LpoB and/or FtsN, was investigated. The continuous fluorescence GTase assay, described in section 3.2, was used with PBP1B (1 µM) in the presence or absence of YbgF (40 µM) and TolA(sol) (40 µM). TolA(sol) was included to test whether its known dissociation of YbgF trimers had any impact. The K_D of the TolA(sol)-YbgF interaction is 40 µM (188), prompting us to use these proteins at high concentration. YbgF had no effect on the GTase activity of PBP1B either alone or in combination with TolA(sol) (Fig. 3.30 A).

Next, GTase reactions of PBP1B (1 µM) in the presence of TolA-His (3 µM) with and without YbgF (40 µM) were performed. TolA-His had a moderate stimulatory effect on PBP1B GTase activity, increasing the rate of reaction 1.9 ± 0.5-fold. The presence of YbgF had no impact on this stimulation (Fig. 3.30 B).

Whether YbgF or TolA-His had any impact on the stimulatory effects of LpoB or FtsN on PBP1B GTase activity was also investigated. YbgF (40 µM) alone had no effect on the stimulation of PBP1B (1 µM) GTase by LpoB (1 µM) or FtsN (1 µM) (Fig. 3.31 A and B). TolA-His further stimulated PBP1B GTase in the presence of LpoB, FtsN or both LpoB and FtsN (Fig. 3.33). This experiment was performed alongside those shown in section 3.2.9 at the same conditions. At these conditions LpoB increased the rate of reaction 9.3 ± 0.9-fold; FtsN 4.6 ± 0.4-fold; LpoB and FtsN together 16.9 ± 0.9-fold; and LpoB, FtsN and TolA together stimulated 24.8 ± 1.6-fold.

The effect of adding YbgF along with other members of the Tol-Pal complex on the stimulatory effects of TolA were also investigated. TolB interacts with TolA via it's "TolA box" at the N-terminus, this motif is sequestered by conformational change upon binding of TolB to Pal, and thus TolB is thought to switch between these two states of interaction (185). This switch may have a functional context with regard to the function of the Tol-Pal complex alone, and also with regard to the effect of TolA on PBP1B. Therefore, protocols for the purification of hexahistidine tagged TolB and Pal were developed (2.3.5). TolB was overproduced in its native form, other than the C-terminal his-tag, to ensure proper cellular processing of its N-terminal motif. The addition of

TolB-His (10 µM) with or without His-Pal (10 µM) had no effect on the stimulation of PBP1B GTase activity by TolA (Fig. 3.34). TolB, Pal and YbgF also had no effect on the synergistic stimulation of PBP1B by TolA and LpoB (Fig. 3.32 A and 3.35) or TolA and FtsN (Fig. 3.32 B and 3.36). Nor did they have any effect on the stimulation exerted by LpoB, FtsN and TolA simultaneously (Fig. 3.37).

To summarise; YbgF alone or with TolA(sol) had no direct effect on the GTase activity of PBP1B. TolA-His had a moderate stimulatory effect on PBP1B GTase activity, which is synergistic with the effects of LpoB and FtsN described in section 3.2 of this work. This stimulatory effect of TolA was independent of YbgF, and of TolB with and without Pal.

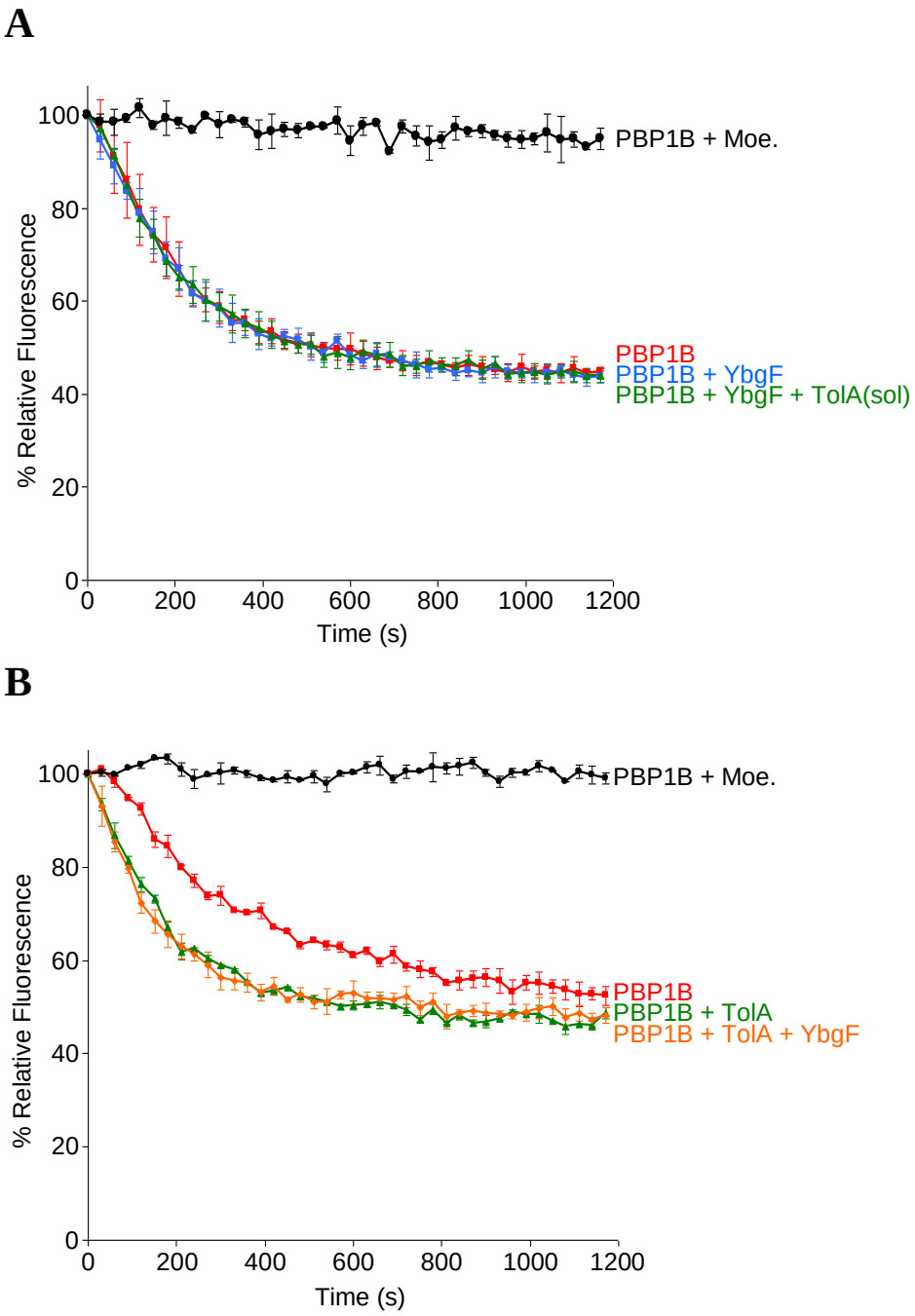

Figure 3.30 Effect of YbgF and TolA on PBP1B GTase activity

(A) GTase reactions of PBP1B (1 µM) alone and in the presence of YbgF (40 µM) with and without TolA(sol) (40 µM), or moenomycin (50 µM). The Triton X-100 concentration was 0.04%. YbgF had no effect on the rate of PBP1B GTase activity, the addition of TolA(sol) to YbgF did not alter this (n = 6).
(B) GTase reactions of PBP1B (1 µM) alone and in the presence of TolA-His (3 µM) with and without YbgF (40 µM), or moenomycin (50 µM). The Triton X-100 concentration was 0.065%. TolA-His increased the rate of PBP1B GTase reaction by 1.9 ± 0.5-fold (n = 8).

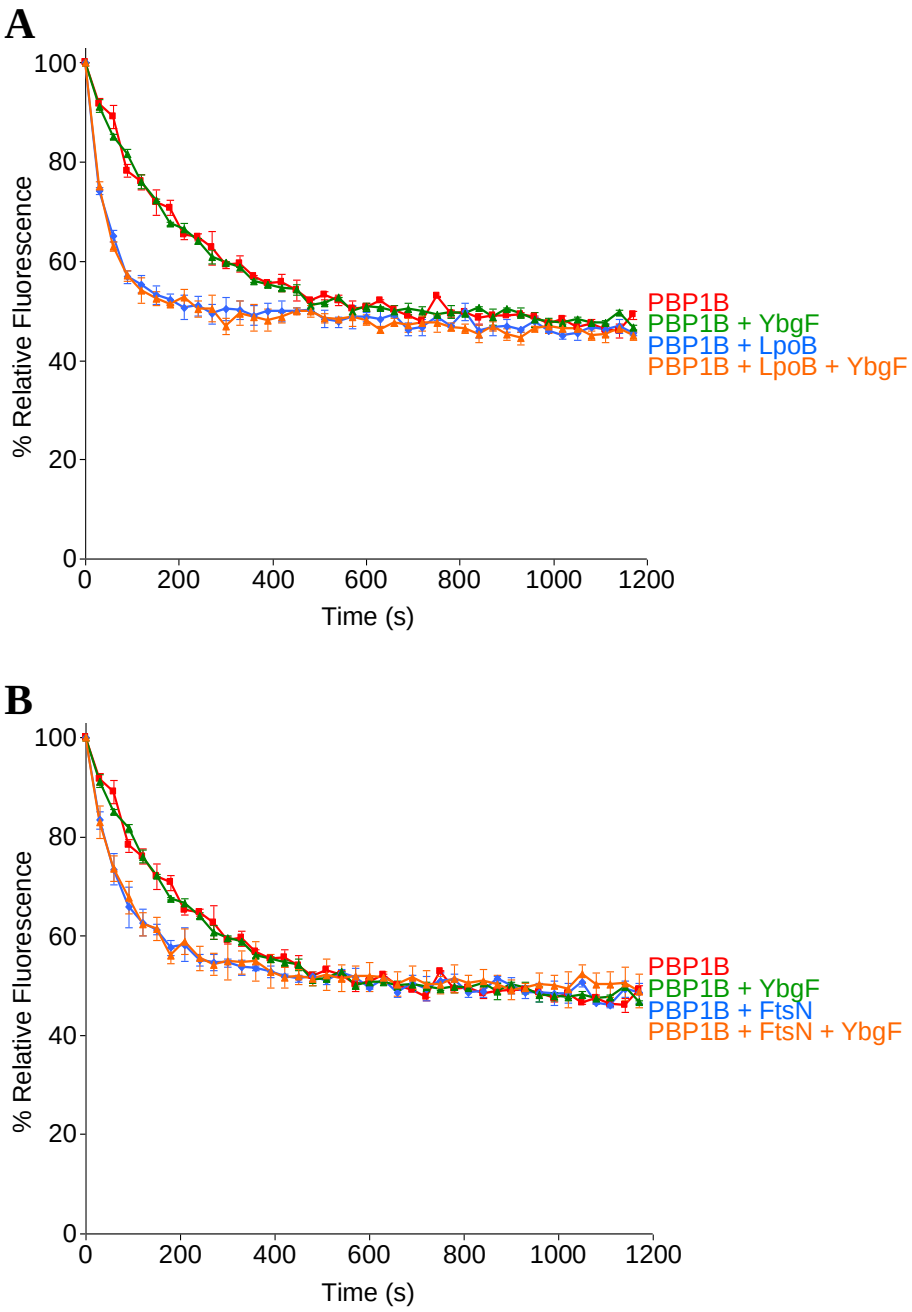

Figure 3.31 Effect of YbgF on stimulation of PBP1B GTase by LpoB and FtsN

(A) GTase reactions of PBP1B (1 µM) alone and in the presence of LpoB (1 µM), YbgF 40 µM, or a combination of these. The Triton X-100 concentration was 0.04%. YbgF had no effect on the stimulation of PBP1B GTase activity by LpoB (n = 4).
(B) GTase reactions of PBP1B (1 µM) alone and in the presence of FtsN (1 µM), YbgF 40 µM, or a combination of these. The Triton X-100 concentration was 0.04%. YbgF had no effect on the stimulation of PBP1B GTase activity by FtsN (n = 4).

A

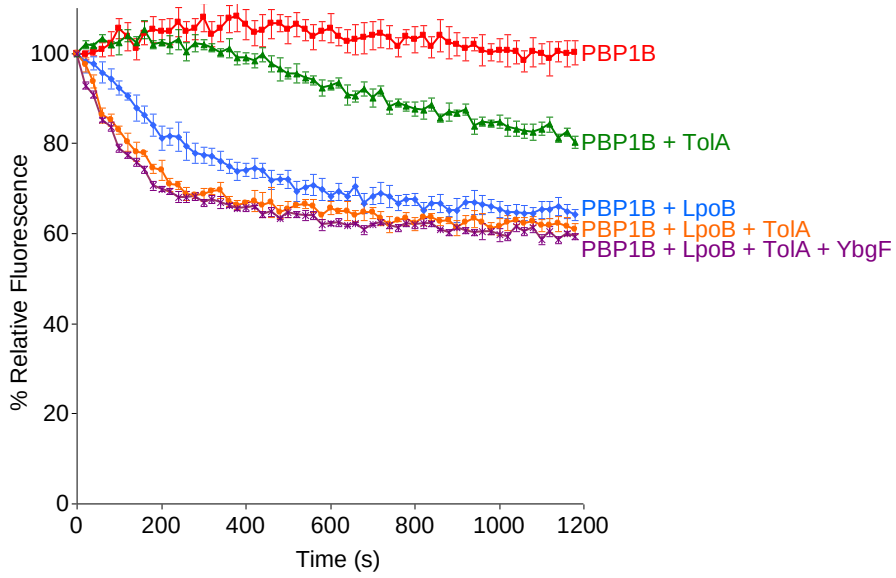

B

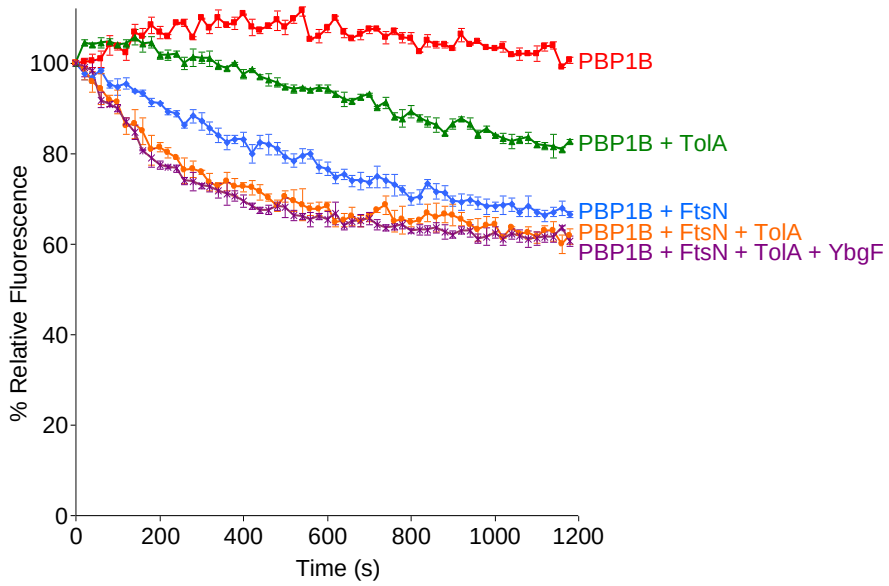

Figure 3.32 The stimulatory effect of TolA on PBP1B GTase activity is cumulative with LpoB and FtsN

(A) GTase reactions of PBP1B (0.25 µM) alone and in the presence of LpoB (0.5 µM), TolA-His (2 µM), YbgF (40 µM) or combinations of these indicated. The reaction temperature was 25°C and the Triton X-100 concentration was 0.04%. The stimulatory effect of TolA-His was synergistic with that of LpoB, YbgF had no impact (n = 4).
(B) Reactions were performed as in (A) with FtsN (0.5 µM) in place of LpoB. The stimulatory effect of TolA-His was also synergistic with that of FtsN, again YbgF had no effect on this (n = 4).

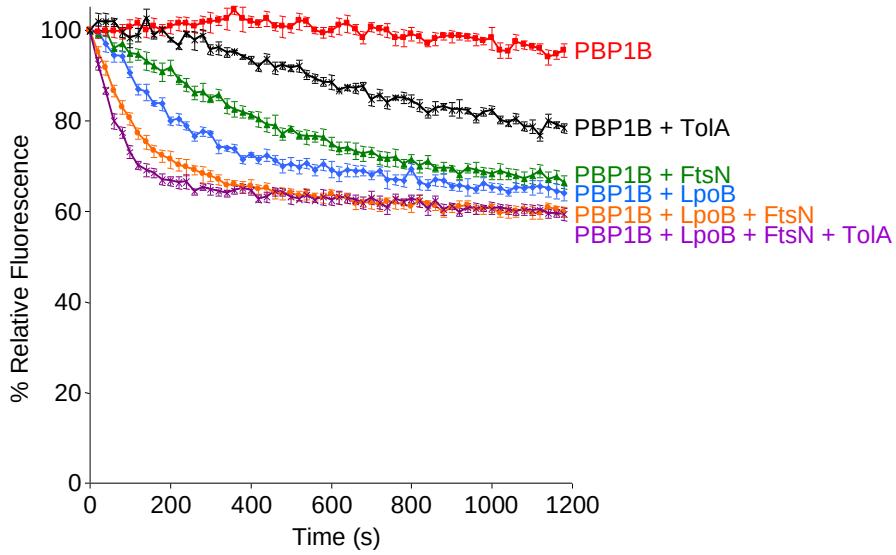

Figure 3.33 The stimulatory effects of TolA, LpoB and FtsN on PBP1B GTase activity are synergistic

GTase reactions of PBP1B (0.25 µM) alone and in the presence of LpoB (0.5 µM), FtsN (0.5 µM), TolA-His (2 µM), or combinations of these. The reaction temperature was 25°C and the Triton X-100 concentration was 0.04%. The presence of TolA-His increased the rate of reaction further than the synergistic effect of LpoB and FtsN (n = 8).

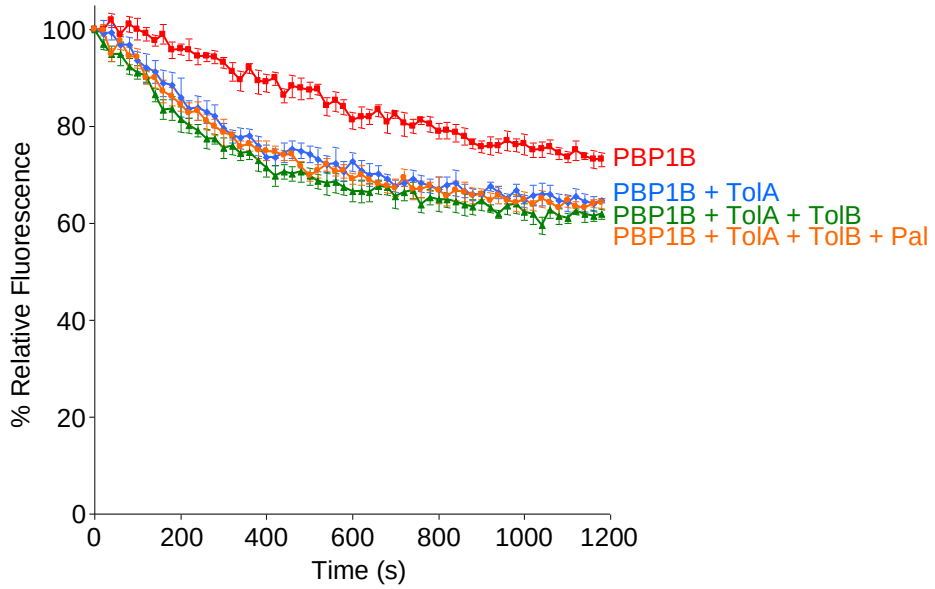

Figure 3.34 Addition of TolB with or without Pal has no effect on the stimulation of PBP1B GTase activity by TolA

GTase reactions of PBP1B (0.5 µM) alone and in the presence of TolA-His (2 µM), TolB-His (10 µM) with and without His-Pal (10 µM). The Triton X-100 concentration was 0.06%. Addition of TolB with or without Pal had no effect on the stimulation of PBP1B by TolA-His (n = 3).

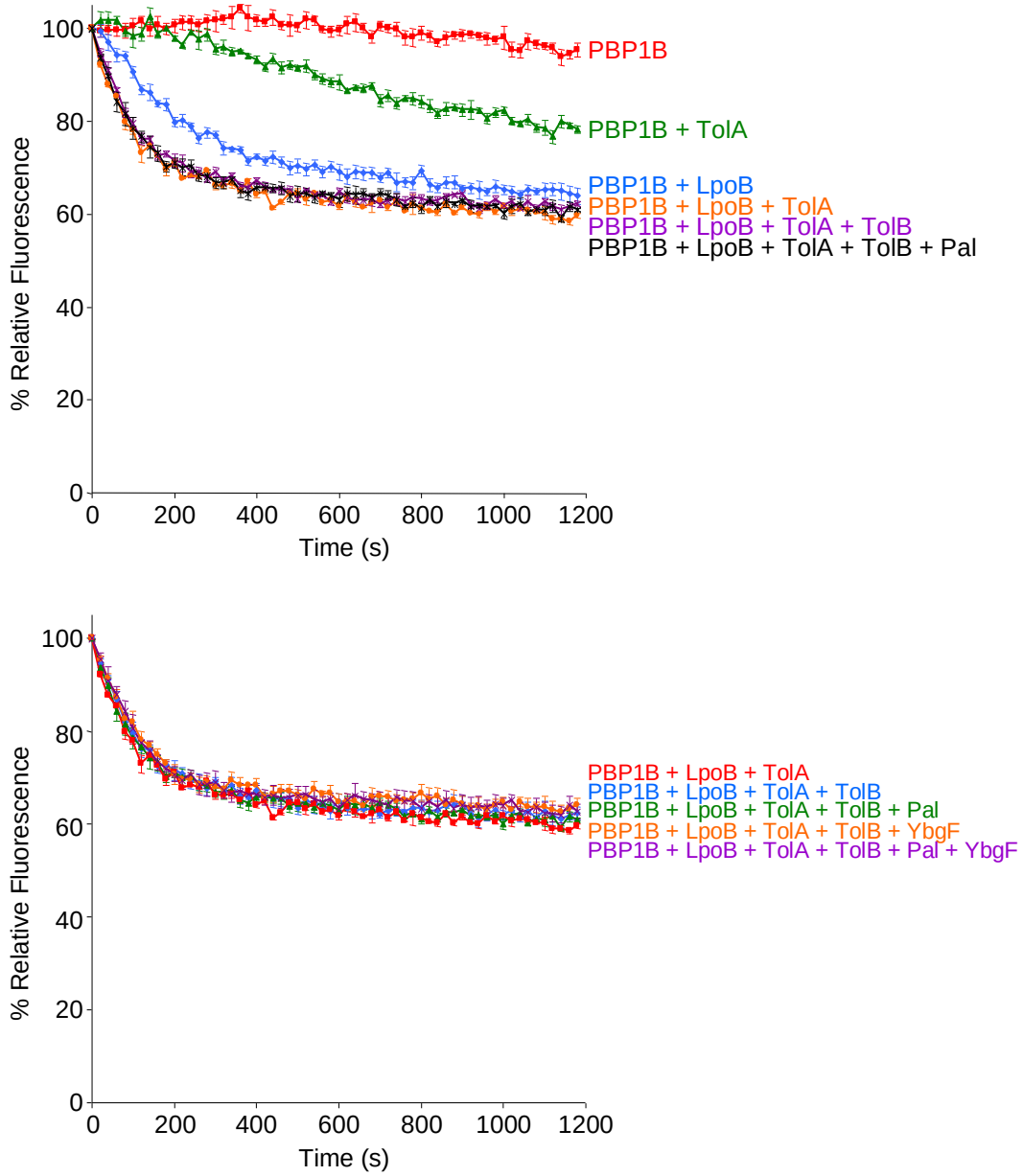

Figure 3.35 TolB, Pal and YbgF have no effect on the cumulative stimulatory effect of TolA and LpoB on PBP1B GTase activity

GTase reactions of PBP1B (0.25 µM) alone and in the presence of LpoB (0.5 µM), TolA-His (2 µM), TolB-His (10 µM), His-Pal (10 µM), YbgF (40 µM) or combinations of these indicated to the right of each curve in the corresponding colour. The Triton X-100 concentration was 0.04%. Addition of TolB, Pal and YbgF in the various combinations shown had no effect on the stimulation of PBP1B GTase by TolA-His and LpoB (n = 4). All reactions were part of the same experiment series but shown in separate graphs due to the large number of protein combinations.

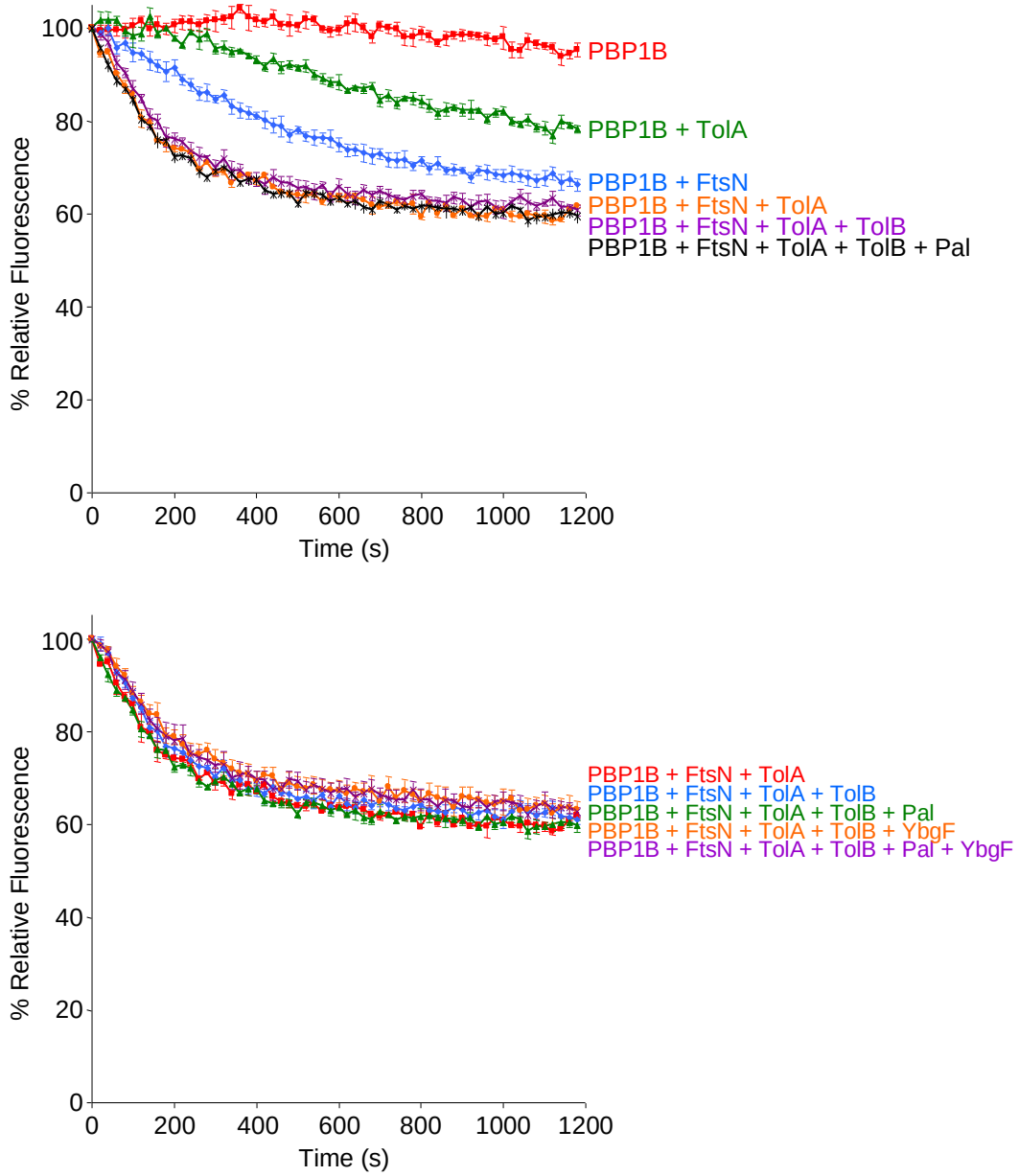

Figure 3.36 TolB, Pal and YbgF have no effect on the cumulative stimulatory effect of TolA and FtsN on PBP1B GTase activity

GTase reactions of PBP1B (0.25 µM) alone and in the presence of either FtsN (0.5 µM), TolA-His (2 µM), TolB-His (10 µM), His-Pal (10 µM), YbgF (40 µM) or combinations of these indicated to the right of each curve in the corresponding colour. The reaction temperature was 25°C and the Triton X-100 concentration was 0.04%. Addition of TolB, Pal and YbgF in the various combinations had no effect on the stimulation of PBP1B GTase by TolA-His and FtsN (n = 4). All reactions were part of the same experiment series but shown in separate graphs due to the large number of protein combinations.

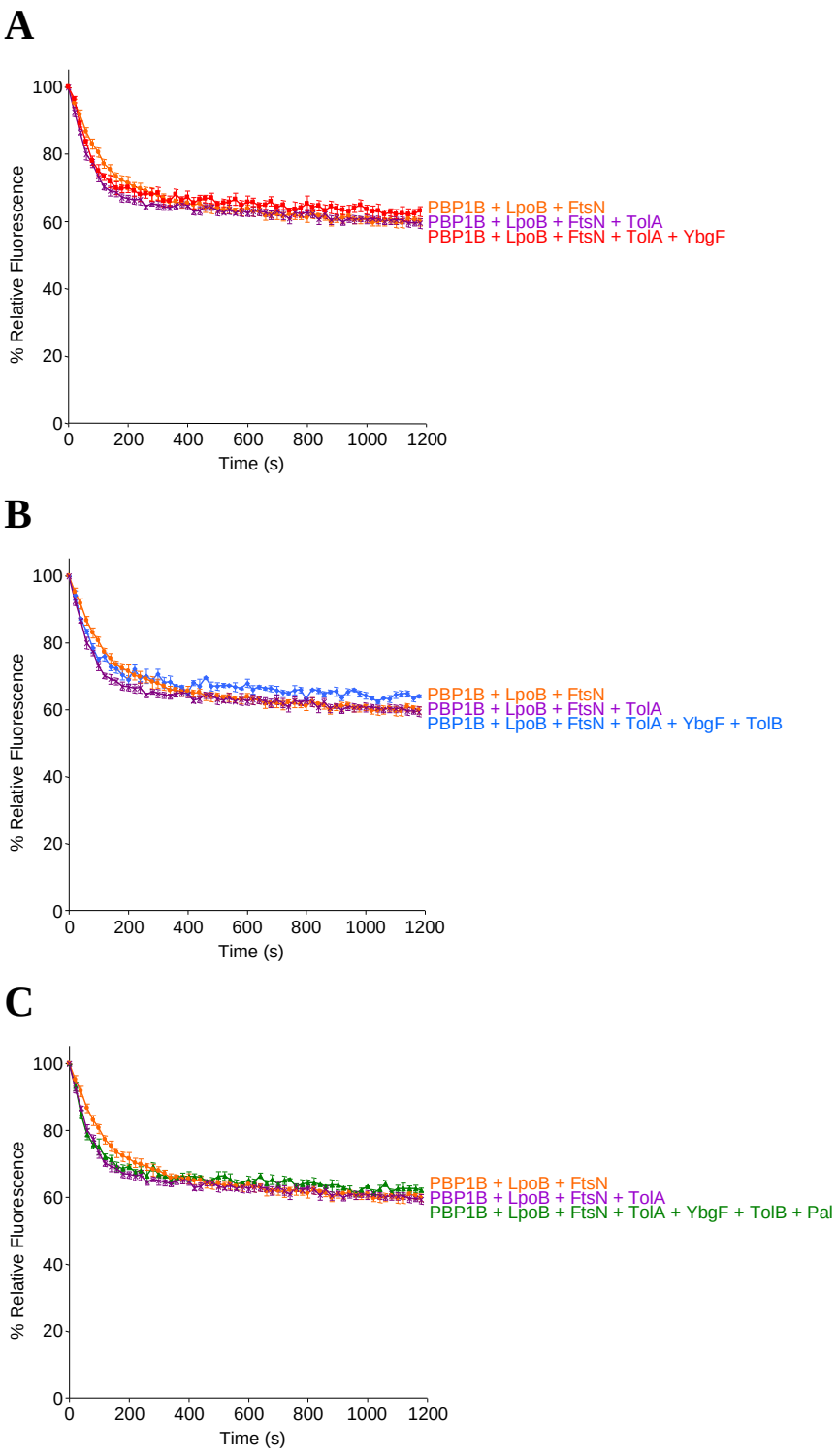

Figure 3.37 TolB, Pal and YbgF have no effect on the cumulative stimulatory effect of TolA, LpoB and FtsN on PBP1B GTase activity

GTase reactions of PBP1B (0.25 µM) in the presence of either LpoB(sol) (0.5 µM) and FtsN-His (0.5 µM) with and without TolA-His (2 µM) and the following; (A) with the addition of YbgF (40 µM), (B) with the further addition of TolB-His (10 µM), (C) with the further addition of His-Pal (10 µM).
Protein combinations indicated to the right of each curve in the corresponding colour. The Triton X-100 concentration was 0.04%. Addition of YbgF, TolB and Pal in the various combinations had no effect on the stimulation of PBP1B GTase by TolA, LpoB and FtsN (n = 4).

3.3.7 TolA and YbgF have no direct effect on PBP1B TPase activity

With the effects of the various combinations of Tol-Pal proteins on the GTase activity of PBP1B established, their effect on the TPase activity was investigated using the *in vitro* PG synthesis assay.

First, we investigated whether any of the purified Tol-Pal proteins had any effect on PBP1B alone. Addition of YbgF (40 µM), TolA-His (3 µM) or a combination of these had no effect on the cross-linking in PG produced by PBP1B (1 µM) (Fig. 3.38 A). The effect of adding TolB-His (10µM) with and without His-Pal (20 µM) was also investigated. No effect was observed (Fig. 3.38 B), which is in agreement with the fact that PBP1B did not interact with TolB in this work (3.3.4).

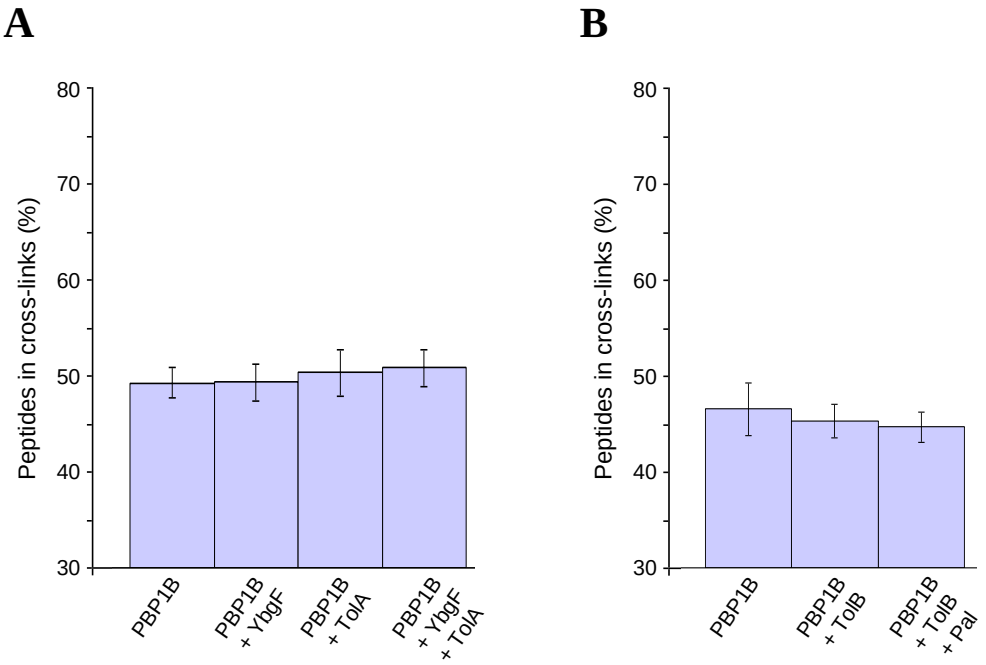

Figure 3.38 PBP1B TPase activity in the presence of Tol-Pal proteins

(A) The percentage of peptides present in cross-links in PG produced by PBP1B (1 µM) alone or in the presence of YbgF (40 µM), TolA-His (3 µM) or both. The presence of YbgF, TolA or a combination of the two had no significant effect (n = 3).
(B) The percentage of peptides participating in cross-links in PG produced by PBP1B (1 µM) alone and in the presence of TolB-His (10 µM) with and without His-Pal (20 µM). The presence of TolB both with and without Pal had no significant effect (n = 3).

3.3.9 The stimulation of PBP1B TPase activity by LpoB is negatively modulated by YbgF, TolA reverses the effect

After it was established that TolA and YbgF have no direct effect on the TPase activity of PBP1B *in vitro* the effect of these proteins on the stimulation of PBP1B TPase by LpoB was investigated.

YbgF (40 µM) was found to have a moderate negative effect on the percentage of peptides present in cross-links in PG produced by PBP1B (1 µM) in the presence of LpoB (1µM), from 68.1 ± 3.1% to 61.0 ± 4.1 ($p = 0.0003$). Addition of TolA-His (3 µM) to the reaction relieved the negative effect, returning the percentage of peptides in cross-links to 67.4 ± 2.6 ($p = 0.0031$). TolA-His alone had no significant effect (Fig. 3.39 A). This experiment series was performed at standard assay conditions with an NaCl concentration of 150 mM (2.4.6). When the concentration of NaCl was increased to 215 mM YbgF completely inhibits stimulation of PBP1B by LpoB (Fig. 3.39 B). Interestingly the negative modulation at standard conditions only affected the percentage of dimeric cross-links but not trimeric cross-links produced (Fig. 3.40). Next, whether the oligomeric state of YbgF affects its regulatory effect on PBP1B was tested. A version of YbgF with point mutations introduced (S49L/H52I) which stabilise its trimerisation by introducing a hydrophobic core in place of the hydrogen bonding hydrophilic core (188) was used. YbgF S49L/H52I, hereafter referred to as YbgF(Tri), interacted with PBP1B but did not exert the negative effect on stimulation by LpoB (Fig. 3.41).

These data supports the evidence presented in section 3.3.6 that PBP1B, LpoB, YbgF and TolA form a quaternary complex *in vitro*. Given the molarities of protein used in this experiment series (1 µM PBP1B, 1 µM LpoB(sol), 40 µM YbgF and 3 µM TolA) the relief effect of TolA is likely dependent upon its direct interaction with PBP1B, as part of the quaternary complex, as the amount of TolA in the reaction is insufficient for the effect to be the result of it simply sequestering YbgF away from the PBP1B-LpoB complex. Krachler *et al.* (188) showed that YbgF and TolA interact with a stoichiometry of 1:1. Thus, assuming 100% complex formation the amount of YbgF would still exceed 37 µM. It will be interesting to test this model in the future, using TolA(sol) in place of full length TolA. As TolA(sol) can still interact with YbgF but not PBP1B, it may not rescue the negative effect if the model were true.

Next, the effect of the addition of TolB with and without Pal was also investigated. There was no significant change in the percentage of peptides participating

in cross-links upon the addition of TolB with and without Pal (Fig. 3.42). Future work will investigate whether TolB and Pal play any role in the regulation of PBP1B-LpoB activity by YbgF and TolA.

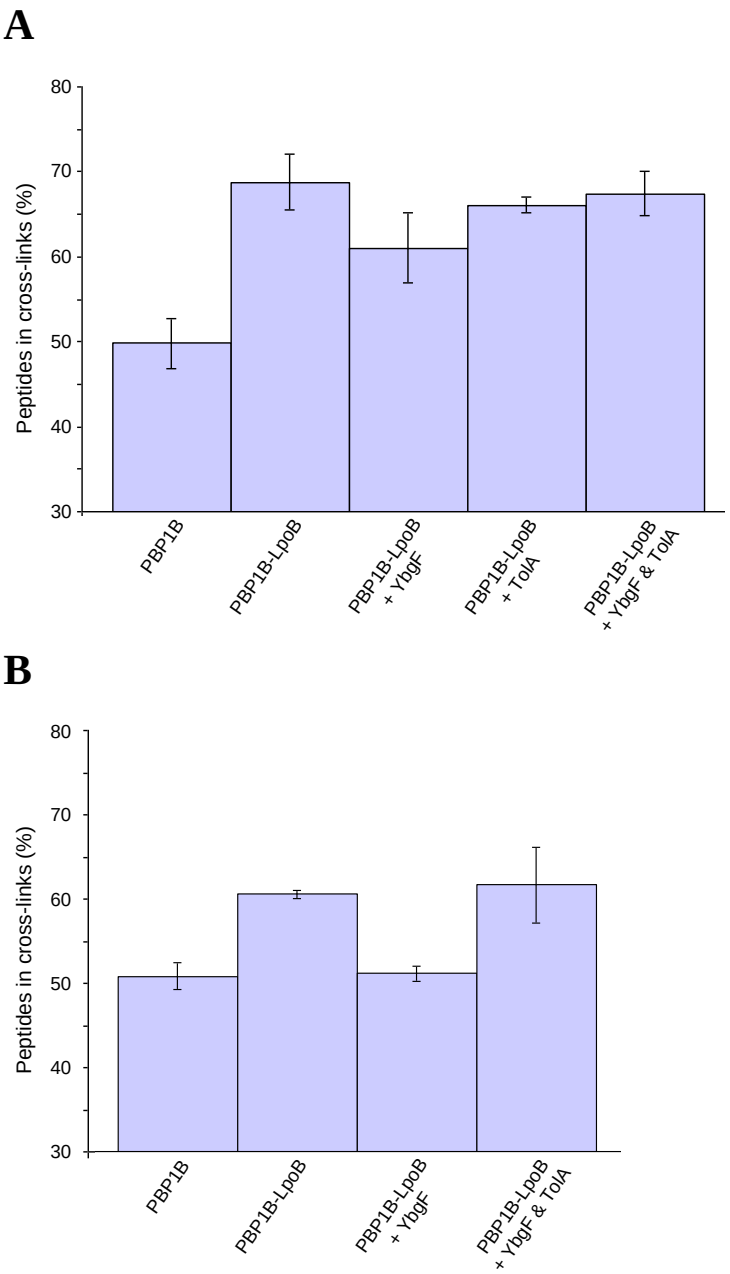

Figure 3.39 YbgF negatively modulates the stimulatory effect of LpoB on PBP1B TPase activity, TolA relieves this effect.

(A) The percentage of peptides in cross-links in PG produced by PBP1B (1 µM) alone and in the presence of LpoB(sol) (1 µM), YbgF (40 µM), TolA-His (3 µM) or combinations of these as indicated below the appropriate bar (n = 4).
(B) The percentage of peptides in cross-links in PG produced by PBP1B (1 µM) alone and in the presence of LpoB(sol) (1 µM), YbgF (40 µM), TolA-His (3 µM) or combinations of these at increased NaCl concentration in the reaction (n = 4).

A

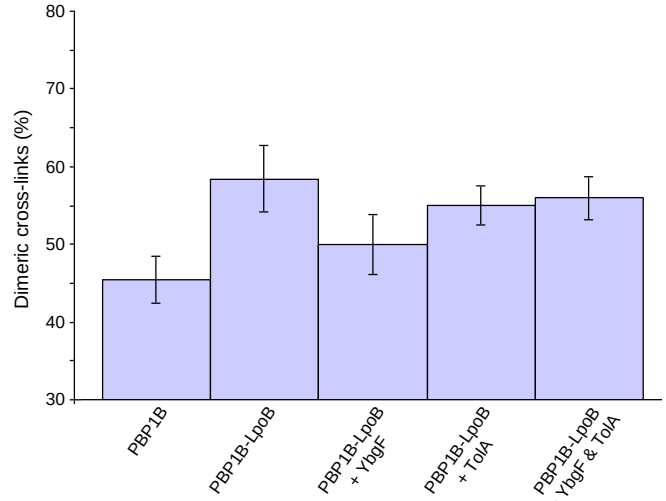

B

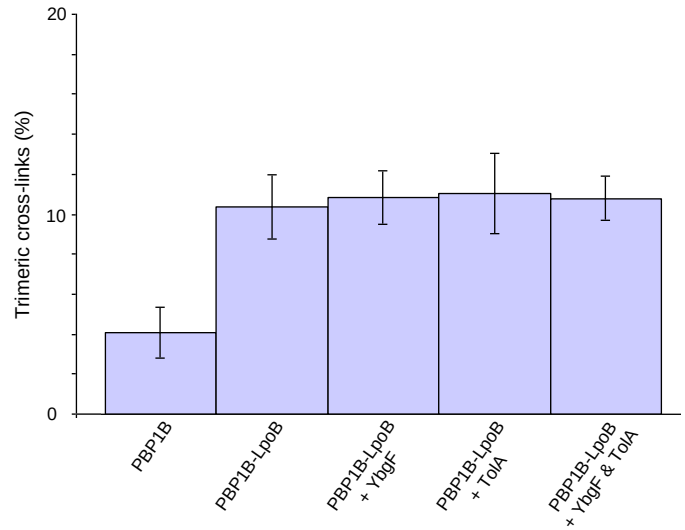

Figure 3.40 The negative modulatory effect of YbgF affects the formation of dimeric but not trimeric cross-links

The percentage of dimeric (A) and trimeric (B) cross-links in PG produced by PBP1B (1 µM) alone and in the presence of LpoB(sol) (1 µM), YbgF (40 µM), TolA-His (3 µM) or combinations of these as indicated below the appropriate bar (n = 4).

A

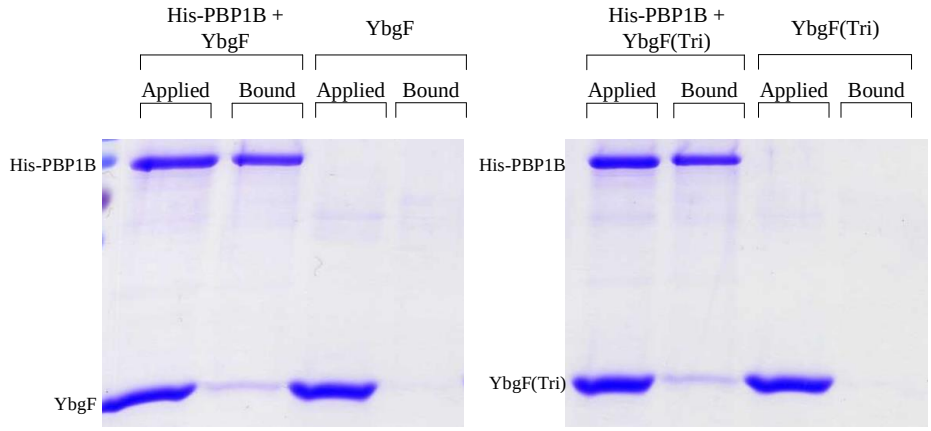

B

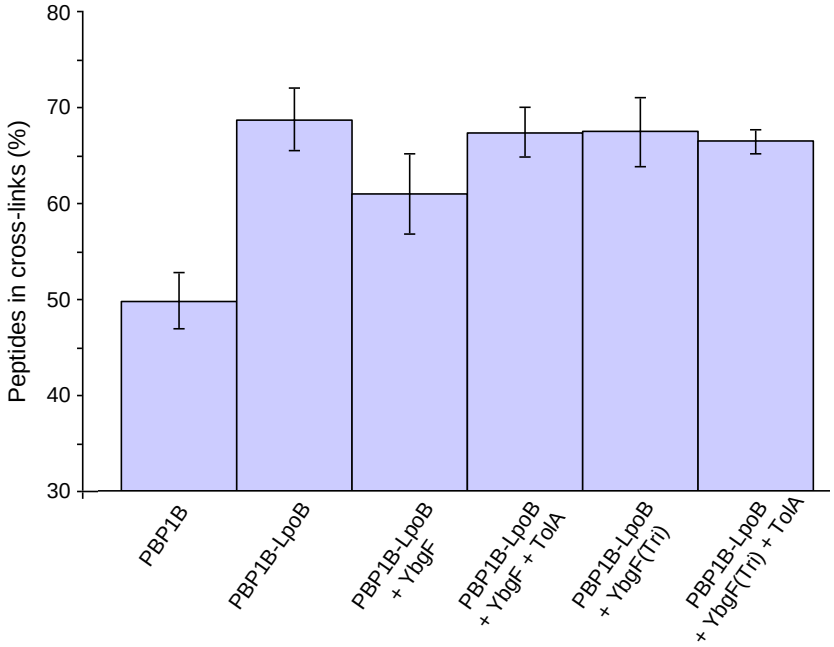

Figure 3.41 Trimeric YbgF still interacts with PBP1B but cannot negatively modulate stimulation by LpoB

(A) Coomassie-stained SDS-PAGE gel of an *in vitro* cross-linking / pulldown experiment. Applied, proteins incubated with the Ni-NTA beads; bound, proteins retained after the wash steps. His-PBP1B (1 µM), and either YbgF (4 µM) or YbgF(Tri) (4 µM) were incubated prior to cross-linking. Both YbgF versions were retained by His-PBP1B.
(B) The percentage of peptides participating in cross-links in PG produced by PBP1B (1 µM) alone and in the presence of combinations LpoB(sol) (1 µM), YbgF or YbgF(Tri) (40 µM), or TolA-His (3 µM). The stabilised trimeric from of YbgF did not negatively modulate the stimulation of PBP1B TPase by LpoB (n = 4).

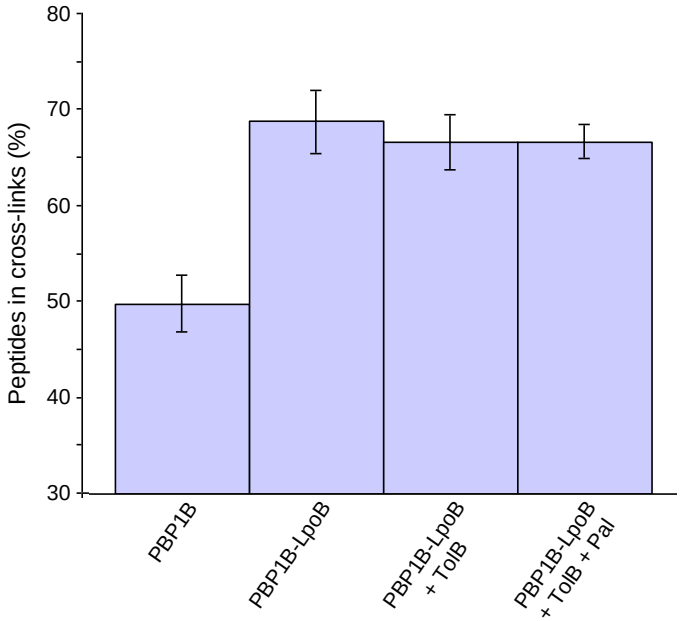

Figure 3.42 TolB with and without Pal has no effect on PBP1B stimulation by LpoB

(A) The percentage of peptides participating in cross-links in PG produced by PBP1B (1 µM) alone and in the presence of TolB-His (10 µM) with and without His-Pal (20 µM). (n = 4).

3.3.10 YbgF exists at 4000 to 5000 copies per cell in exponentially growing culture

The approximate cellular copy number of YbgF in *E. coli* BW25113 during exponential growth in rich medium (LB) was estimated using quantitative western blotting (2.4.13) (Fig. 3.43). The number of copies of YbgF per cell in an exponentially growing *E. coli* BW25113 culture in rich medium was estimated to be 4550 ± 540, which is the mean of 5 replicates ± the standard deviation. PBP1B exists at ~ 130 copies per cell (211), thus at a given time during exponential growth there are approximately 30 molecules of YbgF for every PBP1B. Therefore PBP1B is likely to be continually associated with YbgF.

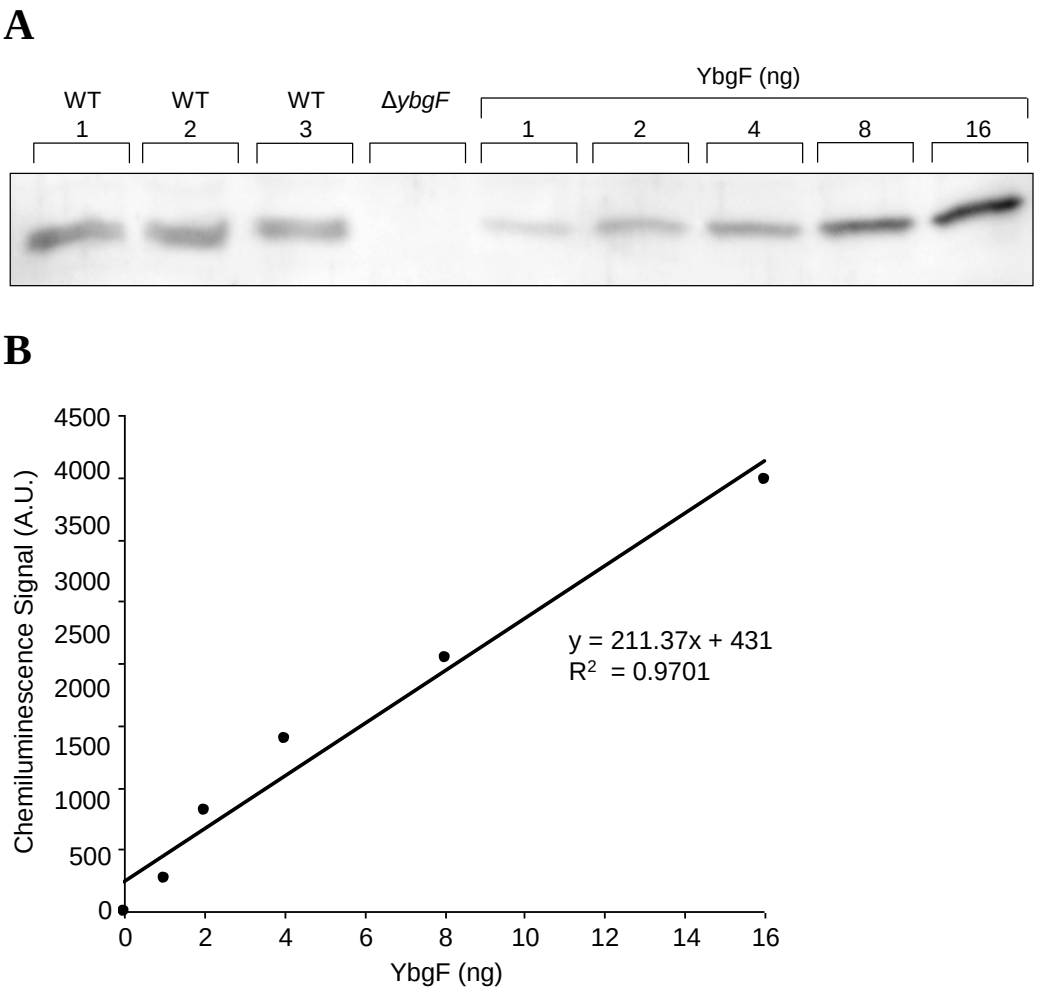

Figure 3.43 Quantitative western blotting of YbgF

(A) An example western blot detection of YbgF from BW25113 whole cell lysate along with purified YbgF standards. Standards were loaded in BW25113Δ*ybgF* lysate to ensure a similar transfer efficiency to endogenous YbgF. Chemiluminescence signal was measured and used to plot a standard curve (B).

3.3.11 Conclusions and discussion

The data presented in this section demonstrate the first evidence of a link between the major PG synthase active during cell division and constituents of the Tol-Pal complex. YbgF, which had a strong phenotypic correlation with PBP1B and LpoB, interacts directly with PBP1B *in vivo* and *in vitro*. The K_D of the YbgF-PBP1B interaction was determined to be 0.28 µM, which is similar to other known binding partners of PBP1B, if not slightly stronger (PBP3, 0.4 µM (67); LpoB, 0.8 µM (3.1.5)). TolA also interacted with PBP1B both *in vivo* (collaborative communication from Andrew Gray) and *in vitro* via its TM domain (domain I), suggesting this interaction occurs in or proximal to the cytoplasmic membrane. TolA and YbgF were also able to interact with PBP1B together, forming a ternary complex and though TolA and YbgF do not interact directly with LpoB, they do interact with PBP1B simultaneously with its lipoprotein activator, forming ternary complexes of TolA-PBP1B-LpoB and YbgF-PBP1B-LpoB. Given that these three individual ternary complexes exist, it is likely that a quaternary complex of all four exists. LpoB and TolB_N are structurally similar. A direct interaction between TolB and PBP1B was tested for by SPR at the same conditions used to demonstrate an interaction between PBP1B and LpoB but no interaction was seen. It is not without precedence that proteins with similar structures share no common function.

With a clear physical interaction of YbgF and TolA with PBP1B established, a functional context with regard to PBP1B's PG synthesis activities was explored. YbgF had no effect on the GTase activity of PBP1B, either alone or in the presence of LpoB or FtsN. TolA moderately stimulated PBP1B GTase, increasing the rate of reaction 1.9 ± 0.5-fold, which is a similar effect to that of PBP2 (3.2.6). The mechanism by which TolA stimulates PBP1B may be distinct from that of FtsN and LpoB as it is able to further stimulate PBP1B in the presence of these two activators, both individually and together. The addition of TolB with and without Pal has no effect on the stimulation of PBP1B GTase by TolA, nor does the addition of YbgF which is consistent with the interaction of TolA with PBP1B occurring via a distinct domain (domain I) to that with YbgF (domain II) and TolB (domain III) (see section 1.4.2.4).

Neither YbgF, TolA, nor a combination of the two proteins had any direct effect on the TPase activity of PBP1B with regard to the amount of cross-linkage in peptidoglycan produced by the enzyme. TolB with or without Pal also had no effect on PBP1B TPase consistent with the fact that no direct interaction was detected between TolB and PBP1B. However in the presence of LpoB, where PBP1B's TPase activity is

increased and presumably is closer to the true situation *in vivo* given the essentiality of LpoB for PBP1B function, YbgF had a moderate negative effect. The percentage of peptides participating in cross-links is decreased from ~ 70% to ~ 60%. This negative effect was reversed in the presence of TolA to the reaction, which returned the degree of cross-linkage back to ~70%. The effect of YbgF only impacted the formation of dimeric cross-links, with the percentage of trimeric cross-links remaining the same as with LpoB alone. Also, the negative effect was responsive to the oligomeric state of YbgF, as a version carrying amino acid substitutions which stabilise YbgF trimerisation was no longer able to exert this modulation. The molecular mechanism behind this is currently unclear and will be investigated. Addition of TolB with and without Pal had no effect on the stimulation of PBP1B TPase by LpoB. It will be worth investigating more complex reaction schema in the future, to test if TolB and/or Pal play any role in the effect of YbgF and TolA on PBP1B-LpoB.

The interaction and activity data suggest that YbgF and TolA are acting to fine tune the TPase activity of PBP1B-LpoB, implicating these as regulators of PBP1B. Given that the level of YbgF in the cell is 30-fold greater than PBP1B, it is possible that YbgF maintains a constant control of PBP1B TPase stimulation, until relieved by TolA. This regulation could control or maintain the degree of cross-linkage during constrictive cell wall synthesis and thus the structural characteristics of the septal PG. A prominent hypothesis of the synthesis of the PG sacculus in the cell is that new material is attached to the existing wall as it is simultaneously removed (as discussed in section 1.2.2). YbgF and TolA may provide a regulatory mechanism for the attachment of the newly synthesised material to the existing material, which may require the formation of transient trimeric cross-links. In the cell it is likely important that the rate of synthesis of new cell wall material be coupled to its insertion into the existing wall, YbgF and TolA may be acting to ensure this co-ordination via this proposed fine tuning of cross-linking. The formation of trimeric cross-links in the *in vitro* PG synthesis assay may represent the attachment of newly synthesised PG to an existing dimer in the reaction. However, this apparent regulation of specific cross-link formation could simply be an effect of the *in vitro* system and may not be truly representative of the *in vivo* situation, and whether or not an increased proportion of trimeric cross-links in the dividing/constricting cell wall is important is unknown and difficult to determine with current techniques. It is also not currently possible to monitor whether YbgF affects the attachment of new PG to existing sacculi by PBP1B *in vitro* by the established method using radioactive lipid II substrate because the experiment requires the separation of intact sacculi from PG

fragments in the supernatant. If a synthase has attached new material to the sacculus it is detected as an increase in radioactivity in the pellet. Unfortunately PBP1B produces glycans *in vitro* which are large enough to pellet with the intact sacculi and therefore the assay cannot distinguish between attached and un-attached PG fragments (50).

Another layer of complexity in understanding the regulatory role of YbgF and TolA is the fact that TolA possibly undergoes conformational changes upon energisation by TolQ and TolR in the cell, in a pmf dependant manner (212). Also, TolA likely participates in a cycling of interaction with TolB and Pal (185). Whether either of these facts have an impact on the system in the cell is unknown but it is possible they could create a cycling between states of TolA, which has previously been suggested (181). This cycling of states may lead to a switch between a configuration which permits the reversal of the negative effect of YbgF by TolA, and one where it is allowed to occur. The effect of the addition of TolB and Pal on the regulation of PBP1B-LpoB by YbgF and TolA *in vitro* will be investigated, however the recreation of the complex of TolQ, TolR and TolA *in vitro* in such a way as it could energise TolA is difficult. It may be possible to observe and effect in liposomes with an artificially generated membrane potential but this is not feasible at this time. A hypothesis / model as to the mechanism of regulation of PBP1B-LpoB by YbgF and TolA is discussed further in section 4.

Data from collaborators in this project provide an *in vivo* context of the work presented in this section. Data communicated by Andrew Gray, Jolanda Verhuel and Tanneke den Blaauwen shows that YbgF, like the other Tol-Pal components, localises at mid-cell during division shown by fluorescence microscopy and immunolocalisation microscopy. This localisation was independent of TolA, PBP1B and LpoB but required FtsZ, PBP3, FtsA and FtsN, indicating a functioning divisome and/or active PG synthesis during division is necessary. A strain lacking *ybgF* showed an increased sensitivity to the β-lactam cefsulodin, which primarily targets PBP1A leaving cells more reliant on PBP1B for growth, suggesting a role of YbgF in PBP1B regulation. In this strain the concentration of PBP1B and LpoB at mid-cell was decreased, suggesting that a loss of YbgF lead to their delocalisation during division. It has previously been shown that some proteins involved in cell wall synthesis do not localise properly if their enzymatic activity is blocked, such as PBP5 (208).

At this stage the *in vivo* situation remains difficult to interpret. A loss of *ybgF* alone had no significant growth phenotype, but in combination with a deletion of *lpoA* a severe growth defect was seen. This strain had impaired OM integrity with leakage of

periplasmic contents (loss of periplasmic mCherry fluorescence), OM blebbing and OM vesicle formation all of which are consistent with impaired Tol-Pal function, indicating that the functional relationship between the PG synthesis proteins of the divisome and Tol-Pal affects the functioning of both. By deletion of *lpoA* the cell now completely relies on PBP1B-LpoB for growth, which would explain the growth defect if the same were true of a deletion of *mrcA*. But this is not the case, as a *ybgF mrcA* double mutant had the same phenotype as a *ybgF* single. This suggests that LpoA has another, YbgF-like, role in the cell, which is currently under further investigation.

Thus, at this stage of the work the main conclusion is that there is a clear functional relationship between PG synthesis and OM invagination/stability during cell division in *E.* coli. YbgF may act as a co-ordinator of PBP1B and Tol-Pal during cell division for the proper synthesis / invagination of key layers of the cell envelope through a fine-tuning of PBP1B PG synthesis activity along with TolA. This is the first evidence for a direct coordination of two aspects of cell envelope synthesis in bacteria which is an exciting development in the field of cell wall synthesis. It may be that other aspects of envelope synthesis are linked, such as the cytoplasmic membrane and periplasm, but this is currently unknown. Much further work is needed to elucidate these processes.

4. Discussion

Insights into the regulation of PG synthases - biochemical evidence of multiprotein complexes for PG synthesis during cell division in *E. coli*

In the years since Höltje proposed that bacteria employ a three-for-one strategy in order to enlarge their peptidoglycan cell wall without suffering lysis, based on Koch's 'make before break' hypothesis, evidence has been growing for the existence of multiprotein complexes for the spatial and temporal regulation of this fundamental aspect of bacterial life (17, 42). It was later discovered that cell wall synthesis is controlled by cytoskeletal elements from inside the cell, and (in *E. coli*) by outer membrane regulators (1, 4). During cell division in *E. coli* more than 20 different proteins are recruited to mid cell for the synthesis and invagination of the key layers of the cell envelope, including the peptidoglycan sacculus and outer membrane. Though many elements have been identified more are being discovered, and the mechanisms remain poorly understood. Several studies have demonstrated the existence of functional interactions between PG synthases, hydrolases and several other proteins which localise at the site of future division in *E. coli*. This work elaborated on the functional interaction of known binding partners of the major peptidoglycan synthase active during cell division in *E. coli* and also discovered novel regulators which not only control PG synthesis by PBP1B, but may coordinate this with invagination of the outer membrane.

Mechanisms of regulation

The high resolution structure of the OM lipoprotein regulator of PBP1B, LpoB, was solved by NMR spectroscopy. This revealed a globular domain with structural similarity to the N-terminal domain of TolB (TolB_N) attached to a large, unstructured, flexible region. This region could allow LpoB to reach from the OM through pores in the PG sacculus to interact with and activate PBP1B. A loss of this region has no impact on the interaction of LpoB with PBP1B *in vitro*, or its stimulatory effects on the synthase, though it renders the protein non-functional in the cell. This is likely because the truncated LpoB versions can no longer reach PBP1B (Fig. 4.1). The non-catalytic UB2H domain, situated between the GTase and TPase domains of PBP1B was shown to be the binding site for LpoB and specific amino acid residues in both proteins required for the interaction were identified, which is the first dissection of the interaction site between a PG synthase and its activator. This showed a relatively large interaction interface consisting of several residues. The interface corresponds with a positively

charged patch on the surface of LpoB, which is conserved in 64 different species. Interestingly, one residue within this patch, when substituted, severely impaired the interaction with PBP1B but only moderately affected the activation of its activities (LpoB Y178). This suggests that binding is required but not sufficient for stimulation, i.e. with the Y178A substitution the affinity of LpoB for PBP1B is decreased, but upon binding its stimulatory effect is not impaired. This is consistent with a mechanism of activation whereby binding of LpoB to certain residues induces conformational changes in PBP1B which positively affect its enzymatic activity. These changes possibly impact on the environment of the catalytic Glu233 residue within the GTase domain of PBP1B. Much more evidence must be gathered before the mechanisms are revealed. It should be tested whether conformational changes occur in PBP1B and/or isolated UB2H upon binding of LpoB. This could be done by NMR spectroscopy using labelled UB2H, or by obtaining crystals of an LpoB-UB2H or LpoB-PBP1B complex for x-ray crystallography. Though crystallisation of LpoB failed previously we now know the likely cause was the long flexible region and could use the LpoB version lacking this region. Another possibility could be using site-directed methyl group labelling to measure structural dynamics in PBP1B by NMR spectroscopy, as this method can provide insights into distance constraints across a protein (213). Isothermal titration calorimetry (ITC) could also be used to analyse entropic changes in PBP1B upon LpoB binding.

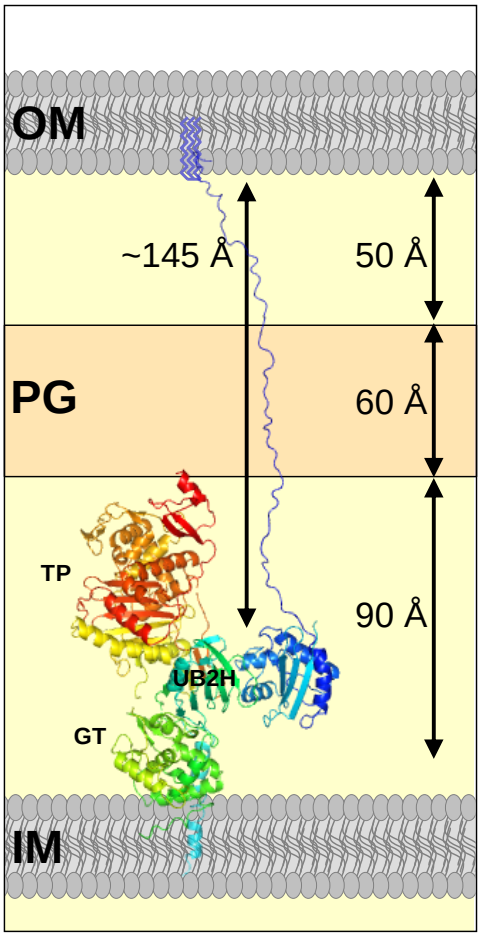

Figure 4.1 LpoB spans the periplasm to interact with the UB2H domain of PBP1B and stimulate the synthase

A model of the stimulation of PBP1B by LpoB in the bacterial envelope. PBP1B is shown with its GT, TP and UB2H domains labelled, LpoB (Blue) reaches from its membrane anchor in the OM via its ~145 Å long, flexible N-terminal region spanning the majority of the periplasm. This places its globular domain in position to interact with the UB2H domain of PBP1B and in turn activate its PG synthase activities. The cell envelope distances and PG thickness were taken from (11).

A summary of all PBP1B activity data presented in this work is shown in Fig. 4.2 below. All proteins tested by GTase and TPase assays are shown in the context of five active complexes; PBP1B, PBP1B-LpoB, PBP1B-FtsN, PBP1B-LpoB-FtsN and PBP1A.

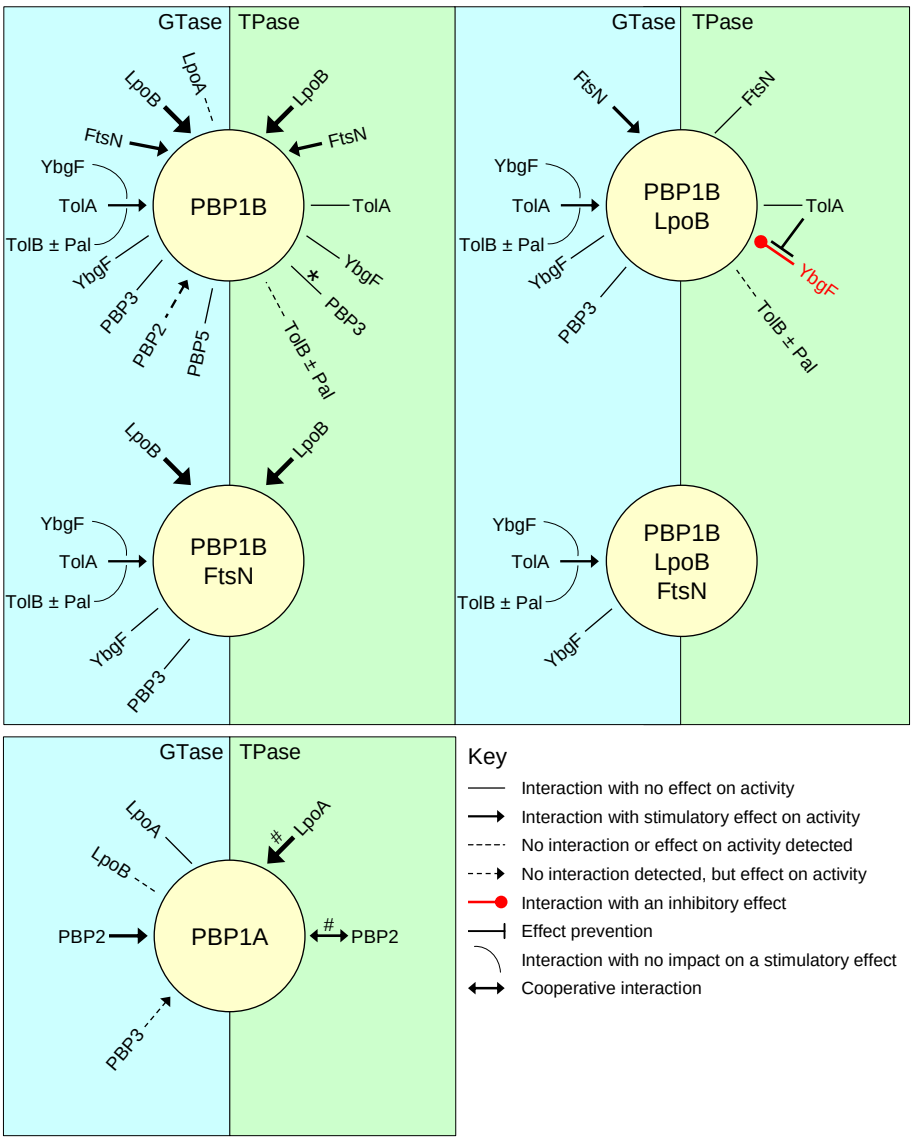

Figure 4.2 Summary of all activity data in this work

The activity data shown in this work is summarised, with all the tested potential effectors of GTase and TPase shown with regard to five active complexes; PBP1B, PBP1B-LpoB, PBP1B-FtsN, PBP1B-LpoB-FtsN and PBP1A. A key describing the meaning of each line / arrow is shown. Arrows are roughly scaled to represent the degree of the given effect. *, tested by Khai Bui (Newcastle University); #, tested by Manuel Banzhaf (Newcastle University) (60).

Stimulation of both synthetic activities of PBP1B appears to be interdependent, as all the amino acid substitutions in LpoB and PBP1B affecting the interaction interface affects both activities similarly, which is consistent with the fact that TPase activity requires ongoing GTase (53). Recent evidence presented by Lupoli *et al.* suggests that the main effect of LpoB is on the GTase domain (69), which is in agreement with data presented in this work. The magnitude of FtsN's effect on PBP1B GTase (3.2-fold increase) is approximately 2.5-fold less than that of LpoB (8-fold increase), which is mirrored in its effect on TPase, which is 2.8-fold less than that of

LpoB, suggesting that the increase in TPase activity may be a direct result of the increased rate of GTase. However, while LpoB and FtsN together exert a synergistic effect on PBP1B GTase activity they do not further increase the percentage of peptides in cross-links (TPase). This may be due to the inherent limitation of the end-point measurement of TPase activity, such that the percentage reached with LpoB alone may be the maximum possible, but the TPase rate could be greater in the presence of both activators. A continuous TPase assay would be useful not only for further understanding this mechanism, but also for studying the effects of YbgF and TolA, and should therefore be pursued in future work. An adaptation of the D-Ala release assay used for studying CPase activity may be suitable as the formation of cross-links also involves release of the terminal D-Ala (214). Further to this, a more precise investigation of the mechanisms of stimulation of PBP1B by LpoB and FtsN is required. An important question is whether the proteins alter the binding of PBP1B to lipid II or the growing glycan. New biophysical techniques such as microscale thermophoresis make experiments to answer these questions more feasible (215, 216).

Considering the above, we propose that the negative effect of YbgF on PBP1B-LpoB is through un-coupling the TPase domain from the GTase domain of PBP1B, and not through interfering with LpoB's binding or induction of conformational change as YbgF has no effect on the stimulation of GTase activity by LpoB, FtsN, TolA or all three together (Fig. 4.3). The ability to selectively uncouple the PG synthesis activities of PBP1B may provide a key functional flexibility during cell division, when the mode of cell wall synthesis must be constrictive.

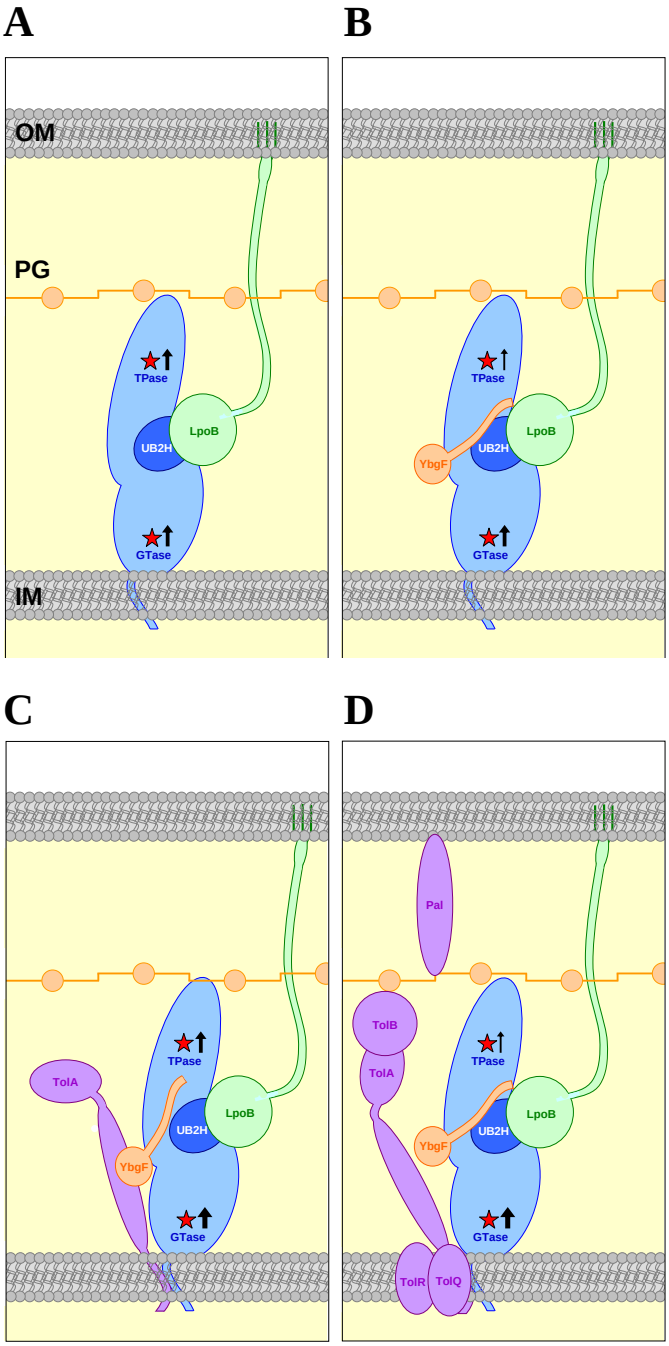

Figure 4.3 Simplified scheme showing the fine-tuning of PG synthesis by YbgF and TolA

Simplified cartoon representation of PBP1B, with the GTase and TPase active sites represented (stars). Upon binding of LpoB to the UB2H domain the GTase activity is increased, in turn increasing the TPase activity (A). Binding of YbgF partially uncouples the two catalytic domains by yet unknown mechanism (B). TolA interacts with PBP1B, likely via its membrane proximal domain (I), and prevents YbgF from exerting its negative, uncoupling effect possibly through its interaction with YbgF (C). Though it is unknown at this stage, TolA may cycle between YbgF bound and unbound states in response to other members of the Tol-Pal system such as energisation by TolQ / TolR, or interaction with TolB upon its release from Pal (D).

The multiprotein complex for PBP1B activity

The fact that LpoB, FtsN and TolA exert a synergistic effect on PBP1B GTase and that YbgF and TolA regulate stimulation of PBP1B by LpoB further supports the hypothesis that multiprotein complexes exist for the regulation of PG synthesis. It is interesting that LpoB, FtsN and TolA share similar structural characteristics, in that they possess long, flexible regions. This flexibility may be vital for the functioning of PBP1B in the dynamic multiprotein divisome, allowing these regulators to exert their effects somewhat distally and to accommodate the additional protein-protein interactions of PBP1B within the divisome, such as FtsW and PBP3 which interact with several other proteins themselves. PBP1B is shown along with its regulatory and accessory proteins during cell division as the PG synthetic sub-section of the divisome (Fig. 4.4). In the state shown LpoB, FtsN and TolA are bound and activate PBP1B, with TolA preventing the negative effect of YbgF. Thus this state could be considered the fully 'on' state. As discussed above, it is possible that TolA cycles between states of permitting and preventing YbgF exerting the negative modulation. Whether this cycling also affects FtsN in any way is not yet known. Regardless, it is likely that this complex needs to be highly dynamic in order to achieve its essential cellular function in a controlled manner and enhanced flexibility would allow this.

PBP1A is able to substitute for PBP1B in the divisome with only a small impact on cell width and timing of division (60). The mechanisms of PG synthesis during division, though further elucidated by this work, still remain unclear. Evidence presented shows that both PBP1A and PBP1B are mildly stimulated by their non-cognate class B PBP suggesting that PBP2 and PBP3 may facilitate this redundancy to a degree, but how, if at all, is PBP1A-LpoA co-ordinated with Tol-Pal? The yet unexplained *ybgF lpoA* phenotype may hint at a YbgF-like function for LpoA not yet discovered, such that in the absence of PBP1B or YbgF, it is able to co-ordinate PBP1A and Tol-Pal function in some way during cell elongation and when PBP1A is active during cell division. Further experiments are required to understand this possible role of LpoA.

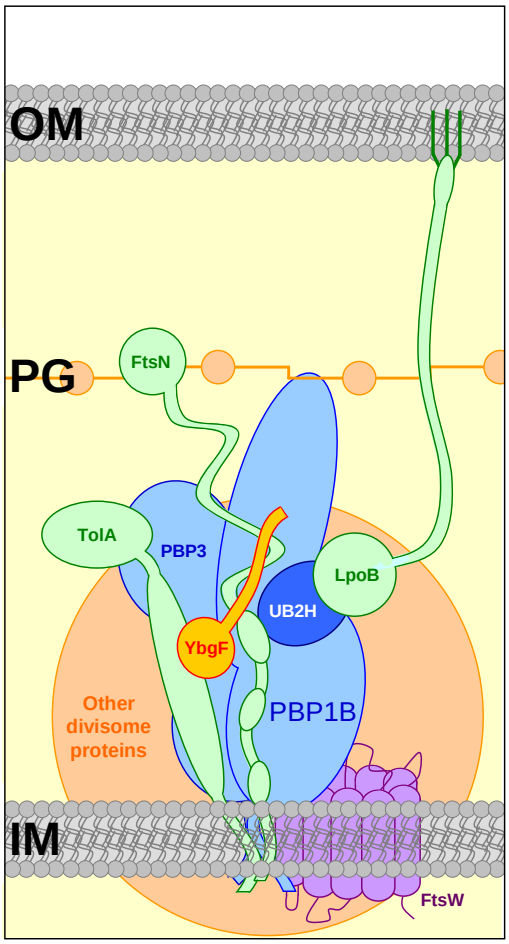

Figure 4.4 Simplified scheme of the proposed PBP1B regulatory complex

A simplified cartoon representation of PBP1B within the divisome along with its regulatory binding partners LpoB, FtsN, TolA and YbgF and other binding partners likely important for its function during cell division, the essential TPase PBP3 and the lipid II flippase FtsW (purple), which likely delivers the cell wall precursor directly to the PG synthases. Proteins are shown as connected ovals or spheres roughly corresponding to known specific structural features/domains, but not strictly to scale. Synthases are shown in blue, positive regulators in green, the negative regulator YbgF in red/gold, and the lipid II flippase in purple. Other members of the divisome are represented as an orange sphere for simplicity. In the state shown, PBP1B is activated by LpoB, FtsN and TolA with TolA preventing the negative effect of YbgF (i.e. a fully 'on' state). Though PBP1B is known to form homodimers, and likely acts as a dimer in the cell, a monomer is shown for simplicity.

Coordination of cell envelope constriction

Cell division in Gram-negative bacteria likely requires coordination of processes across all layers of the cell envelope: inner membrane constriction, septal peptidoglycan synthesis and cleavage, and outer membrane constriction. It is a logical assumption that the systems which achieve these processes are functionally linked for a coordinated constriction of the cell envelope during division. As part of a collaborative project this work elaborates on the initial discovery by Gerding *et al.* and Typas *et al.* who

demonstrated the involvement of the Tol-Pal proteins (27, 177), with evidence of a clear functional link between the major PG synthase active during cell division PBP1B, and the Tol-Pal system. This is the first characterisation of a mechanism for synchronisation of PG synthesis and OM constriction. At this stage, the main conclusion is that YbgF and TolA interact with PBP1B, modulating its PG synthesis activity and, through currently unknown mechanisms, also modulates the activity of the Tol-Pal system as evidenced by a decrease in OM stability in the absence of by a decrease in OM stability in the absence *ybgF* and *lpoA*. This YbgF mediated co-ordination is important for proper PBP1B function in the cell. YbgF is the first known negative regulator of a PG synthase, as it modulates the stimulation of PBP1B by LpoB. TolA acts to reverse this negative modulation, likely through altering the interaction of YbgF and PBP1B (see Fig. 4.2 and 4.3) and further to this rescuing effect, TolA is also capable of moderately increasing the rate of PBP1B GTase activity.

Final word

This work presents major new insights into the regulation of PBP1B, linking it with proteins involved in OM invagination during cell division and providing the first evidence for multiple protein-protein interactions exerting synergistic and modulatory effects on the activity of the synthase, with the first demonstration of a negative regulator, YbgF. Improving our understanding of the regulation of fundamental processes in bacteria is a key step in the development of new antimicrobial therapeutics, an endeavour which has become more and more pressing with the increasing prevalence of pathogens resistant to multiple compounds.

5. Appendix

5.1 Materials

5.1.1 Chemicals

30% Acrylamide (Rotiphorese)	Roth
Acetic acid	Sigma
Agar	Fluka
Ammonium peroxodisulfate (APS)	Serva
Bromphenol blue	Sigma
Calcium chloride	Sigma
Casein	VWR
Chloroform	Fisher
CNBr-activated sepharose	GE Healthcare
Coomassie Brilliant Blue R-250	Roth
DTSSP	Pierce/Thermo Scientific
EDTA	Sigma
EGTA	Sigma
Ethanol	Fisher
Glycerol	Sigma
Glucose	Sigma
Glycine	Sigma
HEPES	VWR
Hydrochloric acid	Sigma
Imidazole	Sigma
Isopropanol	Sigma
Magnesium chloride	VWR
β-mercaptoethanol	Sigma
Methanol	Fisher
Methylene blue	Sigma
Milli-Q H2O	Millipore dispenser
Phosphoric acid	Sigma
Protease inhibitor cocktail (P8465)	Sigma
Rubidium chloride	Sigma
Sucrose	Sigma
Sodium acetate	Sigma
Sodium azide	Merck

Sodium borate	Sigma
Sodium borohydride	Sigma
Sodium chloride	VWR
Sodium dihydrogenphosphate	VWR
di-Sodium orthophosphate	VWR
Sodium dodecyl sulphate	Melford
Sodium hydroxide	Sigma
Sodium phosphate	Sigma
Trizma™ base (Tris)	Sigma
TEMED	Sigma
Tryptone	VWR
Tween 20	Serva
Yeast extract	Deutshe Hefewerke

5.1.2 Antibiotics

Kanamycin	Sigma
Ampicillin	Sigma
Bocillin FL	Molecular probes
Chloramphenicol	Sigma
Aztreonam	Sigma

5.1.3 Enzymes for PG analysis and assays

Pronase E (*Streptomyces grisens*)	Boehringer
α-Amylase (*Bacillus subtilis*)	Fluka
Cellosyl (*Streptomyces coelicolor*)	Hoechst
DNase (Bovine Pancreatic)	Sigma
VIM-4 β-lactamse (*pseudomonas aueruginosa*)	Adeline Derouaux

5.1.4 Molecular weight markers

PageRuler™ prestained marker	Thermo Scientific
Spectra™ high range marker	Thermo Scientific

5.1.5 Kits

Pierce BCA protein assay kit	Thermo Scientific
ProteON™ general amine coupling kit	BioRad
GenElute™ HP plasmid midi-prep kit	Sigma
Zinc staining kit	BioRad

5.1.6 Other materials

Chemiluminescence (ECL) reagents	GE Healthcare
Dialysis cassettes MWc.o. 6 – 8 kDa	Novagen
Dialysis tubing MWc.o. 6 – 8 kDa	Spectrumlabs
[^{14}C]-Glc*N*Ac lipid II	Eefjan Breukink, Manuel Banzhaf
Dansyl-lipid II	Eefjan Breukink, Jules Phillipe
FloScint III liquid scintilant	Perkin Elmer
HisTrap HP (5 ml)	GE Healthcare
HiTrap Q HP (5 ml)	GE Healthcare
HiTrap SP HP (5 ml)	GE Healthcare
Ni^{2+}-NTA superflow beads	QIAGEN
Nitrocellulose membrane	BioRad
ProteON™ GLC sensorchip	BioRad
Protein G-coupled agarose	Pierce/Thermo Scientific
Superdex75 HiLoad 16/60	GE Healthcare
Superdex75 10/300 GL	GE Healthcare
Superdex200 HiLoad 16/600	GE Healthcare
Superdex200 10/300 GL	GE Healthcare
VivaSpin 6 columns (MWc.o. 5 kDa)	Sartorius Stedim

5.1.7 Antibodies

Antibody	Working dilution	Source
α-PBP1A	1 in 1000	Tanja Kallis[1]
α-PBP1B	1 in 5000	Ute Bertsche[1] and this work
α-LpoA	1 in 2000	Manuel Banzhaf[2]
α-LpoB	1 in 2000	Manuel Banzhaf[2]
α-PBP3	1 in 5000	Ute Bertsche[1]
α-MltA	1 in 1000	Waldemar Vollmer[1,2]
α-FtsN	1 in 5000	Waldemar Vollmer[1,2]
α-YbgF	1 in 7500	This work
α-TolA	1 in 5000	This work
α-TolB	1 in 5000	This work
α-Pal	1 in 5000	This work
Goat α-rabbit-HRP conjugated	1 in 10000	Sigma
TrueBlot™ α-rabbit	1 in 2000	eBioscience/Rockford

[1] University of Tübingen
[2] Newcastle university

5.1.8 Proteins

Protein	Description	Source
PBP1Bγ	GSHMA-PBP1Bγ	Jacob Biboy[1]
PBP1Bγ E166A	GSH_6MA-PBP1Bγ E166A	This work
PBP1Bγ D163A/E166A	GSH_6MA-PBP1Bγ D163A/E166A	This work
PBP1Bγ E187A/N188A/ R190A/Q191A	GSH_6MA-PBP1Bγ E187A/N188A/R190A/ Q191A	This work
PBP1Bγ D163A/E166A/ E187A/N188A/R190A/ Q191A	GSH_6MA-PBP1Bγ D163A/E166A/E187A/ N188A/R190A/Q191A	This work
His-UB2H	MGSSH_6SSGLVPRGSHM-PBP1B(108-200)	This work
His-LpoB(sol)	MGSSH_6SSGLVPRGSHM-LpoB(21-213)	This work
LpoB(sol)	GSHM-LpoB(21-213)	This work
LpoB(sol) Y178A	GSHM-LpoB(21-213) Y178A	This work
LpoB(sol) D106A/M195A	GSHM-LpoB(21-213) D106A/M195A	This work
LpoB(sol) N110A/R111A	GSHM-LpoB(21-213) N110A/R111A	This work
LpoB(Δ1-56)	GSHM-LpoB(57-213)	This work
LpoB(Δ1-73)	GSHM-LpoB(74-213)	This work
PBP1A	GSHMASMTGGQQMGA-PBP1A	Jacob Biboy[1]
His-LpoA(sol)	MGSSH_6SSGLVPRGSHM-LpoA(28-652)	This work
His-PBP3	MRGSH_6GSIEGR-PBP3	This work
PBP5	MGSSH_6GLVPRGSHMAS-PBP5(33-403)	Jacob Biboy[1]
PBP2	MASH_6-PBP2	Manuel Banzhaf[1]
FtsN-His	FtsN-GSH_6	This work
FtsNΔ1-57-His	FtsN(58-319)-GSH_6	This work
His-YbgF	MGSSH_6SSGLVPRGSHM-YbgF(26-263)	This work
YbgF	GSHM-YbgF(26-263)	This work
YbgF(Tri)	GSHM-YbgF(26-263) S49L/H52L	This work
His-TolA(sol)	MGSSH_6SSGLVPRGSHM-TolA(74-421)	This work
TolA(sol)	GSHM-TolA(74-421)	This work
TolA-His	TolA-LEH_6	This work
TolA	GSHM-TolA	This work
TolB-His	TolB-LEH_6	This work
His-Pal(sol)	MGSSH_6SSGLVPRGSHM-Pal(29-173)	This work
BSA	Bovine serum albumin	Pierce

[1] Newcastle University

5.1.9 Plasmids

Strain/Plasmid	Properties	Ref. / Source
pDML924	Overproduction of His-PBP1Bγ	(40)
pET28-His-LpoB(sol)	Overproduction of His-LpoBΔ1-20	(27)
pET28-His-LpoA(sol)	Overproduction of His-LpoAΔ1-27	(27)
pET15-His-UB2H	Overproduction of His-UB2H (*mrcB* 108-200)	(56)
pFE42	Overproduction of FtsN-His	(145)
pHis17-ECN2	Overproduction of FtsNΔ1-57-His	(145)
pMvR-1	Overproduction of His-PBP3	(67)
pDACAhis	Overproduction of PBP5	(208)
pET28-His-YbgF(Δ1-25)	Overproduction of His-YbgFΔ1-25	A. Gray[1]
pET28-His-TolA(74-421)	Overproduction of His-TolA74-421 – domains II and III	A. Gray[1]
pET28-His-TolA	Overproduction of His-TolA (N-terminally tagged)	A. Gray[1]
pET28-TolA-His	Overproduction of TolA-His (C-terminally tagged)	A. Gray[1]
pET28-TolB-His	Overproduction of TolB-His	A. Gray[1]
pET28-His-Pal(sol)	Overproduction of His-PalΔ1-28	A. Gray[1]
pET28-His-YbgF(Tri)	Overproduction of His-YbgF S49L H52I (mutant stabilised in trimeric state)	A. Gray[1]
pAK20	(pET28-His-PBP1B E166A) Overproduction of His-PBP1Bγ version	A. Koumoutsi[1]
pAK43	(pET28-His-PBP1B D163A/E166A) Overproduction of His-PBP1Bγ version	A. Koumoutsi[1]
pAK47	(pET28-His-PBP1B E187A/N188A/R190A/ Q191A) Overproduction of His-PBP1Bγ version	A. Koumoutsi[1]
pAK55	(pET28-His-PBP1B D163A/E166A/E187A/ N188A/R190A/Q191A) Overproduction of His-PBP1Bγ version	A. Koumoutsi[1]
pAK44	(pET28-His-LpoB(sol) D106A/M195A) Overproduction of His-LpoB(sol) version	A. Koumoutsi[1]
pAK35	(pET28-His-LpoB(sol) N110A/R111A) Overproduction of His-LpoB(sol) version	A. Koumoutsi[1]
pAK52	(pET28-His-LpoB(sol) Y178A) Overproduction of His-LpoB(sol) version	A. Koumoutsi[1]

[1] Plasmid prepared for this work/collaborative projects

5.1.10 *E. coli* strains

Strain/Plasmid	Relevant Property/Genotype	Ref. / Source
MC1061	Laboratory strain	(217)
BW25113	KIEO laboratory strain	(218, 219)
BL21(DE3)	Expression strain F- *ompT, dcm hsdS* (rB- mB-) *gal* (λDE3)	Novagen
XL1-Blue	Expression strain *recA1, endA1, gyrA96, thi-1, hsdR17, supE44, relA1, lac*	Stratagene
DH5α	Non-expression strain *huA2, lacU169, phoA, glnV44, Φ80' lacZ, gyrA96, recA1, relA1, endA1, thi-1, hsdR17*	Invitrogen
BW25113Δ*lpoB*	*lpoB* deletion strain	(218, 219)[1]
BW25113Δ*lpoA*	*lpoA* deletion strain	(218, 219)[1]
BW25113Δ*ybgF*	*ybgF* deletion strain	(218, 219)[1]
BW25113Δ*tolB*	*tolB* deletion strain	(218, 219)[1]
BW25113Δ*tolA*	*tolA* deletion strain	(218, 219)[1]
BW25113Δ*pal*	*pal* deletion strain	(218, 219)[1]
JOE309 pJC83	*ftsN* depletion strain	(125)
CAG606366	*mrcB*Δ144-191 PBP1BΔUB2H	(27)

[1] Gift from Kenn Gerdes, Newcastle University

5.1.11 Laboratory equipment

Agilent 1200 HPLC system	Agillent technologies
Autoclave	Astell
ÄKTA Prime^{+}	GE Healthcare
Avanti J-26 XP centrifuge	Beckman-Coulter
β-RAM model5 scintilation flow-cell	LabLogic
Developer	Konica SRX-101A
Digital sonifier	Branson
Epson perfection 3490 scanner	Epson
Gel tank, for SDS-PAGE	BioRad
ImageQuant LAS4000mini	GE Healthcare
Kern EG balance	Kern
Kern PFB balance	Kern
Mettler Toledo Classic plus balance	Mettler
FLUOstar Optima plate reader	BMG labtech

Micro 200R microfuge	Hettich
MilliQ PF plus water purification system	Millipore
Optima™ ultracentrifuge	Beckman-Coulter
Optima™ TLX ultracentrifuge	Beckman-Coulter
pH meter	Jenway
Prism microfuge	Labnet
ProteON™ XPR36	BioRad
ScanVac SpeedVac system	UniEqzip
Sigma 3-16k centrifuge	Scientific Laboratory Supplies
Spectrophotometer	Biochrom Libra S22
Thermomixer	Eppendorf
Typhoon scanner	GE Healthcare
Water bath with thermostat	Clifton
Wet-Blot transfer chamber	BioRad

5.2 Supplementary figures

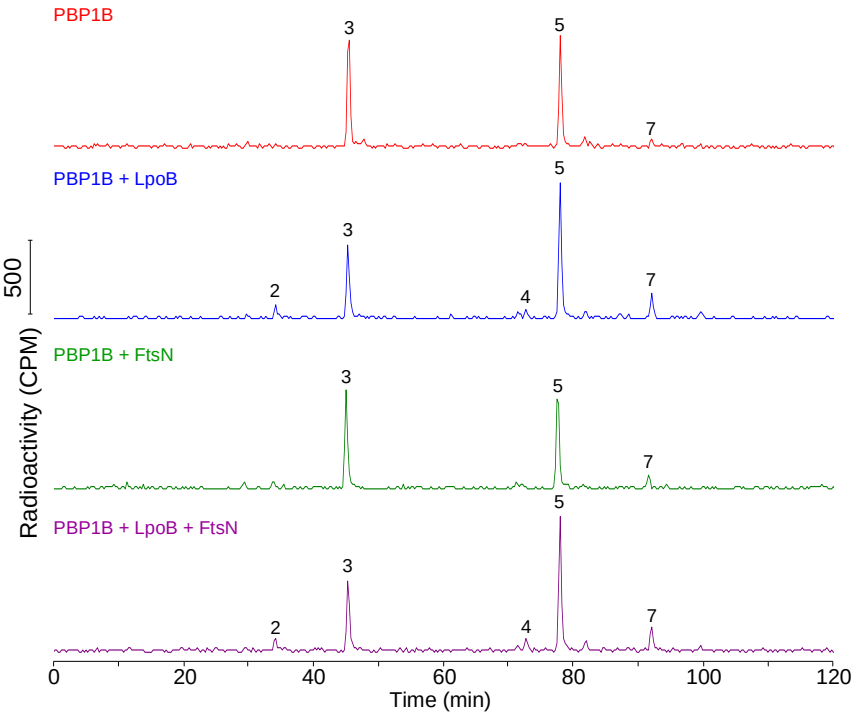

Figure 5.1 HPLC chromatograms corresponding to Fig. 3.20

Representative HPLC chromatograms corresponding to Fig 3.20 B showing counts per minute (CPM) against time (min). Muropeptide peaks are annotated as in figure 2.12.

A

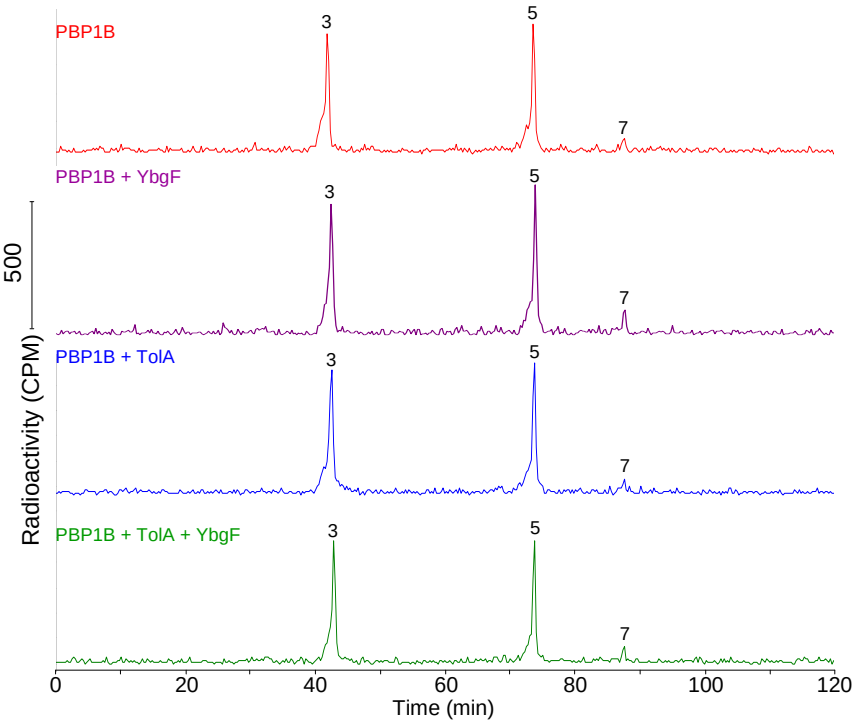

B

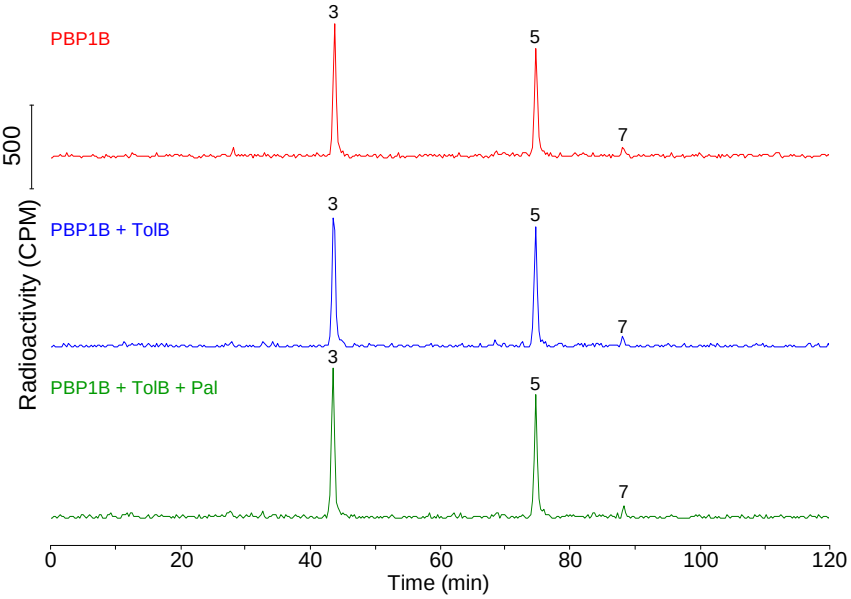

Figure 5.2 HPLC chromatograms corresponding to Fig. 3.40

Representative HPLC chromatograms corresponding to Fig 3.38 A (A) and Fig. 3.38 B (B), showing counts per minute (CPM) against time (min). Muropeptide peaks are annotated as in figure 2.12.

A

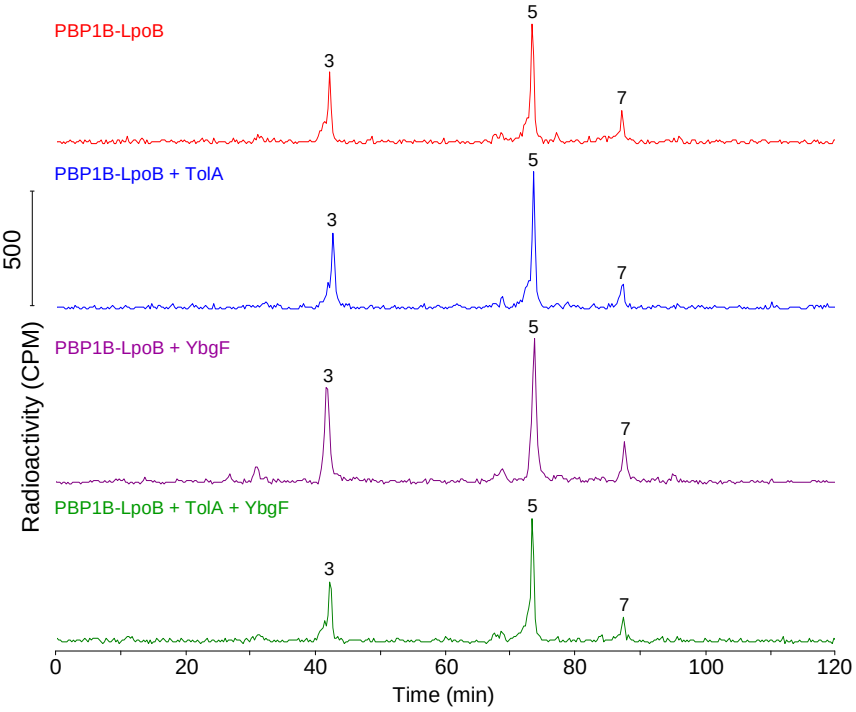

B

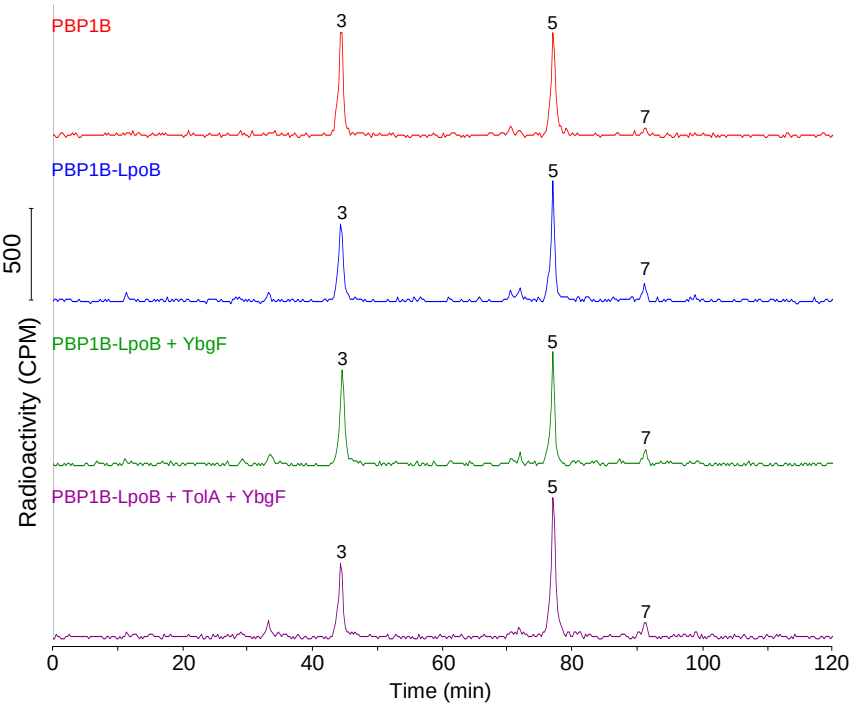

Figure 5.3 HPLC chromatograms corresponding to Fig. 3.41

(A) Representative HPLC chromatograms corresponding to Fig 3.39 A (A) and Fig. 3.39 B (B), showing counts per minute (CPM) against time (min). Muropeptide peaks are annotated as in figure 2.12.

A

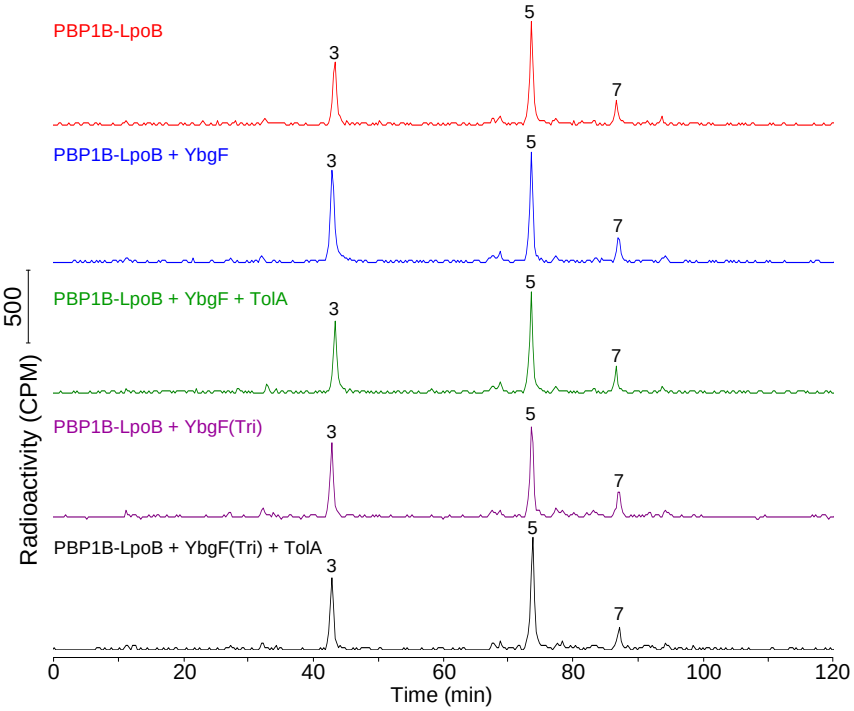

B

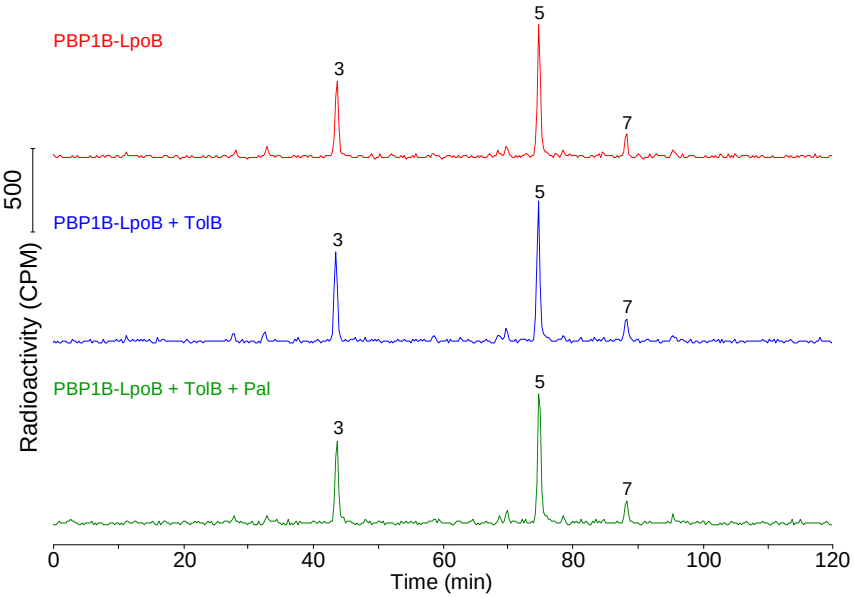

Figure 5.4 HPLC chromatograms corresponding to Fig. 3.43 and 3.44

(A) Representative HPLC chromatograms corresponding to Fig 3.41 (A) and Fig. 3.42 (B), showing counts per minute (CPM) against time (min). Muropeptide peaks are annotated as in figure 2.12.

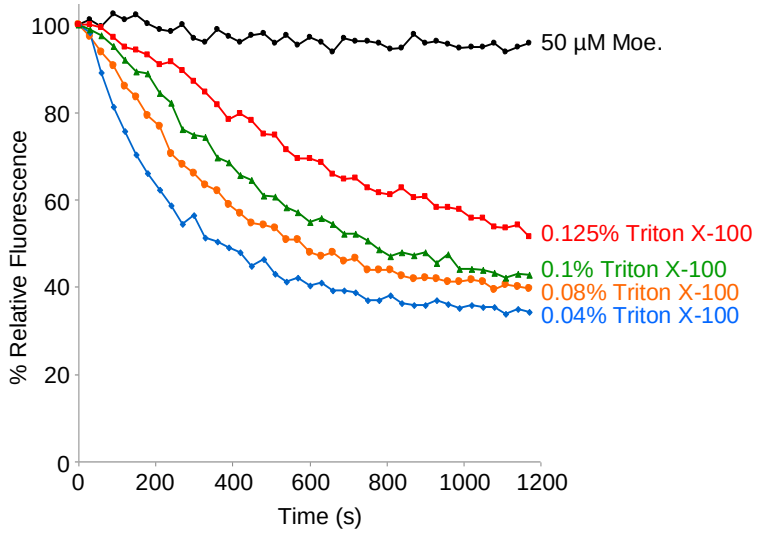

Figure 5.5 The effect of increasing Triton X-100 concentration on GTase activity

GTase reactions of PBP1B (1 µM) in the presence of various Triton X-100 concentrations (indicated to the right of the corresponding curve). 0.125, 0.1, 0.08 and 0.04% were used. A moenomycin (50 µM) control was also included.

6. Publications and submitted/prepared manuscripts

Banzhaf, M., van den Berg van Saparoea, B., Terrak, M., Fraipont, C., Egan, A., Philippe, J., Zapun, A., Breukink, E., Nguyen-Distèche, M., den Blaauwen, T., Vollmer, W. (2012). Cooperativity of peptidoglycan synthases active in bacterial cell elongation. *Molecular Microbiology*, 85(1), 179–194.

Egan, A. J. F. and Vollmer, W. (2013) The Physiology of bacterial cell division. *Annals of the New York Academy of Sciences*, 1277, 8–28.

Jean, N. L., Bougault, C. M., Lodge, A., Derouaux, A., Callens, G., Egan, A. J. F., Lewis, R. J., Vollmer, W., Simorre, J-P. (2014). The elongated molecular structure of the outer-membrane activator of peptidoglycan synthesis LpoA: implications in PBP1A-stimulation. In press at *Structure*.

Egan, A. J. F., Jean, N. L., Koumoutsi, A., Bougault, C. M., Biboy, J., Sassine, J., Solovyova, A. S., Breukink, E., Typas, A., Vollmer, W., Simorre, J-P. (2014). The outer-membrane lipoprotein LpoB spans the periplasm to stimulate the peptidoglycan synthase PBP1B. In press at *Proceedings of the National Academy of Sciences USA*.

A manuscript on the "Coordination of peptidoglycan synthesis and outer membrane constriction during cell division in *E. coli*" is in preparation. Precise authorship and target journal to be confirmed.

7. References

1. **Egan AJF, Vollmer W**. 2013. The physiology of bacterial cell division. Ann. N. Y. Acad. Sci. **1277**:8–28.

2. **Vollmer W, Blanot D, de Pedro MA**. 2008. Peptidoglycan structure and architecture. FEMS Microbiol. Rev. **32**:149–167.

3. **Weidel W, Pelzer H**. 1964. Bagshaped macromolecules - a new outlook on bacterial cell walls. Adv. Enzymol. Relat. Areas Mol. Biol. **26**:193–232.

4. **Typas A, Banzhaf M, Gross CA, Vollmer W**. 2012. From the regulation of peptidoglycan synthesis to bacterial growth and morphology. Nat. Rev. Microbiol. **10**:123–136.

5. **Hantke K, Braun V**. 1973. Covalent binding of lipid to protein. Diglyceride and amide-linked fatty acid at the N-terminal end of the murein-lipoprotein of the *Escherichia coli* outer membrane. Eur. J. Biochem. **34**:284–296.

6. **Vollmer W, Seligman SJ**. 2010. Architecture of peptidoglycan: more data and more models. Trends Microbiol. **18**:59–66.

7. **Schleifer KH, Kandler O**. 1972. Peptidoglycan types of bacterial cell walls and their taxonomic implications. Bacteriol. Rev. **36**:407–477.

8. **Vollmer W**. 2008. Structural variation in the glycan strands of bacterial peptidoglycan. FEMS Microbiol. Rev. **32**:287–306.

9. **Vollmer W, Höltje J-V**. 2004. The Architecture of the murein (peptidoglycan) in Gram-negative bacteria: vertical scaffold or horizontal layer. J. Bacteriol. **186**:5978–5987.

10. **Yao X, Jericho M, Pink D, Beveridge T**. 1999. Thickness and elasticity of Gram-negative murein sacculi measured by atomic force microscopy. J. Bacteriol. **181**:6865–6875.

11. **Matias VRF, Al-amoudi A, Dubochet J, Beveridge TJ, Matias RF**. 2003. Cryo-transmission electron microscopy of frozen-hydrated sections of *Escherichia coli* and *Pseudomonas aeruginosa*. J. Bacteriol. **185**:6112–6118.

12. **Gan L, Chen S, Jensen GJ**. 2008. Molecular organization of Gram-negative peptidoglycan. Proc. Natl. Acad. Sci. U. S. A. **105**:18953–18957.

13. **Glauner B**. 1988. Separation and quantification of muropeptides with high-performance liquid chromatography. Anal. Biochem. **172**:451–464.

14. **Glauner B, Höltje J V, Schwarz U**. 1988. The composition of the murein of *Escherichia coli*. J. Biol. Chem. **263**:10088–10095.

15. **Dmitriev B, Toukach F, Ehlers S**. 2005. Towards a comprehensive view of the bacterial cell wall. Trends Microbiol. **13**:569–574.

16. **Beeby M, Gumbart JC, Roux B, Jensen GJ**. 2013. Architecture and assembly of the Gram-positive cell wall. Mol. Microbiol. **88**:664–672.

17. **Höltje J-V**. 1998. Growth of the stress-bearing and shape-maintaining murein sacculus of *Escherichia coli*. Microbiol. Mol. Biol. Rev. **62**:181–203.

18. **Daniel RA, Errington J**. 2003. Control of cell morphogenesis in bacteria: two distinct ways to make a rod-shaped cell. Cell **113**:767–776.

19. **Domínguez-Escobar J, Chastanet A, Crevenna AH, Fromion V, Wedlich-Söldner R, Carballido-López R**. 2011. Processive movement of MreB-associated cell wall biosynthetic complexes in bacteria. Science **333**:225–228.

20. **Garner EC, Bernard R, Wang W, Zhuang X, Rudner DZ, Mitchison T**. 2011. Coupled, circumferential motions of the cell wall synthesis machinery and MreB filaments in B. subtilis. Science **333**:222–225.

21. **Van Teeffelen S, Wang S, Furchtgott L, Huang KC, Wingreen NS, Shaevitz JW, Gitai Z**. 2011. The bacterial actin MreB rotates, and rotation depends on cell-wall assembly. Proc. Natl. Acad. Sci. U. S. A. **108**:15822–15827.

22. **Olshausen P V, Defeu Soufo HJ, Wicker K, Heintzmann R, Graumann PL, Rohrbach A**. 2013. Superresolution imaging of dynamic MreB filaments in B. subtilis-a multiple-motor-driven transport? Biophys. J. **105**:1171–1181.

23. **Margolin W**. 2005. FtsZ and the division of prokaryotic cells and organelles. Nat. Rev. Mol. Cell Biol. **6**:862–871.

24. **Szwedziak P, Löwe J**. 2013. Do the divisome and elongasome share a common evolutionary past? Curr. Opin. Microbiol. **16**:745–751.

25. **Varma A, de Pedro MA, Young KD**. 2007. FtsZ directs a second mode of peptidoglycan synthesis in Escherichia coli. J. Bacteriol. **189**:5692–5704.

26. **Aaron M, Charbon G, Lam H, Schwarz H, Vollmer W, Jacobs-Wagner C**. 2007. The tubulin homologue FtsZ contributes to cell elongation by guiding cell wall precursor synthesis in *Caulobacter crescentus*. Mol. Microbiol. **64**:938–952.

27. **Typas A, Banzhaf M, van den Berg van Saparoea B, Verheul J, Biboy J, Nichols RJ, Zietek M, Beilharz K, Kannenberg K, von Rechenberg M, Breukink E, den Blaauwen T, Gross CA, Vollmer W**. 2010. Regulation of peptidoglycan synthesis by outer-membrane proteins. Cell **143**:1097–1109.

28. **Paradis-Bleau C, Markovski M, Uehara T, Lupoli TJ, Walker S, Kahne DE, Bernhardt TG**. 2010. Lipoprotein cofactors located in the outer membrane activate bacterial cell wall polymerases. Cell **143**:1110–1120.

29. **Barreteau H, Kovac A, Boniface A, Sova M, Gobec S, Blanot D**. 2008. Cytoplasmic steps of peptidoglycan biosynthesis. FEMS Microbiol. Rev. **32**:168–207.

30. **Zawadzke LE, Bugg TD, Walsh CT**. 1991. Existence of two D-alanine-D-alanine ligases in *Escherichia coli*: cloning and sequencing of the ddlA gene and purification and characterization of the DdlA and DdlB enzymes. Biochemistry **30**:1673–1682.

31. **Bouhss A, Trunkfield AE, Bugg TDH, Mengin-Lecreulx D**. 2008. The biosynthesis of peptidoglycan lipid-linked intermediates. FEMS Microbiol. Rev. **32**:208–233.

32. **Mohammadi T, van Dam V, Sijbrandi R, Vernet T, Zapun A, Bouhss A, Diepeveen-de Bruin M, Nguyen-Distèche M, de Kruijff B, Breukink E**. 2011. Identification of FtsW as a transporter of lipid-linked cell wall precursors across the membrane. EMBO J. **30**:1425–1432.

33. **Barrett D, Wang T-SA, Yuan Y, Zhang Y, Kahne D, Walker S**. 2007. Analysis of glycan polymers produced by peptidoglycan glycosyltransferases. J. Biol. Chem. **282**:31964–31971.

34. **Perlstein DL, Zhang Y, Wang T-S, Kahne DE, Walker S**. 2007. The direction of glycan chain elongation by peptidoglycan glycosyltransferases. J. Am. Chem. Soc. **129**:12674–12675.

35. **Perlstein DL, Wang T-SA, Doud EH, Kahne D, Walker S**. 2010. The role of the substrate lipid in processive glycan polymerization by the peptidoglycan glycosyltransferases. J. Am. Chem. Soc. **132**:48–49.

36. **Terrak M, Sauvage E, Derouaux A, Dehareng D, Bouhss A, Breukink E, Jeanjean S, Nguyen-Distèche M**. 2008. Importance of the conserved residues in the peptidoglycan glycosyltransferase module of the class A penicillin-binding protein 1b of *Escherichia coli*. J. Biol. Chem. **283**:28464–28470.

37. **Lovering AL, Safadi SS, Strynadka NCJ**. 2012. Structural perspective of peptidoglycan biosynthesis and assembly. Annu. Rev. Biochem. **81**:451–478.

38. **Glauner B, Höltje J V**. 1990. Growth pattern of the murein sacculus of *Escherichia coli*. J. Biol. Chem. **265**:18988–18996.

39. **Sauvage E, Kerff F, Terrak M, Ayala J a, Charlier P**. 2008. The penicillin-binding proteins: structure and role in peptidoglycan biosynthesis. FEMS Microbiol. Rev. **32**:234–258.

40. **Terrak M, Ghosh TK, van Heijenoort J, Van Beeumen J, Lampilas M, Aszodi J, Ayala J a, Ghuysen JM, Nguyen-Distèche M**. 1999. The catalytic, glycosyl transferase and acyl transferase modules of the cell wall peptidoglycan-polymerizing penicillin-binding protein 1b of *Escherichia coli*. Mol. Microbiol. **34**:350–364.

41. **Burman LG, Park JT**. 1984. Molecular model for elongation of the murein sacculus of *Escherichia coli*. Proc. Natl. Acad. Sci. U. S. A. **81**:1844–1848.

42. **Koch AL**. 1995. Bacterial Growth and Form. Chapman & Hall, New York.

43. **Fenton AK, Gerdes K**. 2013. Direct interaction of FtsZ and MreB is required for septum synthesis and cell division in *Escherichia coli*. EMBO J. **32**:1953–1965.

44. **Van der Ploeg R, Verheul J, Vischer NOE, Alexeeva S, Hoogendoorn E, Postma M, Banzhaf M, Vollmer W, den Blaauwen T**. 2013. Colocalization and interaction between elongasome and divisome during a preparative cell division phase in *Escherichia coli*. Mol. Microbiol. **87**:1074–1087.

45. **Vollmer W, Joris B, Charlier P, Foster S**. 2008. Bacterial peptidoglycan (murein) hydrolases. FEMS Microbiol. Rev. **32**:259–286.

46. **Goodellt EW, Schwarz ULI**. 1985. Release of cell wall peptides into culture medium by exponentially growing *Escherichia coli*. J. Bacteriol. **162**:391–397.

47. **Park JT**. 1993. Turnover and recycling of the murein sacculus in oligopeptide permease-negative strains of *Escherichia coli*: indirect evidence for an alternative permease system and for a monolayered sacculus. J. Bacteriol. **175**:7–11.

48. **Singh SK, SaiSree L, Amrutha RN, Reddy M**. 2012. Three redundant murein endopeptidases catalyse an essential cleavage step in peptidoglycan synthesis of *Escherichia coli* K12. Mol. Microbiol. **86**:1036–1051.

49. **Denome SA, Elf PK, Henderson TA, Nelson DE, Young KD**. 1999. *Escherichia coli* mutants lacking all possible combinations of eight penicillin binding proteins: viability , characteristics , and implications for peptidoglycan synthesis. J. Bacteriol. **181**:3981–3993.

50. **Born P, Breukink E, Vollmer W**. 2006. In vitro synthesis of cross-linked murein and its attachment to sacculi by PBP1A from *Escherichia coli*. J. Biol. Chem. **281**:26985–26993.

51. **Chalut C, Charpentier X, Remy M-H, Masson J-M**. 2001. Differential responses of *Escherichia coli* cells expressing cytoplasmic domain mutants of

penicillin-binding protein 1b after impairment of penicillin-binding proteins 1a and 3. J. Bacteriol. **183**:200–206.

52. **Henderson TA, Dombrosky PM, Young KD**. 1994. Artifactual processing of penicillin-binding proteins 7 and 1b by the OmpT protease of *Escherichia coli*. J. Bacteriol. **176**:256–259.

53. **Bertsche U, Breukink E, Kast T, Vollmer W**. 2005. In vitro murein peptidoglycan synthesis by dimers of the bifunctional transglycosylase-transpeptidase PBP1B from *Escherichia coli*. J. Biol. Chem. **280**:38096–38101.

54. **Zijderveld CA, Aarsman ME, den Blaauwen T, Nanninga N**. 1991. Penicillin-binding protein 1B of *Escherichia coli* exists in dimeric forms. J. Bacteriol. **173**:5740–5746.

55. **Lovering AL, de Castro LH, Lim D, Strynadka NCJ**. 2007. Structural insight into the transglycosylation step of bacterial cell-wall biosynthesis. Science. **315**:1402–1405.

56. **Sung M-T, Lai Y-T, Huang C-Y, Chou L-Y, Shih H-W, Cheng W-C, Wong C-H, Ma C**. 2009. Crystal structure of the membrane-bound bifunctional transglycosylase PBP1b from *Escherichia coli*. Proc. Natl. Acad. Sci. U. S. A. **106**:8824–8829.

57. **Lovering AL, De Castro L, Strynadka NCJ**. 2008. Identification of dynamic structural motifs involved in peptidoglycan glycosyltransfer. J. Mol. Biol. **383**:167–177.

58. **Matteï P-J, Neves D, Dessen A**. 2010. Bridging cell wall biosynthesis and bacterial morphogenesis. Curr. Opin. Struct. Biol. **20**:749–755.

59. **Goffin C, Fraipont C, Ayala J, Terrak M, Nguyen-Distèche M, Ghuysen JM**. 1996. The non-penicillin-binding module of the tripartite penicillin-binding protein 3 of *Escherichia coli* is required for folding and/or stability of the penicillin-binding module and the membrane-anchoring module confers cell septation activity on the folded. J. Bacteriol. **178**:5402–5409.

60. **Banzhaf M, van den Berg van Saparoea B, Terrak M, Fraipont C, Egan A, Philippe J, Zapun A, Breukink E, Nguyen-Distèche M, den Blaauwen T, Vollmer W**. 2012. Cooperativity of peptidoglycan synthases active in bacterial cell elongation. Mol. Microbiol. **85**:179–194.

61. **Den Blaauwen T, Aarsman MEG, Vischer NOE, Nanninga N**. 2003. Penicillin-binding protein PBP2 of *Escherichia coli* localizes preferentially in the lateral wall and at mid-cell in comparison with the old cell pole. Mol. Microbiol. **47**:539–547.

62. **Weiss DS, Pogliano K, Carson M, Guzman LM, Fraipont C, Nguyen-Distèche M, Losick R, Beckwith J**. 1997. Localization of the *Escherichia coli* cell division protein Ftsl (PBP3) to the division site and cell pole. Mol. Microbiol. **4**:671–681.

63. **Adam M, Fraipont C, Rhazi N, Lakaye B, Devreese B, Beeumen J Van, Heijenoort Y Van, Adam M, Fraipont C, Rhazi N, Nguyen-diste M**. 1997. The bimodular G57-V577 polypeptide chain of the class B penicillin-binding protein 3 of *Escherichia coli* catalyzes peptide bond formation from thiolesters and does not catalyze glycan chain polymerization from the lipid II intermediate. The Bimodular G57. J. Bacteriol. **179**:6005–6009.

64. **Berardino M Di, Dijkstra A, Sttiber D, Keck W, Gubler M**. 1996. The monofunctional glycosyltransferase of *Escherichia coli* is a member of a new class of peptidoglycan-synthesising enzymes. FEBS Lett. **392**:184–188.

65. **Spratt BG, Zhou J, Taylor M., Merrick MJ**. 1996. Monofunctional biosynthetic peptidoglycan transglycosylases. Mol. Microbiol. **19**:639–640.

66. **Derouaux A, Wolf B, Fraipont C, Breukink E, Nguyen-Distèche M, Terrak M**. 2008. The monofunctional glycosyltransferase of *Escherichia coli* localizes to the cell division site and interacts with penicillin-binding protein 3, FtsW, and FtsN. J. Bacteriol. **190**:1831–184.

67. **Bertsche U, Kast T, Wolf B, Fraipont C, Aarsman MEG, Kannenberg K, von Rechenberg M, Nguyen-Distèche M, den Blaauwen T, Höltje J-V,**

Vollmer W. 2006. Interaction between two murein (peptidoglycan) synthases, PBP3 and PBP1B, in *Escherichia coli*. Mol. Microbiol. **61**:675–690.

68. **Del Portillo FG, de Pedro MA, Ayala JA**. 1991. Identification of a new mutation in *Escherichia coli* that suppresses a pbpB (Ts) phenotype in the presence of penicillin-binding protein 1B. FEMS Microbiol. Lett. **68**:7–13.

69. **Lupoli TJ, Lebar MD, Markovski M, Bernhardt T, Kahne D, Walker S**. 2014. Lipoprotein activators stimulate *Escherichia coli* penicillin-binding proteins by different mechanisms. J. Am. Chem. Soc. **136**:52–55.

70. **Turner RD, Hurd AF, Cadby A, Hobbs JK, Foster SJ**. 2013. Cell wall elongation mode in Gram-negative bacteria is determined by peptidoglycan architecture. Nat. Commun. **4**.

71. **Mohammadi T, Karczmarek A, Crouvoisier M, Bouhss A, Mengin-Lecreulx D, den Blaauwen T**. 2007. The essential peptidoglycan glycosyltransferase MurG forms a complex with proteins involved in lateral envelope growth as well as with proteins involved in cell division in *Escherichia coli*. Mol. Microbiol. **65**:1106–1121.

72. **Van den Ent F, Johnson CM, Persons L, de Boer PAJ, Löwe J**. 2010. Bacterial actin MreB assembles in complex with cell shape protein RodZ. EMBO J. **29**:1081–1090.

73. **Salje J, Van den Ent F, de Boer P, Löwe J**. 2011. Direct membrane binding by bacterial actin MreB. Mol. Cell **43**:478–487.

74. **Shiomi D, Sakai M, Niki H**. 2008. Determination of bacterial rod shape by a novel cytoskeletal membrane protein. EMBO J. **27**:3081–3091.

75. **Bendezú FO, Hale CA, Bernhardt TG, de Boer PAJ**. 2009. RodZ (YfgA) is required for proper assembly of the MreB actin cytoskeleton and cell shape in *E. coli*. EMBO J. **28**:193–204.

76. **Alyahya SA, Alexander R, Costa T, Henriques AO, Emonet T, Jacobs-Wagner C**. 2009. RodZ, a component of the bacterial core morphogenic apparatus. Proc. Natl. Acad. Sci. U. S. A. **106**:1239–1244.

77. **Shiomi D, Toyoda A, Aizu T, Ejima F, Fujiyama A, Shini T, Kohara Y, Niki H**. 2013. Mutations in cell elongation genes mreB, mrdA and mrdB suppress the shape defect of RodZ-deficient cells. Mol. Microbiol. **87**:1029–1044.

78. **Kruse T, Bork-Jensen J, Gerdes K**. 2005. The morphogenetic MreBCD proteins of Escherichia coli form an essential membrane-bound complex. Mol. Microbiol. **55**:78–89.

79. **Van den Ent F, Leaver M, Bendezu F, Errington J, de Boer PAJ, Löwe J**. 2006. Dimeric structure of the cell shape protein MreC and its functional implications. Mol. Microbiol. **62**:1631–1642.

80. **Ikeda M, Sato T, Wachi M, Jung HK, Ishino F, Kobayashi Y, Matsuhashi M**. 1989. Structural similarity among *Escherichia coli* FtsW and RodA proteins and Bacillus subtilis SpoVE protein, which function in cell division, cell elongation, and spore formation, respectively. J. Bacteriol. **171**:6375–6378.

81. **Fumitoshi I, Park W, Tomioka S, Shigeo T, Takasesn I, Kunugitas K, Matsuzawa H, Asoh S, Ohta T, Spratt BG, Matsuhashis M**. 1986. Peptidoglycan synthetic activities in membranes of *Escherichia coli* caused by overproduction of penicillin-binding protein 2 and RodA potein. J. Biol. Chem. **261**:7024–7031.

82. **El Ghachi M, Matteï P-J, Ecobichon C, Martins A, Hoos S, Schmitt C, Colland F, Ebel C, Prévost M-C, Gabel F, England P, Dessen A, Boneca IG**. 2011. Characterization of the elongasome core PBP2:MreC complex of *Helicobacter pylori*. Mol. Microbiol. **82**:68–86.

83. **White CL, Kitich A, Gober JW**. 2010. Positioning cell wall synthetic complexes by the bacterial morphogenetic proteins MreB and MreD. Mol. Microbiol. **76**:616–633.

84. **Bi E, Lutkenhaus J**. 1991. FtsZ ring structure associated with division in *Escherichia coli*. Nature **354**:161–164.

85. **Löwe J, Amos LA**. 1998. Crystal structure of the bacterial cell-division protein FtsZ. Nature **391**:203–206.

86. **Mukherjee A, Lutkenhaus J**. 1998. Dynamic assembly of FtsZ regulated by GTP hydrolysis. EMBO J. **17**:462–469.

87. **Erickson HP, Anderson DE, Osawa M**. 2010. FtsZ in bacterial cytokinesis: cytoskeleton and force generator all in one. Microbiol. Mol. Biol. Rev. **74**:504–528.

88. **Li Z, Trimble MJ, Brun Y V, Jensen GJ**. 2007. The structure of FtsZ filaments in vivo suggests a force-generating role in cell division. EMBO J. **26**:4694–4708.

89. **Mateos-Gil P, Paez A, Hörger I, Rivas G, Vicente M, Tarazona P, Vélez M**. 2012. Depolymerization dynamics of individual filaments of bacterial cytoskeletal protein FtsZ. Proc. Natl. Acad. Sci. U. S. A. **109**:8133–8138.

90. **Anderson DE, Gueiros-filho FJ, Erickson P, Erickson HP**. 2004. Assembly dynamics of FtsZ rings in *Bacillus subtilis* and *Escherichia coli* and effects of FtsZ-regulating proteins. J. Bacteriol. **186**:5775–5781.

91. **Raskin DM, de Boer PAJ**. 1999. Rapid pole-to-pole oscillation of a protein required for directing division to the middle of *Escherichia coli*. Proc. Natl. Acad. Sci. U. S. A. **96**:4971–4976.

92. **Hale CA, Meinhardt H, de Boer PAJ**. 2001. Dynamic localization cycle of the cell division regulator MinE in *Escherichia coli*. EMBO J. **20**:1563–1572.

93. **Park K-T, Wu W, Battaile KP, Lovell S, Holyoak T, Lutkenhaus J**. 2011. The Min oscillator uses MinD-dependent conformational changes in MinE to spatially regulate cytokinesis. Cell **146**:396–407.

94. **Wu LJ, Errington J**. 2004. Coordination of cell division and chromosome segregation by a nucleoid occlusion protein in *Bacillus subtilis*. Cell **117**:915–925.

95. **Bernhardt TG, de Boer PAJ**. 2005. SlmA, a nucleoid-associated, FtsZ binding protein required for blocking septal ring assembly over chromosomes in *E. coli*. Mol. Cell **18**:555–564.

96. **Tonthat NK, Arold ST, Pickering BF, Van Dyke MW, Liang S, Lu Y, Beuria TK, Margolin W, Schumacher MA**. 2011. Molecular mechanism by which the nucleoid occlusion factor, SlmA, keeps cytokinesis in check. EMBO J. **30**:154–164.

97. **Cho H, McManus HR, Dove SL, Bernhardt TG**. 2011. Nucleoid occlusion factor SlmA is a DNA-activated FtsZ polymerization antagonist. Proc. Natl. Acad. Sci. U. S. A. **108**:3773–3778.

98. **Tonthat NK, Milam SL, Chinnam N, Whitfill T, Margolin W, Schumacher MA**. 2013. SlmA forms a higher-order structure on DNA that inhibits cytokinetic Z-ring formation over the nucleoid. Proc. Natl. Acad. Sci. **110**:15163–15163.

99. **Adams DW, Errington J**. 2009. Bacterial cell division: assembly, maintenance and disassembly of the Z ring. Nat. Rev. Microbiol. **7**:642–653.

100. **Wu LJ, Errington J**. 2012. Nucleoid occlusion and bacterial cell division. Nat. Rev. Microbiol. **10**:8–12.

101. **F.J. Trueba**. 1982. On the precision and accuracy achieved by *Escherichia coli* cells at fission about their middle. Arch. Microbiol. **131**:55–59.

102. **Yu XC, Margolin W**. 1999. FtsZ ring clusters in min and partition mutants: role of both the Min system and the nucleoid in regulating FtsZ ring localization. Mol. Microbiol. **32**:315–326.

103. **Männik J, Wu F, Hol FJH, Bisicchia P, Sherratt DJ, Keymer JE, Dekker C**. 2012. Robustness and accuracy of cell division in Escherichia coli in diverse cell shapes. Proc. Natl. Acad. Sci. U. S. A. **109**:6957–6962.

104. **Aarsman MEG, Piette A, Fraipont C, Vinkenvleugel TMF, Nguyen-Distèche M, den Blaauwen T**. 2005. Maturation of the *Escherichia coli* divisome occurs in two steps. Mol. Microbiol. **55**:1631–45.

105. **Vollmer W, Bertsche U**. 2008. Murein (peptidoglycan) structure, architecture and biosynthesis in *Escherichia coli*. Biochim. Biophys. Acta **1778**:1714–1734.

106. **Haney SA, Glasfeld E, Hale C, Keeney D, He Z, de Boer PAJ**. 2001. Genetic analysis of the *Escherichia coli* FtsZ.ZipA interaction in the yeast two-hybrid system. Characterization of FtsZ residues essential for the interactions with ZipA and with FtsA. J. Bol. Chem. **276**:11980–11987.

107. **Pichoff S, Lutkenhaus J**. 2002. Unique and overlapping roles for ZipA and FtsA in septal ring assembly in *Escherichia coli*. EMBO J. **21**:685–693.

108. **Pichoff S, Lutkenhaus J**. 2005. Tethering the Z ring to the membrane through a conserved membrane targeting sequence in FtsA. Mol. Microbiol. **55**:1722–1734.

109. **Krupka M, Rivas G, Rico AI, Vicente M**. 2012. Key role of two terminal domains in the bidirectional polymerization of FtsA protein. J. Biol. Chem. **287**:7756–7765.

110. **Szwedziak P, Wang Q, Freund SM V, Löwe J**. 2012. FtsA forms actin-like protofilaments. EMBO J. **31**:2249–2260.

111. **Hale CA, Rhee AC, Boer PAJ De, Rhee AMYC**. 2000. ZipA-Induced Bundling of FtsZ Polymers Mediated by an Interaction between C-Terminal Domains. J. Bacteriol. **182**:5153–5166.

112. **Gueiros-filho FJ, Losick R**. 2002. A widely conserved bacterial cell division protein that promotes assembly of the tubulin-like protein FtsZ. Genes Dev. **16**:2544–2556.

113. **Low HH, Moncrieffe MC, Löwe J**. 2004. The crystal structure of ZapA and its modulation of FtsZ polymerisation. J. Mol. Biol. **341**:839–852.

114. **Durand-Heredia JM, Yu HH, De Carlo S, Lesser CF, Janakiraman A**. 2011. Identification and characterization of ZapC: a stabilizer of the FtsZ-ring in *Escherichia coli*. J. Bacteriol. **193**:1405–1413.

115. **Durand-Heredia J, Rivkin E, Fan G, Morales J, Janakiraman A**. 2012. Identification of ZapD as a cell division factor that promotes the assembly of FtsZ in *Escherichia coli*. J. Bacteriol. **194**:3189–3198.

116. **Hale CA, Shiomi D, Liu B, Bernhardt TG, Margolin W, Niki H, de Boer PAJ**. 2011. Identification of *Escherichia coli* ZapC (YcbW) as a component of the division apparatus that binds and bundles FtsZ polymers. J. Bacteriol. **193**:1393–1404.

117. **Ebersbach G, Galli E, Møller-Jensen J, Löwe J, Gerdes K**. 2008. Novel coiled-coil cell division factor ZapB stimulates Z ring assembly and cell division. Mol. Microbiol. **68**:720–735.

118. **Galli E, Gerdes K**. 2010. Spatial resolution of two bacterial cell division proteins: ZapA recruits ZapB to the inner face of the Z-ring. Mol. Microbiol. **76**:1514–1526.

119. **Galli E, Gerdes K**. 2012. FtsZ-ZapA-ZapB interactome of *Escherichia coli*. J. Bacteriol. **194**:292–302.

120. **Espéli O, Borne R, Dupaigne P, Thiel A, Gigant E, Mercier R, Boccard F**. 2012. A MatP-divisome interaction coordinates chromosome segregation with cell division in E. coli. EMBO J. **31**:3198–3211.

121. **De Leeuw E, Graham B, Phillips GJ, ten Hagen-Jongman CM, Oudega B, Luirink J**. 1999. Molecular characterization of *Escherichia coli* FtsE and FtsX. Mol. Microbiol. **31**:983–993.

122. **Corbin BD, Wang Y, Beuria TK, Margolin W**. 2007. Interaction between cell division proteins FtsE and FtsZ. J. Bacteriol. **189**:3026–3035.

123. **Arends SJR, Kustusch RJ, Weiss DS**. 2009. ATP-binding site lesions in FtsE impair cell division. J. Bacteriol. **191**:3772–3784.

124. **Reddy M**. 2007. Role of FtsEX in cell division of *Escherichia coli*: viability of ftsEX mutants is dependent on functional SufI or high osmotic strength. J. Bacteriol. **189**:98–108.

125. **Chen JC, Beckwith J**. 2001. FtsQ, FtsL and FtsI require FtsK, but not FtsN, for co-localization with FtsZ during *Escherichia coli* cell division. Mol. Microbiol. **42**:395–413.

126. **Di Lallo G, Fagioli M, Barionovi D, Ghelardini P, Paolozzi L**. 2003. Use of a two-hybrid assay to study the assembly of a complex multicomponent protein machinery: bacterial septosome differentiation. Microbiology **149**:3353–3359.

127. **Karimova G, Dautin N, Ladant D**. 2005. Interaction network among *Escherichia coli* membrane proteins involved in cell division as revealed by bacterial two-hybrid analysis. J. Bacteriol. **187**:2233–2243.

128. **Aussel L, Barre FX, Aroyo M, Stasiak A, Stasiak AZ, Sherratt D**. 2002. FtsK Is a DNA motor protein that activates chromosome dimer resolution by switching the catalytic state of the XerC and XerD recombinases. Cell **108**:195–205.

129. **Bigot S, Sivanathan V, Possoz C, Barre F-X, Cornet F**. 2007. FtsK, a literate chromosome segregation machine. Mol. Microbiol. **64**:1434–1441.

130. **Grenga L, Luzi G, Paolozzi L, Ghelardini P**. 2008. The *Escherichia coli* FtsK functional domains involved in its interaction with its divisome protein partners. FEMS Microbiol. Lett. **287**:163–167.

131. **Löwe J, Ellonen A, Allen MD, Atkinson C, Sherratt DJ, Grainge I**. 2008. Molecular mechanism of sequence-directed DNA loading and translocation by FtsK. Mol. Cell **31**:498–509.

132. **Dubarry N, Possoz C, Barre F-X**. 2010. Multiple regions along the *Escherichia coli* FtsK protein are implicated in cell division. Mol. Microbiol. **78**:1088–1100.

133. **Geissler B, Margolin W**. 2005. Evidence for functional overlap among multiple bacterial cell division proteins: compensating for the loss of FtsK. Mol. Microbiol. **58**:596–612.

134. **Buddelmeijer N, Beckwith J**. 2004. A complex of the *Escherichia coli* cell division proteins FtsL, FtsB and FtsQ forms independently of its localization to the septal region. Mol. Microbiol. **52**:1315–1327.

135. **Chen JC, Minev M, Beckwith J**. 2002. Analysis of ftsQ mutant alleles in Escherichia coli: complementation, septal localization, and recruitment of downstream cell division proteins. J. Bacteriol. **184**:695–705.

136. **Van den Ent F, Vinkenvleugel TMF, Ind A, West P, Veprintsev D, Nanninga N, den Blaauwen T, Löwe J**. 2008. Structural and mutational analysis of the cell division protein FtsQ. Mol. Microbiol. **68**:110–123.

137. **Gonzalez MD, Akbay EA, Boyd D, Beckwith J**. 2010. Multiple interaction domains in FtsL, a protein component of the widely conserved bacterial FtsLBQ cell division complex. J. Bacteriol. **192**:2757–2768.

138. **Villanelo F, Ordenes A, Brunet J, Lagos R, Monasterio O**. 2011. A model for the *Escherichia coli* FtsB/FtsL/FtsQ cell division complex. BMC Struct. Biol. **11**.

139. **Masson S, Kern T, Le Gouëllec A, Giustini C, Simorre J-P, Callow P, Vernet T, Gabel F, Zapun A**. 2009. Central domain of DivIB caps the C-terminal regions of the FtsL/DivIC coiled-coil rod. J. Biol. Bhemistry **284**:27687–27700.

140. **Goehring NW, Gonzalez MD, Beckwith J**. 2006. Premature targeting of cell division proteins to midcell reveals hierarchies of protein interactions involved in divisome assembly. Mol. Microbiol. **61**:33–45.

141. **Lara B, Ayala JA**. 2002. Topological characterization of the essential *Escherichia coli* cell division protein FtsW. FEMS Microbiol. Lett. **216**:23–32.

142. **Alexeeva S, Gadella TWJ, Verheul J, Verhoeven GS, den Blaauwen T**. 2010. Direct interactions of early and late assembling division proteins in E*scherichia coli* cells resolved by FRET. Mol. Microbiol. **77**:384–398.

143. **Fraipont C, Alexeeva S, Wolf B, van der Ploeg R, Schloesser M, den Blaauwen T, Nguyen-Distèche M**. 2011. The integral membrane FtsW protein and peptidoglycan synthase PBP3 form a subcomplex in *Escherichia coli*. Microbiology **157**:251–259.

144. **Mercer KLN, Weiss DS**. 2002. The *Escherichia coli* cell division protein FtsW is required to recruit its cognate transpeptidase, FtsI (PBP3), to the division site. J. Bacteriol. **184**:904–912.

145. **Müller P, Ewers C, Bertsche U, Anstett M, Kallis T, Breukink E, Fraipont C, Terrak M, Nguyen-Distèche M, Vollmer W**. 2007. The essential cell division

protein FtsN interacts with the murein (peptidoglycan) synthase PBP1B in *Escherichia coli*. J. Biol. Chem. **282**:36394–36402.

146. **Busiek KK, Eraso JM, Wang Y, Margolin W**. 2012. The early divisome protein FtsA interacts directly through its 1c subdomain with the cytoplasmic domain of the late divisome protein FtsN. J. Bacteriol. **194**:1989–2000.

147. **Yang J-C, Van Den Ent F, Neuhaus D, Brevier J, Löwe J**. 2004. Solution structure and domain architecture of the divisome protein FtsN. Mol. Microbiol. **52**:651–660.

148. **Ursinus A, Van Den Ent F, Brechtel S, De Pedro M, Höltje J-V, Lowe J, Vollmer W**. 2004. Murein (peptidoglycan) binding property of the essential cell division protein FtsN from *Escherichia coli*. J. Bacteriol. **186**:6728–6737.

149. **Arends SJR, Williams K, Scott RJ, Rolong S, Popham DL, Weiss DS**. 2010. Discovery and characterization of three new *Escherichia coli* septal ring proteins that contain a SPOR domain: DamX, DedD, and RlpA. J. Bacteriol. **192**:242–255.

150. **Gerding MA, Liu B, Bendezú FO, Hale CA, Bernhardt TG, de Boer PAJ**. 2009. Self-enhanced accumulation of FtsN at Division Sites and Roles for Other Proteins with a SPOR domain (DamX, DedD, and RlpA) in *Escherichia coli* cell constriction. J. Bacteriol. **191**:7383–7401.

151. **Dai K, Xu Y, Lutkenhaus J**. 1996. Topological characterization of the essential *Escherichia coli* cell division protein FtsN. J. Bacteriol. **178**:1328–1334.

152. **Goehring NW, Robichon C, Beckwith J**. 2007. Role for the nonessential N terminus of FtsN in divisome assembly. J. Bacteriol. **189**:646–649.

153. **Bernard CS, Sadasivam M, Shiomi D, Margolin W**. 2007. An altered FtsA can compensate for the loss of essential cell division protein FtsN in *Escherichia coli*. Mol. Microbiol. **64**:1289–1305.

154. **Rico AI, García-Ovalle M, Palacios P, Casanova M, Vicente M**. 2010. Role of *Escherichia coli* FtsN protein in the assembly and stability of the cell division ring. Mol. Microbiol. **76**:760–771.

155. **Tarry M, Arends SJR, Roversi P, Piette E, Sargent F, Berks BC, Weiss DS, Lea SM**. 2009. The *Escherichia coli* cell division protein and model Tat substrate SufI (FtsP) localizes to the septal ring and has a multicopper oxidase-like structure. J. Mol. Biol. **386**:504–519.

156. **Samaluru H, SaiSree L, Reddy M**. 2007. Role of SufI (FtsP) in cell division of *Escherichia coli*: evidence for its involvement in stabilizing the assembly of the divisome. J. Bacteriol. **189**:8044–8052.

157. **Heidrich C, Templin MF, Ursinus A, Merdanovic M, Berger J, Schwarz H, de Pedro M a, Höltje J V**. 2001. Involvement of N-acetylmuramyl-L-alanine amidases in cell separation and antibiotic-induced autolysis of *Escherichia coli*. Mol. Microbiol. **41**:167–178.

158. **Kerff F, Petrella S, Mercier F, Sauvage E, Herman R, Pennartz A, Zervosen A, Luxen A, Frère J-M, Joris B, Charlier P**. 2010. Specific structural features of the N-acetylmuramoyl-L-alanine amidase AmiD from *Escherichia coli* and mechanistic implications for enzymes of this family. J. Mol. Biol. **397**:249–259.

159. **Uehara T, Park JT**. 2007. An anhydro-N-acetylmuramyl-L-alanine amidase with broad specificity tethered to the outer membrane of *Escherichia coli*. J. Bacteriol. **189**:5634–5641.

160. **Bernhardt TG, de Boer PAJ**. 2003. The *Escherichia coli* amidase AmiC is a periplasmic septal ring component exported via the twin-arginine transport pathway. Mol. Microbiol. **48**:1171–1182.

161. **Uehara T, Parzych KR, Dinh T, Bernhardt TG**. 2010. Daughter cell separation is controlled by cytokinetic ring-activated cell wall hydrolysis. EMBO J. **29**:1412–1422.

162. **Lupoli TJ, Taniguchi T, Wang T-S, Perlstein DL, Walker S, Kahne DE**. 2009. Studying a cell division amidase using defined peptidoglycan substrates. J. Am. Chem. Soc. **131**:18230–18231.

163. **Heidrich C, Ursinus A, Berger J, Schwarz H, Höltje J-V**. 2002. Effects of multiple deletions of murein hydrolases on viability, septum cleavage, and

sensitivity to large toxic molecules in *Escherichia coli*. J. Bacteriol. **184**:6093–6099.

164. **Korsak D, Liebscher S, Vollmer W**. 2005. Susceptibility to antibiotics and β -lactamase induction in murein hydrolase mutants of *Escherichia coli*. Antimicrob. Agents Chemother. **49**:1409–2005.

165. **Park JT, Uehara T**. 2008. How bacteria consume their own exoskeletons (turnover and recycling of cell wall peptidoglycan). Microbiol. Mol. Biol. Rev. **72**:211–227.

166. **Uehara T, Park JT**. 2008. Growth of *Escherichia coli*: significance of peptidoglycan degradation during elongation and septation. J. Bacteriol. **190**:3914–3922.

167. **Olrichs NK, Aarsman MEG, Verheul J, Arnusch CJ, Martin NI, Hervé M, Vollmer W, de Kruijff B, Breukink E, den Blaauwen T**. 2011. A novel in vivo cell-wall labeling approach sheds new light on peptidoglycan synthesis in *Escherichia coli*. Chembiochem **12**:1124–1133.

168. **Uehara T, Dinh T, Bernhardt TG**. 2009. LytM-domain factors are required for daughter cell separation and rapid ampicillin-induced lysis in *Escherichia coli*. J. Bacteriol. **191**:5094–5107.

169. **Peters NT, Dinh T, Bernhardt TG**. 2011. A fail-safe mechanism in the septal ring assembly pathway generated by the sequential recruitment of cell separation amidases and their activators. J. Bacteriol. **193**:4973–4983.

170. **Yang DC, Peters NT, Parzych KR, Uehara T, Markovski M, Bernhardt TG**. 2011. An ATP-binding cassette transporter-like complex governs cell-wall hydrolysis at the bacterial cytokinetic ring. Proc. Natl. Acad. Sci. U. S. A. **108**:1052–1060.

171. **Yang DC, Tan K, Joachimiak A, Bernhardt TG**. 2012. A conformational switch controls cell wall-remodelling enzymes required for bacterial cell division. Mol. Microbiol. **85**:768–781.

172. **Bos MP, Robert V, Tommassen J**. 2007. Biogenesis of the Gram-negative bacterial outer membrane. Annu. Rev. Microbiol. **61**:191–214.

173. **Cowles CE, Li Y, Semmelhack MF, Cristea IM, Silhavy TJ**. 2011. The free and bound forms of Lpp occupy distinct subcellular locations in *Escherichia coli*. Mol. Microbiol. **79**:1168–1181.

174. **Bernadac A, Gavioli M, Lazzaroni J, Raina S, Lloubès R**. 1998. *Escherichia coli tol-pal* mutants form outer membrane vesicles. J. Bacteriol. **180**:4872–4878.

175. **Cascales E, Bernadac A, Gavioli M, Lazzaroni J, Lloubes R, Lyon CB, Cedex V**. 2002. Pal lipoprotein of *Escherichia coli* plays a major role in outer membrane integrity. J. Bacteriol. **184**:754–759.

176. **Sturgis JN**. 2001. Organisation and evolution of the tol-pal gene cluster. J. Mol. Microbiol. Biotechnol. **3**:113–122.

177. **Gerding MA, Ogata Y, Pecora ND, Niki H, de Boer PAJ**. 2007. The trans-envelope Tol-Pal complex is part of the cell division machinery and required for proper outer-membrane invagination during cell constriction in *E. coli*. Mol. Microbiol. **63**:1008–1025.

178. **Lazzaroni J-C, Dubuisson J-F, Vianney A**. 2002. The Tol proteins of *Escherichia coli* and their involvement in the translocation of group A colicins. Biochimie **84**:391–397.

179. **Journet L, Rigal A, Lazdunski C, Bénédetti H**. 1999. Role of TolR N-terminal, central, and C-terminal domains in dimerization and interaction with TolA and TolQ. J. Bacteriol. **181**:4476–4484.

180. **Parsons LM, Grishaev A, Bax A**. 2008. The periplasmic domain of TolR from *Haemophilus influenzae* forms a dimer with a large hydrophobic groove: NMR solution structure and comparison to SAXS data. Biochemistry **47**:3131–3142.

181. **Godlewska R, Wiśniewska K, Pietras Z, Jagusztyn-Krynicka EK**. 2009. Peptidoglycan-associated lipoprotein (Pal) of Gram-negative bacteria: function, structure, role in pathogenesis and potential application in immunoprophylaxis. FEMS Microbiol. Lett. **298**:1–11.

182. **Derouiche R, Lloubès R, Sasso S, Bouteille H, Oughideni R, Lazdunski C, Loret E**. 1999. Circular dichroism and molecular modeling of the *E. coli* TolA periplasmic domains. Biospectroscopy **5**:189–198.

183. **Lubkowski J, Hennecke F, Plückthun A, Wlodawer A**. 1999. Filamentous phage infection: crystal structure of g3p in complex with its coreceptor, the C-terminal domain of TolA. Structure **7**:711–722.

184. **Abergel C, Bouveret E, Claverie JM, Brown K, Rigal A, Lazdunski C, Bénédetti H**. 1999. Structure of the *Escherichia coli* TolB protein determined by MAD methods at 1.95 A resolution. Structure **7**:1291–1300.

185. **Bonsor DA, Hecht O, Vankemmelbeke M, Sharma A, Krachler AM, Housden NG, Lilly KJ, James R, Moore GR, Kleanthous C**. 2009. Allosteric beta-propeller signalling in TolB and its manipulation by translocating colicins. EMBO J. **28**:2846–2857.

186. **Derouiche R, Bénédetti H, Lazzaroni J-C, Lazdunski C, Lloubès R**. 1995. Protein complex within *Escherichia coli* inner membrane. TolA N-terminal domain interacts with TolQ and TolR proteins. J. Biol. Chem. **270**:11078–11084.

187. **Lazzaroni JC, Vianney A, Popot JL, Bénédetti H, Samatey F, Lazdunski C, Portalier R, Géli V**. 1995. Transmembrane alpha-helix interactions are required for the functional assembly of the *Escherichia coli* Tol complex. J. Mol. Biol. **246**:1–7.

188. **Krachler AM, Sharma A, Cauldwell A, Papadakos G, Kleanthous C**. 2010. TolA modulates the oligomeric status of YbgF in the bacterial periplasm. J. Mol. Biol. **403**:270–285.

189. **Germon P, Ray M, Vianney A, Lazzaroni C**. 2001. Energy-Dependent conformational change in the TolA protein of *Escherichia coli* involves its N-terminal domain , TolQ , and TolR. J. Bacteriol. **183**:4110–4114.

190. **Cascales E, Gavioli M, Sturgis JN, Lloubès R**. 2000. Proton motive force drives the interaction of the inner membrane TolA and outer membrane pal proteins in *Escherichia coli*. Mol. Microbiol. **38**:904–915.

191. **Cascales E, Lloubès R**. 2003. Deletion analyses of the peptidoglycan-associated lipoprotein Pal reveals three independent binding sequences including a TolA box. Mol. Microbiol. **51**:873–885.

192. **Yeh Y-C, Comolli LR, Downing KH, Shapiro L, McAdams HH**. 2010. The *Caulobacter* Tol-Pal complex is essential for outer membrane integrity and the positioning of a polar localization factor. J. Bacteriol. **192**:4847–4858.

193. **Vollmer W, von Rechenberg M, Höltje J-V**. 1999. Demonstration of molecular interactions between the murein polymerase PBP1B, the lytic transglycosylase MltA, and the scaffolding protein MipA of *Escherichia coli*. J. Biol. Chem. **274**:6726–3734.

194. **Schwartz B, Markwalder JA, Seitz SP, Wang Y, Stein RL**. 2002. A kinetic characterization of the glycosyltransferase activity of *Eschericia coli* PBP1b and development of a continuous fluorescence assay. Biochemistry **41**:12552–12561.

195. **Offant J, Terrak M, Derouaux A, Breukink E, Nguyen-Distèche M, Zapun A, Vernet T**. 2010. Optimization of conditions for the glycosyltransferase activity of penicillin-binding protein 1a from *Thermotoga maritima*. FEBS J. **277**:4290–4298.

196. **Zhao G, Meier TI, Kahl SD, Gee KR, Blaszczak LC**. 1999. BOCILLIN FL , a sensitive and commercially available reagent for detection of penicillin-binding proteins. Antimicrob. Agents Chemother. **43**:1124–1128.

197. **Hayashi K**. 1975. A rapid determination of sodium dodecyl sulfate with methylene blue. Anal. Biochem. **67**:503–506.

198. **Demchick P, Koch AL**. 1996. The permeability of the wall fabric of *Escherichia coli* and *Bacillus subtilis*. J. Bacteriol. **178**:768–773.

199. **Vázquez-laslop N, Lee H, Hu R, Alex A**. 2001. Molecular sieve mechanism of selective release of cytoplasmic proteins by osmotically shocked *Escherichia coli*. J. Bacteriol. **183**:2399–2404.

200. **Holm L, Rosenström P**. 2010. Dali server: conservation mapping in 3D. Nucleic Acids Res. **38**:W545–549.

201. **Cai X, Lu J, Wu Z, Yang C, Xu H, Lin Z, Shen Y**. 2013. Structure of *Neisseria meningitidis* lipoprotein GNA1162. Acta Crystallogr. Sect. F. Struct. Biol. Cryst. Commun. **69**:362–368.

202. **Stoker NG, Broome-smith JK, Edelman A, Spratt BG**. 1983. Organization and subcloning of the dacA-rodA-pbpA cluster of cell shape genes in *Escherichia coli*. J. Bacteriol. **155**:847–853.

203. **Nelson DE, Young KD**. 2001. Contributions of PBP5 and DD -carboxypeptidase penicillin binding proteins to maintenance of cell shape in *Escherichia coli*. J. Bacteriol. **183**:3055–3064.

204. **Potluri L-P, de Pedro M, Young KD**. 2012. *E. coli* low molecular weight penicillin binding proteins help orient septal FtsZ, and their absence leads to asymmetric cell division and branching. Mol. Microbiol. **84**:203–224.

205. **Markiewicz K, Broome-Smith K, Schwarz U, Spratt BG**. 1982. Spherical *E. coli* due to elevated levels of D-alanine carboxypeptidase. Nature **297**:702–704.

206. **Begg KJ, Dewar SJ, Donachie WD**. 1995. A new *Escherichia coli* cell division gene, ftsK. J. Bacteriol. **177**:6211–6222.

207. **Draper GC, Mclennan N, Begg K, Donachie WD, Lennan NMC, Begg KEN, Masters M**. 1998. Only the N-terminal domain of FtsK functions in cell division. J. Bacteriol. **180**:4621–4627.

208. **Potluri L, Karczmarek A, Verheul J, Piette A, Wilkin J-M, Werth N, Banzhaf M, Vollmer W, Young KD, Nguyen-Distèche M, den Blaauwen T**. 2010. Septal and lateral wall localization of PBP5, the major D,D-carboxypeptidase of *Escherichia coli*, requires substrate recognition and membrane attachment. Mol. Microbiol. **77**:300–323.

209. **Otero LH, Rojas-altuve A, Llarrull LI, Carrasco-lópez C, Kumarasiri M, Lastochkin E, Fishovitz J, Dawley M, Hesek D, Lee M, Johnson JW, Fisher JF, Chang M, Mobashery S, Hermoso JA**. 2013. How allosteric control of *Staphylococcus aureus* penicillin binding protein 2a enables methicillin resistance and physiological function. Proc. Natl. Acad. Sci. **110**:16808–16813.

210. **Nichols RJ, Sen S, Choo YJ, Beltrao P, Zietek M, Chaba R, Lee S, Kazmierczak KM, Lee KJ, Wong A**. 2010. Phenotypic landscape of a bacterial cell. Cell **144**:143–156.

211. **Dougherty TJ, Kennedy K, Kessler RE, Pucci MJ**. 1996. Direct quantitation of the number of individual penicillin-binding proteins per cell in *Escherichia coli*. J. Bacteriol. **178**:6110–6115.

212. **Cascales E, Lloubès R, Sturgis JN**. 2001. The TolQ-TolR proteins energize TolA and share homologies with the flagellar motor proteins MotA-MotB. Mol. Microbiol. **42**:795–807.

213. **Religa TL, Ruschak AM, Rosenzweig R, Kay LE**. 2011. Site-directed methyl group labeling as an NMR probe of structure and dynamics in supramolecular protein systems: applications to the proteasome and to the ClpP protease. J. Am. Chem. Soc. **133**:9063–9068.

214. **Clarke TB, Kawai F, Park S-Y, Tame JRH, Dowson CG, Roper DI**. 2009. Mutational analysis of the substrate specificity of *Escherichia coli* penicillin binding protein 4. Biochemistry **48**:2675–2683.

215. **Seidel SAI, Wienken CJ, Geissler S, Jerabek-Willemsen M, Duhr S, Reiter A, Trauner D, Braun D, Baaske P**. 2012. Label-free microscale thermophoresis discriminates sites and affinity of protein-ligand binding. Angew. Chem. Int. Ed. Engl. **51**:10656–10659.

216. **Radke MB, Taft MH, Stapel B, Hilfiker-kleiner D, Preller M, Manstein DJ**. 2014. Small molecule-mediated refolding and activation of myosin motor function. Elife **3**:e01603.

217. **Casadaban MJ, Cohen SN**. 1980. Analysis of gene control signals by DNA fusion and cloning in *Escherichia coli*. J. Mol. Biol. **138**:179–207.

218. **Baba T, Ara T, Hasegawa M, Takai Y, Okumura Y, Baba M, Datsenko K A, Tomita M, Wanner BL, Mori H**. 2006. Construction of *Escherichia coli* K-12 in-frame, single-gene knockout mutants: the Keio collection. Mol. Syst. Biol. **2**:2006.0008.

219. **Yamamoto N, Nakahigashi K, Nakamichi T, Yoshino M, Takai Y, Touda Y, Furubayashi A, Kinjyo S, Dose H, Hasegawa M, Datsenko K A, Nakayashiki T, Tomita M, Wanner BL, Mori H**. 2009. Update on the Keio collection of *Escherichia coli* single-gene deletion mutants. Mol. Syst. Biol. **5**.